UNIVERSITÀ
DEGLI STUDI
DI PADOVA

Sede Amministrativa: Università degli Studi di Padova

Dipartimento di Scienze Chimiche

CORSO DI DOTTORATO DI RICERCA IN: SCIENZE MOLECOLARI
CURRICOLO: SCIENZE CHIMICHE
CICLO XXX

L'ELETTROCHIMICA QUALE STRUMENTO FONDAMENTALE PER ACCRESCERE LA COMPRENSIONE E L'IMPLEMENTAZIONE DELLA POLIMERIZZAZIONE RADICALICA PER TRASFERIMENTO DI ATOMO

ELECTROCHEMISTRY AS A CRUCIAL TOOL TO BROADEN ATOM TRANSFER RADICAL POLYMERIZATION UNDERSTANDING AND IMPLEMENTATION

Coordinatore: Ch.mo Prof. Leonard Jan Prins
Supervisore: Ch.mo Prof. Armando Gennaro

Dottoranda : Francesca Lorandi

Contents:

Glossary of Acronyms

AA	Acrylic acid
AIBN	Azobisisobutyronitrile
ARGET	Activator regenerated by electron transfer
AsAc	Ascorbic acid
AT	Atom transfer
ATRP	Atom transfer radical polymerization
BA	Butyl acrylate
BMA	Butyl methacrylate
BB	Benzyl bromide
BC	Benzyl chloride
BDFE	Bond dissociation free energy
BiBA	2-bromoisobutyric acid
BMIm	1-butyl-3-methylimidazolium
BPA	Bromo phenylaceticacid
BPED	*N*,*N*'-bis(pyridin-2-ylmethyl 3-hexoxo-3-oxopropyl)ethane 1,2-diamine
BPMEA	*N*,*N*-bis(2-pyridylmethyl)-2-hydroxyethylamine
BPMODA	Bis(2-pyridylmethyl)octadecylamine
BPMODA*	Bis[2-(4-methoxy-3,5-dimethyl)pyridylmethyl]octadecylamine
BPMPrA	*N*,*N*-bis(2-pyridylmethyl)propylamine
BPN	Bromopropionitrile
Bpy	2,2'-Bypiridine
Brji 98	Polyoxyethylene (20) oleyl ether
Bu_4NClO_4	Tetra butylammonium perchlorate
Bu_4NPF_6	Tetra butylammonium hexafluorophosphate
CAN	Chloroacetonitrile
CE	Counter electrode
CiBA	2-chloroisobutyric acid
CPAA	Chlorophenylacetic acid
CPN	Chloroproprionitrile
CRP	Controlled radical polymerization
CRT	Catalytic radical termination
CV	Cyclic voltammetry

$Đ$	Molecular weight dispersity (M_w/M_n)
DCF	Dead-chain fraction
DCPA	2,2-dichloropropionic acid
DET	Dissociative electron transfer
DMF	Dimethylformamide
dNbpy	4,4'-Dinonyl-2,2'-bipyridine
DP	Degree of polymerization
*e*ATRP	Electrochemically mediated atom transfer radical polymerization
EBiB	Ethyl α-bromoisobutyrate
EBPA	α-bromophenylacetate
EBA	Ethyl bromoacetate
ECP	Ethyl 2-chloropropionate
ESI-MS	Electrospray ionization mass spectroscopy
ET	Electron transfer
Et_4NCl	Tetraethylammonium chloride
Et_4NBr	Tetraethylammonium bromide
Et_4NBF_4	Tetraethylammonium tetrafluoroborate
Fc	Ferrocene
FT-IR	Fourier transform infrared spectroscopy
GC	Glassy carbon
GPC	Gel permeation chromatography
HD	Hexadecane
HEBiB	2-hydroyethyl 2-bromoisobutyrate
HMTETA	1,1,4,7,10,10-Hexamethyltriethylenetetramine
ICAR	Initiators for continuous activator regeneration
ICP-MS	Inductively coupled plasma mass spectroscopy
I_{eff}	Initiator efficiency ($M_{n,th}/M_n$)
IL	Ionic liquid
ISET	Inner-sphere electron transfer
ITRP	Iodine transfer radical polymerization
M	Monomer
MA	Methyl acrylate
MAA	Methacrylic acid
MBiB	Methyl α-bromoisobutyrate

MBP	Methyl 2-bromopropionate
MCP	Methyl 2-chloropropionate
Me_6TREN	Tris(2-(dimethylamino)ethyl)amine
MMA	Methyl methacrylate
M_n	Number average molecular weight
M_w	Weight average molecular weight
MW	Molecular weight
NMP	Nitroxide mediated polymerization
NMR	Nuclear magnetic resonance
NiPAM	*N*-isopropyl acrylamide
OEOBP	Oligo(ethylene glycol) methyl ether 2-bromopropionate
OEOMA	Oligo(ethylene glycol) methyl ether methacrylate, average M_n = 500
OMRP	Organometallic mediated radical polymerization
OSET	Outer-sphere electron transfer
OTf	Trifluoromethanesulfonate
PEB	1-phenylethyl bromide
PEC	1-phenylethyl chloride
PMDETA	*N*,*N*,*N*',*N*',*N*''-pentamethyldiethylenetriamine
PRE	Persistent radical effect
RAFT	Reversible addition fragmentation chain transfer polymerization
RDRP	Reversible deactivation radical polymerization
RDE	Rotating disk electrode
RE	Reference electrode
RP	Radical polymerization
RT	Conventional radical termination
RX	Organic halide (ATRP initiator)
SARA	Supplemental activator and reducing agent
SCE	Saturated calomel electrode
SDA	Sodium dodecanoic acid
SDBS	Sodium dodecylbenzenesufonate
SDS	Sodium dodecyl sufate
SEM	Scanning electron microscope
SET-LRP	Single electron transfer living radical polymerization
SFRP	Stable free-radical polymerization

SR&NI	Simultaneous reverse & normal initiation
*t*BA	*tert*-butyl acrylate
*t*BMA	*tert*-butyl methacrylate
TCAA	Trichloroacetic acid
TEMPO	2,2,6,6-tetramethylpiperidinyl-1-oxy
TPEDA	*N*,*N*,*N*',*N*'-tetra[(2-pyridal)methyl]ethylenediamine
TPMA	Tris-[(2-pyridyl)methyl]amine
TPMA*1	(4-methoxy-3,5-dimethyl-pyridin-2-ylmethyl)-pyridin-2-ylmethyl-amine
TPMA*2	Bis-(4-methoxy-3,5-dimethyl-pyridin-2-ylmethyl)-pyridin-2-ylmethyl-amine
TPMA*3	Tris-(4-methoxy-3,5-dimethyl-pyridin-2-ylmethyl)-pyridin-2-ylmethyl-amine
WE	Working electrode

Riassunto

La possibilità di controllare processi per via elettrochimica riveste crescente attenzione nel mondo della chimica organica e della sintesi di polimeri. L'elettrochimica offre diversi parametri per intervenire sulle proprietà dei sistemi in oggetto, senza introdurre altri agenti chimici e spesso aumentando la tolleranza del sistema verso le impurezze. Di conseguenza la gestione del processo e il passaggio tra diversi stadi risultano facilitati.

Negli ultimi dieci anni, il principale interesse nel campo della sintesi polimerica riguarda la preparazione di macromolecole con architetture predeterminate. La polimerizzazione radicalica per trasferimento di atomo (ATRP) è la tecnica più versatile e affermata per la costruzione di polimeri ben definiti, con stretta distribuzione di pesi molecolari ed eccellente ritenzione di funzionalità di fine catena. L'ATRP si basa sulla disattivazione reversibile dei radicali propaganti, in modo da allungare il tempo di vita delle catene in crescita. La concentrazione di radicali in soluzione rimane sempre molto bassa, portando così a minimizzare la probabilità dei radicali stessi di essere soggetti a terminazione.

L'equilibrio di attivazione-disattivazione è generalmente governato da un catalizzatore metallico, composto da un centro di rame e un legante amminico polidentato. Nella sua forma attiva, $[Cu^{I}L]^{+}$, il catalizzatore genera radicali per rottura riduttiva del legame C–X nell'alogenuro alchilico, RX, utilizzato come iniziatore. La specie disattivante $[X–Cu^{II}L]^{+}$ si forma in seguito al trasferimento elettronico e atomico, che avvengono in contemporanea. I radicali generati riescono ad addizionare solo poche molecole di monomero (reazione di propagazione), prima di essere riconvertiti al loro stato dormiente tramite reazione con $[X–Cu^{II}L]^{+}$. In ATRP è importante che gli iniziatori siano altamente reattivi, in modo da garantire la crescita simultanea di tutte le catene e quindi poter ottenere pesi molecolari predeterminati. Le funzionalità di fine catena non vengono intaccate durante la polimerizzazione e questo permette di sottoporre il polimero a processi di post-polimerizzazione e di costruire copolimeri con varie composizioni e topologie.

Lo scopo di questa tesi di dottorato è quello di affermare l'elettrochimica come fondamentale, accessibile ed efficace risorsa per l'analisi meccanicistica dei processi di ATRP e per condurre questo tipo di polimerizzazioni. Meno di venti anni fa, studi elettrochimici furono per la prima volta utilizzati in ATRP: i potenziali standard di

riduzione di alcuni catalizzatori comunemente usati furono determinati tramite voltammetria ciclica (CV) e correlati alle performances catalitiche di questi composti. Da allora, la CV è la tecnica per eccellenza per lo studio delle proprietà redox dei catalizzatori per ATRP, nonché per la determinazione delle affinità relative delle specie di Cu^{I} e Cu^{II} per gli ioni alogenuro, quindi per predire l'attività dei complessi nella polimerizzazione. Inoltre, diverse procedure elettrochimiche sono state messe a punto per misurare con elevata precisione la costante cinetica di attivazione, k_{act}, che riguarda quindi la reazione tra $[Cu^{I}L]^{+}$ e RX. Valori di k_{act} che coprono 12 ordini di grandezza sono stati misurati con diverse tecniche, in vari ambienti.

Tra le suddette tecniche, l'utilizzo di un elettrodo a disco rotante (RDE) consente misure rapide, facilmente realizzabili e altamente riproducibili. Il RDE è stato usato in questo lavoro di tesi per definire una semplice procedura elettrochimica per la determinazione della costante termodinamica di equilibrio di ATRP, K_{ATRP}. Sostanzialmente con questo strumento è stata seguita la reazione tra Cu^{I} e RX, come avveniva per la misura di k_{act}, ma in questo caso non si è introdotto nel sistema un catturatore radicalico, che serviva per isolare cineticamente lo step di attivazione. Quindi le reazioni di attivazione, disattivazione e terminazione radicalica sono state contemporaneamente monitorate e il valore di K_{ATRP} è stato ottenuto dall'elaborazione del responso elettrochimico tramite un'equazione, originariamente proposta da Fischer e in seguito opportunamente modificata. Il metodo è stato applicato a diversi catalizzatori, iniziatori, combinazioni di solvente e monomero e temperature, osservando dei trends nelle costanti in accordo con i principi di ATRP.

K_{ATRP} e k_{act} devono essere determinate in assenza di ioni alogenuro, i quali influenzano fortemente la speciazione dei complessi di Cu^{I}. Infatti, la quantità della specie attiva $[Cu^{I}L]^{+}$ viene diminuita a causa della formazione di specie di Cu^{I} variamente alogenate, di conseguenza la sua reazione con RX risulta rallentata. Dalla riduzione nella velocità con cui Cu^{I} viene consumato al variare di C_{X^-} è stato possibile stimare la costante di associazione di X^- a $[Cu^{I}L]^{+}$ (o alidofilicità di Cu^{I}, K_X^I). Viene quindi presentata una procedura per stimare K_X^I dai valori di K_{ATRP}^{app}, determinati *via* RDE in presenza di diverse concentrazioni di X^-.

Oltre a fornire strumenti per studi di tipo meccanicistico, l'elettrochimica viene usata anche come *driving force* del processo di polimerizzazione. Infatti, un potenziale o una

corrente possono essere applicati al sistema per rigenerare la specie di Cu^{I}, da $[X–Cu^{II}L]^{+}$ che si accumula in seguito al verificarsi di reazioni di terminazione radicalica. La polimerizzazione radicalica per trasferimento di atomo mediata elettrochimicamente (*e*ATRP) sfrutta gli elettroni come agenti riducenti, quindi non porta alla formazione di sottoprodotti e consente di usare come reagente un sale di Cu^{II}, stabile all'aria, che viene poi ridotto *in situ*. Il tradizionale setup per *e*ATRP richiede però un potenziostato e costosi elettrodi di Platino. Durante il mio periodo di dottorato ho cercato di semplificare il setup di *e*ATRP, così da rendere questa tecnica più conveniente e realizzabile su larga scala. Alcuni materiali non costosi e facilmente funzionalizzabili sono stati testati come catodi in solventi organici e in sistemi acquosi. Polimerizzazioni ben controllate sono state ottenute con gli elettrodi lavoranti analizzati, anche operando in modalità galvanostatica (*i.e.* applicando step a corrente costante), la quale consente di utilizzare due elettrodi anziché tre, e di sostituire il potenziostato con un semplice generatore di corrente. Inoltre, questi catodi hanno dato ottimi risultati in combinazione con un anodo sacrificale di Alluminio, quindi realizzando un setup completamente Pt-free. Infine, è stato dimostrato che questi materiali non rilasciano ioni metallici in soluzione e che la loro morfologia non viene modificata nel corso delle polimerizzazioni, pertanto possono essere riutilizzati in reazioni successive.

Caratteristica distintiva dell'*e*ATRP e della ATRP in generale è l'eccezionale versatilità di queste tecniche, che consentono di polimerizzare diverse tipologie di monomeri. Per molti anni però, fu ritenuto impossibile controllare la polimerizzazione di monomeri acidi *via* ATRP. Nel 2016, Fantin et al. hanno dimostrato che le catene propaganti di poli(acido metacrilico) tendono a ciclizzare, con conseguente perdita della funzionalità C–X, quindi terminazione. Una volta definite le condizioni adatte per evitare questa pericolosa reazione secondaria, è stato possibile controllare efficacemente la polimerizzazione dell'acido metacrilico tramite *e*ATRP.

Questa importante vittoria mi ha permesso di lavorare con successo alla polimerizzazione dell'acido acrilico (AA), monomero biocompatibile, usato in moltissimi settori. Innanzitutto è stato dimostrato che la propagazione di AA è affetta dalla stessa reazione parassita di ciclizzazione, quindi alcune delle condizioni che hanno permesso l'efficace *e*ATRP dell'acido metacrilico, sono state adattate al sistema analizzato. *i*) Il sale bromurato è stato sostituito da un sale clorurato, *ii*) la velocità di polimerizzazione è stata massimizzata usando un elettrodo lavorante con elevata area superficiale, applicando un

potenziale molto più negativo di quello standard di riduzione del catalizzatore e ottimizzando la composizione del sistema.

Un modo efficace per aumentare l'applicabilità della ATRP consiste nella sintesi di leganti che conferiscano particolari proprietà al centro metallico. Nella tesi sono riportati 4 nuovi leganti, in cui lo scheletro del legante tris(2-metilpiridil)ammina (TPMA), comunemente usato in ATRP, è stato modificato con sostituenti fenilici variamente funzionalizzati in posizione *meta*. La caratterizzazione elettrochimica dei complessi di Cu con questi leganti ha portato a predire una loro minore attività rispetto al tradizionale Cu/TPMA. Questa è stata confermata dalla determinazione di k_{act} tramite RDE. Ciononostante, questi complessi sono risultati efficaci catalizzatori in *e*ATRP di metil metacrilato in DMF, e di oligo(etilene glicole)metil etere metacrilato e di acido metacrilico in acqua. Nonostante la non elevata attività, i complessi analizzati hanno mostrato buona stabilità in acqua, anche a pH acido, e si propongono come catalizzatori adeguati per sistemi altamente reattivi.

La versatilità di queste polimerizzazioni si riflette nella possibilità di applicazione in un'ampia varietà di ambienti. Grande interesse, ad esempio, è rivolto all'utilizzo di Liquidi Ionici (ILs) come solventi di polimerizzazione "green". Pertanto, le proprietà redox di alcuni catalizzatori e iniziatori, frequentemente usati in ATRP, sono state studiate tramite CV in 1-butil-3-metilimidazolio trifluorometansolfonato. Nello stesso sono stati effettuati studi cinetici *via* RDE. Queste analisi hanno permesso di affermare che il comportamento dei composti di Cu e degli alogenuri alchilici in IL è del tutto simile a quello osservato nei solventi organici tradizionali. Perciò, i liquidi ionici si confermano come solventi adatti a processi di polimerizzazione controllata. Appare infine auspicabile realizzare *e*ATRP in ILs, perché la buona conducibilità elettrica di questi solventi consente di evitare l'aggiunta di un elettrolita di supporto.

Un ulteriore ambiente sostenibile di polimerizzazione è rappresentato dai sistemi dispersi. Sebbene moltissime polimerizzazioni su scala industriale si basino su sistemi in (mini)emulsione, la maggior parte della letteratura che tratta di ATRP riporta processi in soluzione omogenea. La realizzazione di ATRP in miniemulsione ha richiesto la sintesi di opportuni leganti super-idrofobici, che consentissero di confinare il catalizzatore nella fase dispersa idrofobica, dove potesse esercitare il suo effetto. Durante il mio dottorato ho trascorso sei mesi come *visiting student* presso la Carnegie Mellon University, nel laboratorio del Prof. Matyjaszewski, che scoprì l'ATRP nel 1995. In quel periodo ho potuto

lavorare estesamente su ATRP in miniemulsione ed emulsione. Un nuovo sistema catalitico è stato messo a punto e applicato con efficacia in *e*ATRP e ARGET-ATRP (attivatori rigenerati per trasferimento elettronico ATRP, in cui un agente riducente è usato per rigenerare continuamente Cu^{I}). Catalizzatori idrofilici tradizionali sono stati usati in combinazione con surfattanti anionici poco costosi, formando coppie ioniche capaci di entrare negli agglomerati monomerici e catalizzare la polimerizzazione. L'interazione tra le specie reagenti è stata provata attraverso caratterizzazioni elettrochimiche e spettrochimiche, che hanno permesso di definire il diverso contributo di catalisi interfacciale e via coppie ioniche. Grazie a questo approccio sono stati prodotti copolimeri a blocchi, a stella e a spazzola. Inoltre il Cu residuo nei polimeri precipitati è risultato estremamente poco, in alcuni casi inferiore ad 1 ppm, quindi i polimeri non necessitano di ulteriore purificazione. Il sistema catalitico è stato poi applicato in ARGET-ATRP in emulsione, sfruttando la presenza di un catalizzatore idrofilico, essenziale in emulsione dove la polimerizzazione deve verificarsi in fase acquosa. ARGET-ATRP ben controllate in emulsione *ab initio* sono state ottenute, anche con basse quantità di surfattante, ottimizzando la procedura di pre-emulsificazione, la velocità di mescolamento e selezionando opportuni iniziatori idrofilici.

Abstract

Controlling processes by electrochemical means is increasingly attracting the attention of organic and polymer chemists. Electrochemistry provides tunable parameters without requiring the addition of external compounds, often increasing system tolerance to impurities, thus facilitating reaction handling and switching among different stages.

In the last decades, the main interest in polymer chemistry concerned the preparation of predetermined macromolecular architectures. Atom transfer radical polymerization (ATRP) is the most powerful and versatile method to build well-defined polymers, with narrow molecular-weight distribution and excellent retention of chain-end functionalities. ATRP is based on the reversible deactivation of propagating radicals, such as to extend the lifetime of polymer chains. Radical concentration in solution is always very low, ultimately minimizing their probability of terminating.

The activation-deactivation equilibrium is generally governed by a metal catalyst, composed by copper and a polydentate amine ligand. The active form of the catalyst, $[Cu^{I}L]^{+}$, generates radicals by reductive cleavage of the C–X bond in the alkyl halide initiator, RX. As a consequence of the electron transfer and the concurrent atom transfer, the deactivator $[X–Cu^{II}L]^{+}$ is formed. Generated radicals add to few monomer molecules (*i.e.* propagation reaction), then they are reverted to their dormant state by reacting with $[X–Cu^{II}L]^{+}$. Importantly, RX initiators should be highly reactive, as to ensure the simultaneous growth of all chains, thereby targeting pre-determined molecular weights. Chain-end functionalities are preserved during the polymerization, thus enabling several post-polymerization process and the building of copolymers with various compositions and topologies.

The aim of this thesis is to affirm electrochemical tools as a primary, effective and accessible source for ATRP triggering and mechanistic analysis. Less than 20 years ago, electrochemistry was involved for the first time in ATRP, when standard reduction potentials of some common catalysts were determined by cyclic voltammetry (CV) and correlated to their catalytic performances. Since then, CV is a well-established technique to study the redox properties of ATRP catalysts and the relative affinity of Cu^{I} and Cu^{II} species for halide ions, hence predicting their activity in the polymerization. Moreover, many electrochemical procedures were arranged for the precise measurement of the

activation rate constant, $\underline{k}_{act}$, which concerns the reaction between $[Cu^{I}L]^{+}$ and RX. $\underline{k}_{act}$ values spanning over a range of 12 orders of magnitude were measured with different techniques, in many environments.

Among these techniques, the use of a rotating disk electrode allowed a fast, easy and highly reproducible measurement. This instrument was further exploited in this thesis work to set up a facile electrochemical procedure for the determination of the thermodynamic equilibrium constant of ATRP, K_{ATRP}. Essentially, the reaction between Cu^{I} species and RX was followed as for k_{act} determination, but in the absence of a radical scavenger that had been used to kinetically isolate the activation step. The interplay between activation, deactivation and radical termination was monitored, and K_{ATRP} was obtained by elaborating the electrochemical response through an equation proposed by Fischer and recently slightly modified. The method was applied to different Cu catalysts, initiators, solvent/monomer combinations and temperatures, observing some trends in accordance with general ATRP understanding.

Both k_{act} and K_{ATRP} must be measured in the absence of halide ions, which strongly affect the speciation of Cu^{I}. Indeed, the amount of active $[Cu^{I}L]^{+}$ is reduced by the formation of various halogenated Cu^{I} species, thus slowing down the reaction with RX. However, the drop in the rate of Cu^{I} consumption in the presence of different C_{X^-} was used to estimate the association constant of X^{-} to $[Cu^{I}L]^{+}$ (*i.e.* Cu^{I} halidophilicity constant, K_X^I). A procedure to measure K_X^I from K_{ATRP}^{app}, obtained under various C_{X^-}, was reported and verified for an independently determined K_X^I value.

Electrochemistry is not only used to study ATRP mechanism, but also to effectively trigger the polymerization process. In fact, an applied current or potential is used to re-generate Cu^{I} from $[X–Cu^{II}L]^{+}$, which accumulates in solution because of termination events. Electrochemically mediated ATRP (*e*ATRP) uses electrons as a reducing agent, thus it is free of by-products and allows to start from a minimum amount of air-stable Cu^{II}, which is reduced *in situ*. Nonetheless, the traditional *e*ATRP setup required a potentiostat and expensive Platinum electrodes. During my Ph.D., I tried to simplify the setup as to make *e*ATRP a cost-effective and scalable technique. Various inexpensive and easily functionalizable materials were successfully used as cathodes for *e*ATRP in both organic and aqueous media. These working electrodes allowed well-controlled polymerizations even under galvanostatic conditions (*i.e.* constant current steps), which permitted the use

of two, instead of three electrodes, and the replacement of the potentiostat with a common current generator. Furthermore, these cathodes were coupled to a sacrificial Aluminum anode in a completely Pt-free setup. Finally, these materials did not release metal ions in solution during the polymerization, and their morphology was not modified, thus they could be re-used in consecutive experiments.

One important feature of *e*ATRP and ATRP in general is their high versatility. Actually, various types of monomers are suitable for these techniques. Instead, controlled polymerization of acidic monomers *via* ATRP was considered impossible, until very recently. In 2016, Fantin at al. proved that growing chains of poly(methacrylic acid) in ATRP were affected by a cyclization reaction with loss of C–X functionalities, *i.e.* termination. Suitable conditions to overcome this issue were proposed and successful *e*ATRPs of methacrylic acid were reported.

This important achievement was extended to acrylic acid (AA), which is a biocompatible, largely used monomer. In this thesis, it is proved that AA polymerization was hampered by the same cyclization side reaction, during *e*ATRP. Indeed, some conditions that were suitable for methacrylic acid, were successfully adapted to *e*ATRP of AA. *i*) Chloride ions replaced bromides, and *ii*) polymerization rate was enhanced by using a cathode with large surface area, applying a strongly negative potential, if compared to E^{e} of the catalyst, and optimizing the amount and the nature of other reactants.

One way to broaden the applicability of ATRP is to design new ligands able to convey particular features to Cu catalysts. Herein, 4 new ligands are presented, in which the skeleton of the traditionally used tris(2-methylpyridyl)amine (TPMA) was modified with *m*-functionalized phenyl substituents. Electrochemical characterizations of Cu complexes with these ligands allowed to predict a lower activity toward RX, compared to parent TPMA, which was proved by k_{act} determination. Nevertheless, these complexes were used to catalyze well-controlled *e*ATRPs of methyl methacrylate in DMF, and oligo (ethylene glycol) methyl ether methacrylate and methacrylic acid in water. Despite the low activity, these compounds were very stable even at acidic pH and can be used to tune the polymerization in extremely reactive systems.

The versatility of ATRP is also reflected by the application in different environments. Ionic liquids for example are attracting great interest as green solvents for polymerizations. In 1-butyl-3-methylimidazolium trifluoromethanesulfonate, the redox properties of

common ATRP catalysts and initiators were investigated by CV, whereas kinetic studies were performed *via* rotating disk electrode. This work proved that the behavior of Cu complexes and RX in ILs is similar to the one observed in traditional organic solvents. Therefore, ILs are suitable media for controlled polymerizations, and particularly they should be applied as solvent for *e*ATRP because they are sufficiently conductive without added supporting electrolytes.

Dispersed media represent another eco-friendly environment for polymerizations. Although many industrial processes are based on (mini)emulsion systems, the vast majority of literature reports on ATRP concerns experiments in homogeneous solutions. ATRP in miniemulsion required the design of super hydrophobic catalysts that remained confined into hydrophobic droplets, whereby tuning the polymerization. During my Ph.D., I spent six months as a visiting student at Carnegie Mellon University, in the laboratory of Prof. Matyjaszewski, who discovered ATRP in 1995. There, I had the opportunity to work on ATRP in miniemulsion and emulsion. A new catalytic system was arranged, and effectively applied to *e*ATRP and activators re-generated by electron transfer (ARGET) ATRP, in which a reducing agent is added to continuously re-generate Cu^{I} species. Common hydrophilic catalysts were combined to inexpensive surfactants, to form ion pairs able to enter the monomer droplets and catalyze the process. Electrochemical and spectrochemical characterizations proved the interactions between the compounds and defined the different contributions from ion-pair and interfacial catalysis. Block copolymers, polymer stars and brushes were easily synthetized with this approach. Moreover, residual copper in precipitated polymers was very low, even < 1 ppm, thus avoiding the need of further purifications. The system was then adapted to emulsion ARGET-ATRP, taking advantage of the water-solubility of the catalyst, which is a requirement of emulsion polymerizations, where the process should occur in the aqueous phase. By using suitable hydrophilic initiators and finely tuning the stirring rate and the pre-emulsification procedure, well controlled *ab initio* emulsion ARGET-ATRPs were obtained, even with low surfactant amounts.

Chapter 1.

Introduction

Table of contents

1.1. From electropolymerizations to the electrochemical mediation of ATRP

Electrochemistry always played a distinct role in the world of macromolecules.[1] The use of an electrochemical stimulus to trigger a polymerization is an environmentally friendly approach, which avoids externally added reactants to initiate the process and/or the application of drastic conditions. Moreover, electrochemistry pioneered the modern concept of switching, by offering a facile manipulation of polymerizations, playing on the redox properties of system components.[2, 3]

Classical electropolymerizations have huge impact in the field of polymer chemistry.[4] Electropolymerizations are known since many years and typically concern a redox-active monomer (*e.g.* aniline, pyrrole, …).[5, 6] These processes generally follow a step-growth mechanism, in which monomers react at the electrode, forming rather insoluble coatings. Electrodeposited polymers are extensively used as biosensors and membranes.[7, 8] Electrochemically controlled supramolecular polymerizations are another, very recently developed, example of step-growth electropolymerizations.[9]

Many radical polymerizations (RPs), following a chain-growth mechanism, involve redox-active metals that can act as initiating or catalytic systems. Hence, electrochemistry was exploited to regenerate some redox initiators or catalysts, to prepare polyacrylamides[10, 11] or cationic polymethacrylates,[12] respectively. Some of these systems showed the possibility of slightly controlling the growth of polymer chains.

Actually, an enormous interest is focused on controlling macromolecular architectures during polymerizations, but, for a long time, this was considered impossible for radical polymerizations.[13, 14] Indeed, the lifetime of radicals in RPs is too short if compared to other living ionic polymerizations; they terminate at a diffusion-controlled rate. In this context, controlled radical polymerizations (CRPs) completely revolutionized polymer chemistry, by proposing ways to extend radicals lifetime and precisely direct their growth.[15, 16] The main concept at the basis of each controlled RP technique is the reversible deactivation of active radicals, thereby establishing an equilibrium between propagating and dormant species (**Scheme 1.1**). Therefore, these techniques are overall called reversible-deactivation radical polymerizations (RDRPs).

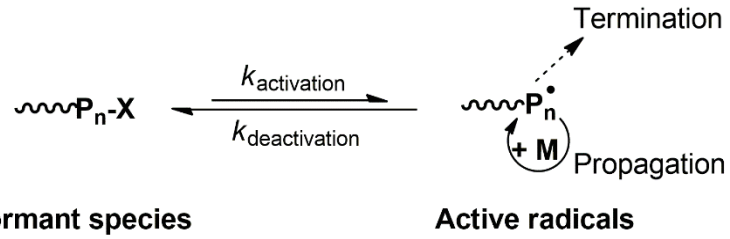

Scheme 1.1. General equilibrium between active radicals and dormant species in a reversible-deactivation radical polymerization (RDRP).

Atom transfer radical polymerization (ATRP) is the most used and versatile RDRP method, as will be discussed in the next section.[17] ATRPs are catalyzed by redox metals, thus electrochemistry was naturally required to investigate the polymerization mechanism.[18] Electrochemistry was also used as an external stimulus to trigger the

process.[19, 20] Electrochemically mediated ATRP (*e*ATRP) is one of the most recent and successful results of the interaction between electrochemistry and polymer chemistry. My Ph.D. project is centered on *e*ATRP and more generally on the use of electrochemistry as a diagnostic tool and driving force in ATRP.

This chapter presents ATRP, analyzing the role of some components and polymerization conditions, and discussing the mechanism of atom and electron transfer (AT and ET, respectively). Particular attention is given to the redox properties of various compounds and how electrochemical characterizations are important to define the thermodynamics and kinetics of the system. *e*ATRP is then described in details, in terms of experimental apparatus and synthetic advantages. **Chapter 2** offers a chronological summary of contributions given by electrochemistry to mechanistic understanding in ATRP, as well as to the preparation of well-defined polymeric materials. Finally, the outline of this thesis work is presented and contextualized in the described state of the art.

1.2. ATRP: general mechanism and low-ppm catalyst loading

In RDRP methods, the dynamic equilibrium between dormant and active species is established in two different ways. A first class of techniques is based on the intermittent deactivation-(re)activation of propagating radicals, by means of a catalyst, as in atom transfer radical polymerization (ATRP), or spontaneously, as in nitroxide mediated polymerization (NMP, also known as stable free radical polymerization, SFRP)[21] or organometallic-mediated radical polymerization (OMRP).[22] Instead, a second class involves a degenerate transfer between propagating and dormant radicals, as in reversible addition-fragmentation chain-transfer polymerization (RAFT)[23, 24] or iodine transfer radical polymerization (ITRP).[25, 26]

All mentioned RDRP processes faced a huge growth in the last decades, impacting both academies and industries. ATRP stands out among the others as the most used and versatile, and the yearly increase in the average number of publications and patents reported in **Figure 1.1** supports this statement. Actually, ATRP allows to obtain polymers with pre-determined molecular weights (MWs), extremely narrow molecular weight distribution and high retention of chain-end functionalities.[27] Homopolymers and copolymers with complex architectures, and different compositions and topologies, as well as variously functionalized and hybrid organic-inorganic materials were built by ATRP.[28, 29]

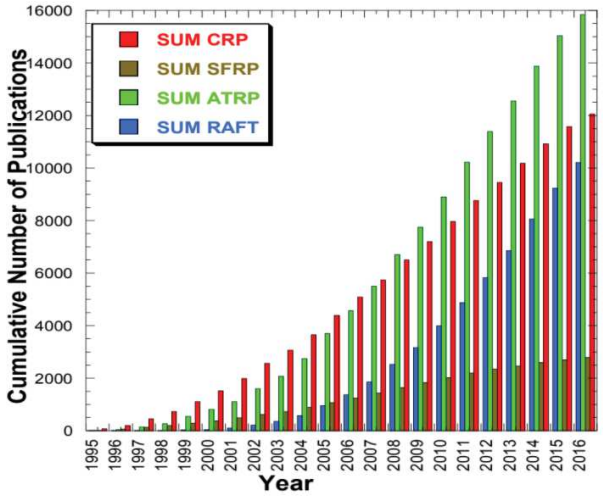

Figure 1.1. Results of SCIFinder search on various RDRP methods as of October 2016.

In ATRP, the reversible equilibrium between dormant and active species is mediated by a catalyst, which is generally a complex of copper with a polidentate amine ligand. The complex in its lower oxidation state, $[Cu^{I}L]^{+}$, activates the process by reductive cleavage of the C–X bond in the initiator (RX) or in the dormant chain (P_n–X). Following this activation step, the catalyst is oxidized and the halogen atom is transferred to the Cu complex, forming the deactivator $[X–Cu^{II}L]^{+}$. Meanwhile, a radical is generated, which can add to few monomer molecules (*i.e.* propagation) before interacting with $[X–Cu^{II}L]^{+}$, hence being reverted to its dormant state (**Scheme 1.2**).

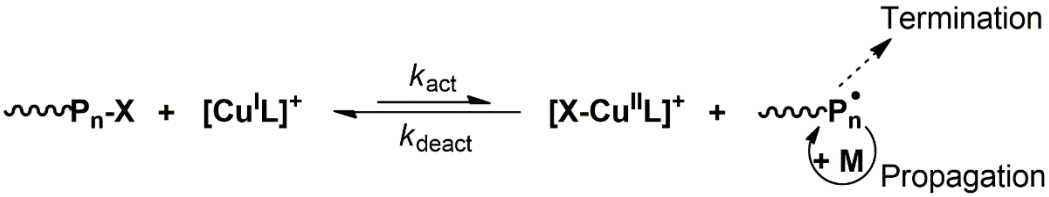

Scheme 1.2. Mechanism of atom transfer radical polymerization (M = monomer).

In conventional radical polymerizations radicals live approximately 1 s, which means that at any time essentially all chains are dead. Conversely, in ATRP the lifetime of radicals is extended to hours or even days, in the sense that they lay in a dormant state for most of the time. As a consequence, the fraction of terminated chains is very small, usually below 10%.[14]

Although radical termination events are minimized in ATRP, they cannot be completely avoided. Regardless of whether radicals terminate by radical-radical coupling or disproportionation, each termination reaction causes the accumulation of one molecule of deactivator $[X–Cu^{II}L]^{+}$. This phenomenon is called persistent radical effect (PRE).[30]

Indeed, if R is the propagating chain and Y the deactivator, R is a transient radical that can disappear both by termination and cross reaction (*i.e.* reacting with Y), whereas Y is a "persistent radical" that can disappear only by cross-reaction (**Scheme 1.3**). Each self-termination of R causes the build-up of excess Y. However, the permanent increase in Y amount accelerates the cross-reaction at the expense of the self-termination, which never stops completely, but becomes increasingly less important. A dynamic equilibrium is reached when the rate of the cross-reaction matches that of the radical generation.

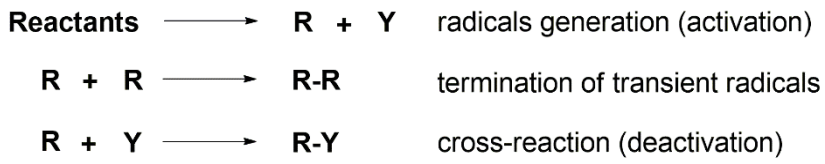

Scheme 1.3. Schematic representation of reactions defining the persistent radical effect (PRE), where R is the transient radical and Y the persistent radical.

Traditional ATRPs were performed by starting with a huge amount of Cu^{I} catalyst (*ca.* 0.1 M), to face the irreversible oxidation of part of the catalyst to Cu^{II} species. High catalyst loading is clearly inconvenient in terms of production cost, system manipulation and polymer purification. Moreover, many Cu^{I} salts are not air-stable. A reverse ATRP process was initially proposed, which started by oxidation-stable Cu^{II} complexes that were reduced *in situ* by a free radical initiator.[31] However, copolymers could not be obtained with this technique, thus a simultaneous reverse and normal initiation ATRP (SR&NI) was developed.[32, 33] In this case, a low amount of more active Cu^{II} complexes are used and reduced *in situ* by a small amount of a free radical initiator in the presence of a larger amount of an alkyl halide initiator.

Many efforts were devoted to drastically decrease the initial copper amount, spawning a series of techniques based on the re-generation of the active Cu^{I} species from the persistent radical, $[X–Cu^{II}L]^{+}$ (**Scheme 1.4**).[34] In activators regenerated by electron transfer (ARGET) ATRP, few ppm of catalyst can be used in the presence of a reducing agent, such as a Sn^{II} salt, ascorbic acid, glucose, hydrazine, or even small amounts of inexpensive ligands, and also zero-valent metals like Mg, Zn and Fe.[35, 36] Metallic copper can be used as a reducing agent but it is also able to activate C–X chain ends, thus RDRP in the presence of Cu^{0} is called supplemental activator and reducing agent (SARA) ATRP.[17, 37-39] The main drawback of ARGET-ATRP is that oxidation of the reducing agent in solution generates by-products that must be separated from the polymer, besides being eventually toxic (*e.g.* Sn^{IV}). In initiators for continuous activator regeneration (ICAR) ATRP, a source of organic

free radicals (*e.g.* AIBN) is used to re-generate Cu^{I}.[40, 41] The rate of the polymerization depends on the rate of decomposition of the added initiator. More recently, a "green" process, called photo-ATRP, was proposed. It uses UV or visible light to reduce Cu^{II} species to Cu^{I}.[42, 43] Finally, in 2016 mechano-ATRP was developed. This technique uses ultrasound and piezo-electricity of functionalized ZnO nanoparticles to re-generate the Cu^{I} activator.[44, 45]

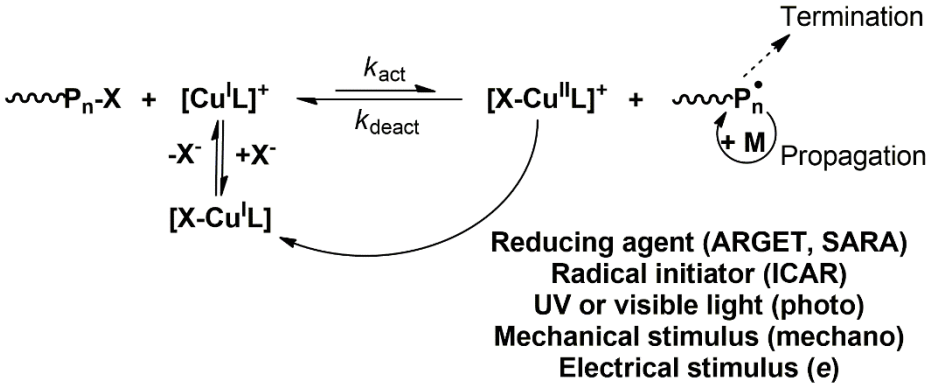

Scheme 1.4. Mechanism of ATRP with (re)generation of active Cu^{I} species.

The use of an electrical stimulus, *i.e.* an applied potential or current, was proposed in 2011 by Magenau et al.[46] Electrochemically mediated ATRP (*e*ATRP) is based on the straightforward reduction of Cu^{II} species to Cu^{I} by means of an imposed electrical stimulus. In this sense, besides being in essence similar to ARGET-ATRP in the regeneration mechanism, *e*ATRP avoids the need of external reducing agents, and the formation of by-products. Instead, electrons act as "reducing agents", thus *e*ATRP emerges as an environmentally-friendly and flexible method. Moreover, all advantages provided by other techniques are preserved: *i*) start from an air-stable Cu^{II} species that is reduced *in situ*, *ii*) increased tolerance to oxygen, *iii*) use of few ppm catalyst loadings.

The setup of *e*ATRP and the great advantages provided by this technique will be described in **Section 1.4** and in **Chapter 2**.

1.3. ATRP basics: fundamental parameters, components, transfer mechanisms

In ATRP, the polymerization rate depends on the propagation rate constant, k_p, and the concentrations of monomer and propagating chains. In turn, the amount of active chains is related to the thermodynamic equilibrium constant of ATRP, K_{ATRP}, and the concentrations of dormant species, activators and deactivators, as expressed by Eq. 1.1.[14, 47]

$$R_p = k_p C_M C_{P_n^\bullet} = k_p K_{ATRP} \left(\frac{C_{[P_nX]} C_{[Cu^I L]^+} C_M}{C_{[XCu^{II}L]^+}} \right) \quad (1.1)$$

K_{ATRP} is defined by the ratio between the activation rate constant and the deactivation rate constant, k_{act}/k_{deact}. The structure of the ligand, *i.e.* the reducing power of the catalyst (as explained in **Section 1.3.1**), and the structure of monomer/dormant species, and reaction conditions (solvent, temperature and pressure), affect both k_{act} and k_{deact}, thus K_{ATRP}. Actually, k_{deact} values are generally very high, even approaching the diffusion-controlled limit, and less influenced than k_{act} by the previously mentioned parameters.

R_p increases with K_{ATRP}, thus ATRP rate is generally higher with highly active catalysts. However, the higher the activity of the catalyst, the higher the amount of generated radicals, thereby increasing the likelihood of terminations, as well as the amount of $[XCu^{II}L]^+$ because of the PRE, thus slowing down the polymerization.

In a well-controlled polymerization, chains should grow simultaneously, and this is evaluated by a parameter called molecular weight dispersity (M_w/M_n or $Đ$), defined as the ratio between weight average molecular weight (M_w) and number average molecular weight (M_n). $Đ$ is influenced by the amount of dormant species and deactivator, by the rates of propagation, and deactivation, and by monomer conversion (p) and targeted degree of polymerization (DP = C_M^0/C_{RX}^0, where superscript "0" stands for initial concentration), according to Eq. 1.2.[14]

$$Đ = \frac{M_w}{M_n} = 1 + \frac{1}{DP} + \left(\frac{k_p C_{[P_nX]}}{k_{deact} C_{[XCu^{II}L]^+}} \right) \left(\frac{2}{p} - 1 \right) \quad (1.2)$$

This equation is derived for the ideal case of complete and fast initiation, and no termination or chain transfer. In agreement with Eq. 1.2, if the deactivation of propagating chains is fast, and/or $C_{[XCu^{II}L]^+}$ is relatively high, narrower MW distributions can be achieved.[47]

Figure 1.2a, b shows typical features of a well-controlled ATRP-like process. The kinetics of monomer consumption is first-order, while measured molecular weights increase linearly with monomer conversion. Dispersity should be low, particularly $Đ < 1.5$ at the end of the process. Normally, dispersity decreases with conversion, except at high conversion, when the depletion of monomer and the high viscosity favor radical termination reactions. Monomer conversion is determined by ^{1}H NMR, whereas molecular weight and dispersity of the polymer are measured by Gel Permeation Chromatography in a suitable eluent. If MWs values measured by GPC are close to values obtained from NMR data of

monomer conversion, the initiator efficiency is good. This parameter is defined as I_{eff} = $M_{n,th}$ (from NMR data)/M_n (measured by GPC), and it reflects the amount of chains that start growing simultaneously.

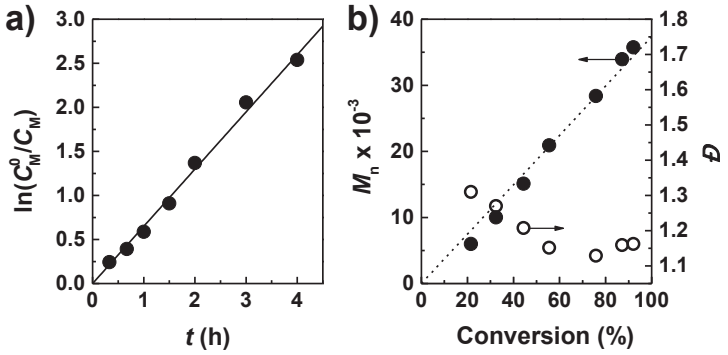

Figure 1.2. Typical graphs of a well-controlled ATRP: a) a first-order kinetic plot of monomer consumption and b) molecular weights and dispersity evolution with monomer conversion.

Besides dispersity, the retention of chain-end functionalities is strongly correlated to the extent of termination reactions in ATRP. Terminated chains cannot be further functionalized or extended with other monomers, thus it is important to estimate the dead-chain fraction (DCF). This parameter is defined as the ratio between the amount of terminated chains, T, and the initial concentration of initiator, and depends on the targeted DP, monomer conversion, propagation and termination rate constants, and reaction time t.[14, 48]

$$\mathrm{DCF} = \frac{C_\mathrm{T}}{C^0_\mathrm{RX}} = \frac{2\mathrm{DP}k_\mathrm{t}[\ln(1-p)]^2}{C^0_\mathrm{M}k^2_\mathrm{p}t} \tag{1.3}$$

Terminations are generally diffusion-controlled processes, thus k_t values for different monomers are similar. In contrast, k_p is strongly affected by monomer type and structure. However, reaction conditions can be tuned so as to decrease $k_t/(k_p)^2$. If the temperature is raised, k_p increases much more than k_t. Nevertheless, an enhancement in T tends to increase the rate of side-reactions, dramatically affecting both monomer conversion and MW distribution. An increase in pressure will enhance k_p and decrease k_t at the same time, because radical propagation has a negative volume of activation, whereas termination has a positive activation volume. Indeed, a high pressure favored well-controlled ATRPs of high-MW polymers and hybrids. Other strategies such as compartmentalization[49] (which will be slightly discussed in **Chapter 8**) and confined spaces were proposed to minimize termination reactions.[50]

1.3.1. Catalyst

A suitable ATRP catalyst must reversibly activate dormant species with a terminal C-X bond by abstraction of the halogen atom, which involves also a mono-electronic oxidation of the metal center. Thus, the metal complex used as catalyst should *i*) own at least two oxidation states separated by one electron count; *ii*) have a good halogen affinity and an expandable coordination sphere to accommodate X^-; *iii*) possess high electron density on the metal center. Indeed, during the activation step, one electron is formally transferred from the catalyst to the dormant chain end. It follows that late transition metals in a lower oxidation state are good ATRP catalysts, although some early transition metals have also been employed. Examples include Ru, Cu, Fe, Ni, Mo, Mn, Os, Co, etc. The Cu^I/Cu^{II} redox couple is definitely the most used in ATRP, mainly for the facile handling and easy availability of copper salts.[14]

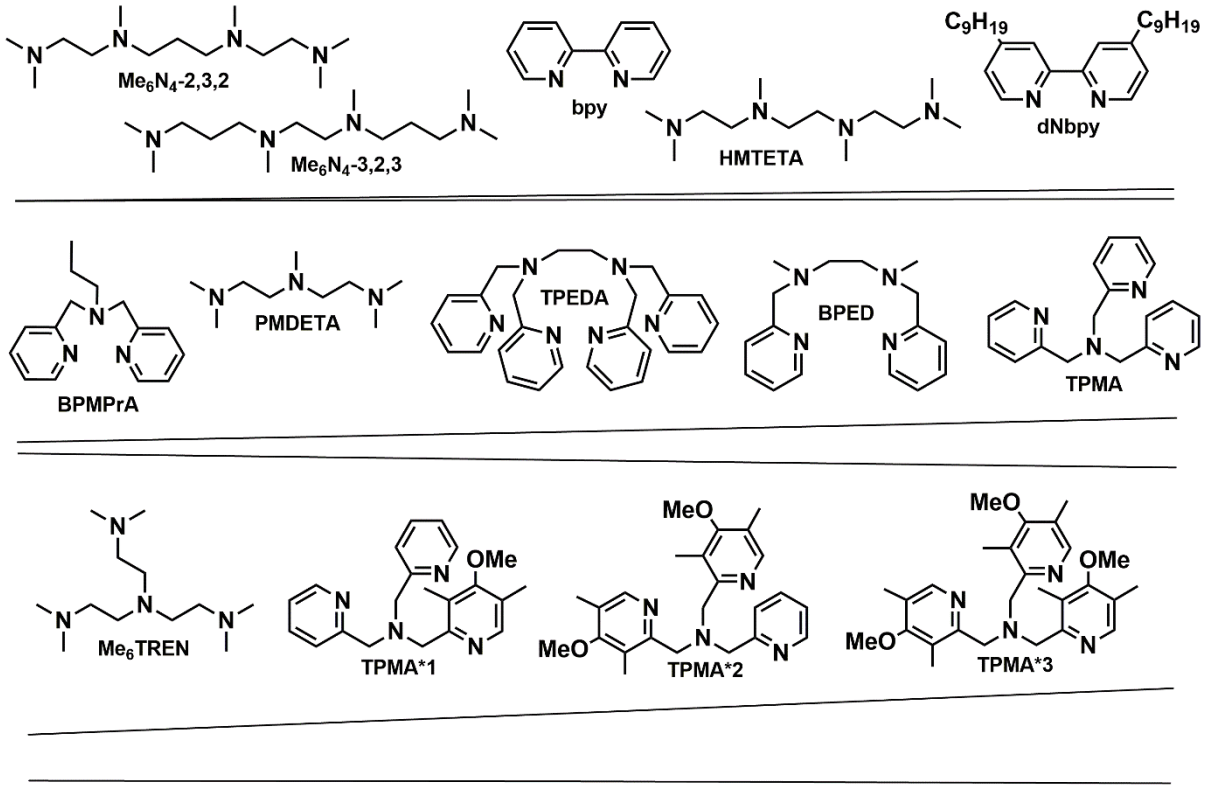

Figure 1.3. Chemical structures of common ATRP ligands, ordered according to increasing reducing power of respective Cu complexes.

The activity of copper complexes in ATRP depends on the nature of the polydentate-amine ligand and increases in the order bidentate < tetradentate (linear) < tridentate < tetradentate (cyclic) < tetradentate (branched) < tetradentate (cyclic-bridged). Moreover, the nature of nitrogen atoms in the ligand affects the catalytic activity of Cu complexes,

which increases in the order imine < aliphatic amines ≈ pyridines < aromatic amines.[51, 52] Structures of common and recently synthesized[53] ATRP ligands are reported in **Figure 1.3**.

Regarding the geometrical structure of these complexes, the d^{10} Cu^{I} activator has 4 occupied coordination sites and a tetrahedral or square pyramidal geometry with most common ATRP ligands (**Scheme 1.5a**). Instead, the d^{9} Cu^{II} deactivator is generally pentacoordinated, with (pseudo)halide ions or solvent molecules filling the sites unoccupied by the amine ligand. Cu^{II} species is either trigonal bipyramidal or square pyramidal (**Scheme 1.5b, c**).[54]

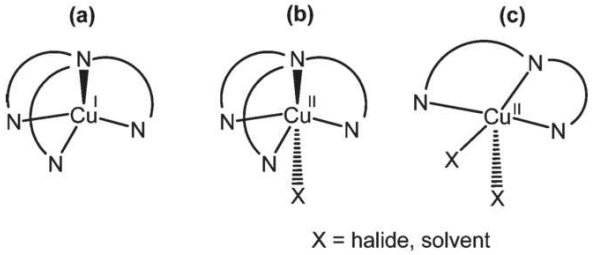

Scheme 1.5. Schematic representations of the molecular geometry of Cu complexes with a,b) Me_6TREN, or c) PMDETA as ligand (reprinted with permission from Ref. [55]. Copyright 2010, American Chemical Society).

Redox properties of ATRP catalysts are strictly related to thermodynamic and kinetic aspects of the ATRP process, hence the electrochemical behavior of copper-ligands complexes needs to be carefully investigated.[56] Cyclic voltammetry provides several information on the catalytic system.[57] The typical voltammetric pattern of a common ATRP catalyst is reported in **Figure 1.4**. Each signal is associated to the monoelectronic reduction of Cu^{II} species. In the absence or presence of amine ligands, the reversible redox processes in Eq. 1.4 and 1.5 occur. Standard reduction potentials of each redox couple, $E^{\ominus}$, is generally estimated from the half-wave potential $E_{1/2} = (E_{pa} + E_{pc})/2$, where E_{pa} and E_{pc} are the anodic and cathodic peak potentials, respectively. The presence of a polydentate amine ligand shifts the quasi-reversible peak couple of the solvated Cu^{2+}/Cu^{+} ions to more negative potentials. The shift in $E^{\ominus}$ values is correlated to the stability constants of $[Cu^{I}L]^{+}$ and $[Cu^{II}L]^{2+}$, β^{I} and β^{II}, respectively, according to Eq. 1.6.

$$Cu^{2+} + e^{-} \rightleftharpoons Cu^{+} \qquad E^{\ominus}_{Cu^{2+}/Cu^{+}} \qquad (1.4)$$

$$[Cu^{II}L]^{2+} + e^{-} \rightleftharpoons [Cu^{I}L]^{+} \qquad E^{\ominus}_{[Cu^{II}L]^{2+}/[Cu^{I}L]^{+}} \qquad (1.5)$$

$$E^{\ominus}_{[Cu^{II}L]^{2+}/[Cu^{I}L]^{+}} = E^{\ominus}_{Cu^{2+}/Cu^{+}} + \frac{RT}{F}\ln\frac{\beta^{I}}{\beta^{II}} \qquad (1.6)$$

where R is the gas constant and F is the Faraday constant. β^{I} and β^{II} are stability constants of copper complexes, according to the equilibria in Eq. 1.7 and 1.8, respectively.

$$Cu^{+} + L \rightleftharpoons [Cu^{I}L]^{+} \qquad \beta^{I} \qquad (1.7)$$

$$Cu^{2+} + L \rightleftharpoons [Cu^{II}L]^{2+} \qquad \beta^{II} \qquad (1.8)$$

Clearly, the determination of standard reduction potentials of variously coordinated Cu complexes is crucial in defining the speciation of ATRP catalysts.[55]

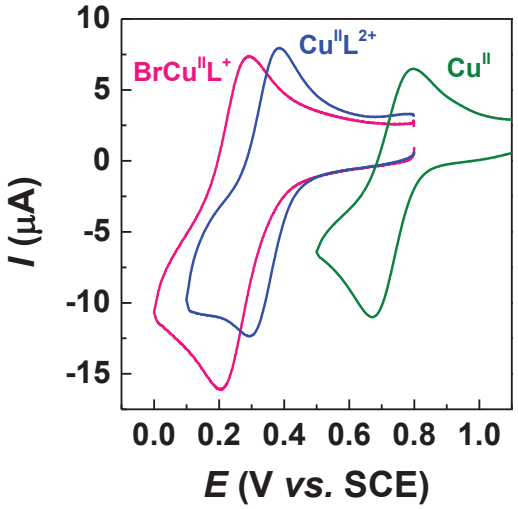

Figure 1.4. CVs of $Cu^{II}(OTf)_2$ (green), $[Cu^{II}Me_6TREN]^{2+}$ (blue) and $[BrCu^{II}Me_6TREN]^{+}$ (pink) in MMA/DMF 1/1 (v/v) + 0.1 M Et_4NBF_4; scan rate (υ) = 0.2 V s^{-1}, T = 25 °C, recorded on a glassy carbon disk.

$E^{\ominus}_{[Cu^{II}L]^{2+}/[Cu^{I}L]^{+}}$ of common ATRP catalysts varies between -0.2 and +0.2 V *vs.* SCE in organic solvents,[58] whereas in water $E^{\ominus}_{[Cu^{II}L]^{2+}/[Cu^{I}L]^{+}}$ reaches values as low as -0.4 V *vs.* SCE.[59] Independently from the environment, in general $E^{\ominus}_{[Cu^{II}L]^{2+}/[Cu^{I}L]^{+}} \ll E^{\ominus}_{Cu^{2+}/Cu^{+}}$, beacuse ligands form very stable complexes with Cu^{II}, leading to high β^{II}/β^{I} ratios, thus negatively shifting $E^{\ominus}$ (Eq 1.6). The more negative the standard potential, the higher the reducing power of the $[Cu^{II}L]^{2+}/[Cu^{I}L]^{+}$ couple, *i.e.* higher catalytic activity. For some common catalysts, $\beta^{I} \approx 10^{7}$ M^{-1} was measured by potentiometric titration in CH_3CN, and β^{II} values in the range 10^{23}-10^{27} M^{-1} were reported.[55] A little smaller gap between β^{I} and β^{II} was measured in water, with β^{I} values in the range 10^{8}-10^{13} M^{-1} and β^{II} values from 10^{15} to 10^{20}.[59] Such high stability constants make binary complexes very stable even at extremely low concentrations, and in the presence of acids[60] or small amounts of non-complexing impurities.

However, the stability of Cu^{I} species is hampered by their strong tendency to disproportionate. The disproportionation process (Eq. 1.11) can be seen as the sum of reactions in Eq. 1.5, 1.9 and 1.10, thus the disproportionation/comproportionation equilibrium constant can be calculated from Eq. 1.12.

$$[Cu^{I}L]^{+} \rightleftharpoons Cu^{+} + L \qquad 1/\beta^{I} \qquad (1.9)$$

$$Cu^{+} + e^{-} \rightleftharpoons Cu^{0} \qquad E^{\ominus}_{Cu^{+}/Cu^{0}} \qquad (1.10)$$

$$[Cu^{I}L]^{+} \rightleftharpoons [Cu^{II}L]^{2+} + e^{-} \qquad E^{\ominus}_{[Cu^{II}L]^{2+}/[Cu^{I}L]^{+}} \qquad (1.5)$$

$$2[Cu^{I}L]^{+} \rightleftharpoons [Cu^{II}L]^{2+} + Cu^{0} + L \qquad K_{disp} \qquad (1.11)$$

$$\ln K_{disp} = \frac{F}{RT}\left(E^{\ominus}_{Cu^{+}/Cu^{0}} - E^{\ominus}_{[Cu^{II}L]^{2+}/[Cu^{I}L]^{+}}\right) - \ln \beta^{I} \qquad (1.12)$$

K_{disp} is a fundamental parameter in SARA ATRP, where comproportionation between Cu^{0} and Cu^{II}/L is the driving force of the reaction (**Scheme 1.6**).[37] K_{disp} is higher in water than in organic solvents; in particular, disproportionation is negligible in CH_3CN. K_{disp} is much higher for alkylamine ligands than for pyridinic ones, which indeed ensure better performances in aqueous media. In water, K_{disp} correlates linearly with the rate constant of disproportionation, k_{disp}.[59] The latter can be directly measured by electrochemical techniques. Actually, a rotating disk electrode can be used to follow the disappearance of Cu^{I} species in a selected solvent, in the presence of the ligand and eventually of halogen ions, but in the absence of initiator or any other compound.[39] The same technique was used to determine the activation rate constant, k_{act}, of some catalyst-initiator systems, and it will be explained in details in **Chapter 3**.

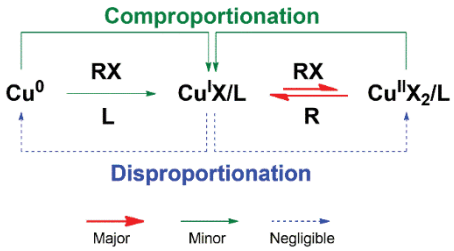

Scheme 1.6. Schematic representation of SARA-ATRP mechanism, with emphasis on Cu species and indication of the importance of each equilibrium.

When few equivalents of halogen ions are present together with a Cu^{II} salt and a polydentate amine ligand, the ternary complex $[X–Cu^{II}L]^{+}$ is formed. Generally, $E^{\ominus}_{[XCu^{II}L]^{+}/[XCu^{I}L]} \ll E^{\ominus}_{[Cu^{II}L]^{2+}/[Cu^{I}L]^{+}}$. In this case, the shift of $E^{\ominus}$ depends on the relative affinity of Cu^{I} and Cu^{II} species for halide ions, expressed by the thermodynamic association

constant, K_X^I and K_X^{II} (Eq. 1.14 and 1.15). The ratio between these two constants can be estimated from the shift in standard potential, according to Eq. 1.16, and it is strongly affected by the nature of ligand, halide ions, solvent and monomer, as well as their relative amounts.

$$[XCu^{II}L]^+ + e^- \rightleftharpoons [XCu^{I}L] \qquad E^{\ominus}_{[XCu^{II}L]^+/[XCu^{I}L]} \qquad (1.13)$$

$$[Cu^{I}L]^+ + X^- \rightleftharpoons [XCu^{I}L] \qquad K_X^I \qquad (1.14)$$

$$[Cu^{II}L]^{2+} + X^- \rightleftharpoons [XCu^{II}L]^+ \qquad K_X^{II} \qquad (1.15)$$

$$E^{\ominus}_{[XCu^{II}L]^+/[XCu^{I}L]} = E^{\ominus}_{[Cu^{II}L]^{2+}/[Cu^{I}L]^+} + \frac{RT}{F}\ln\frac{K_X^I}{K_X^{II}} \qquad (1.16)$$

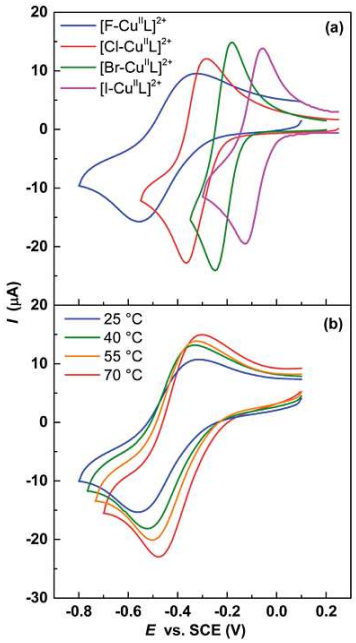

Figure 1.5. CVs of a) $[XCu^{II}TPMA]^+$ (X = F, Cl, Br, I) at T =25 °C, and b) $[FCu^{II}TPMA]^+$ at different temperatures, recorded in DMF + 0.1 M *n*-Bu_4NPF_6 at υ = 0.1 V s^{-1} on a glassy carbon disk electrode (reprinted with permission from Ref. [61]. Copyright 2017, American Chemical Society).

The electrochemical determination of $E^{\ominus}$ allows to define catalyst stability and speciation in the selected solvent, provided that one of the two affinity constants is known. K_X^{II} can be independently determined by spectrophotometric titration of $[Cu^{II}L]^{2+}$ with known amounts of halide salts.[62] $E^{\ominus}_{[XCu^{II}L]^+/[XCu^{I}L]}$ mostly depends on the K_X^{II} value, whereas K_X^I plays a minor role. Indeed, it has been observed for different halogens, copper complexes, and solvents that K_X^{II} varies over several orders of magnitude, while K_X^I is roughly constant (*ca.* 10^2 M^{-1}).[55, 59, 63] In organic solvents for example, $E^{\ominus}_{[XCu^{II}L]^+/[XCu^{I}L]}$

strongly depends on X, increasing in the order F < pseudohalide ~ Cl < Br < I (**Figure 1.5a**).[61] In contrast, in pure water the trend is different for some ligands, with $E^{\ominus}_{[XCu^{II}L]^+/[XCu^{I}L]} > E^{\ominus}_{[Cu^{II}L]^{2+}/[Cu^{I}L]^+}$.[59]

Actually, Cu speciation varies with the environment. In water, K_X^{II} is very small, thus a large excess of Br^- is required to have an amount of deactivator species suitable for polymerization control.[59, 64] Conversely, in organic solvents $[XCu^{II}L]^+$ deactivator is so stable that it is the prevalent species even at $C_{[Cu^{II}L]^{2+}}/C_{X^-} = 1$. Moreover, $K_X^{II} \gg K_X^{I}$, accounting for the negative shift in $E^{\ominus}$ of the ternary complex.[55] Cu^I speciation is more complicated than Cu^{II} speciation, since many species other than $[Cu^IL]^+$ are already present at $C_{[Cu^IL]^+}/C_{X^-} = 1$. This will be highlighted in **Chapter 3**.

Despite the multitude of Cu^I species present in solution, only $[Cu^IL]^+$ was proved to be able to activate the C–X bond, thus $[Cu^IL]^+$ is the real ATRP catalyst.[65] The experimentally measured rate of RX activation was found to vary with $C_{[Cu^IL]^+}$, while increasing amounts of X^- were added in solution (**Figure 1.6**). Thus, all other Cu^I species, *e.g.* $[XCu^IL]$, and $[Cu^IX_2]^-$ are inactive, or much less active.

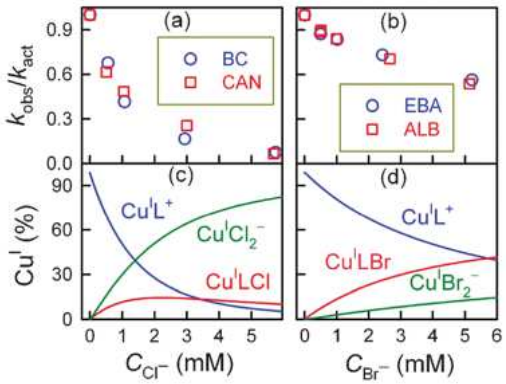

Figure 1.6. Effect of halide ions on a,b) activation rate constant, k_{act}, and c,d) speciation of Cu^I. k_{obs} = experimentally observed rate constant in the presence of X^-. Distribution diagrams were calculated for the ternary $Cu^I/L/X^-$ system at $C^0_{Cu^I} = C_L = 0.5$ mM in CH_3CN + 0.1 M Et_4NBF_4 at $T = 25$ °C (reprinted with permission from Ref. [65]. Copyright 2011 The Royal Society of Chemistry).

Lastly, the temperature has a strong effect on the redox properties of the catalysts (**Figure 1.5b**): $E^{\ominus}_{[XCu^{II}L]^+/[XCu^{I}L]}$ becomes more positive while increasing T, which means that the reducing power of the catalyst decreases at higher temperatures.[61] However, ATRP rate is generally enhanced at higher T, mainly because of the easier dissociation of the C-X bond and/or the increase in propagation rate constants, with raising T.[14]

1.3.2. Initiator

Alkyl halides are used as initiators for ATRP, mainly RBr and RCl. Their reactivity strongly depends on the structure of the alkyl part (*i.e.* stability of the radical fragment), increasing in the order primary < secondary < tertiary.[66] Electrochemical reduction of RX is a bielectronic irreversible process, thus a single cathodic peak is observed in CV. The peak is located at potentials much more negative than $E^{\ominus}$ of Cu catalysts. RX undergoes a concerted dissociative electron transfer (DET, Eq. 1.17) followed by reduction of the generated radical (Eq. 1.18):[65]

$$RX + e^- \rightleftharpoons R^\bullet + X^- \qquad E^{\ominus}_{RX/R^\bullet+X^-} \qquad (1.17)$$

$$R^\bullet + e^- \rightleftharpoons R^- \qquad E^{\ominus}_{R^\bullet/R^-} \qquad (1.18)$$

The reduction process occurs at a peak potential $E_{pc} \ll E^{\ominus}_{RX/R^\bullet+X^-}$ because of the large overpotential associated with the C–X bond breaking. As a consequence, it is not possible to extract information about the standard reduction potential of RX from its voltammetric response. In general, however, alkyl halides with highly negative E_{pc} are more difficult to reduce and therefore are less active ATRP initiators (*e.g.* RX reactivity follows the order HEBiB > OEOBP >> NiPAM,[67] **Figure 1.7**).

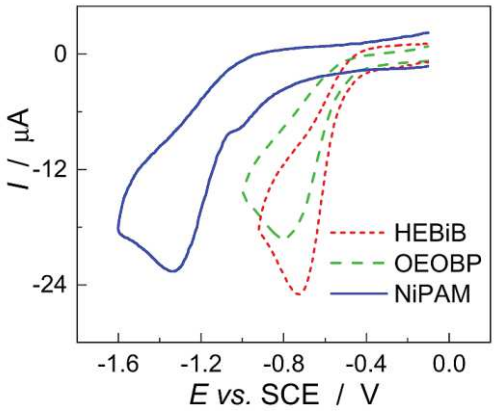

Figure 1.7. CVs of 10^{-3} M RX in H_2O + 0.1 M Et_4NBF_4, recorded on a glassy carbon electrode at $\upsilon = 0.2$ V s^{-1}, $T = 25$ °C.

$E^{\ominus}_{RX/R^\bullet+X^-}$ values have been estimated by means of a thermodynamic cycle, which takes into account the Gibbs free energy of homolytic bond dissociation in RX, $\Delta_{BD}G^{\ominus}$, and $E^{\ominus}_{X^\bullet/X^-}$.[68, 69] The latter can be found in the literature for different halogens in water, CH_3CN, and DMF.[68] $\Delta_{BD}G^{\ominus}$ can be obtained from tabulated BDE and $\Delta_{BD}S^{\ominus}_{(g)}$ values.[70, 71]

$E^{\ominus}_{RX/R^{\bullet}+X^{-}}$ values varies between -0.4 V and -1.0 V *vs.* SCE for RBr, and between -0.5 V and -1.2 V *vs.* SCE for RCl, in organic solvents.[68] This trend reflects the more difficult reduction and lower ATRP reactivity of RCl compared to RBr. $E^{\ominus}_{RX/R^{\bullet}+X^{-}}$ is more positive for more substituted RX, increasing in the order tertiary > secondary > primary, in agreement with their reactivity as ATRP initiators.

An indirect electrochemical method based on homogeneous redox catalysis was used to determine $E^{\ominus}_{R^{\bullet}/R^{-}}$ of some radicals that mimic common ATRP propagating radicals.[72] A stable precursor D was first reduced to generate aromatic radical anions $D^{\bullet-}$ (Eq. 1.19). DET between $D^{\bullet-}$ and RX yields an intermediate radical $R^{\bullet}$ (Eq. 1.20), which further reacts with $D^{\bullet-}$ either by radical coupling (Eq. 1.21) or by ET, which regenerates the original D (Eq. 1.22). The rate of the last ET depends on the relative standard potentials of the two reagents, $E^{\ominus}_{D/D^{\bullet-}}$ and $E^{\ominus}_{R^{\bullet}/R^{-}}$. This electrocatalytic process causes an increase in the cathodic peak of D and a reduction (or disappearance) of its anodic partner (**Figure 1.8**). Examination of the competition between coupling and ET allows determination of the standard reduction potential of $R^{\bullet}$ ($E^{\ominus}_{R^{\bullet}/R^{-}}$).

$$D + e^{-} \rightleftharpoons D^{\bullet-} \quad (1.19)$$

$$D^{\bullet-} + RX \rightarrow R^{\bullet} + X^{-} + D \quad (1.20)$$

$$R^{\bullet} + D^{\bullet-} \rightarrow RD^{-} \quad (1.21)$$

$$R^{\bullet} + D^{\bullet-} \rightleftharpoons R^{-} + D \quad (1.22)$$

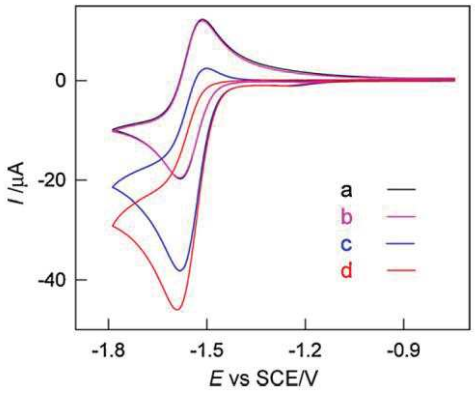

Figure 1.8. CVs of methyl 3-nitrobenzoate (D) in CH_3CN+ 0.1 M Et_4NBF_4 recorded on a glassy carbon disk, at υ = 0.04 V s^{-1} in the presence and absence of RX = methyl 2-iodopropionate. a) 1.036 mM D; b) 1.036 mM D + 2.1 mM benzamide; c) as b) + 1.036 mM RX; d) as b) + 2.07 mM RX. Benzamide was added to avoid self-protonation reactions (reprinted with permission from Ref. [72]. Copyright 2010 Elsevier).

$E^{\ominus}_{R^{\bullet}/R^-}$ obtained for $^{\bullet}CH_2CN$, $^{\bullet}CH_2CO_2Et$ and $^{\bullet}CH(CH_3)CO_2\,CH_3$ are −0.72, −0.63 and −0.66 V *vs.* SCE, respectively.[72] These values are similar to the corresponding $E^{\ominus}_{RX/R^{\bullet}+X^-}$ values of RBr.[70] However, at an inert electrode, the overall reduction of RX is a $2e^-$ process, since heterogeneous reduction of $R^{\bullet}$ is more favored than that of RX, mostly because of the contribution of C–X bond dissociation energy to the ET barrier. Conversely, in ATRP conditions in solution, homogenous reduction of $R^{\bullet}$ is often less favored than reduction of RX for the following reasons: *i*) concentrations of both reducing agent (*e.g.* $[Cu^IL]^+$) and $R^{\bullet}$ are low; *ii*) reduction of RX by copper complexes is a catalytic process, whereas reduction of $R^{\bullet}$ is not.[18]

1.3.3. Atom transfer and electron transfer

Atom transfer in ATRP proceeds by formation of a bonded transition state (TS) during the reaction between $[Cu^IL]^+$ and RX. In the TS, the halogen atom acts as a bridge between R and Cu.

From a thermodynamic point of view, the reversible AT reaction between a Cu^I complex and an alkyl halide can be expressed as the sum of Eqs. 1.5, 1.15, and 1.17, as follows:

$$RX + e^- \rightleftharpoons R^{\bullet} + X^- \qquad E^{\ominus}_{RX/R^{\bullet}+X^-} \qquad (1.17)$$

$$[Cu^IL]^+ \rightleftharpoons [Cu^{II}L]^{2+} + e^- \qquad E^{\ominus}_{[Cu^{II}L]^{2+}/[Cu^IL]^+} \qquad (1.5)$$

$$[Cu^{II}L]^{2+} + X^- \rightleftharpoons [XCu^{II}L]^+ \qquad K^{II}_X \qquad (1.15)$$

$$[Cu^IL]^+ + RX \rightleftharpoons [XCu^{II}L]^+ + R^{\bullet} \qquad K_{ATRP} \qquad (1.23)$$

Therefore, the ATRP equilibrium constant, K_{ATRP}, can be expressed as:

$$\ln K_{ATRP} = \ln K^{II}_X + \frac{F}{RT}\left(E^{\ominus}_{RX/R^{\bullet}+X^-} - E^{\ominus}_{[Cu^{II}L]^{2+}/[Cu^IL]^+}\right) \qquad (1.24)$$

Eq. 1.24 can be used to estimate K_{ATRP} of very active systems that are difficult to analyze by conventional experimental techniques.[59] The reduction of RX by $[Cu^IL]^+$ is an endoergonic process, because $E^{\ominus}_{RX/R^{\bullet}+X^-}$ is more negative than $E^{\ominus}$ of copper complexes. Thus, the equilibrium is always shifted towards the reactants, ensuring a low radical concentration (*i.e.* $K_{ATRP} < 1$). Indeed, $\Delta G^{\ominus}_{ATRP}$ values as high as 59 kJ mol^{-1} in acetonitrile and ≤ 21.5 kJ mol^{-1} in pure water have been reported.[29]

Surprisingly, $\ln K_{ATRP}$ does not correlate with $E^{\ominus}_{[Cu^{II}L]^{2+}/[Cu^{I}L]^{+}}$ (red dots in **Figure 1.9**) as expected from Eq. 1.24, because K_X^{II} considerably varies with L.[58] Conversely, $\ln K_{ATRP}$ correlates to $E^{\ominus}_{[XCu^{II}L]^{+}/[XCu^{I}L]}$ (black squares in **Figure 1.9**) according to Eq. 1.25, obtained by rearranging Eq. 1.24 and taking into account Eq. 1.16.

$$\ln K_{ATRP} = \ln K_X^{I} + \frac{F}{RT}\left(E^{\ominus}_{RX/R^{\bullet}+X^{-}} - E^{\ominus}_{[XCu^{II}L]^{+}/[XCu^{I}L]}\right) \quad (1.25)$$

Since K_X^{I} is roughly constant in the same solvent for a series of copper complexes (with X = Br), linear correlations between $\ln K_{ATRP}$ and $E^{\ominus}_{[XCu^{II}L]^{+}/[XCu^{I}L]}$ were observed.[58]

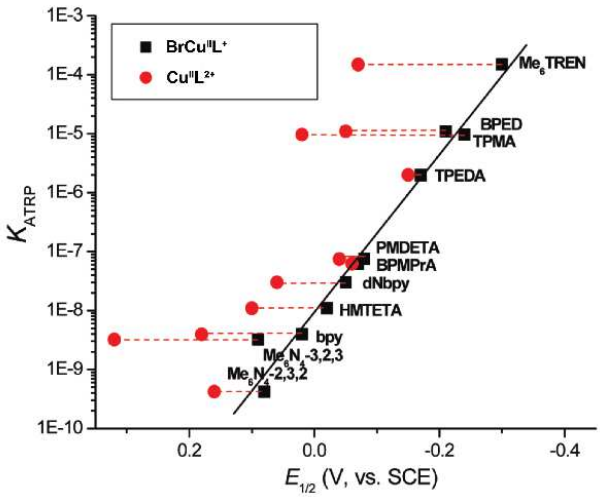

Figure 1.9. Comparison of $[Cu^{II}L]^{2+}$ and $[BrCu^{II}L]^{+}$ redox potentials correlated with K_{ATRP} values (measured with RX = EBiB) in CH_3CN, at T = 25 °C. L structures in **Figure 1.3** (reprinted with permission from Ref. [58]. Copyright 2009 American Chemical Society).

Eq. 1.25 was used to estimate the trend of K_{ATRP} for the reaction between $[Cu^{I}TPMA]^{+}$ and different benzyl halides in DMF (BnX, with X = F, Cl, Br, I).[61] K_{ATRP} reaches a maximum for X = Br. This maximum results from the interplay of two opposing factors: *i*) the carbon−halogen bond becomes stronger moving from C−I to C−F, hampering the atom transfer, *ii*) concurrently, the Cu^{II}–X interaction becomes more favorable (I < Br < Cl < F), facilitating halogen abstraction.

The electron transfer between $[Cu^{I}L]^{+}$ and dormant species can follow different pathways (**Scheme 1.7**): inner sphere electron transfer-concerted atom transfer (ISET-AT) or outer sphere electron transfer (OSET). The latter can be either concerted (OSET-C) or a two-step process with a radical anion intermediate (OSET-SW).[70]

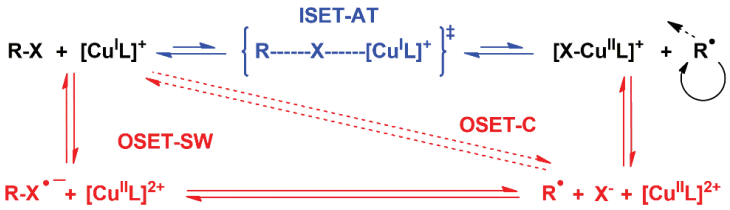

Scheme 1.7. Hypothetical OSET (concerted and stepwise) *vs.* ISET pathways in ATRP.

Experiments proved that reduction of common RX follows a concerted mechanism, thus the OSET-SW pathway should be discarded.[73, 74] Thermodynamic requirements for ISET-AT and OSET-C are essentially the same, therefore, their relative TS energies must be considered to discriminate between the two pathways. The rate constant of the hypothetical OSET-C reaction between bromoacetonitrile and $[Cu^{I}TPMA]^{+}$ complex was estimated using Marcus theory for the ET processes, as $k_{OSET} \approx 10^{-11}$ M^{-1} s^{-1}.[70] This value is more than 12 orders of magnitude smaller than the experimentally measured activation rate constant ($k_{act} \approx 82$ M^{-1} s^{-1} at 25 °C in CH_3CN), clearly indicating that the ISET mechanism is strongly preferred. This was confirmed by measuring activation rate constants of RX by outer sphere electron donors, $D^{\bullet-}$, and $[Cu^{I}L]^{+}$ complexes. In all cases, activation by $[Cu^{I}L]^{+}$ was 7-10 orders of magnitude faster than activation by $D^{\bullet-}$.[72] The energetic requirements of the ISET-AT and OSET pathways are shown in **Figure 1.10**.

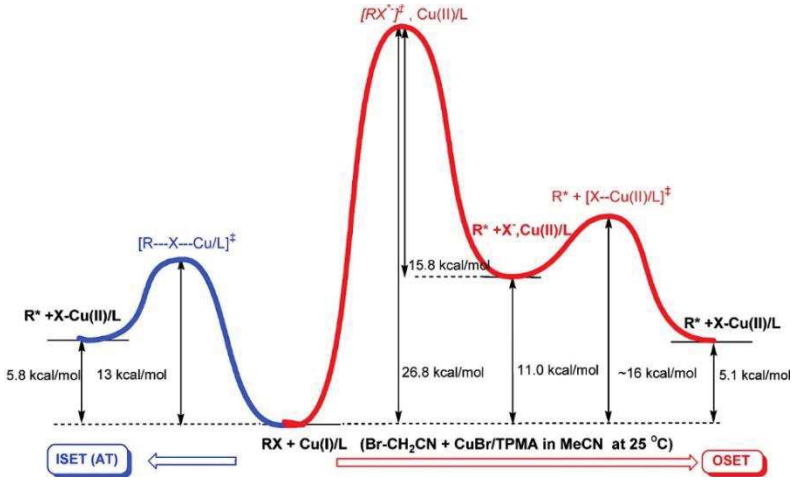

Figure 1.10. Comparison of free energies during ISET-AT and concerted OSET processes for the reaction of bromoacetonitrile with $[Cu^{I}TPMA]^{+}$ in CH_3CN, at $T = 25$ °C (reprinted with permission from Ref. [70]. Copyright 2008 American Chemical Society).

Finally, one-electron reduction of the propagating alkyl radical to carbanion is kinetically favored over reduction of the corresponding alkyl halide to $R^{\bullet}$ and X^{-}, thus, catalysts favoring ISET-AT over OSET are required in order to avoid chain-breaking side reactions.

1.4. *e*ATRP: traditional setup and principal advantages

The use of electrochemistry to trigger ATRP requires a dedicated setup. A traditional *e*ATRP experiment is performed in an electrochemical cell equipped with a three-electrode system, connected to a potentiostat/galvanostat.

A three-electrode cell is common in electrochemical measurements. With this setup, the current flows between the electrode of interest, which is called working electrode (WE), and a counter electrode (CE). The potential of the WE is monitored by coupling it with an electrode of known constant equilibrium potential, called reference electrode (RE), placed nearby the WE. Then, the potential difference between the WE and RE is generally measured by means of a potentiostat, through a high input impedance circuit, so that a negligible current flows through the RE. In this way, the potential of the RE remains constant and equal to its open-circuit value. The potentiostat enables also the electronic compensation of the resistive term due to the working solution between WE and RE, as well as any resistive contributions from the WE itself. The CE should not release by electrolysis substances that can cause interfering processes at the WE. For this reason, the CE is normally separated from the working electrode compartment by a sintered-glass disk or other type of separator.[75]

The described arrangement is adopted in *e*ATRP, by employing the following set of electrodes (**Figure 1.11**):[46]

i) A saturated calomel electrode (SCE) is used as RE in aqueous media, whereas a Ag/AgX/(X^- in a non-aqueous solvent) reference electrode is employed in organic solvents. Unlike SCE, the potential of the non-aqueous RE is not well defined. For this reason, a reference redox couple is generally added to the solution at the end of the experiment to allow the conversion of measured potentials to the SCE scale.

ii) The CE is made of Platinum and can be a small ring for voltammetric analysis, but a larger surface (*e.g.* a Pt foil or mesh) is needed during electrolysis experiments. Moreover, the CE is placed in a separated compartment to avoid side reactions like Cu^I oxidation and contamination of the working solution by oxidation products arising from the anodic process. As will be discussed in the following chapters, the Pt foil can be replaced with an Aluminum wire, directly immersed into the working solution. The wire acts as a sacrificial anode, which

is actually consumed during the polymerization, but does not produce oxidation products that interfere with the process. Since the electrochemical apparatus is simplified by using a sacrificial CE, this approach was called simplified *e*ATRP (*se*ATRP).[76]

iii) A Pt mesh with large surface area is used as the WE. The main role of the WE is to provide electrons for the reduction of Cu^{II} species, thus a vast surface area grants access to many Cu^{II} molecules eventually enhancing the polymerization rate.

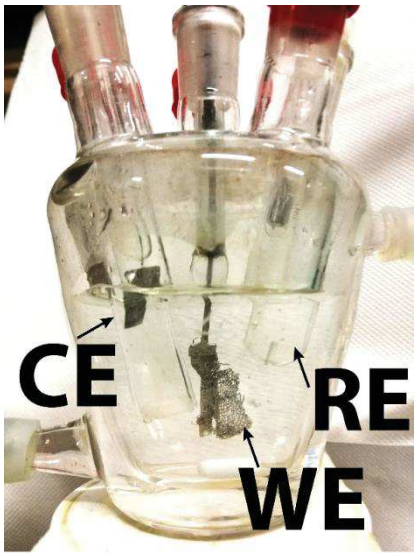

Figure 1.11. Electrochemical cell for *e*ATRP, equipped with a magnetic stirrer, and a traditional three-electrode system: Pt mesh as working electrode (WE), Pt foil as counter electrode (CE) in a separated compartment, and SCE as reference electrode (RE) in aqueous media.

Two different electrochemical stimuli can be applied to run an *e*ATRP, *i.e.* potential or current. When a constant potential is applied to the system, E_{app}, a potentiostatic approach is adopted.[46, 64] Conversely, one or more steps at a fixed current value, I_{app}, are used when working under galvanostatic conditions.[77]

Initially, *e*ATRPs were performed under potentiostatic conditions, accurately analyzing the effect of E_{app} value on polymerization outcomes.[46, 64] Indeed, E_{app} must be carefully selected considering the redox properties of the catalyst in the operating system. This requirement is one of the key strengths of this technique; in fact before the advent of *e*ATRP, very few electrochemical characterizations of ATRP components were reported. Thus, the knowledge of redox properties of ATRP catalysts was limited, despite being of primary importance to defining the polymerization mechanism. *e*ATRP allows, and even

demands a simultaneous evaluation of the electrochemical parameters affecting the catalyst and its interplay with the initiator, in the selected monomer/solvent combination and at the operative temperature. This evaluation can be performed also at the end of the polymerization, collecting important information on the stability of the catalyst.[60]

The applied potential establishes the ratio between Cu^{I} and Cu^{II} species, according to the Nernst equation (Eq. 1.26). Thus, if $E_{app} = E_{1/2}$ ($\approx E^{\circ}$), $C_{Cu^{I}} = C_{Cu^{II}}$. Instead, if $E_{app} = E_{1/2} - 0.06$ V, $C_{Cu^{I}} \approx 10 C_{Cu^{II}}$, thereby generating a higher amount of radicals, eventually enhancing the polymerization rate. Conversely, if $E_{app} = E_{1/2} + 0.06$ V, $C_{Cu^{II}} \approx 10 C_{Cu^{I}}$, thus very few species are activated at any cycle and this can be particularly important for very fast polymerizing systems. In brief, the selection of E_{app} determines the ratio $C_{Cu^{I}}/C_{Cu^{II}}$, which in turn affects the polymerization rate, according to Eq. 1.1.

$$E_{app} = E_{1/2} - \frac{RT}{F} \ln \frac{C_{Cu^{I}}}{C_{Cu^{II}}} \tag{1.26}$$

The value of E_{app} can span over a wider range of values, as reported in **Figure 1.12a** for the *e*ATRP of BA (56 vol%) in DMF, using $[BrCu^{II}TPMA]^{+}$ as catalyst and EBiB as initiator.[77] E_{app} was varied from $E_{1/2}$ to $E_{1/2} - 0.18$ V, and concurrently polymerization rate increased until $E_{app} = E_{1/2} - 0.125$ V, then it remained constant, because the system approached the mass transport limitation (**Figure 1.12b**). Despite the high rate (*i.e.* relatively high concentration of radicals), the control was preserved with this setup (**Figure 1.12c**). However, other monomers exhibited completely different behaviors[59, 64] as will be displayed in the following chapters.

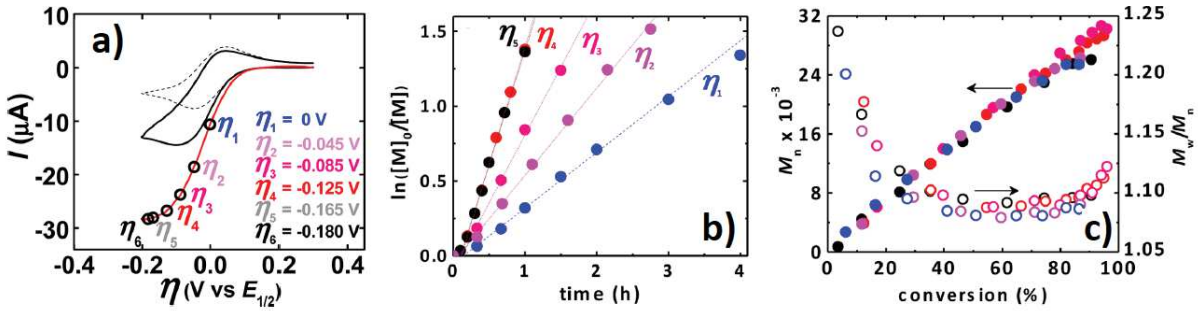

Figure 1.12. a) CVs of 1.17 mM $[Br\text{-}Cu^{II}Me_6TREN]^{+}$ in the absence (dashed line) and presence of 12.9 mM EBiB, in BA 56 vol% in DMF + 0.2 M *n*-Bu_4NClO_4, $\upsilon = 0.05$ V s^{-1}, $\eta_i = E_{app} - E_{1/2}$. b) Kinetic plots and c) MW and dispersity evolution *vs.* conversion, for *e*ATRP at various η_i (reprinted with permission from Ref. [77]. Copyright 2013, American Chemical Society).

Interestingly, the applied potential can be changed throughout the electrolysis, switching the polymerization from "on" to "off".[46, 60] If termination events are minimized, chain-end functionalities are retained, thus, once stopped, the process can be re-started by restoring the previous E_{app} value, and this cycle can be repeated many times. **Figure 1.13** reports one example of intermittent polymerization. R_p during "on" stages should equal the rate of continuous polymerization at the same E_{app}.

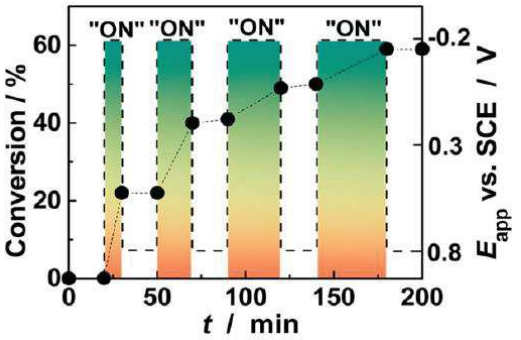

Figure 1.13. Monomer conversion *vs.* time, during ON/OFF switching in aqueous *e*ATRP of MAA, at pH = 0.9 and T = 25 °C (reprinted with permission from Ref. [60]. Copyright 2016, American Chemical Society).

*e*ATRP can be conducted also in galvanostatic mode, by selecting one or more appropriate I_{app} values. Generally, the chronoamperometry (current behavior *vs.* time) recorded during a potentiostatic experiment on the same system, is divided into two steps (**Figure 1.14a**).[77] The first one should correspond to a relatively high I_{app} value, as to reduce a huge portion of Cu^{II} to Cu^{I} species, then a lower I_{app} provides electrons to re-generate Cu^{I} from cumulated Cu^{II}. The charge (Q) passed during each step is obtained by integration of the area of I *vs.* t plot. Thus, I_{app} values are selected for each step and applied for the desired time, as to theoretically produce the same charge. In this way, galvanostatic *e*ATRPs were showed to reproduce the results obtained under potentiostatic control (**Figure 1.14b, c**).[77] The length of each step is not trivial. Indeed, if the potential at the WE is monitored during the polymerization, a progressive decrease in E values is observed in the last part of each step. The drop is due to: *i*) larger overpotentials required to provide the imposed current value; *ii*) the increased viscosity of the solution, *i.e.* higher resistivity. If I_{app} is maintained for longer times, a significant potential drop can be observed (**Figure 1.14d**), congruent with metallic copper deposition on the WE, thus irreversible loss of active catalyst.[77] Indeed, copper deposition arises from reduction of Cu^{I} species to Cu^{0}. Some studies showed that by increasing the number of current steps a better monitoring of the WE potential was achieved, and this can lead to an improved control over the process.[76]

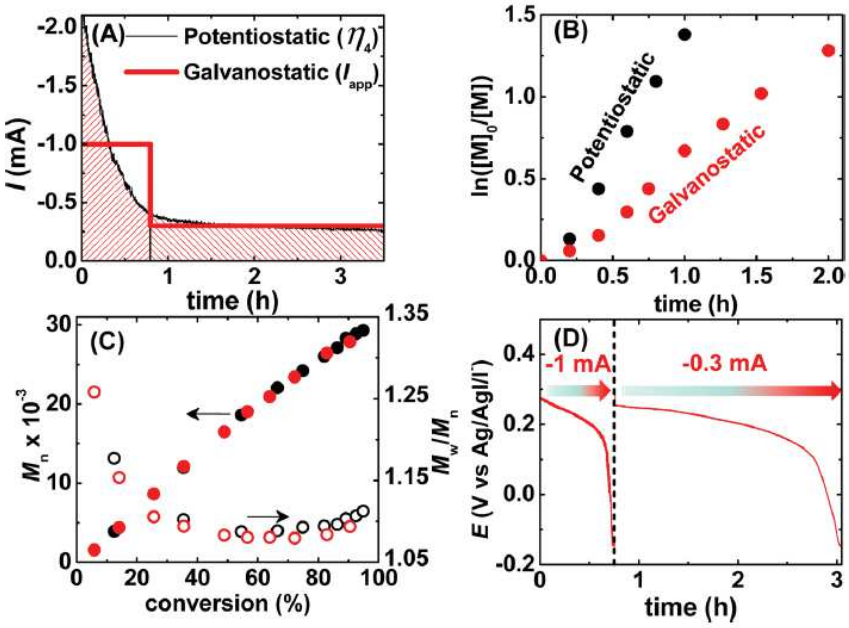

Figure 1.14. a) Chronoamperometry recorded during potentiostatic *e*ATRP and splitting into two constant, applied current, I_{app}, intervals. Comparison between potentiostatic and galvanostatic *e*ATRPs: b) kinetic plots and c) MW and dispersity evolution *vs.* conversion. d) Potential drop of the WE recorded during galvanostatic *e*ATRP (reprinted with permission from Ref. [77]. Copyright 2013, American Chemical Society).

The galvanostatic mode has some attractive features: firstly, only two electrodes are needed, WE and CE. Secondly, the expensive potentiostat can be replaced by a cheaper and more common current generator. Thus, the experimental setup is highly simplified and production cost is reduced, and this is advantageous both for academic and industrial purposes. However, it should be noted that *e*ATRPs reported in the literature always adopted a three-electrode setup also when operating at constant current, in order to gain a feedback on *E* variations happening at the WE.[77]

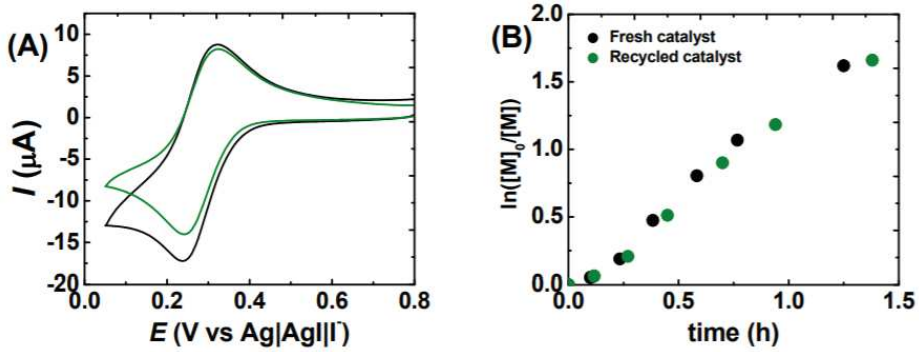

Figure 1.15. a) CVs of fresh (black) and recycled (green) [Br–Cu^{II}TPMA]$^+$, prior to the first and second polymerization, respectively, recorded at $\upsilon = 0.1$ V s^{-1}, and $T = 44$ °C. b) Kinetic plots of two sequential *e*ATRPs with fresh (black) and recycled (green) copper catalyst.

As mentioned earlier, large overpotentials can cause the deposition of metallic copper on the WE. This apparent drawback can be turned into an advantage, because copper can be recycled by electrodeposition on the WE.[77, 78] Actually, it was demonstrated that by applying a sufficiently negative potential at the end of the polymerization, Cu^0 was deposited on the cathode, without altering the final polymer features. Magenau et al. were able to recover 95% of the catalyst in 4 h of electrolysis, taking advantage of the positive shift in the reduction potential of Cu^I species to Cu^0 by increasing *T*. A successive *e*ATRP was performed by immersing the copper-coated WE into a new polymerization solution containing all polymerization components except Cu^{II}. Initially, no response was obtained when a CV was performed with the coated cathode. Then, Cu^0 was stripped from the electrode surface by applying a potential more positive than the oxidation potential of Cu^I to Cu^{II}. The stripping process was fast and the formation of $[X–Cu^{II}L]^+$ was confirmed by a color change in the solution and by CV (**Figure 1.15a**). The following *e*ATRP gave comparable results to the one conducted on the fresh catalyst (**Figure 1.15b**), proving that copper can be efficiently recycled by an electrodeposition-stripping cycle.[77]

Besides the benefit of catalyst recyclability, the possibility of copper electrodeposition is important for the purification of obtained polymers. Indeed, many applications require very low metal content in targeted polymers, thus purification procedures are generally performed after the synthesis. Simple column filtration may not be sufficient to obtain the desired purity, thus other methods were developed (ion exchange resins, dialysis, and heterogeneous systems that will be explained in **Chapter 8**). In this context, *e*ATRP offers a facile and relatively fast method that does not require any additional equipment.

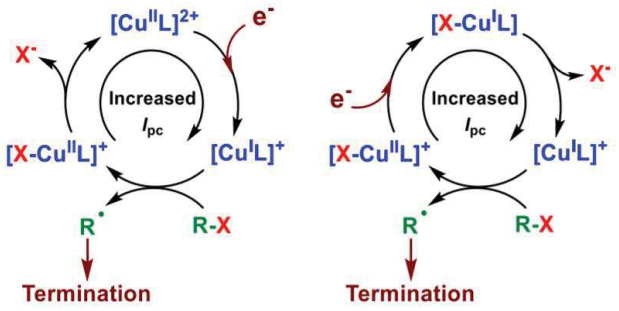

Scheme 1.8. Catalytic cycle involving radical termination and heterogenous ET to Cu^{II}.

Finally, *e*ATRP exclusively provides some useful insights into the polymerization mechanism. Fantin et al. used the total amount of charge passed, *Q*, during the synthesis to estimate the extent of radical-radical termination in *e*ATRP of methacrylic acid.[60] In fact, **Scheme 1.8** highlights that one Cu^{II} complex should be formed for each terminated radical.

Cu^{II} species must be reduced to Cu^{I} at the WE, to further activate C–Br bonds. Therefore, each termination event is accompanied by the successive one-electron reduction of a Cu^{II} complex, with the consumption of one elementary charge. It follows that, by recording the total consumed charge during an *e*ATRP experiment, the number of active chains lost by radical-radical termination can be evaluated using Eq. 1.27. This equation considers that copper is initially present as Cu^{II}, thus the total measured charge Q is the sum of two contributions: *i*) Q_0 for the initial reduction of Cu^{II} species to Cu^{I}, *ii*) Q_R for the reduction of Cu^{II} species accumulated due to radical-radical termination reactions.

$$Q = Q_0 + Q_R = -(n_0 + n_R)F \quad (1.27)$$

n_0 is the number of moles of Cu^{II} species initially converted to Cu^{I}, n_R is the number of moles of chains terminated by radical-radical reactions, and F is the Faraday constant. n_0 is estimated by using the Nernst equation (Eq. 1.26), neglecting the small overpotential related to the passage of current. Clearly n_0 and Q_0 depend on the value of E_{app}, *i.e.* on the amount of electro-generated Cu^{I}. The number of growing chains should equal the number of moles of initiator, n_{RX}, assuming 100% initiator efficiency. Therefore, the fraction of radical-radical terminated chains, n_R/n_{RX}, is immediately obtained, and it should be lower than 10% of total chains for a well-controlled process. Actually, this procedure does not take into account possible contributions to Q from reduction of oxygen or other impurities, or reduction of H^+ to hydrogen, thus the final percentage can be slightly overestimated.

In summary, *e*ATRP enables to precisely control the polymerization, analyze redox and stability features of system components, estimate the extent of termination, remove and recycle the catalyst and intermittently activate the process. All these properties make *e*ATRP a powerful technique that has been greatly used and improved, as will be described in **Chapter 2**.

References

1. Plamper, F. A. *Colloid and Polymer Science* **2014,** 292, 777-783.
2. Blanco, V.; Leigh, D. A.; Marcos, V. *Chemical Society Reviews* **2015,** 44, 5341-5370.
3. Teator, A. J.; Lastovickova, D. N.; Bielawski, C. W. *Chemical Reviews* **2016,** 116, 1969-1992.
4. Cosnier, S.; Karyakin, A., *Electropolymerization: concepts, materials and applications*. John Wiley & Sons: 2011.

5. Bardini, L.; Ceccato, M.; Hinge, M.; Pedersen, S. U.; Daasbjerg, K.; Marcaccio, M.; Paolucci, F. *Langmuir* **2013,** 29, 3791-3796.

6. Sadki, S.; Schottland, P.; Brodie, N.; Sabouraud, G. *Chemical Society Reviews* **2000,** 29, 283-293.

7. Ates, M. *Materials Science and Engineering: C* **2013,** 33, 1853-1859.

8. Otero, T. F.; Martinez, J. G.; Arias-Pardilla, J. *Electrochimica Acta* **2012,** 84, 112-128.

9. Yan, Q.; Feng, A.; Zhang, H.; Yin, Y.; Yuan, J. *Polymer Chemistry* **2013,** 4, 1216-1220.

10. Saraç, A. S.; Erbil, C.; Soydan, A. B. *Journal of Applied Polymer Science* **1992,** 44, 877-881.

11. Saraç, A. S.; Soydan, A. B.; Coka, V. *Journal of Applied Polymer Science* **1996,** 62, 111-116.

12. Lin, T. Y.; Chou, T. C. *Journal of The Electrochemical Society* **1997,** 144, 835-840.

13. Moad, G.; Solomon, D. H., *The Chemistry of Radical Polymerization*. Elsevier: 2006, 2nd edition.

14. Matyjaszewski, K. *Macromolecules* **2012,** 45, 4015-4039.

15. Braunecker, W. A.; Matyjaszewski, K. *Progress in Polymer Science* **2007,** 32, 93-146.

16. Tsarevsky, N. V.; Sumerlin, B. S. *Fundamentals of Controlled/Living Radical Polymerization*. Royal Society of Chemistry: 2013.

17. Konkolewicz, D.; Krys, P.; Góis, J. R.; Mendonça, P. V.; Zhong, M.; Wang, Y.; Gennaro, A.; Isse, A. A.; Fantin, M.; Matyjaszewski, K. *Macromolecules* **2014,** 47, 560-570.

18. Fantin, M.; Lorandi, F.; Gennaro, A.; Isse, A. A.; Matyjaszewski, K. *Synthesis* **2017,** 49, 3311-3322.

19. Chmielarz, P.; Fantin, M.; Park, S.; Isse, A. A.; Gennaro, A.; Magenau, A. J.; Sobkowiak, A.; Matyjaszewski, K. *Progress in Polymer Science* **2017**, 67, 47-68.

20. Lorandi, F.; Fantin, M.; Isse, A. A.; Gennaro, A. *Current Opinion in Electrochemistry*, *submitted*.

21. Nicolas, J.; Guillaneuf, Y.; Lefay, C.; Bertin, D.; Gigmes, D.; Charleux, B. *Progress in Polymer Science* **2013,** 38, 63-235.

22. Allan, L. E. N.; Perry, M. R.; Shaver, M. P. *Progress in Polymer Science* **2012,** 37, 127-156.

23. Rizzardo, E.; Moad, G.; Thang, S. H., Reversible Addition–Fragmentation Chain Transfer Polymerization. In *Encyclopedia of Polymer Science and Technology*, John Wiley & Sons, Inc.: 2002.

24. Hill, M. R.; Carmean, R. N.; Sumerlin, B. S. *Macromolecules* **2015,** 48, 5459-5469.

25. Matyjaszewski, K.; Gaynor, S.; Wang, J.-S. *Macromolecules* **1995,** 28, 2093-2095.

26. Boyer, C.; Lacroix-Desmazes, P.; Robin, J.-J.; Boutevin, B. *Macromolecules* **2006,** 39, 4044-4053.

27. Matyjaszewski, K.; Xia, J. *Chemical Reviews* **2001,** 101, 2921-2990.

28. Coessens, V.; Pintauer, T.; Matyjaszewski, K. *Progress in Polymer Science* **2001,** 26, 337-377.

29. Matyjaszewski, K.; Tsarevsky, N. V. *Journal of the American Chemical Society* **2014,** 136, 6513-6533.

30. Fischer, H. *Chemical Reviews* **2001,** 101, 3581-3610.

31. Xia, J.; Matyjaszewski, K. *Macromolecules* **1997,** 30, 7692-7696.

32. Krys, P.; Schroeder, H.; Buback, J.; Buback, M.; Matyjaszewski, K. *Macromolecules* **2016,** 49, 7793-7803.

33. Tang, W.; Matyjaszewski, K. *Macromolecular Theory and Simulations* **2008,** 17, 359-375.

34. Pintauer, T.; Matyjaszewski, K. *Chemical Society Reviews* **2008,** 37, 1087-1097.

35. Jakubowski, W.; Matyjaszewski, K. *Macromolecules* **2005,** 38, 4139-4146.

36. Matyjaszewski, K.; Jakubowski, W.; Min, K.; Tang, W.; Huang, J.; Braunecker, W. A.; Tsarevsky, N. V. *Proceedings of the National Academy of Sciences* **2006,** 103, 15309-15314.

37. Konkolewicz, D.; Wang, Y.; Zhong, M.; Krys, P.; Isse, A. A.; Gennaro, A.; Matyjaszewski, K. *Macromolecules* **2013,** 46, 8749-8772.

38. Anastasaki, A.; Nikolaou, V.; Nurumbetov, G.; Wilson, P.; Kempe, K.; Quinn, J. F.; Davis, T. P.; Whittaker, M. R.; Haddleton, D. M. *Chemical Reviews* **2015,** 116, 835-877.

39. Lorandi, F.; Fantin, M.; Isse, A. A.; Gennaro, A. *Polymer* **2015,** 72, 238-245.

40. D'Hooge, D. R.; Konkolewicz, D.; Reyniers, M. F.; Marin, G. B.; Matyjaszewski, K. *Macromolecular Theory and Simulations* **2012,** 21, 52-69.

41. Konkolewicz, D.; Magenau, A. J.; Averick, S. E.; Simakova, A.; He, H.; Matyjaszewski, K. *Macromolecules* **2012,** 45, 4461-4468.

42. Konkolewicz, D.; Schröder, K.; Buback, J.; Bernhard, S.; Matyjaszewski, K. *ACS Macro Letters* **2012,** 1, 1219-1223.

43. Tasdelen, M. A.; Ciftci, M.; Yagci, Y. *Macromolecular Chemistry and Physics* **2012,** 213, 1391-1396.

44. Mohapatra, H.; Kleiman, M.; Esser-Kahn, A. P. *Nature Chemistry* **2016**, 9, 135-139.

45. Wang, Z.; Pan, X.; Li, L.; Fantin, M.; Yan, J.; Wang, Z.; Wang, Z.; Xia, H.; Matyjaszewski, K. *Macromolecules* **2017**, DOI: 10.1021/acs.macromol.7b01597.

46. Magenau, A. J.; Strandwitz, N. C.; Gennaro, A.; Matyjaszewski, K. *Science* **2011,** 332, 81-84.

47. Krys, P.; Matyjaszewski, K. *European Polymer Journal* **2017**, 89, 482-523.

48. Wang, Y.; Soerensen, N.; Zhong, M.; Schroeder, H.; Buback, M.; Matyjaszewski, K. *Macromolecules* **2013,** 46, 683-691.

49. Kagawa, Y.; Zetterlund, P. B.; Minami, H.; Okubo, M. *Macromolecular Theory and Simulations* **2006,** 15, 608-613.

50. Silies, L.; Didzoleit, H.; Hess, C.; Stühn, B.; Andrieu-Brunsen, A. *Chemistry of Materials* **2015,** 27, 1971-1981.

51. Matyjaszewski, K.; Göbelt, B.; Paik, H.-j.; Horwitz, C. P. *Macromolecules* **2001,** 34, 430-440.

52. Tang, W.; Matyjaszewski, K. *Macromolecules* **2006,** 39, 4953-4959.

53. Kaur, A.; Ribelli, T. G.; Schröder, K.; Matyjaszewski, K.; Pintauer, T. *Inorganic Chemistry* **2015,** 54, 1474-1486.

54. Pintauer, T.; Matyjaszewski, K. *Coordination Chemistry Reviews* **2005,** 249, 1155-1184.

55. Bortolamei, N.; Isse, A. A.; Di Marco, V. B.; Gennaro, A.; Matyjaszewski, K. *Macromolecules* **2010,** 43, 9257-9267.

56. Matyjaszewski, K. *Macromolecules* **1998,** 31, 4710-4717.

57. Qiu, J.; Matyjaszewski, K.; Thouin, L.; Amatore, C. *Macromolecular Chemistry and Physics* **2000,** 201, 1625-1631.

58. Braunecker, W. A.; Tsarevsky, N. V.; Gennaro, A.; Matyjaszewski, K. *Macromolecules* **2009,** 42, 6348-6360.

59. Fantin, M.; Isse, A. A.; Gennaro, A.; Matyjaszewski, K. *Macromolecules* **2015,** 48, 6862-6875.

60. Fantin, M.; Isse, A. A.; Venzo, A.; Gennaro, A.; Matyjaszewski, K. *J. Am. Chem. Soc* **2016,** 138, 7216-7219.

61. Lanzalaco, S.; Fantin, M.; Scialdone, O.; Galia, A.; Isse, A. A.; Gennaro, A.; Matyjaszewski, K. *Macromolecules* **2016,** 50, 192-202.

62. Golub, G.; Lashaz, A.; Cohen, H.; Paoletti, P.; Bencini, A.; Valtancoli, B.; Meyerstein, D. *Inorganica Chimica Acta* **1997,** 255, 111-115.

63. Bell, C. A.; Bernhardt, P. V.; Monteiro, M. J. *Journal of the American Chemical Society* **2011,** 133, 11944-11947.

64. Bortolamei, N.; Isse, A. A.; Magenau, A. J.; Gennaro, A.; Matyjaszewski, K. *Angewandte Chemie International Edition* **2011,** 123, 11593-11596.

65. De Paoli, P.; Isse, A. A.; Bortolamei, N.; Gennaro, A. *Chemical Communications* **2011,** 47, 3580-3582.

66. Tang, W.; Matyjaszewski, K. *Macromolecules* **2007,** 40, 1858-1863.

67. Fantin, M.; Isse, A. A.; Matyjaszewski, K.; Gennaro, A. *Macromolecules* **2017,** 50, 2696-2705.

68. Isse, A. A.; Lin, C. Y.; Coote, M. L.; Gennaro, A. *The Journal of Physical Chemistry B* **2010,** 115, 678-684.

69. Saveant, J.-M. *Advances in Physical Organic Chemistry* **2000,** 35, 117-192.

70. Lin, C. Y.; Coote, M. L.; Gennaro, A.; Matyjaszewski, K. *Journal of the American Chemical Society* **2008,** 130, 12762-12774.

71. Lin, C. Y.; Marque, S. R.; Matyjaszewski, K.; Coote, M. L. *Macromolecules* **2011,** 44, 7568-7583.

72. Bortolamei, N.; Isse, A. A.; Gennaro, A. *Electrochimica Acta* **2010,** 55, 8312-8318.

73. Isse, A. A.; Gennaro, A.; Lin, C. Y.; Hodgson, J. L.; Coote, M. L.; Guliashvili, T. *Journal of the American Chemical Society* **2011,** 133, 6254-6264.

74. Isse, A. A.; Bortolamei, N.; De Paoli, P.; Gennaro, A. *Electrochimica Acta* **2013,** 110, 655-662.

75. Bard, A. J.; Faulkner, L. R., *Electrochemical methods: fundamentals and applications*. J. Wiley, New York: 2001, 2nd edition.

76. Park, S.; Chmielarz, P.; Gennaro, A.; Matyjaszewski, K. *Angewandte Chemie International Edition* **2015,** 127, 2418-2422.

77. Magenau, A. J.; Bortolamei, N.; Frick, E.; Park, S.; Gennaro, A.; Matyjaszewski, K. *Macromolecules* **2013,** 46, 4346-4353.

78. Jasinski, N.; Lauer, A.; Stals, P. J.; Behrens, S.; Essig, S.; Walther, A.; Goldmann, A. S.; Barner-Kowollik, C. *ACS Macro Letters* **2015,** 4, 298-301.

Chapter 2.

Present and future of the partnership between electrochemistry and ATRP

Table of contents

2.1. Electrochemistry and ATRP: state of the art

The electrochemical analysis of ATRP and its components started in 2000, when Qui et al. proposed the use of electrochemistry as a screening tool for the selection of suitable ATRP catalysts.[1] They firstly used cyclic voltammetry to measure the standard reduction potentials, $E^{\ominus}$, in CH_3CN of several ternary copper complexes, carrying Br or Cl atom. $E^{\ominus}$ values were correlated to the reducing power of catalysts, *i.e.* to their activity and performances in ATRP of methyl acrylate. Prior to this work, literature data were used to correlate electrochemical properties of few catalysts to their performances in ATRP.[2]

Since then, CV has become a well-established characterization tool to predict the reactivity of novel copper complexes from their E^{e}. Indeed, many efforts were devoted to the synthesis of new ligands to build highly reducing Cu complexes,[3] to be used as effective catalyst in ATRPs of less reactive monomers, such as vinyl acetate, or in heterogeneous environments.[4]

In 2008, thermodynamic and electrochemical properties of alkyl halides were collected and integrated with redox properties of radicals obtained by *ab initio* molecular orbital calculations. Then, Marcus theory for electron transfer processes allowed to estimate the rate constants of hypothetical OSET mechanisms, concluding that the ISET pathway is strongly preferred.[5]

A detailed work addressed the effect of polymerization solvent on K_{ATRP} and catalyst activity.[6] Moreover, the equilibrium constants of each step involved in the ATRP process were estimated or calculated, for some catalysts, in CH_3CN. In the same solvent, the speciation of Cu/Me_6TREN and Cu/PMDETA was completely defined for both Cu^{I} and Cu^{II} species in the presence of Cl^- or Br^-.[7] Adopted techniques were potentiometric and spectrophotometric titrations. The speciation of common catalysts was deeply analyzed also in water, taking into account the effect of pH on redox properties and stability of the complexes.[8] Halidophilicity constants were measured, thereby identifying for the first time the strong tendency of $[X–Cu^{II}L]^+$ to dissociate in X^- and $[Cu^{II}L]^{2+}$, in aqueous media.

Much more recently, the affinity for Cu complexes for fluorine and iodine was analyzed, proving that the trend is opposite to that of standard reduction potentials: $[F–Cu^{II}L]^+ < [Br–Cu^{II}L]^+ < [Cl–Cu^{II}L]^+ << [I–Cu^{II}L]^+$. This study helped rationalizing the behavior of K_{ATRP} for a certain catalyst/RX combination when the halogen atom was varied. The observed K_{ATRP} order was $K_{ATRP,F} << K_{ATRP,Cl} < K_{ATRP,I} < K_{ATRP,Br}$.[9]

Electrochemical reduction of alkyl halides was largely studied,[10] and ATRP benefited from such investigations. Importantly, the possibility of a radical-anion intermediate was excluded for the DET of organic halides used as initiators, thus affirming the inconsistency of proposed OSET mechanism. Instead, a good catalyst for controlled radical polymerizations should be able to react with RX or dormant species by an ISET-AT.[11]

The strong denial of OSET mechanism made electrochemical investigations a crucial tool in the debate on SARA ATRP *vs.* SET-LRP (single electron transfer living radical polymerization)[12] mechanisms, proposed to describe RDRP processes in the presence of

Cu^0.[13] Indeed, SET-LRP affirmed that Cu^0 is the main activator and the mechanism of RX activation follows an OSET pathway. The debate is still not completely resolved, although many works supported the SARA ATRP mechanism.[14, 15]

A very important achievement was reported in 2011 by De Paoli et al., who identified the real ATRP active catalytic species, which is $[Cu^IL]^+$.[16] Speciation studies were merged with the electrochemical study of the activation reaction of RX by Cu^I species, in the absence and presence of halide ions. The same work proposed the use of an electrochemical tool, a rotating disk electrode (RDE) to analyze the kinetics of ATRP activation step and determine the activation rate constant, k_{act}. By means of RDE, k_{act} values up to *ca.* 5×10^3 M^{-1} s^{-1} can be easily measured.[17]

Other electrochemical techniques were used to measure k_{act} values spanning over a very wide range, approximately from 10^{-3} to 10^8 M^{-1} s^{-1}, thus permitting kinetic studies of fast systems, such as very active catalysts or polar solvents.[18, 19] These methods include analysis of homogeneous redox catalysis by CV and digital simulations of CVs. In some cases, CV combined with digital simulations allows the simultaneous evaluation of k_{act} and K_{ATRP}. Moreover, these techniques were employed to analyze and quantify the halidophilicity of some Cu^I and Cu^{II} complexes. Bell et al. used digital simulations of CVs in the absence and presence of a radical scavenger to measure k_{act}[20] and then independently determine k_{deact} for the same system.[21]

Recently, the same authors identified the formation of organometallic intermediates, *i.e.* $[R\text{-}Cu^{II}/L]$, by observing the CVs of some catalyst/initiator systems.[22] This is a relevant side reaction known as Cu^I induced catalytic radical termination, CRT (more details in **Chapter 3**), whose mechanism is not well-defined yet.[23, 24] Again, by superimposing CVs and digital simulations, they were able to evaluate the kinetics of organometallic species generation.

Electrochemical monitoring of activation kinetics was also crucial in the SARA-ATRP *vs.* SET-LRP debate. Indeed, activation rates of RX by both Cu^I and Cu^0 were measured and the superior activity of Cu^I was affirmed, under typical conditions.[14] Particularly, during my master thesis work, I determined by RDE both k_{act} and the rate constant of Cu^I disproportionation, k_{disp}, in some selected systems.[25] Overall, k_{disp} was shown to be much smaller and even negligible if compared to k_{act} of catalysts and conditions traditionally used in RDRPs in the presence of Cu^0. As a consequence, we definitely affirmed that Cu^0

generated by Cu^{I} dispropotionation cannot be the principal activator of dormant species. Indeed, Cu^{I} is immediately involved in RX activation ($k_{act} >> k_{disp}$) and it does not have time to generate a significant amount of Cu^{0} by disproportionation.

Finally, electrochemistry plays an important role in the selection of suitable catalysts for metal-free ATRP. Indeed, this process employs photo-redox catalysts like phenothiazine derivatives and related compounds. Redox properties of selected catalysts and the corresponding radical cations were characterized by CV and the DET reaction was analyzed by using Marcus theory.[26] The electrochemistry of a wide range of possible catalysts was studied, including polycyclic aromatic hydrocarbons, phenothiazines, phenazines, phenoxazines, and carbazoles.[27]

Concluding this first part of the overview, electrochemistry clearly was and still is an essential tool in the investigation and understanding of ATRP, as well as related techniques. Electrochemical characterizations allow to predict catalyst activity, measure many parameters and deeply analyze the mechanism of ET and AT.

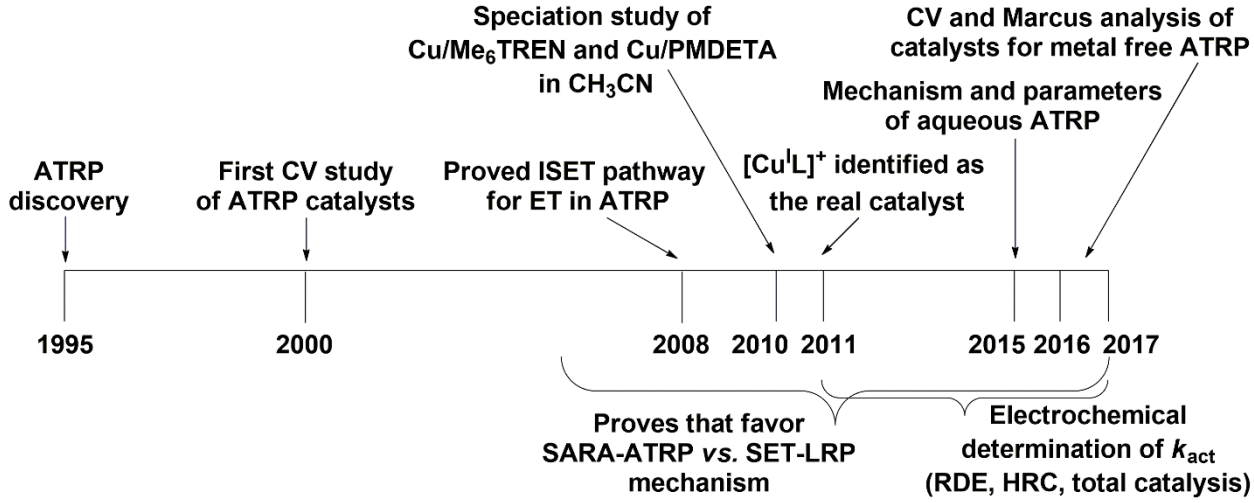

Figure 2.1. Timeline of fundamental contributions of electrochemistry to the study of ATRP mechanism.

2.2. Electrochemical mediation of ATRP: state of the art

The second part of this overview is entirely dedicated to *e*ATRP, which was born in 2011, when Magenau et al. reported the electrochemically triggered ATRP of methyl acrylate in CH_3CN.[28] A traditional three-electrode setup and potentiostatic conditions were used, and then adapted to aqueous media, where it is much more challenging to achieve a

well-controlled process.[29] Later, conditions for *e*ATRP of OEOMA in water were carefully optimized, taking advantage of the exhaustive electrochemical characterization of various ATRP catalysts in this solvent.[8]

Galvanostatic *e*ATRP was firstly proposed for the polymerization of BA in DMF.[30] In the same work, copper was electrodeposited on the WE surface at the end of the reaction and re-used in a subsequent polymerization. The same system was used to develop the simplified electrochemically mediated ATRP (*se*ATRP), by using an Aluminum wire as sacrificial anode in an undivided cell.[31]

Block copolymers were effectively produced by both *e*ATRP and *se*ATRP in organic solvents, proving the good retention of chain-end functionalities with these techniques.[32] More complex architectures, like polymeric stars, were obtained by starting from various macroinitiators with many C–X sites (*e.g.* β-cyclodextrins, and functionalized glucose molecules).[33, 34]

The redox couple Fe^{II}/Fe^{III} is sometimes used as ATRP catalyst, showing good versatility and offering the possibility to avoid the presence of organic ligands, under particular conditions. Iron-mediated *e*ATRP of MMA in CH_3CN was performed with Me_6TREN as ligand and without a polydentate amine.[35] The effect of catalyst loading, supporting electrolyte and applied potential was carefully analyzed.[36]

Aqueous *e*ATRP was then extended to other monomers: acrylamide,[37] and N-isopropyl acrylamide, starting from a PEO macroinitiator.[38] More important, *e*ATRP of methacrylic acid (MAA) in water at very low pH was recently reported.[39] For the first time a well-controlled ATRP of MAA was achieved, taking advantage of electrochemical characterizations to identify and solve polymerization issues. More details will be given in **Chapter 5**

Not only water-soluble monomers are polymerized in water, but also hydrophobic polymers can be grown in this eco-friendly solvent. Actually, polymerizations in dispersed media, *e.g.* miniemulsion and emulsion, are very attractive but not highly developed, mainly because of not-easy understanding and handling of heterogeneous processes. A double-catalyst system was set up by Fantin et al. to effectively run *e*ATRPs in miniemulsion.[40] Two catalysts are required to take the electrochemical stimulus from the electrode and transfer it inside the hydrophobic monomer droplets. This complex but fascinating environment will be deeply discussed in **Chapter 8**.

The working electrode was used simultaneously as electron source and site for the growth of polymer chains, in the so-called surface initiated *e*ATRP (SI-*e*ATRP).[41] Some polymer brushes were grown from an initiator-decorated gold electrode, tuning the final thickness by varying the amount of RX and the applied potential. Moreover, the system worked even if exposed to air, and the solution was successfully recycled after polymerization. This pioneering work was followed by a series of hybrid materials formed by different polymers grafted from various types of surface (*e.g.* carbon fibers, mesoporous carbon).[42, 43]

Another approach to SI-*e*ATRP used non-conductive surfaces, modified with ATRP initiating sites and placed close to the WE in a traditional three-electrode equipment. In this case, polymers grow on the functionalized non conductive platform, instead of on the working electrode. It was shown that by changing the orientation of this platform with respect to the WE, Cu diffused with different rates to different regions of the surface, thus gradient polymers were obtained.[44] This approach was adopted on polyethersulfone membranes, nanoparticles, silica layers.[45-47]

The possibility of growing controlled polymer chains on surfaces covered by an initiator layer is extremely attractive in the field of sensors and biosensors (*e.g.* enzyme covered surfaces, dendrimers or protein template),[48, 49] and "smart" coatings (*e.g.* surfaces with enhanced anti-fouling features).[50]

A very smart variant of SI-*e*ATRP concerned the use of a bipolar electrode to produce gradient and patterned polymer brushes. Indeed, by generating a potential gradient on a bipolar electrode, a concentration gradient of Cu^{I} was created, thus obtaining a gradient growth of polymer chains on the initiator-decorated surface, located close to the electrode. A 3D gradient, tunable in terms of thickness, modified area and steepness was realized with PNIPAM and MMA as monomer.[51]

*e*ATRP kinetics were modelled in order to explain some characteristic features observed, mainly regarding MWs and dispersity evolution.[52] Other techniques were used to study surface initiated processes: *in situ* AFM for example provided simultaneous investigations on growth mechanism and surface/polymer morphology.[53] Recently, electrochemistry was combined with surface plasmon resonance (EC-SPR), developing a new useful tool for *in situ* monitoring of the effect of E_{app} at an initiator-functionalized electrode, on polymerization kinetics.[54]

In summary, since 2011 *e*ATRP has established as a versatile, powerful low-ppm catalyst ATRP technique. The simplification of the experimental apparatus and the application of *e*ATRP in "green" media are paving the way to the scale-up of this process.

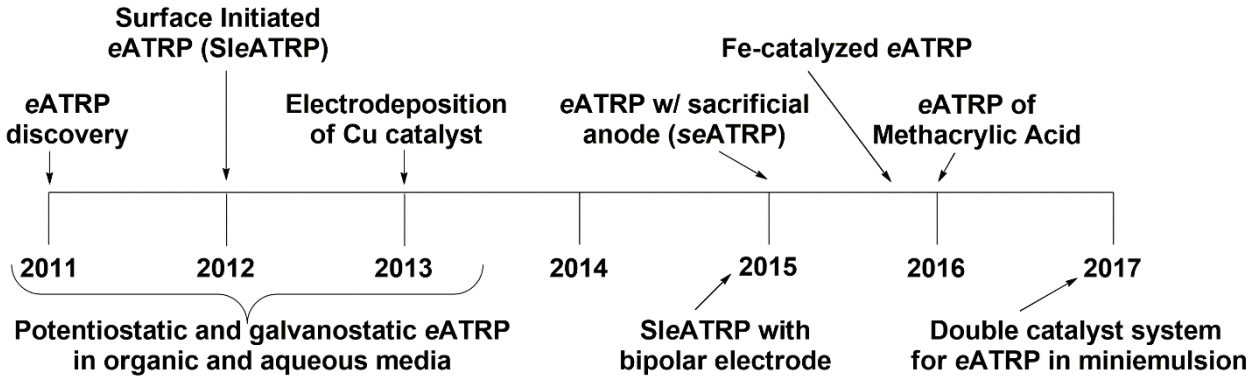

Figure 2.2. Timeline of major landmarks in *e*ATRP history.

2.3. Thesis outline

The presented overview affirms the importance of electrochemistry for atom transfer radical polymerization, and shows that the number of achievements is increasing. My Ph.D. work enters this scene, by dealing with both mechanistic analyses and development of new systems and setups.

Chapter 3 presents a new protocol for the determination of the thermodynamic equilibrium constant of ATRP, K_{ATRP}. A simple and highly reproducible technique was built, based on the use of a rotating disk electrode, which was already exploited for the determination of the activation rate constant, k_{act}. The method is discussed in details, also examining some correlations between thermodynamic and kinetic parameters.

The effective electrochemical triggering of ATRP is the main subject of all other chapters, touching a plethora of conditions. In **Chapter 4**, materials different from Platinum, which are less expensive and more easily functionalizable, are tested as cathodes for *e*ATRP in both organic and aqueous media. Performances comparable with a traditional Pt cathode are reported, together with good re-usability of electrodes and negligible release of metal ions in solution. A completely Pt-free setup is developed, by combining the new cathodes to a sacrificial Al anode, as in the simplified *e*ATRP setup. Moreover, a coupled copper cathode/anode setup is proposed, were copper is the only metal present, acting as electrodic material and catalyst.

Moving from the setup to the reactants, **Chapter 5** reports the first well-controlled polymerization of acrylic acid (AA), by an ATRP technique. In fact, the recent work performed on methacrylic acid is used to understand the issues affecting polymerization of AA, and optimize the conditions for *e*ATRP of this monomer.

Chapter 6 is focused on new polydentate amines, obtained by modifying the skeleton of TPMA, and their complexes with copper. Redox properties of these complexes are characterized, also in the presence of halide ions. The activity of one of the new catalysts is tested by measuring k_{act} and the performance in *e*ATRPs in both organic and aqueous media, also comparing the results with traditional Cu/TPMA catalyst.

Finally, the interest is devoted to polymerization media in the last two chapters. Indeed, **Chapter 7** shows the characterization of common ATRP catalysts and initiators in the Ionic Liquid (IL) [BMIm][OTf]. ILs are extremely attractive for their "green" features, and this work is a necessary precursor for the development of *e*ATRP in ILs.

Chapter 8 presents an extensive work that I mainly conducted during my stay as visiting student at Carnegie Mellon University (Pittsburgh, PA), in the group of Prof. Matyjaszewski. Miniemulsions are used as polymerization media, taking advantage of the good heat transfer and low viscosity achieved by polymerizing hydrophobic monomers in water. The recently developed dual-catalyst system is much simplified, by exploiting the interaction between hydrophilic Cu complexes with pyridinic ligands, and anionic surfactants. Electrochemical and spectroscopic characterizations are used to analyze the polymerization mechanism, and the approach is applied to *e*ATRP and ARGET-ATRP, building various homopolymers, block copolymers and more complex architectures. Moreover, the hydrophilicity of the catalyst made it suitable for emulsion systems, in combination with a hydrophilic initiator. Indeed, the first well-controlled ARGET-ATRP in a true *ab initio* emulsion system is developed by a careful optimization of setup conditions.

References

1. Qiu, J.; Matyjaszewski, K.; Thouin, L.; Amatore, C. *Macromolecular Chemistry and Physics* **2000,** 201, 1625-1631.

2. Matyjaszewski, K. *Macromolecules* **1998,** 31, 4710-4717.

3. Kaur, A.; Ribelli, T. G.; Schröder, K.; Matyjaszewski, K.; Pintauer, T. *Inorganic Chemistry* **2015,** 54, (4), 1474-1486.

4. Elsen, A. M.; Burdyńska, J.; Park, S.; Matyjaszewski, K. *Macromolecules* **2012,** 45, 7356-7363.

5. Lin, C. Y.; Coote, M. L.; Gennaro, A.; Matyjaszewski, K. *Journal of the American Chemical Society* **2008,** 130, 12762-12774.

6. Braunecker, W. A.; Tsarevsky, N. V.; Gennaro, A.; Matyjaszewski, K. *Macromolecules* **2009,** 42, 6348-6360.

7. Bortolamei, N.; Isse, A. A.; Di Marco, V. B.; Gennaro, A.; Matyjaszewski, K. *Macromolecules* **2010,** 43, 9257-9267.

8. Fantin, M.; Isse, A. A.; Gennaro, A.; Matyjaszewski, K. *Macromolecules* **2015,** 48, 6862-6875.

9. Lanzalaco, S.; Fantin, M.; Scialdone, O.; Galia, A.; Isse, A. A.; Gennaro, A.; Matyjaszewski, K. *Macromolecules* **2016,** 50, 192-202.

10. Isse, A. A.; Lin, C. Y.; Coote, M. L.; Gennaro, A. *The Journal of Physical Chemistry B* **2011,** 115, 678-684.

11. Isse, A. A.; Gennaro, A.; Lin, C. Y.; Hodgson, J. L.; Coote, M. L.; Guliashvili, T. *Journal of the American Chemical Society* **2011,** 133, 6254-6264.

12. Percec, V.; Guliashvili, T.; Ladislaw, J. S.; Wistrand, A.; Stjerndahl, A.; Sienkowska, M. J.; Monteiro, M. J.; Sahoo, S. *Journal of the American Chemical Society* **2006,** 128, 14156-14165.

13. Konkolewicz, D.; Wang, Y.; Zhong, M.; Krys, P.; Isse, A. A.; Gennaro, A.; Matyjaszewski, K. *Macromolecules* **2013,** 46, 8749-8772.

14. Konkolewicz, D.; Krys, P.; Góis, J. R.; Mendonça, P. V.; Zhong, M.; Wang, Y.; Gennaro, A.; Isse, A. A.; Fantin, M.; Matyjaszewski, K. *Macromolecules* **2014,** 47, 560-570.

15. Konkolewicz, D.; Wang, Y.; Krys, P.; Zhong, M.; Isse, A. A.; Gennaro, A.; Matyjaszewski, K. *Polymer Chemistry* **2014,** 5, 4396-4417.

16. De Paoli, P.; Isse, A. A.; Bortolamei, N.; Gennaro, A. *Chemical Communications* **2011**, 47, 3580-3582.

17. Isse, A. A.; Bortolamei, N.; De Paoli, P.; Gennaro, A. *Electrochimica Acta* **2013,** 110, 655-662.

18. Fantin, M.; Isse, A. A.; Bortolamei, N.; Matyjaszewski, K.; Gennaro, A. *Electrochimica Acta* **2016,** 222, 393-401.

19. Fantin, M.; Isse, A. A.; Matyjaszewski, K.; Gennaro, A. *Macromolecules* **2017,** 50, 2696-2705.

20. Bell, C. A.; Bernhardt, P. V.; Monteiro, M. J. *Journal of the American Chemical Society* **2011,** 133, 11944-11947.

21. Zerk, T. J.; Bernhardt, P. V. *Inorganic chemistry* **2014,** 53, 11351-11353.

22. Zerk, T. J.; Bernhardt, P. V. *Inorganic Chemistry* **2017,** 56, 5784-5792.

23. Ribelli, T. G.; Wahidur Rahaman, S.; Daran, J.-C.; Krys, P.; Matyjaszewski, K.; Poli, R. *Macromolecules* **2016,** 49, 7749-7757.

24. Schröder, K.; Konkolewicz, D.; Poli, R.; Matyjaszewski, K. *Organometallics* **2012,** 31, 7994-7999.

25. Lorandi, F.; Fantin, M.; Isse, A. A.; Gennaro, A. *Polymer* **2015,** 72, 238-245.

26. Pan, X.; Fang, C.; Fantin, M.; Malhotra, N.; So, W. Y.; Peteanu, L. A.; Isse, A. A.; Gennaro, A.; Liu, P.; Matyjaszewski, K. *Journal of the American Chemical Society* **2016,** 138, 2411-2425.

27. Theriot, J. C.; McCarthy, B. G.; Lim, C. H.; Miyake, G. M. *Macromolecular Rapid Communications* **2017**, *38*, 1700040.

28. Magenau, A. J.; Strandwitz, N. C.; Gennaro, A.; Matyjaszewski, K. *Science* **2011,** 332, 81-84.

29. Bortolamei, N.; Isse, A. A.; Magenau, A. J.; Gennaro, A.; Matyjaszewski, K. *Angewandte Chemie* **2011,** 123, 11593-11596.

30. Magenau, A. J.; Bortolamei, N.; Frick, E.; Park, S.; Gennaro, A.; Matyjaszewski, K. *Macromolecules* **2013,** 46, 4346-4353.

31. Park, S.; Chmielarz, P.; Gennaro, A.; Matyjaszewski, K. *Angewandte Chemie* **2015,** 127, 2418-2422.

32. Chmielarz, P.; Sobkowiak, A.; Matyjaszewski, K. *Polymer* **2015,** 77, 266-271.

33. Chmielarz, P. *Polymer* **2016,** 102, 192-198.

34. Chmielarz, P. *Chemical Papers* **2017,** 71, 161-170.

35. Guo, J.-K.; Zhou, Y.-N.; Luo, Z.-H. *Macromolecules* **2016,** 49, 4038-4046.

36. Guo, J. K.; Yin-Ning, Z.; Zheng-Hong, L. *AIChE Journal* **2017**, DOI: 10.1002/aic.15978.

37. Chmielarz, P.; Park, S.; Simakova, A.; Matyjaszewski, K. *Polymer* **2015,** 60, 302-307.

38. Chmielarz, P.; Krys, P.; Park, S.; Matyjaszewski, K. *Polymer* **2015,** 71, 143-147.

39. Fantin, M.; Isse, A. A.; Venzo, A.; Gennaro, A.; Matyjaszewski, K. *J. Am. Chem. Soc* **2016,** 138, 7216-7219.

40. Fantin, M.; Park, S.; Wang, Y.; Matyjaszewski, K. *Macromolecules* **2016,** 49, 8838-8847.

41. Li, B.; Yu, B.; Huck, W. T.; Zhou, F.; Liu, W. *Angewandte Chemie* **2012,** 124, 5182-5185.

42. Zhang, J.; Yi, X.-B.; Ju, W.; Fan, H.-L.; Wang, Q.-C.; Liu, B.-X.; Liu, S. *Electrochemistry Communications* **2017,** 74, 19-23.

43. Jin, G.-P.; Fu, Y.; Bao, X.-C.; Feng, X.-S.; Wang, Y.; Liu, W.-H. *Journal of Applied Electrochemistry* **2014,** 44, 621-629.

44. Li, B.; Yu, B.; Huck, W. T.; Liu, W.; Zhou, F. *Journal of the American Chemical Society* **2013,** 135, 1708-1710.

45. Chmielarz, P.; Krys, P.; Wang, Z.; Wang, Y.; Matyjaszewski, K. *Macromolecular Chemistry and Physics* **2017**, 218, 1700106.

46. Chmielarz, P.; Yan, J.; Krys, P.; Wang, Y.; Wang, Z.; Bockstaller, M. R.; Matyjaszewski, K. *Macromolecules* **2017**, 50, 4151-4159.

47. Wu, J.; Song, H.; Li, D.; Zhao, W.; Zhang, W.; Kang, L.; Ran, F.; Zhao, C. *Surfaces and Interfaces* **2017**, 8, 119-126.

48. Sun, Y.; Zhang, J.; Li, J.; Zhao, M.; Liu, Y. *RSC Advances* **2017,** 7, 28461-28468.

49. Hu, Q.; Wang, Q.; Sun, G.; Kong, J.; Zhang, X. *Analytical Chemistry* **2017,** 89, 9253-9259.

50. Hu, Y.; Yang, G.; Liang, B.; Fang, L.; Ma, G.; Zhu, Q.; Chen, S.; Ye, X. *Acta Biomaterialia* **2015,** 13, 142-149.

51. Shida, N.; Koizumi, Y.; Nishiyama, H.; Tomita, I.; Inagi, S. *Angewandte Chemie International Edition* **2015,** 54, 3922-3926.

52. Guo, J. K.; Zhou, Y. N.; Luo, Z. H. *AIChE Journal* **2015,** 61, 4347-4357.

53. Li, B.; Yu, B.; Zhou, F. *Macromolecular rapid communications* **2013,** 34, 246-250.

54. Chen, D.; Hu, W. *Analytical Chemistry* **2017,** 89, 4355-4358.

Chapter 3.

Electrochemical determination of K_{ATRP} *via* rotating disk electrode

Table of contents

3.1. Introduction and aim of the work

The incessant increase in ATRP development and application requires a continuous analysis of the intrinsic mechanism of the process, thereby determining the parameters affecting each step of polymerization.[1, 2] Indeed, fully understanding and quantifying all different contributions allows to make reliable predictions and overcome problems.

As explained in **Chapter 1** (**Section 1.3**) ATRP equilibrium between active and dormant species is governed by a thermodynamic constant, K_{ATRP}, which depends on the particular combination of catalyst, initiator, solvent, monomer and temperature.[3] K_{ATRP} can be expressed as the ratio between the kinetic activation rate constant and deactivation rate constant, k_{act}/k_{deact}. The equilibrium constant varies from 10^{-12}, for less active catalysts, to values in the order of 10^{-1} that were estimated for very active catalysts in aqueous media.[4-6] K_{ATRP} is traditionally determined by using UV-Visible spectroscopy or gas chromatography to follow the evolution of Cu^{II} species or RX concentration, respectively, during the reaction between ATRP catalysts and initiators.[3, 7-9] These techniques normally require relatively high amounts of Cu and RX to obtain reliable signals. K_{ATRP} is then derived from the rate of $[X–Cu^{II}L]^+$ formation or RX consumption, by using an equation originally proposed by Fisher and Fukuda,[10, 11] and later modified as to be valid for faster systems.[3]

No electrochemical tools are available to determine K_{ATRP}, despite the established use of electrochemical techniques to measure k_{act}, in the broad range of *ca.* 10^{-4}-10^{8} M^{-1} s^{-1}.[12-15] Among these, the use of a rotating disk electrode (RDE) sticks out as a very fast, simple and reproducible method, with the only drawback to be limited to slow or moderate activations ($k_{act} < 5 \times 10^3$ $M^{-1}s^{-1}$).[14] The procedure for k_{act} determination requires the use of a radical scavenger (generally the stable nitroxide radical TEMPO) to kinetically isolate the activation step, by rapidly trapping all generated radicals (**Scheme 3.1**).

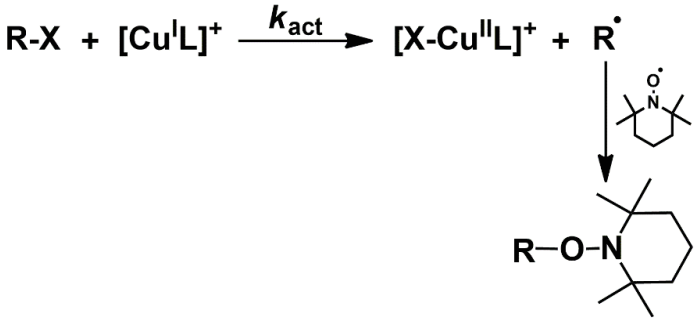

Scheme 3.1. Mechanism of ATRP in the presence of the radical scavenger TEMPO, for k_{act} determination.

An important aspect emerged from k_{act} determination: the presence of halogen ions makes impossible the determination of true k_{act} values; only "apparent" rate constants are measured, strongly dependent on C_{X^-}.[12, 13, 16] Actually, X^- affects the speciation of both Cu^I and Cu^{II}, mainly reducing the amount of active catalyst $[Cu^IL]^+$.[16, 17] It follows that k_{act} and K_{ATRP} values measured in the presence of X^- are underestimated.[3, 9] Instead, the constant

per se corresponds to the value extrapolated to $C_{X^-} = 0$, or measured in the absence of X^-. Traditionally, Cu^IBr or Cu^ICl were employed as a copper source for kinetic experiments, mainly because they are easily purchasable and used in polymerization setups. Thus, it is important to evaluate the overall experimental conditions when looking at literature data.

In contrast, halogen ions generated by reductive cleavage of RX, *i.e.* activation step, immediately bind to the simultaneously formed Cu^{II} species, because generally $K_X^{II} \gg K_X^I$ (K_X^{II} and K_X^I are the association constants of X^- to Cu^{II} and Cu^I, respectively).[17] Thus, generated X^- does not affect Cu^{II} speciation during the ATRP process.

In this work, the RDE is used to accurately and easily measure the equilibrium constant K_{ATRP}. Indeed, by using the same technique adopted for k_{act} measurement, but avoiding the addition of TEMPO, the interplay between activation, deactivation and radical termination (RT, **Scheme 3.2a**) can be monitored. Following the oxidation of Cu^I, K_{ATRP} was obtained from the current versus time behavior, by using Levich and Fischer's laws. The reproducibility of the measure, as well as its applicability to different ligands, initiators (**Figure 3.1**), solvents and temperatures, was evaluated.

a) ATRP mechanism with conventional radical termination (RT)

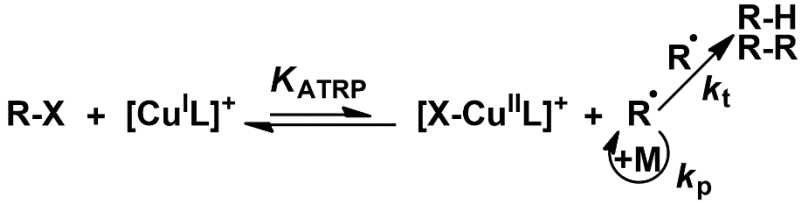

b) Cu^I induced catalytic radical termination (CRT)

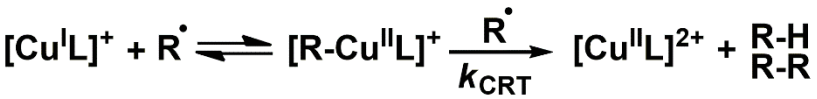

Scheme 3.2. Comparison between the mechanism of a) conventional radical termination (RT) and b) Cu^I induced catalytic radical termination (CRT).

Measured K_{ATRP} values are in agreement with general ATRP understanding and previous reports, if the effect of halogen ions was considered and an excess of RX was used. The latter allowed to avoid the contribution of undesired reactions, like Cu^I induced catalytic radical termination (CRT, **Scheme 3.2b**), which is known to affect ATRP systems,[18-20] as will be further discussed in **Section 3.1**. A method for the evaluation of the association constant between $[Cu^IL]^+$ and X^-, K_X^I, is also proposed, by exploiting the decrease in measured K_{ATRP}^{app} in the presence of different amounts of X^-.

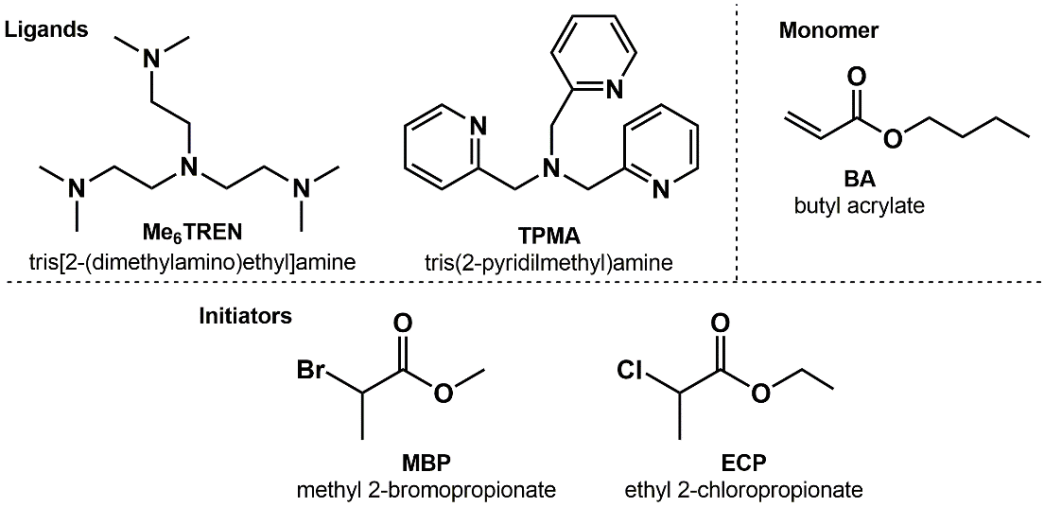

Figure 3.1. Structures of compounds relevant to the present Chapter.

3.2. Theoretical background

To determine k_{act}, the disappearance of Cu^I caused by its reaction with the alkyl halide initiator was followed by means of a rotating disk electrode (RDE).[12, 13, 16] The presence of a radical scavenger was required to kinetically isolate the activation step. Oxidation of Cu^I was monitored under diffusion control by selecting an appropriate constant potential, E_{app}. In the absence of RX, there was no homogeneous chemical reaction involving $[Cu^IL]^+$. Therefore, applying the selected E_{app} at the RDE produced a constant limiting current (I_L), as expected according to **Figure 3.2a**. Injecting RX into the cell caused a continuous decrease of I_L because the bulk concentration of $[Cu^IL]^+$ decreased. I_L depends on $C_{[Cu^IL]^+}$ according to the Levich equation (Eq. 3.1):

$$I_L = 0.62nFAD^{2/3}\nu^{-1/6}\omega^{1/2}C_{[Cu^IL]^+} \quad (3.1)$$

where D is the diffusion coefficient of $[Cu^IL]^+$, n is the number of exchanged electrons, F is the Faraday constant, ν is the kinematic viscosity, and ω is the angular velocity of the RDE. C_{Cu^I} was tracked according to Eq. 3.2:

$$\frac{I_L}{I_L^0} = \frac{C_{[Cu^IL]^+}}{C^0_{[Cu^IL]^+}} \quad (3.2)$$

where the superscript "0" indicates the initial values. Appropriate experimental conditions (second-order with $C^0_{Cu^IL^+} = C^0_{RX}$ or pseudo-first-order with $C^0_{RX} \gg C^0_{Cu^IL^+}$) were chosen,

depending on the activity of the catalyst/initiator couple. **Figure 3.2b,c** reports an example of k_{act} measurement *via* RDE, under second-order conditions.

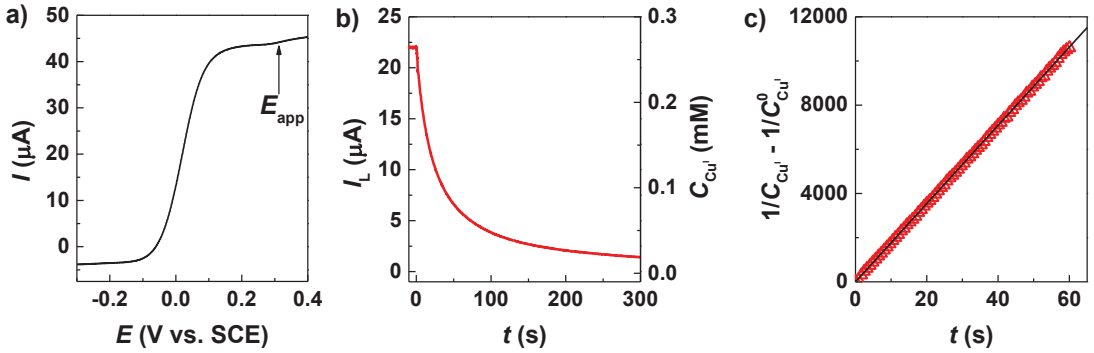

Figure 3.2. a) Linear sweep voltammetry of 5×10^{-3} M $[Cu^{I}TPMA]^{+}$ in CH_3CN + 0.1 M Et_4NBF_4, recorded on a GC RDE at $\upsilon = 0.005$ V s^{-1} and $\omega_{RDE} = 2500$ rpm. b) Decay of limiting current *vs.* time, and c) data elaboration for k_{act} determination in CH_3CN + 0.1 M Et_4NBF_4: $C^0_{MBP}/C^0_{[Cu^{I}TPMA]^+}/C^0_{TEMPO} = 1/1/20$, $C^0_{[Cu^{I}TPMA]^+} = 2.6 \times 10^{-4}$ M, $T = 25$ °C, $\omega_{RDE} = 4000$ rpm.

A similar approach can be used to determine K_{ATRP}. This parameter is generally derived from experimental data by using the equation proposed by Fischer and Fukuda for the persistent radical effect.[10, 11] Fischer's equation, reported below (Eq. 3.3) for the case of initial equimolar amounts of catalyst and initiator ($C^0_{[Cu^{I}L]^+} = C_0 = I_0 = C^0_{RX}$), defines a linear relationship between deactivator concentration ($Y = C_{[X-Cu^{II}L]^+}$) and $t^{1/3}$.

$$Y = (6k_t K^2_{ATRP} I_0^2 C_0^2)^{1/3} t^{1/3} \tag{3.3}$$

However, Tang et al. showed that this expression is not suitable for fast ATRP equilibria, where a curvature in Fischer's plot was observed.[3] As a consequence, a modification of the original equation was derived and tested both theoretically and experimentally. Eq. 3.4 and Eq. 3.5 were the resulting relations for $C_0 = I_0$ and $C_0 \neq I_0$, respectively.

$$F(Y) = \left(\frac{C_0^2}{3(C_0-Y)^3} - \frac{C_0}{(C_0-Y)^2} + \frac{1}{C_0-Y}\right) = 2k_t K^2_{ATRP} t + c' \tag{3.4}$$

$$F(Y) = \left(\frac{I_0 C_0}{(C_0-I_0)}\right)^2 \left(\frac{1}{C_0^2(I_0-Y)} + \frac{2}{C_0 I_0 (C_0-I_0)} \ln\left(\frac{I_0-Y}{C_0-Y}\right) + \frac{1}{I_0^2(C_0-Y)}\right) = 2k_t K^2_{ATRP} t + c'' \tag{3.5}$$

where c' and c'' are constants. Fischer's law is valid if activation, deactivation and radical termination are concurrently occurring in the analyzed system. Hence, for K_{ATRP} determination, the chronoamperometric oxidation of Cu^{I} is followed through the RDE, without adding any radical scavenger. Similarly to the case of k_{act} measurement, when the selected E_{app} was applied, a constant limiting current was observed and when after few

seconds RX was added, it started decreasing because of the reaction between $[Cu^{I}L]^{+}$ and RX (**Figure 3.3a**). The concentration of $[Cu^{I}L]^{+}$, $C_{[Cu^{I}L]^{+}}$, was obtained from Eq. 3.2. The concentration of the deactivator Cu^{II} at any instant was then calculated as $Y = C_{[X-Cu^{II}L]^{+}} = C^{0}_{[Cu^{I}L]^{+}} - C_{[Cu^{I}L]^{+}}$, and substituted into Eq. 3.4 or 3.5. After obtaining the slope of $F(Y)$ *vs. t* (**Figure 3.3b**) by linear regression analysis, K_{ATRP} was extracted from Eq. 3.6, where $k_t = 2.5 \times 10^9$ M^{-1} s^{-1}, which generally accounts for termination reactions of small molecules in many solvents.[21]

$$K_{ATRP} = \sqrt{\frac{slope}{2k_t}} \tag{3.6}$$

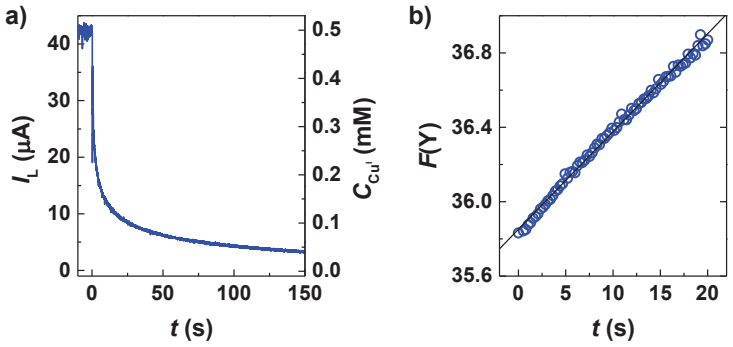

Figure 3.3. a) Decay of limiting current *vs.* time and b) data elaboration according to Eq. 3.5 for K_{ATRP} determination in CH_3CN + 0.1 M Et_4NBF_4: $C^{0}_{MBP}/C^{0}_{[Cu^{I}TPMA]^{+}} = 50$, $C^{0}_{[Cu^{I}TPMA]^{+}} = 5 \times 10^{-4}$ M, $T = 25$ °C, $\omega_{RDE} = 2500$ rpm.

3.3. Feasibility and reproducibility of K_{ATRP} measurement *via* RDE

K_{ATRP} was determined *via* RDE for a model Cu^{I}/RX system in CH_3CN; Me_6TREN was selected as one of the most active and common ATRP ligands,[22] whereas MBP was selected to mimic the chain-end of acrylates. This case is interesting because the secondary propionyl radical terminates by both RT and CRT.[20, 23]

In fact, the application of Fischer's equation requires that no processes other than activation, deactivation, and radical termination occur in the system. Thus, side reactions that may contribute either to Cu^{II} accumulation or radical termination should be avoided. However, it was recently showed that Cu^{I} is able to induce radical termination through a process called catalytic radical termination (CRT, **Scheme 3.b**).[18, 20] This reaction can be relevant, particularly for acrylates; therefore, it must be taken into account, especially for secondary radicals. CRT occurs in two steps: *i*) formation of an organometallic

intermediate, $[RCu^{II}L]^+$, and *ii*) termination by reaction of $[RCu^{II}L]^+$ with a second radical or by β-H elimination. The second step is considered rate determining.[20]

According to the kinetic expressions of conventional radical termination (RT) and CRT, the latter is minimized if $C_{RX} \gg C_{Cu^{II}}$ (Eq. 3.7). Indeed, a large excess of RX with respect to Cu^I was used in K_{ATRP} determination. Since in the analyzed system Cu^{II} is generated by the reaction between $[Cu^IL]^+$ and RX, $C^0_{RX}/C^0_{[Cu^IL]^+} = 50$ was typically used, thus $C_{RX}/C_{Cu^{II}} > 50$, which ensured $v_{RT} > 10v_{CRT}$. For example, $v_{RT} \approx 100v_{CRT}$ for the $[Cu^IMe_6TREN]^+$/MBP system, for which $K_{ATRP} = 1.1 \times 10^{-5}$ (**Table 3.3 entry 1**, in CH_3CN) and $k_{CRT} = 10^4$ M^{-1} s^{-1} (in CH_3CN /methyl acrylate). The rate of termination of two small radicals without an unusual steric effect is governed by diffusion, therefore $k_t = 2.5 \times 10^9$ M^{-1} s^{-1} was used.

$$\frac{v_{RT}}{v_{CRT}} = \frac{k_t C^2_{R^\bullet}}{k_{CRT} C_{Cu^I} C_{R^\bullet}} = \frac{k_t C_{R^\bullet}}{k_{CRT} C_{Cu^I}} = \frac{k_t C_{RX}}{k_{CRT} C_{Cu^{II}}} K_{ATRP} \quad (3.7)$$

K_{ATRP} was determined by chronoamperometry under steady state conditions to monitor the decay of $[Cu^IL]^+$, according to the procedure reported in **Section 3.2** (experimental details in **Appendix B2**). To ensure the validity and reproducibility of the method, K_{ATRP} determination was repeated multiple times under different conditions (**Table 3.1**). Changing $C^0_{RX}/C^0_{Cu^I}$ or changing the initial C_{Cu^I} had minor effects on measured K_{ATRP} values, confirming that $v_{RT} >> v_{CRT}$ under the selected conditions. Repeated K_{ATRP} determinations at $C^0_{RX}/C^0_{Cu^I} = 50$ also gave very reproducible results. Overall, K_{ATRP} for the model system $[Cu^IMe_6TREN]^+$/MBP was determined as $(1.05 \pm 0.07) \times 10^{-5}$.

Table 3.1. Reproducibility test on K_{ATRP} determination by RDE, for $[Cu^IMe_6TREN]^+$/MBP system in CH_3CN, $T = 25$ °C.[a]

$C^0_{Cu^I}$ (10^3 M)	$C^0_{MBP}/C^0_{Cu^I}$	K_{ATRP}
0.5	50	9.83×10^{-6}
0.5	50	1.02×10^{-5}
0.5	50	1.08×10^{-5}
0.2	50	1.18×10^{-5}
1	50	1.00×10^{-5}
0.5	35	1.03×10^{-5}
0.5	100	1.08×10^{-5}

[a] 0.1 M Et_4NBF_4 as supporting electrolyte. $C_L = 1.5C^0_{Cu^I}$.

3.4. Effect of Cu^I induced CRT on K_{ATRP} determination

To test the need of RX excess, K_{ATRP} was measured starting from equimolar amounts of MBP and Cu^I, $C^0_{MBP} = C^0_{Cu^I}$, varying $C^0_{Cu^I}$ from 2×10^{-4} to 10^{-3} M (**Table 3.2**). However, by using Fischer's law for $C_0 = I_0$ (Eq. 3.4), 3 different K_{ATRP} values that increased by decreasing $C^0_{Cu^I}$ were obtained.

Recently, Wang et al. proposed an equation (Eq. 3.8) to evaluate the rate constant of the reaction between Cu^I and RX, when CRT was the dominant cause of radical termination.[18] Eq. 3.8 can be used to calculate k_{CRT}, provided that K_{ATRP} is independently measured for the analyzed system. However, if applied to the recorded kinetics for $C^0_{MBP} = C^0_{Cu^I}$, 3 different k_{CRT} values were obtained, which increased with decreasing C_{Cu^I}, (**Table 3.2**).

In summary, both functions $F(Y)$ and $G(Y)$ seemed not suitable to define the system when $C^0_{MBP} = C^0_{Cu^I}$. Therefore, it can be concluded that CRT contribution to ATRP equilibrium cannot be neglected under the imposed conditions, even though CRT is not predominant over RT. Please notice that the precise mechanism of CRT is currently under investigation,[19, 23] thus more detailed analysis of the CRT process will be addressed in future works.

$$G(Y) = \int_0^Y \frac{Y}{(I_0 - Y)(C_0 - Y)} dY = k_{CRT} K_{ATRP} t \quad (3.8)$$

Table 3.2. Attempts of K_{ATRP} and k_{CRT} determination for $[Cu^IMe_6TREN]^+$/MBP, in CH_3CN, $T = 25$ °C.[a]

Entry	$C^0_{MBP}/C^0_{Cu^I}$	$C^0_{Cu^I}$ (M)	K_{ATRP} [b]	k_{CRT} (M^{-1} s^{-1}) [c]
1	50	-	1.1×10^{-5} [d]	-
2	1	2×10^{-4}	1.6×10^{-5}	1.8×10^5
3	1	5×10^{-4}	1.0×10^{-5}	8.2×10^4
4	1	1×10^{-3}	9.6×10^{-6}	4.9×10^4

[a] 0.1 M Et_4NBF_4 as supporting electrolyte. $C_L = 1.5C^0_{Cu^I}$. [b] Calculated from Eq. 3.4. [c] Calculated from Eq. 3.8. [d] Average of values measured in different conditions (see **Table 3.1**).

3.5. K_{ATRP} values for different systems

A large $C^0_{RX}/C^0_{Cu^I}$ ratio was necessary to suppress CRT, therefore, $C^0_{RX}/C^0_{Cu^I}$ = 50 was used to measure K_{ATRP} of all systems in the present work. Cu^I/Me_6TREN and Cu^I/TPMA were investigated in CH_3CN, DMF, and 50% (v/v) mixtures with *n*-butyl acrylate (BA) (**Table 3.3**). In the presence of BA, monomer conversion was small (**Figure 3.4**) and thus only short oligomers were formed (DP < 20). Due to the presence of relatively short chains, the same value of k_t, 2.5×10^9 M^{-1} s^{-1}, typical for small molecules, was used for all systems.

K_{ATRP} was higher for $[Cu^IMe_6TREN]^+$ than for $[Cu^ITPMA]^+$, accounting for the higher activity of Cu complex with Me_6TREN.[22] K_{ATRP} for $[Cu^IMe_6TREN]^+$ reaction with ethyl 2-chloropropionate (ECP) was nearly one order of magnitude lower than K_{ATRP} of the $[Cu^IMe_6TREN]^+$/MBP system, in agreement with the lower reactivity of RCl than RBr of the same structure.[24] With both complexes, K_{ATRP} diminished by about one order of magnitude when switching from pure DMF to pure CH_3CN. Indeed, CH_3CN tends to occupy the free coordination site of $[Cu^IL]^+$, strongly stabilizing the active catalyst, thus decreasing its activity.[17] The presence of 50% (v/v) monomer diminished K_{ATRP} by a factor of ~10 in DMF and a factor of ~2 in CH_3CN. A similar trend was previously observed.[9]

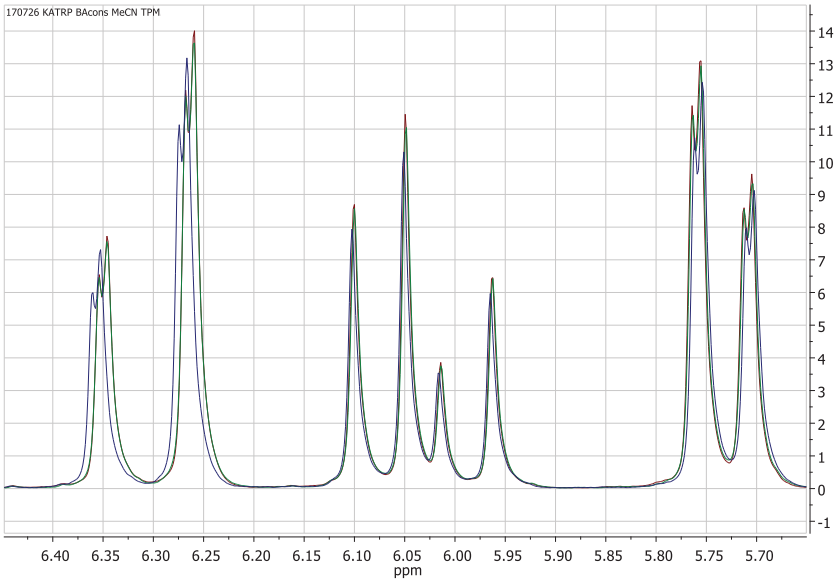

Figure 3.4. ^{1}H NMR signals of BA at t = 0 s (–), t = 20 s (–), t = 100 s (–),corresponding to a monomer conversion of 0, 1.7, and 4.7 % ($M_{n,th(PBA)}$ = 0, 943, 2285), respectively. Recorded spectra were normalized on the signal of CH_2 groups of $[(C_2H_5)_4N]^+$ (supporting electrolyte cation). General conditions: CH_3CN/BA 1/1 (v/v), $C^0_{[Cu^ITPMA]^+}$ = 0.5 mM, $C^0_{MBP}/C^0_{[Cu^ITPMA]^+} = 50$ (**Table 3.3, entry 5**).

Table 3.3. Determination of K_{ATRP} by RDE in various environment, T = 25 °C.[a]

Entry	L	Solvent	Monomer[b]	RX	$E^{\ominus}_{[BrCu^{II}L]^+/[BrCu^{I}L]}$ (V *vs.* SCE)	K_{ATRP}	k_{act} (M^{-1} s^{-1})[c]	k_{deact} (M^{-1} s^{-1})[d]
1	Me_6TREN	CH_3CN	-	MBP	-0.330	1.1×10^{-5}	2.1×10^{3} [e]	1.9×10^{8}
2	Me_6TREN	CH_3CN	-	ECP	-0.431[f]	2.3×10^{-6}	1.7×10^{1} [e]	7.4×10^{6}
3	TPMA	CH_3CN	-	MBP	-0.242	3.5×10^{-6}	2.2×10^{2} [e]	6.3×10^{7}
4	Me_6TREN	CH_3CN	BA	MBP	-0.252	7.2×10^{-6}	1.2×10^{3}	1.7×10^{8}
5	TPMA	CH_3CN	BA	MBP	-0.203	1.8×10^{-6}	4.4×10^{1} [g]	2.8×10^{7}
6[h]	Me_6TREN	DMF	-	MBP	-0.323	1.3×10^{-4}	$> 10^{4}$ [i]	$> 10^{8}$
7[h]	TPMA	DMF	-	MBP	-0.236	1.6×10^{-5}	7.1×10^{3}	4.4×10^{8}
8	Me_6TREN	DMF	BA	MBP	-0.334	1.9×10^{-5}	7.7×10^{3}	4.1×10^{8}
9	TPMA	DMF	BA	MBP	-0.229	1.7×10^{-6}	7.8×10^{1} [g]	4.9×10^{7}

[a] 0.1 M Et_4NBF_4 as supporting electrolyte. $C^0_{Cu^I}$ = 0.5 mM, $C_L = 1.5C^0_{Cu^I}$, $C^0_{RX} = 50C^0_{Cu^I}$. ω_{RDE} = 2500 rpm. [b] 50% (v/v), if present. [c] Unless otherwise specified, measured *via* RDE in the presence of TEMPO. [d] Calculated as $k_{deact} = k_{act}/K_{ATRP}$. [e] Taken from Ref. [14]. [f] The redox couple was $[ClCu^{II}L]^+/ClCu^{I}L$. [g] Measured in this work in a one-pot experiment together with K_{ATRP} determination. [h] $C^0_{Cu^I}$ = 0.2 mM. [i] The kinetics were too fast to be followed for a longer period than the mixing time.

For slower systems, K_{ATRP} and k_{act} were determined in a single experiment. First, RX was added to a $[Cu^{I}L]^+$ solution, and K_{ATRP} was measured as previously described. Then, a concentrated solution of TEMPO in CH_3CN or DMF was added and k_{act} was measured (**Figure 3.5**). By using a sufficient excess of RX over $[Cu^{I}L]^+$, so that C_{RX} does not change significantly during the experiment, k_{act} values were obtained by kinetic analysis under pseudo-first order conditions (**Table 3.3, entries 5 and 9**). Both values of activation rate constant were also measured independently under second-order conditions with $C^0_{MBP} = C^0_{Cu^I}$, and in the presence of TEMPO from the beginning of the experiment (k_{act} = 49 M^{-1} s^{-1} and k_{act} = 79 M^{-1} s^{-1} for **entries 5 and 9**, respectively obtained). k_{act} values determined with the two different methods perfectly matched.

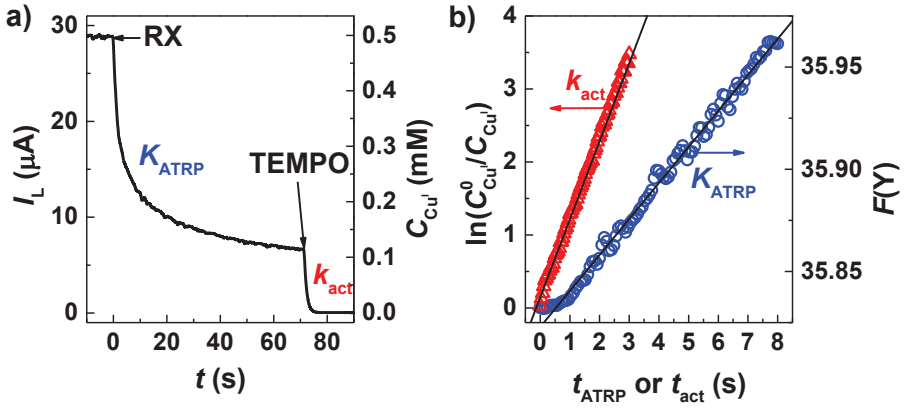

Figure 3.5. a) Decay of limiting current *vs.* time, and b) data elaboration for k_{act} determination (red) or K_{ATRP} determination according to modified Fischer's law, in CH_3CN/BA (1/1 v/v) + 0.1 M Et_4NBF_4: $C^0_{MBP}/C^0_{[Cu^ITPMA]^+} = 50$, $C^0_{Cu^ITPMA^+} = 5 \times 10^{-4}$ M, T = 25 °C, ω_{RDE} = 2500 rpm. $C^0_{TEMPO} = 50C^0_{[Cu^ITPMA]^+}$ was injected *ca.* 70 s after MBP injection.

K_{ATRP} values were correlated with k_{act} and k_{deact} values. k_{act} values were either taken from the literature or measured *via* RDE in the presence of TEMPO. k_{deact} was obtained from the relation $K_{ATRP} = k_{act}/k_{deact}$. **Figure 3.6** shows that k_{act} and k_{deact} in a logarithmic plot correlate linearly with K_{ATRP}, for a fixed RX. This correlation is stronger than the ones previously obtained.[25] It is worth noting that both k_{act} and k_{deact} increase with increasing K_{ATRP}, indicating that the ATRP equilibrium becomes faster at higher K_{ATRP}. k_{act} contributes to the overall value of K_{ATRP} much stronger than $k_{deact.}$.

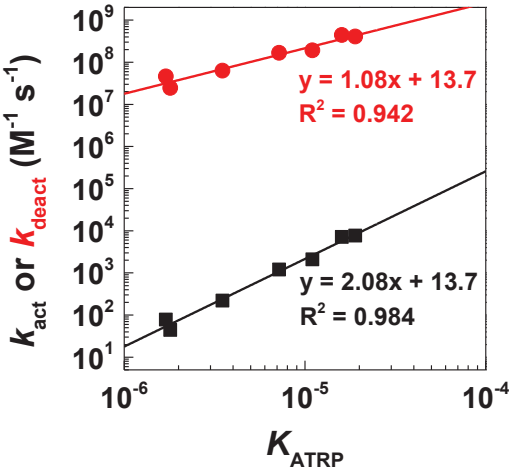

Figure 3.6. Correlation of k_{act} and k_{deact} with K_{ATRP} for various $[Cu^IL]^+$/MBP systems (see data in **Table 3.3**) at 25 °C.

Stronger activators are generally also faster deactivators, exhibiting a trend that was recently observed for ATRP catalysts in water.[6] This trend, however, differs from what was previously observed,[25] which demonstrates that accurate determination of K_{ATRP} is necessary to obtain information about ATRP mechanism.

3.6. Comparison with literature data

A brief comment is needed about the comparison between data collected in the present work and literature values. K_{ATRP} data in **Table 3.3** are generally higher than previously reported values, which were however measured in the presence of X^-, *i.e.* in the presence of a fraction of inactive Cu^I species. Tang et al. measured $K_{ATRP} = 3.3 \times 10^{-7}$ for the Cu^IBr/TPMA/MBP system in CH_3CN.[3] This value is roughly one order of magnitude lower than the value in **Table 3.3**, **entry 3,** $K_{ATRP} = 3.5 \times 10^{-6}$, measured for Cu^I/TPMA/MBP. This discrepancy indicates that only a small fraction of Cu^I was present as active $[Cu^IL]^+$ complex when Cu^IBr was used as a source of copper.[3, 16]

This was further confirmed by measuring K_{ATRP} by means of RDE, under the same conditions used by Wang et al. ($C^0_{[Cu^ITPMA]^+} = 5 \times 10^{-3}$M, $C^0_{MBP} = 20C^0_{[Cu^ITPMA]^+}$, $C^0_{Br^-} = 5 \times 10^{-3}$M). The plot of $F(Y)$ vs. t showed a deviation from linearity in the first 10 s (**Figure 3.7**). Indeed, the data could be fit to two linear segments, one for $t \leq 3$ s and the other for $t > 10$ s. $K_{ATRP} = 5.6\times10^{-7}$ was determined if the linear segment at $t > 10$ s (up to 700 s) was used. This value is quite similar to the one reported by Tang et al. When instead data of the first segment were analyzed, $K_{ATRP} = 1.3 \times 10^{-6}$ was obtained. Furthermore, by using $C^0_{Cu^I} = 5 \times 10^{-3}$ M, $C^0_{MBP}/C^0_{Cu^I} = 50$, in the absence of Br^- ions, and considering only the first 10 s, $K_{ATRP} = 3.6 \times 10^{-6}$ was obtained, which is in perfect agreement with the value reported in **Table 3.3**.

Two aspects should be highlighted: *i*) the importance of avoiding the presence of halide ions, *ii*) the difference between considering the first part of the plot or longer periods. Indeed, side reactions like CRT become much more important at longer times. Considering the ratio between RT and CRT rates (Eq. 3.7), it is possible to see that $\upsilon_{RT}/\upsilon_{CRT}$ decreases during the reaction as $C_{Cu^{II}}$ increases. However, if k_{CRT} is very low, the ratio remains high enough to favor RT up to long times. Otherwise, $\upsilon_{RT} \gg \upsilon_{CRT}$ only in the initial stages of

the reaction, CRT contribution becoming more relevant at longer times, meaning that Fischer's law is no more valid. This observation is more significant for lower K_{ATRP} values.

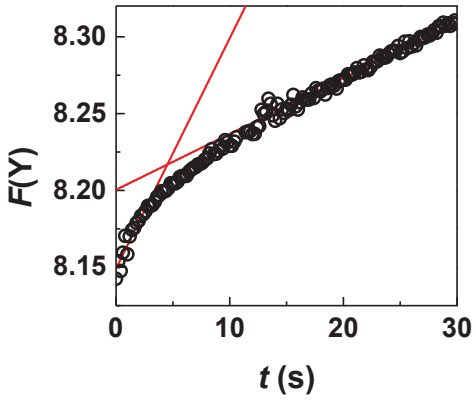

Figure 3.7. Data elaboration according to the modified Fischer's equation for K_{ATRP} determination in CH_3CN + 0.1 M Et_4NBF_4, $\boldsymbol{C^0_{Cu^IBr}}$ = 5 × 10^{-3} M, C_{TPMA} = 1.5$\boldsymbol{C^0_{Cu^IBr}}$, $\boldsymbol{C^0_{MBP}/C^0_{Cu^IBr} = 20}$, T = 25 °C, ω_{RDE} = 2500 rpm.

Finally, by using K^I_{Br} = 396 M^{-1} measured for this system as described in **Section 3.7**, one can calculate that if K_{ATRP} = 3.5 × 10^{-6}, K^{app}_{ATRP} = 1.6 × 10^{-6} for $C^0_{Cu^I}$= $C^0_{Br^-}$ = 5 × 10^{-3} M, which perfectly matches the value measured under these conditions by considering the first 3 s of the plot.

3.7. Determination of the halidophilicity constant for Cu^I from $\boldsymbol{K^{app}_{ATRP}}$ measurements

As previously highlighted, the rigorous determination of thermodynamic and kinetic constants for ATRP requires to work in the absence of halide ions, which affects the speciation of Cu^I species, particularly diminishing the amount of active catalyst $[Cu^IL]^+$.[16] Indeed, slower activation kinetics were observed in the presence of Br^-, compared to the case of $C^0_{Br^-}$ = 0.[12, 13]

Figure 3.8a shows variations of $C_{[Cu^IL]^+}$ during reaction of $[Cu^IMe_6TREN]^+$ with MBP at different $C^0_{Br^-}/C^0_{Cu^I}$ ratios. Analysis of $C_{Cu^{II}}$ by Eq. 3.5 gave straight lines from which apparent equilibrium constants, K^{app}_{ATRP}, were calculated. K^{app}_{ATRP} is defined by Eq. 3.9, and the complete derivation is reported in **Appendix B3**. In accordance with K^{app}_{ATRP} definition, measured values were always smaller than K_{ATRP} (*i.e.* the value calculated with

$C^0_{\mathrm{Br}^-} = 0$), and decreased with increasing $C^0_{\mathrm{Br}^-}$. The values of $K^{\mathrm{app}}_{\mathrm{ATRP}}/K_{\mathrm{ATRP}}$ at different $C^0_{\mathrm{Br}^-}$ are reported in **Figure 3.8b** (orange triangles).

$$K^{\mathrm{app}}_{\mathrm{ATRP}} = \frac{C_{[\mathrm{BrCu^{II}L}]^+} C_{\mathrm{R}^\bullet}}{\left(C^0_{\mathrm{Cu^I}} - C_{[\mathrm{BrCu^{II}L}]^+}\right) C_{\mathrm{RX}}} \tag{3.9}$$

The smaller reactivity of Cu^I in the presence of Br^- was due to the formation of inactive complexes, mainly $BrCu^IMe_6TREN$, but also $[Cu^IBr_2]^-$ and others. The complete speciation of 10^{-3} M Cu^I/Me_6TREN and Cu^I/PMDETA in CH_3CN was previously reported in the presence of both Br^- and Cl^-.[17] **Figure 3.8** presents the speciation of 5×10^{-4} M Cu^I/Me_6TREN in the presence of increasing amounts of Br^- and Cl^-, obtained by using literature data for association constants. In the case of bromides, $[Cu^IL]^+$ and $BrCu^IL$ are the predominant species present in solution under the experimental conditions, *i.e.* different $C^0_{\mathrm{Br}^-}$, used in this work. The contribution of a third species, $[Cu^IBr_2]^-$ is significant only for approximately $C^0_{\mathrm{Br}^-} > 5 \times 10^{-3}$ M.

The fraction of Cu^I present as the active $[Cu^IMe_6TREN]^+$ was calculated considering the reaction in Eq. 3.10 (detailed calculation in **Appendix B3**), *i.e.* the association of Br^- to $[Cu^IMe_6TREN]^+$ (bromidophilicity), with equilibrium constant $K^{\mathrm{I}}_{\mathrm{Br}} = 186\ \mathrm{M}^{-1}$ in CH_3CN.[17]

$$[\mathrm{Cu^IL}]^+ + \mathrm{Br}^- \rightleftharpoons \mathrm{BrCu^IL} \qquad K^{\mathrm{I}}_{\mathrm{Br}} = \frac{C_{\mathrm{BrCu^IL}}}{C_{[\mathrm{Cu^IL}]^+} C_{\mathrm{Br}^-}} \tag{3.10}$$

The ratio between the amount of active catalyst $[Cu^IL]^+$ and the total amount of Cu^I in solution (*i.e.* the initially added Cu^I), $C_{[\mathrm{Cu^IMe_6TREN}]^+}/C^0_{\mathrm{Cu^I}}$, was calculated for each $C^0_{\mathrm{Br}^-}$ and reported in **Figure 3.8b** (blue squares). The experimental values of $K^{\mathrm{app}}_{\mathrm{ATRP}}/K_{\mathrm{ATRP}}$ and the calculated values of $C_{[\mathrm{Cu^IMe_6TREN}]^+}/C^0_{\mathrm{Cu^I}}$ overlapped each other. This confirmed that $[Cu^IL]^+$ is the only active species in ATRP.[16] Moreover, the result enables to use the drop in $K^{\mathrm{app}}_{\mathrm{ATRP}}$ with increasing $C^0_{\mathrm{Br}^-}$ to estimate $K^{\mathrm{I}}_{\mathrm{Br}}$, when this parameter is not known. Obtained $K^{\mathrm{I}}_{\mathrm{Br}}$ value is valid only if $[Cu^IL]^+$ and $BrCu^IL$ are the predominant species in solution, under the experimental conditions of $K^{\mathrm{app}}_{\mathrm{ATRP}}$ determination.

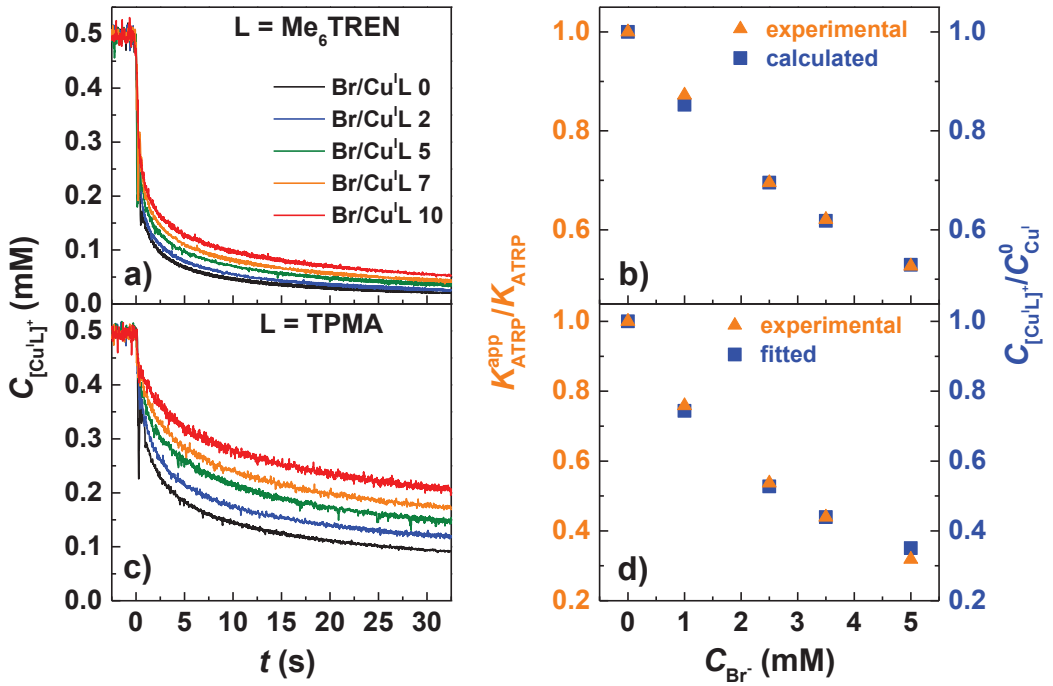

Figure 3.8. a) $C_{[Cu^{I}Me_6TREN]^+}$ and c) $C_{[Cu^{I}TPMA]^+}$ *vs.* time for the reaction of $[Cu^{I}L]^+$ with MBP in the presence of different amounts of Br^-, in CH_3CN + 0.1 M Et_4NBF_4, T = 25 °C. Experimental K_{ATRP}^{app}/K_{ATRP} values (orange triangles), in the presence of increasing $C^0_{Br^-}$, and b) calculated $C_{[Cu^{I}Me_6TREN]^+}/C^0_{Cu^{I}}$ values (blue squares), d) fitting of $C_{[Cu^{I}TPMA]^+}/C^0_{Cu^{I}}$ to Eq. 3.10 to obtain K^{I}_{Br} (blue squares).

The observed overlap between K_{ATRP}^{app}/K_{ATRP} and $C_{[Cu^{I}Me_6TREN]^+}/C^0_{Cu^{I}}$, can be explained considering the expression for K_{ATRP}^{app} in Eq. 3.9. The equation was derived considering the concurrent presence of two equilibria: *i*) ATRP (**Scheme 3.2a**) and *ii*) association of Br^- to $[Cu^{I}L]^+$ (Eq. 3.10). If $C^0_{Br^-} = 0$, $C^0_{Cu^{I}} - C_{[BrCu^{II}L]^+} = C_{[Cu^{I}L]^+}$, thus $K_{ATRP}^{app} = K_{ATRP}$. It follows that the ratio between the apparent and the "true" ATRP constants is expressed by Eq. 3.11:

$$\frac{K_{ATRP}^{app}}{K_{ATRP}} = \frac{C_{[Cu^{I}L]^+}}{C^0_{Cu^{I}} - C_{[XCu^{II}L]^+}} \approx \frac{C_{[Cu^{I}L]^+}}{C^0_{Cu^{I}}} \qquad (3.11)$$

K_{ATRP}^{app}/K_{ATRP} equals the ratio $C_{[Cu^{I}L]^+}/C^0_{Cu^{I}}$, if $C_{[BrCu^{II}L]^+} \ll C^0_{Cu^{I}}$. In the analyzed system: 5×10^{-4} M $[Cu^{I}Me_6TREN]^+$, 2.5×10^{-2} M MBP in CH_3CN, $K_{ATRP} = 1.1 \times 10^{-5}$, thus, at equilibrium, $C_{[BrCu^{II}Me_6TREN]^+} = 1.2 \times 10^{-5}$, which is *ca.* 40-times smaller than $C^0_{Cu^{I}}$.

To prove the flexibility of the method, K^{I}_{Br} for $[Cu^{I}Me_6TREN]^+$ was determined also using $C^0_{Cu^{I}} = 2 \times 10^{-4}$ M and $C^0_{Cu^{I}} = 10^{-3}$ M, and $C^0_{Br^-}/C^0_{Cu^{I}} = 0$, 5, 10 in both cases. K^{I}_{Br} = 221 M^{-1} and 148 M^{-1} were obtained, respectively. These values prove that by simply

measuring K_{ATRP}^{app} with 3 different ratios $C_{Br^-}^0/C_{Cu^I}^0$, a rough estimate of K_{Br}^I is possible. To improve the accuracy of the result, the fitting should be performed on many points (*i.e.* several different $C_{Br^-}^0/C_{Cu^I}^0$ ratios), but $C_{Br^-}^0/C_{Cu^I}^0$ ratios should be carefully selected. Moreover, the measurement of K_{ATRP} in the absence of Br^- should be repeated at least three times, because it is the most critical point in the fitting.

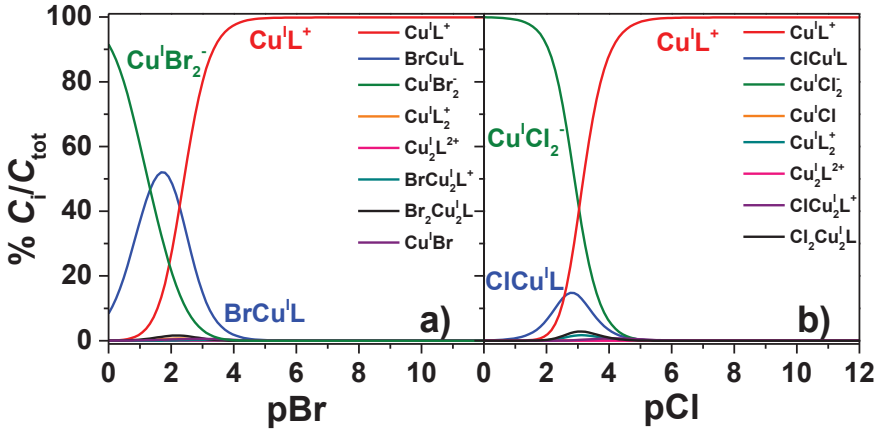

Figure 3.9. Speciation diagrams of 5 × 10^{-4} M Cu^I/Me_6TREN in CH_3CN, T = 25 °C, varying the amount of a) Br^- and b) Cl^-. Species distributions were obtained from thermodynamic parameters in Ref. [17], using HySS software.

The method was applied to determine the bromidophilicity constant for $[Cu^ITPMA]^+$. Speciation of Cu^I/TPMA/Br^- is unknown in CH_3CN. It was assumed that $[Cu^IL]^+$ and $BrCu^IL$ were the major species for $C_{Br^-}^0$ < 5 × 10^{-3} M, as previously determined for $[Cu^IMe_6TREN]^+$ and $[Cu^IPMDETA]^+$.[17] This assumption, however, is invalid in the case of Cl^- because of the higher chloridophilicity compared to bromodophilicity, leading to significant amounts of various Cu^I species even for low $C_{Cl^-}^0$ (**Figure 3.8b**).[17] Consequently, only K_{Br}^I was estimated.

Figure 3.8c shows $C_{[Cu^ITPMA]^+}$ decrease during reaction of the complex with MBP at different $C_{Br^-}^0/C_{Cu^I}^0$ ratios. Analysis of these curves according to the modified Fischer equation provided K_{ATRP}^{app}, which after normalization with respect to K_{ATRP}, gave the K_{ATRP}^{app}/K_{ATRP} ratios reported in **Figure 3.8d** (orange triangles). For different $C_{Br^-}^0$, the ratio $C_{[Cu^ITPMA]^+}/C_{Cu^I}^0$ depends on the unknown constant K_{Br}^I. Then, K_{Br}^I value was iteratively changed to minimize the difference between $C_{[Cu^ITPMA]^+}/C_{Cu^I}^0$ values (blue squares in **Figure 3.8d**), and experimental data of K_{ATRP}^{app}/K_{ATRP}. From a good fit, K_{Br}^I = 396 M^{-1} was

obtained. Also in this case, $C_{[\mathrm{BrCu^{II}L}]^+} \ll C^0_{\mathrm{Cu^I}}$: 5 × 10^{-4} M [Cu$^{\mathrm{I}}$TPMA]$^+$, 2.5 × 10^{-2} M MBP in CH_3CN, K_{ATRP} = 3.5 × 10^{-6}, thus, $C_{[\mathrm{BrCu^{II}TPMA}]^+}$ = 6.5 × 10^{-6}, which is *ca.* 80-times smaller than $C^0_{\mathrm{Cu^I}}$.

Once $K^{\mathrm{I}}_{\mathrm{Br}}$ was determined, the halidophilicity constant for Cu$^{\mathrm{II}}$, $K^{\mathrm{II}}_{\mathrm{Br}}$, was calculated from Eq. 1.16 (**Chapter 1**, **Section 1.3.1**), which correlates the standard reduction potentials of ternary and binary Cu complexes, to the halidophilicity constants $K^{\mathrm{II}}_{\mathrm{X}}$ and $K^{\mathrm{I}}_{\mathrm{X}}$. $E^{\ominus}$ values of the redox couples [Cu$^{\mathrm{II}}$L]$^{2+}$/[Cu$^{\mathrm{I}}$L]$^+$ and [BrCu$^{\mathrm{II}}$L]$^+$/[BrCu$^{\mathrm{I}}$L] were taken from the literature or measured in this work (**Table 3.3**). $K^{\mathrm{II}}_{\mathrm{Br}}$ = 1.5 × 10^6 M^{-1} and 1.1 × 10^7 M^{-1} were obtained for [Cu$^{\mathrm{II}}$Me$_6$TREN]$^{2+}$ and [Cu$^{\mathrm{II}}$TPMA]$^{2+}$, respectively. $K^{\mathrm{II}}_{\mathrm{Br}}$ = 1.3 × 10^6 M^{-1} was previously reported for [Cu$^{\mathrm{II}}$Me$_6$TREN]$^{2+}$ in CH_3CN.[17] $K^{\mathrm{II}}_{\mathrm{Br}}$ values higher than 10^7 M^{-1} are difficult to directly measure by techniques such as spectrophotometry that are commonly used to measure equilibrium constants.

3.8. Temperature effect on K_{ATRP}

The effect of reaction temperature on ATRP equilibrium was investigated by measuring K_{ATRP} for [Cu$^{\mathrm{I}}$TPMA]$^+$/MBP in CH_3CN at different T, and evaluating the enthalpic and entropic contributions. Data reported in **Table 3.4** show that K_{ATRP} increased with increasing T. Analysis of the data according to van't Hoff equation, $d\ln K/d(1/T) = -\Delta H^{\ominus}/R$, yielded the standard enthalpy of reaction as $\Delta H^{\ominus}$ = 13.5 kJ mol^{-1} (**Figure 3.10**). Then, the standard entropy of reaction was obtained from $\Delta G^{\ominus} = -RT \ln K_{ATRP} = \Delta H^{\ominus} - T\Delta S^{\ominus}$. Using the K_{ATRP} value measured at 298,15 K, gave $\Delta G^{\ominus} =$ 31.1 kJ mol^{-1} and $\Delta S^{\ominus} =$ 59 J mol^{-1} K^{-1}.

$\Delta H^{\ominus} = 36$ kJ mol^{-1} was previously measured for Cu$^{\mathrm{I}}$Br/TPMA and ethyl bromopropionate in methyl acrylate (MA) 50 vol % in CH_3CN.[9] The lower value determined herein in the absence of monomer and Br$^-$ (*i.e.* in a more active system) is in line with the prediction from Ref. [9]. However, in the presence of Br$^-$, the temperature can significantly affect also the speciation of Cu$^{\mathrm{I}}$ ions, thus a complete work on T effect on ATRP parameters is required.

Table 3.4. K_{ATRP} determined by RDE, for the system $[Cu^{I}TPMA]^{+}$/MBP in CH_3CN at different temperatures.[a]

T (°C)	K_{ATRP}
10	2.59×10^{-6}
25	3.47×10^{-6}
40	4.34×10^{-6}
55	5.78×10^{-6}

[a] 0.1 M Et_4NBF_4 as supporting electrolyte. $C^0_{Cu^I} = 0.5$ mM, $C_L = 1.5C^0_{Cu^I}$, $C^0_{RX} = 50C^0_{Cu^I}$. ω = 2500 rpm.

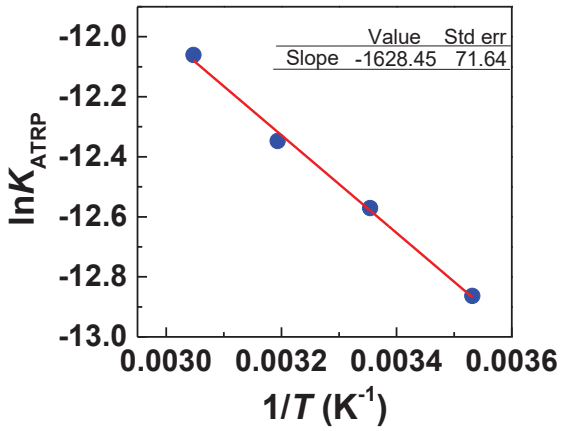

Figure 3.10. van't Hoff plot of K_{ATRP} values at different temperatures, for the $[Cu^{I}TPMA]^{+}$/MBP system in CH_3CN + 0.1 M Et_4NBF_4.

3.9. Conclusions and perspectives

The thermodynamic constant of ATRP equilibrium, K_{ATRP}, was determined for several systems, by following the reaction of $[Cu^{I}L]^{+}$ with RX by means of a rotating disk electrode, and then applying a modified Fischer equation. The procedure is fast and reproducible. For relatively slow systems, K_{ATRP} and k_{act} were measured in a 'one-pot' experiment, by simply adding a radical scavenger a few seconds after the injection of RX.

Competitive equilibria must be minimized. An excess of secondary alkyl halide initiator is required to avoid the influence of catalytic radical termination. A Cu^{I} salt with non-complexing ions (*e.g.* $Cu^{I}OTf$) should be used to avoid the influence of complexing agents, such as halide ions. Indeed, X^- can bind to Cu^{I} species, diminishing the amount of active catalyst and slowing down the process.

The effect of Br^- on K_{ATRP} was used to estimate the bromidophilicity constant for $[Cu^{I}L]^+$ by measuring K_{ATRP}^{app} values in the presence of different amounts of halide ions, and then correlating the decrease of K_{ATRP}^{app} to $C_{Br^-}^0$.

Linear correlations between logK_{ATRP} and logk_{act} and logk_{deact} were found. Both k_{act} and k_{deact} increased with K_{ATRP}, the effect being much more pronounced on k_{act} than on k_{deact}. However, only two Cu complexes were considered in this work, under various conditions. K_{ATRP} of other ligand/initiator combinations should be measured to complete the observed correlation, also considering that the measurement is relatively fast and easy.

References

1. Matyjaszewski, K.; Tsarevsky, N. V. *Journal of the American Chemical Society* **2014,** 136, 6513-6533.
2. Krys, P.; Matyjaszewski, K. *European Polymer Journal* **2017**, 89, 482-523.
3. Tang, W.; Tsarevsky, N. V.; Matyjaszewski, K. *Journal of the American Chemical Society* **2006,** 128, 1598-1604.
4. Braunecker, W. A.; Matyjaszewski, K. *Progress in Polymer Science* **2007,** 32, 93-146.
5. Konkolewicz, D.; Krys, P.; Góis, J. R.; Mendonça, P. V.; Zhong, M.; Wang, Y.; Gennaro, A.; Isse, A. A.; Fantin, M.; Matyjaszewski, K. *Macromolecules* **2014,** 47, 560-570.
6. Fantin, M.; Isse, A. A.; Gennaro, A.; Matyjaszewski, K. *Macromolecules* **2015,** 48, 6862-6875.
7. Pintauer, T.; Zhou, P.; Matyjaszewski, K. *Journal of the American Chemical Society* **2002,** 124, 8196-8197.
8. Smolne, S.; Buback, M. *Macromolecular Chemistry and Physics* **2015,** 216, 894-902.
9. Wang, Y.; Kwak, Y.; Buback, J.; Buback, M.; Matyjaszewski, K. *ACS Macro Letters* **2012,** 1, 1367-1370.
10. Fischer, H. *Chemical reviews* **2001,** 101, 3581-3610.
11. Goto, A.; Fukuda, T. *Progress in Polymer Science* **2004,** 29, 329-385.
12. Isse, A. A.; Bortolamei, N.; De Paoli, P.; Gennaro, A. *Electrochimica Acta* **2013,** 110, 655-662.
13. Lorandi, F.; Fantin, M.; Isse, A. A.; Gennaro, A. *Polymer* **2015,** 72, 238-245.
14. Fantin, M.; Isse, A. A.; Bortolamei, N.; Matyjaszewski, K.; Gennaro, A. *Electrochimica Acta* **2016,** 222, 393-401.
15. Fantin, M.; Isse, A. A.; Matyjaszewski, K.; Gennaro, A. *Macromolecules* **2017,** 50, 2696-2705.
16. De Paoli, P.; Isse, A. A.; Bortolamei, N.; Gennaro, A. *Chemical Communications* **2011,** 47, 3580-3582.
17. Bortolamei, N.; Isse, A. A.; Di Marco, V. B.; Gennaro, A.; Matyjaszewski, K. *Macromolecules* **2010,** 43, 9257-9267.

18. Wang, Y.; Soerensen, N.; Zhong, M.; Schroeder, H.; Buback, M.; Matyjaszewski, K. *Macromolecules* **2013,** 46, 683-691.

19. Ribelli, T. G.; Rahaman, S.; Matyjaszewski, K.; Poli, R. *Chemistry-A European Journal* **2017**, 23, 13879-13882.

20. Ribelli, T. G.; Wahidur Rahaman, S.; Daran, J.-C.; Krys, P.; Matyjaszewski, K.; Poli, R. *Macromolecules* **2016,** 49, 7749-7757.

21. Fischer, H.; Paul, H. *Accounts of chemical research* **1987,** 20, 200-206.

22. Tang, W.; Matyjaszewski, K. *Macromolecules* **2006,** 39, 4953-4959.

23. Ribelli, T. G.; Augustine, K. F.; Fantin, M.; Krys, P.; Poli, R.; Matyjaszewski, K. *Macromolecules* **2017**, 50, 7920-7929.

24. Tang, W.; Matyjaszewski, K. *Macromolecules* **2007,** 40, 1858-1863.

25. Tang, W.; Kwak, Y.; Braunecker, W.; Tsarevsky, N. V.; Coote, M. L.; Matyjaszewski, K. *Journal of the American Chemical Society* **2008,** 130, 10702-10713.

Chapter 4.

Non-Pt electrodes for *e*ATRP

in organic and aqueous media

Table of contents

4.1. Introduction and aim of the work

As described in **Chapter 1** (**Section 1.4**), the traditional equipment for *e*ATRP requires an electrochemical cell, connected to a potentiostat through a 3-electrode system. Both working and counter electrodes are made of Platinum, and the CE is placed in a separated compartment to avoid solution contaminations.[1] Although this setup is affordable on a laboratory scale, implementation in an industrial plant for large production demands a simplification of the apparatus, as well as a severe cut in equipment cost.

An important step toward a cost-effective process consisted in the replacement of the Pt CE with a sacrificial Aluminum wire, thereby working with an undivided cell. This approach was called simplified *e*ATRP (*se*ATRP).[2] Moreover, when a constant current is applied instead of a potential (*i.e.* galvanostatic mode), the reference electrode is not needed, and a cheap current generator can replace the expensive potentiostat.[3]

Up to now, Pt has been the only material used as a cathode in *e*ATRP. Despite being a good electronic conductor and a chemically inert metal, it is extremely expensive and rare. Since the role of the WE is to provide electrons for Cu^{II} reduction, in principle, Pt can be replaced with any other material able to accomplish this task, without being directly involved in the polymerization process.

The cathode is at the core of the *e*ATRP process, *locus* of catalyst reduction, therefore if a stable, nonfouling material is used, it can be viewed as an inexhaustible reducing agent. Thus, inexpensive cathodic materials are more affordable than the commonly used reducing agents.[4]

Moreover, Pt is an extremely inert metal, hindering the possibility of preparing functionalized materials that can find applications in the fields of electronics and biosensors. In contrast, electrodic materials like gold or glassy carbon can be easily functionalized with ATRP initiators containing thiols or diazonium groups, to grow (co)polymers on their surfaces.[5-7]

Following these evaluations, a series of materials was tested as cathodes for *e*ATRP in both organic and aqueous media and the results are presented in the next sections. Chemical structures of ligands, initiators and monomers used in both environments are reported in **Figure 4.1**.

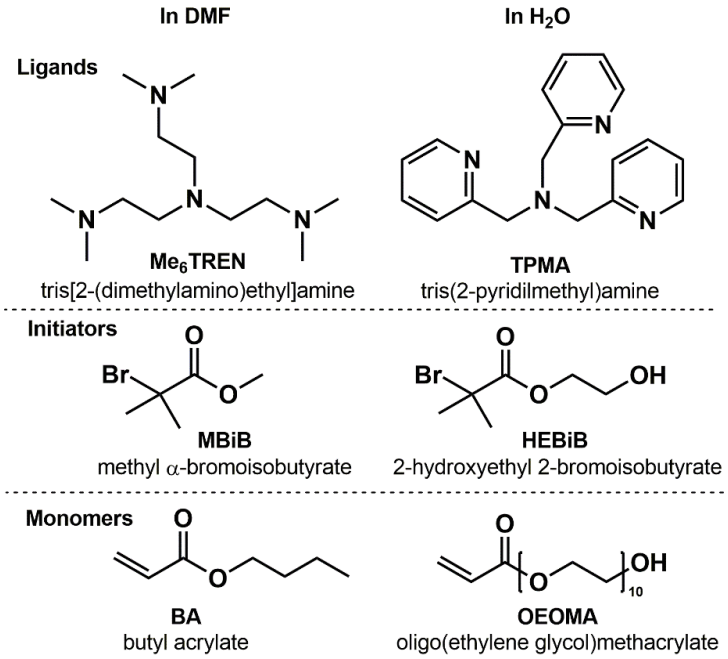

Figure 4.1. Structures of compounds relevant to the present chapter.

4.2. *e*ATRP of BA in DMF with non-Pt cathodes

Three different classes of materials were considered as new cathodes for *e*ATRP in organic solvents (**Figure 4.2**): carbon materials (glassy carbon – GC), pure metals (Fe, Au) and metallic alloys (304 stainless steel – 304SS, NiCr).

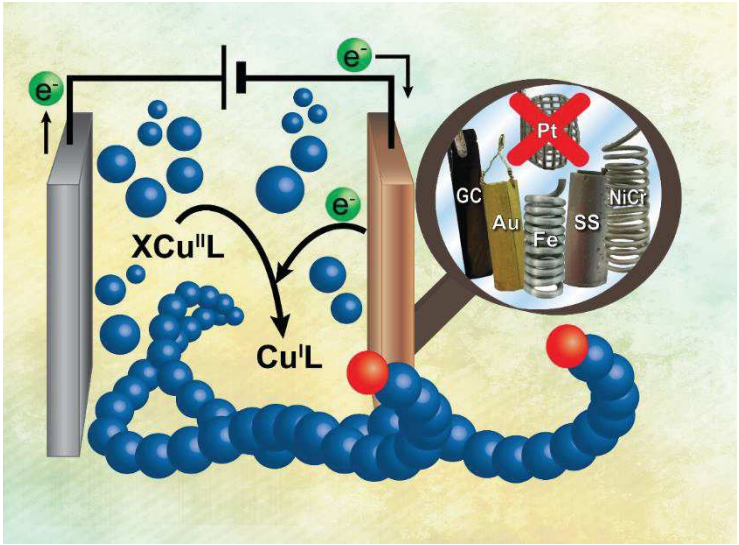

Figure 4.2. Artistic representation of *e*ATRP mechanism. In the lens, pictures of non-Pt materials tested as cathodes (inside cover of Polymer Chemistry, reprinted with permission from Ref. [10]. Copyright 2016, Royal Chemical Society).

Copper was initially discarded because it is well-known that metallic copper can activate alkyl halides and re-generate Cu^{I} by comproportionation with Cu^{II}, as in the SARA-ATRP process.[8, 9] However, some investigations were conducted on the role of Cu as electrodic material in organic solvents, and the results will be presented in **Section 4.4**. The new electrodes were applied on a well-known system to allow the comparison with the traditional setup. BA was hence selected as monomer at 50 vol% in DMF, using $[Br\text{-}Cu^{II}Me_6TREN]^+$ as catalyst, MBiB as initiator, and T = 45 °C to enhance the polymerization rate and limit the viscosity increment with increasing monomer conversion. The catalytic complex was formed *in situ* by adding equal amounts of $Cu^{II}(OTf)_2$, Me_6TREN and Et_4NBr.

Firstly, the system was characterized by cyclic voltammetry, performed on a small GC working electrode. A reversible CV was recorded for the $[Br–Cu^{II}Me_6TREN]^+/[Br–Cu^{I}Me_6TREN]$ redox couple. The standard reduction potential of Cu^{II} was obtained from the peak potentials as half-wave potential, thus $E^{e} \approx E_{1/2} = (E_{pa} + E_{pc})/2 =$ -0.26 V *vs.* SCE (**Figure 4.3**). E_{pa} and E_{pc} are the potentials of the anodic and cathodic peaks, respectively. A previous work on a similar system showed that by imposing $E_{app} < E^{e}$ the polymerization rate was enhanced without losing control over the process.[3] For this reason, $E_{app} = E_{1/2} –$ 0.06 V was selected as the operative potential for the present system, which approximately provides $C_{Cu^{I}}/C_{Cu^{II}} = 10$, according to Nernst equation (Eq. 1.26, **Chapter 1**, **Section 1.4**).

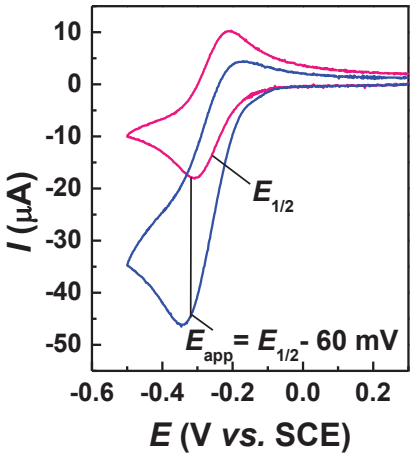

Figure 4.3. CVs of 10^{-3} M $[BrCu^{II}Me_6TREN]^+$ in BA/DMF 1/1 (v/v) + 0.1 M Et_4NBF_4, in the absence (pink) and presence (blue) of 10^{-2} M MBiB. $\upsilon = 0.2$ Vs^{-1}, $T = 45$ °C.

Potentiostatic *e*ATRP with WE = Pt. For comparison, an *e*ATRP was performed on the described system with the traditional setup, *i.e.* WE = Pt (a mesh of geometrical area *ca.* 6

cm^2). 91% conversion was recorded in only 1.5 h and the final PBA showed $Đ$ = 1.16. Both experimental conditions and polymerization results were comparable to those previously obtained with an identical setup. Before testing alternative cathodic materials, the effect of bromide ions concentration on polymerization rate and control was tested, since Br^- dramatically affects catalyst speciation (discussed in **Chapter 3**, **Section 3.7**).[11]

Table 4.5. Effect of C_{Br^-} on potentiostatic *e*ATRP of 50 vol% BA performed at a Pt electrode in DMF.[a]

Entry	C_{Et_4NBr} (mM)	t (h)	Q (C)	Conv. (%)	$M_{n,th}$ (10^{-3})	M_n (10^{-3})	k_p^{app} (h^{-1})	$Đ$
1	-	2	4.9	86	39.7	38.2	1.26	1.22
2	1	1.5	2.4	91	40.9	35.5	1.83	1.16
3	2	2	2.2	92	41.3	35.7	1.37	1.15
4	10	4	2.2	92	41.3	35.7	0.64	1.16

[a] Polymerization conditions: $C_{BA}/C_{MBiB}/C_{[Cu^{II}Me_6TREN]^{2+}}$ = 349/1/0.1 with $C_{Cu^{II}} = 10^{-3}$ M; $C_{Et_4NBF_4}$ = 0.1 M; V_{tot} = 15 mL; $E_{app} = E_{1/2} - 0.06$ V; T = 45 °C.

Potentiostatic *e*ATRPs were carried out with $C_{Cu^{II}(OTf)_2}/C_{Me_6TREN}$ = 1/1[1] and different initial C_{Br^-}, at a fixed $E_{app} = E_{1/2} - 0.06$ V (**Figure 4.4** and **Table 4.5**). In the absence of Br^-, the process was slower and slightly less controlled than the polymerization with 1 or 2 equivalents of Br^-. In fact, bromide ions strongly bind to Cu^{II} species,[11] thereby ensuring the presence of the deactivator $[Br–Cu^{II}L]^+$, and enhancing the rate of deactivation and control over molecular weight distribution. However, when $C_{Cu^{II}}/C_{Br^-}$ = 1/10 the polymerization rate was nearly 3 times slower. Indeed, Br^- also binds to Cu^I species, reducing the amount of active $[Cu^IL]^+$,[11, 12] thus decreasing the polymerization rate. The control did not improve ($Đ$ = 1.16), evidencing that higher C_{Br^-} was not beneficial. Although employing $C_{Cu^{II}}/C_{Br^-}$ =1/2 is interesting from a practical point of view as both species can be simultaneously introduced using $Cu^{II}Br_2$, it slightly decreased the reaction rate with respect to $C_{Cu^{II}}/C_{Br^-}$=1/1. Therefore, exactly equal amounts of $Cu^{II}(OTf)_2$, ligand and Br^- ions were used for *e*ATRPs with all tested electrodic materials.

[1] In the preceding chapter, initial concentrations were indicated with a "0" superscript, to be distinguished from equilibrium concentrations. Starting from this chapter, all reported concentrations should be intended as initial, unless otherwise specified, thus the "0" superscript is omitted.

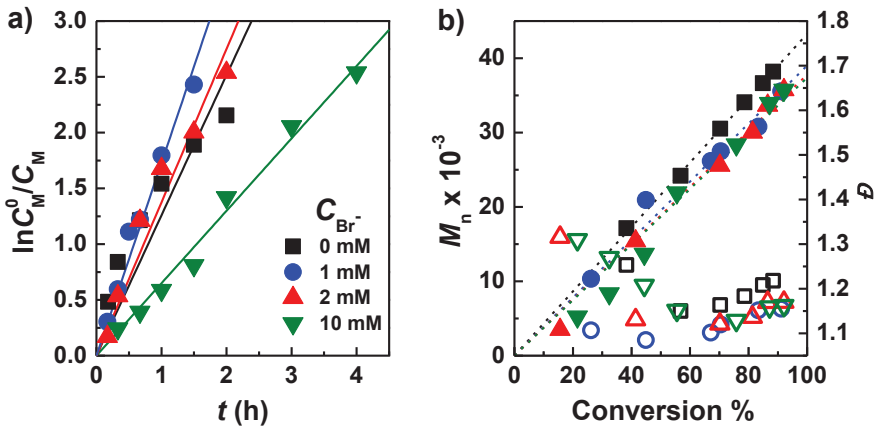

Figure 4.4. *e*ATRP of 50 vol% BA performed at a Pt WE in DMF + 0.1 M Et_4NBF_4, with different amounts of Br^- ions. a) Kinetic plot, and b) evolution of MWs and dispersity *vs.* conversion. $C_{BA}/C_{MBiB}/C_{[Cu^{II}Me_6TREN]^{2+}}$ = 349/1/0.1, $C_{Cu^{II}} = 10^{-3}$ M, V_{tot} = 15 mL, $E_{app} = E_{1/2} - 0.06$ V, T = 45 °C.

4.2.1. *e*ATRP with non-Pt cathodes under potentiostatic and galvanostatic control

Potentiostatic *e*ATRP with non-Pt cathodes. The surface of all tested materials was cleaned and activated by electrochemical, chemical or mechanical procedures, as reported in **Appendix C1**.

A blank test was performed with all selected materials to prove their chemical inertness. After immersion in the working solution for more than 4 h without any applied potential (*i.e.* at open circuit) but under vigorous stirring, no polymer formation or appreciable monomer conversion was observed with each cathode. This suggested that the analyzed materials were not directly involved in the polymerization, but act exclusively as electron carriers.

Potentiostatic *e*ATRP of BA with all tested electrodes exhibited conversions > 85% in less than 2 h (**Table 4.1**). Control over polymer growth was similar to that observed with Pt, obtaining $Đ < 1.2$, good accordance between experimental and theoretical M_n values, and linear increase of M_n with conversion (**Figure 4.5**). These results clearly proved that the nature of the WE did not affect the reduction of Cu^{II} to Cu^{I} species in *e*ATRP.

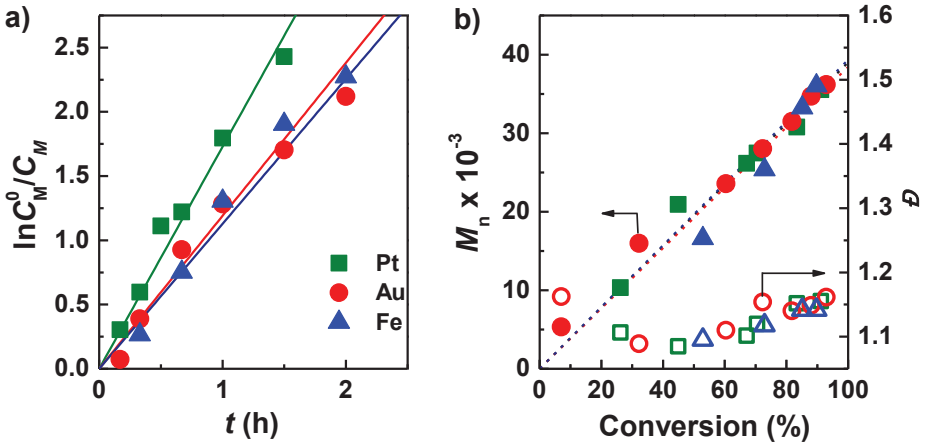

Figure 4.5. Potentiostatic *e*ATRP of 50 vol% BA in DMF + 0.1 M Et_4NBF_4, performed on various WEs. a) Kinetic plot, and b) evolution of MWs and dispersity *vs.* conversion. $C_{BA}/C_{MBiB}/C_{Cu^{II}(OTf)_2}/C_{Me_6TREN}/C_{Et_4NBr}$ = 349/1/0.1/0.1/0.1, $C_{Cu^{II}}$ = 10^{-3} M, V_{tot} = 15 mL, E_{app} = $E_{1/2}$ – 0.06 V, T = 45 °C (adapted with permission from Ref. [10]. Copyright 2016, Royal Chemical Society).

Table 4.1. Potentiostatic *e*ATRP of 50 vol% BA in DMF performed at different cathodes (WEs).[a]

Entry	WE	A [b] (cm^2)	E_{app}-$E_{1/2}$ (V)	t (h)	Q (C)	Conv. (%)	$M_{n,th}$ (10^{-3})	M_n (10^{-3})	k_p^{app} (h^{-1})	$Đ$
1	Pt	5	-0.06	1.5	2.4	91	40.9	35.5	1.83	1.16
2	GC	4	-0.06	2	1.9	89	39.9	33.7	1.11	1.14
3	Au	5	-0.06	2	2.7	88	39.5	34.7	0.95	1.15
4	Fe	4	-0.21	2	2.8	90	40.3	36.1	1.08	1.14
5	SS304	5	-0.16	2	1.9	86	38.4	34.7	1.09	1.14
6[c]	SS304	5	-0.16	3	8.5	93	16.8	13.2	1.02	1.24
7	NiCr	5	-0.3	2.5	5.7	97	43.6	39.0	1.35	1.18
8[c]	NiCr	5	-0.3	2.5	9.8	93	16.8	13.6	1.20	1.24

[a] Polymerization conditions: $C_{BA}/C_{MBiB}/C_{Cu^{II}(OTf)_2}/C_{Me_6TREN}/C_{Et_4NBr}$ = 349/1/0.1/0.1/0.1 with $C_{Cu^{II}}$ = 10^{-3} M; $C_{Et_4NBF_4}$ = 0.1 M; V_{tot} = 15 mL; T = 45 °C. [b] Estimated geometric surface area of WE. [c] C_{BA}/C_{MBiB} = 140/1, all other conditions unchanged (reprinted with permission from Ref. [10]. Copyright 2016, Royal Chemical Society).

It should be noted that the same E_{app} value was not used with all WEs. In particular, non-noble metal electrodes required more negative E_{app} values. Actually, in polymerization conditions, the voltammetric pattern of $[Br–Cu^{II}Me_6TREN]^+$ + MBiB on bulky GC and Au electrodes showed a well-defined cathodic peak similar to the one observed on Pt (**Figure 4.6**, black line). Thus *e*ATRPs with these cathodes were performed at $E_{app} \approx E_{1/2}$ – 0.06 V.

Conversely, cyclic voltammetry of $[BrCu^{II}Me_6TREN]^+$ on NiCr, Fe and SS304 electrodes (**Figure 4.6**, blue line) showed an ill-defined, stretched cathodic peak at more negative potentials than that observed on Pt. A thin layer of resistive oxides might be present on the surface of these non-noble metals, resulting in a significantly lower rate of the heterogeneous electron transfer. To take into account the slower ET on these metals, E_{app} was shifted to more negative values, so as to roughly match the current value observed in the CV of 1 mM $[BrCu^{II}Me_6TREN]^+$ + 10 mM MBiB on the Pt mesh.

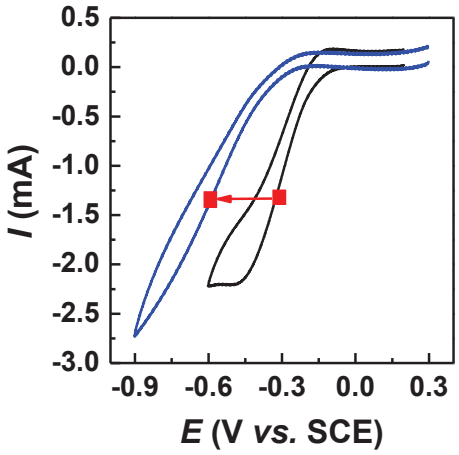

Figure 4.6. CVs of 1 mM $[BrCu^{II}Me_6TREN]^+$ + 10 mM MBiB, in BA/DMF 1/1 (v/v) + 0.1 M Et_4NBF_4, recorded on a a) Pt WE ($A \approx 5$ cm^2), b) NiCr WE ($A \approx 5$ cm^2). $\upsilon = 0.2$ V s^{-1}, $T = 45$ °C.

As explained in **Chapter 1** (**Section 1.4**), *e*ATRP allows to measure the charge consumed during the polymerization, which gives important indications about the extent of termination. According to Eq. 4.1, a theoretical charge Q_{th} = 1.5 C is required for the quantitative reduction of Cu^{II} species to Cu^{I} in the present system.

$$Q_{th} = \nu n_{Cu^{II}} F \quad (4.1)$$

where ν is the number of transferred electron (ν = 1 in this case), $n_{Cu^{II}}$ is the number of moles of Cu^{II} initially present in solution and F is the Faraday constant. For all WEs, except NiCr, Q was in the range of 1.9–2.8 C, *i.e.* less than twice higher than Q_{th}. The excess charge is consumed by regenerating Cu^{I} from cumulated $[BrCu^{II}L]^+$ arising from radical termination. Instead, for WE = NiCr the charge consumption was significantly greater than Q_{th}, possibly because of a contribution due to the reduction of oxides present on the electrode surface. Alternatively, considering the high overpotential applied to face the low rate of electron transfer on this material, the excess Q could be due to partial reduction of

Cu^{I} to Cu^{0},[3] or even reduction of impurities. However, these reactions did not influence control or rate of polymerization.

GPC traces of PBA obtained from potentiostatic *e*ATRPs (*e.g.* **Figure 4.7** in the case of Au) exhibited a small shoulder at high molecular weights for conversions > 70%. The shoulder is indicative of some termination by radical-radical coupling, which is considered the main pathway of radical termination in acrylic monomers.[13, 14] Nevertheless, the extent of termination and its effect on molecular weight distribution were really limited; polymerizations were well-controlled, yielding polymers with $Đ$ always < 1.2. However, radical coupling leads to dead chains that lack the C–X chain end functionality. It follows that, in order to efficiently build copolymers, the process should be stopped at conversions *ca.* 70%. The small discrepancy between $M_{n,th}$ and M_n was previously observed[3] and is attributed to the use of PMMA, instead of PBA, as GPC calibration standards.

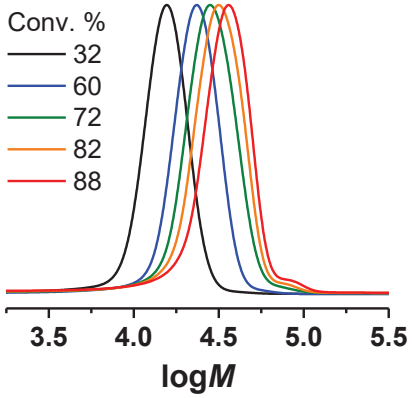

Figure 4.7. GPC traces of PBA produced via *e*ATRP on Au WE. Polymerization conditions as in **Table 4.1** (adapted with permission from Ref. [10]. Copyright 2016, Royal Chemical Society).

Inductively coupled plasma mass spectroscopy (ICP-MS) measurements were conducted on final solutions in order to verify that the cathodes did not release metal ions in the course of polymerizations. Obtained results are reported in **Table 4.2**, together with the analysis of a blank sample (*i.e.* the initial solution prepared in the presence of each component except the WE). Importantly, the amount of Ni, Cr, and Fe ions found in solution after *e*ATRPs with NiCr and SS304 cathodes was practically identical with that of the blank experiment, evidencing that these electrodes do not release undesired ions into the solution during the process. Overall, the amount of metal ions found in final solutions was very small (5×10^{-6} – 2×10^{-4} M), thus exerting a negligible effect on the polymerization process and, in particular, on the purity of the polymer.

Table 4.2. ICP-MS analysis of polymerization media.[a]

Entry	WE	Cu (ppm)	Ni (ppm)	Cr (ppm)	Fe (ppm)
1[b]	-	65.7	0.1	0.3	7.7
2[c]	NiCr	61.4	0.2	1.7	12.0
3[c]	SS304	71.2	0.3	0.4	7.8

[a] 1 ppm = (1 mg of metal)/(1 kg of solution). [b] Blank sample: a solution containing all components of *e*ATRP, except the WE. [c] *e*ATRP of BA 20 vol% in DMF: $C_{BA}/C_{MBiB}/C_{Cu^{II}(OTf)_2}/C_{Me_6TREN}/C_{Et_4NBr}$ = 140/1/0.1/0.1/0.1 with $C_{Cu^{II}} = 10^{-3}$ M; $C_{Et_4NBF_4}$ = 0.1 M; V_{tot} = 15 mL; T = 45 °C. Further details on polymerizations are reported in **entries 6 and 8** in **Table 4.1**.

ICP-MS measurements confirmed that the main role of cathodic materials in *e*ATRP is to act a as source of electrons for Cu^{II} reduction. Moreover, these measurements highlighted that Cu ions were preserved in solution after *e*ATRP. Metal cathodes were mechanically stable and did not participate in side reactions with the Cu catalyst or other components of the polymerization mixture.

Galvanostatic *e*ATRP with non-Pt cathodes. In galvanostatic (*i.e.* fixed current) *e*ATRP, the rate of Cu^{I} generation depends on the applied current, regardless of the nature of the electrodic material. I_{app} values in galvanostatic *e*ATRP of BA were chosen on the basis of chronoamperometry (*I vs. t*) recorded during potentiostatic *e*ATRP with a Pt working electrode (**Figure 4.8a**). Six current steps, with progressively decreasing current and increasing step time, were applied to simulate as much as possible the rate of Cu^{I} generation under potentiostatic conditions. The selected current steps allowed to produce $[Cu^{I}L]^{+}$ at a high rate at the beginning of the polymerization, and successively to slowly regenerate the active catalyst from $[BrCu^{II}L]^{+}$ accumulated after termination reactions.[2, 3] Although galvanostatic syntheses can be performed in a two-electrode setup (WE and CE), herein a RE was employed to monitor the potential of the working electrode during the experiment. An example of the typical trend found for all electrodes is reported in **Figure 4.8b** in the case of galvanostatic *e*ATRP on SS304. The working potential remained close to $E_{1/2}$ – 0.06 V, without falling to extremely negative values, which can promote the deposition of Cu^{0} on the WE or other harmful side reactions.[3]

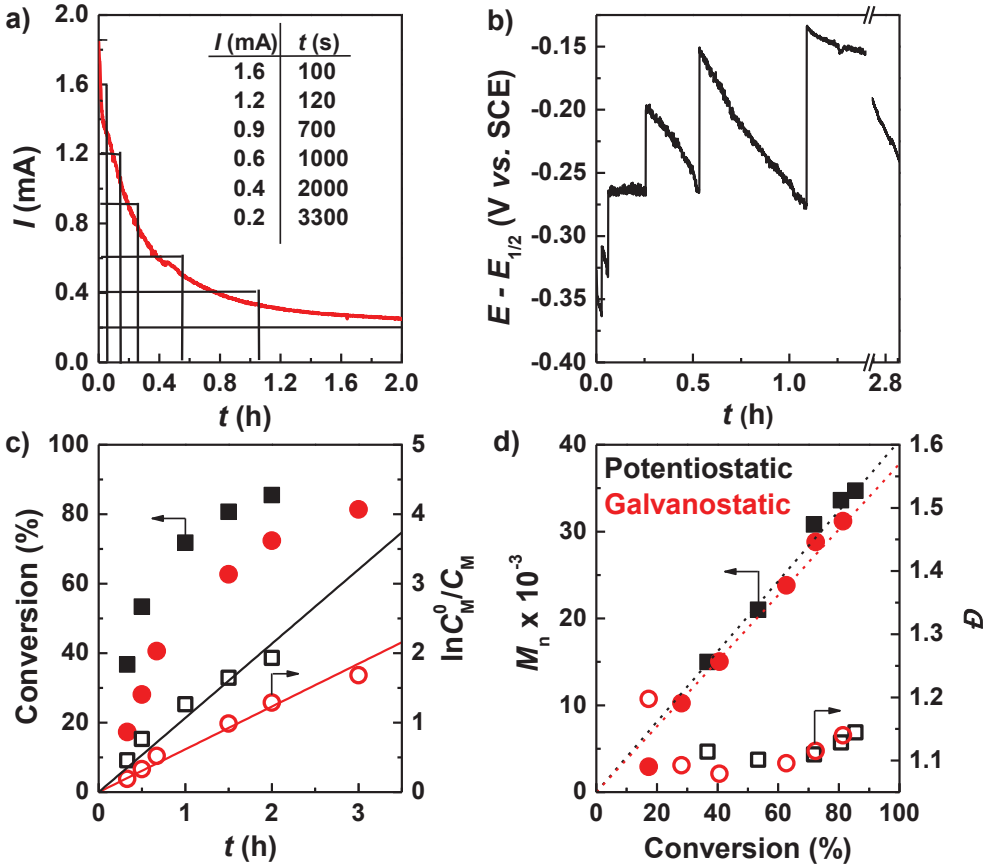

Figure 4.8. a) Chronoamperometry recorded during potentiostatic *e*ATRP on WE = Pt (**Table 4., entry 1**) and splitting in 6 steps. b) Potential behavior recorded on WE = SS304, during a galvanostatic *e*ATRP with 6 constant current steps. c) Kinetic plot, and d) evolution of MWs and dispersity *vs.* conversion, for potentiostatic (black) *vs.* galvanostatic (red) *e*ATRP of 50 vol% BA in DMF + 0.1 M Et_4NBF_4, on WE = SS304. $C_{BA}/C_{MBiB}/C_{Cu^{II}(OTf)_2}/C_{Me_6TREN}/C_{Et_4NBr}$ = 349/1/0.1/0.1/0.1, $C_{Cu^{II}}$ = 10^{-3} M, V_{tot} = 15 mL, E_{app} = $E_{1/2}$ – 0.06 V, T = 45 °C (adapted with permission from Ref. [10]. Copyright 2016, Royal Chemical Society).

Galvanostatic *e*ATRP with all tested electrodes (**Table 4.3** and **Figure 4.8c-d**) exhibited linear growth of M_n with conversion, $M_n \approx M_{n,th}$ and final PBA with $Đ \leq 1.15$. The results showed that all tested materials could be used as cathodes in galvanostatic *e*ATRP with the application of a fixed current/time program, to achieve a well-controlled polymerization process. However, polymerizations performed in a galvanostatic mode were in some cases slightly slower than the corresponding potentiostatic *e*ATRP processes, as previously reported.[3]

Table 4.3. Galvanostatic *e*ATRP of 50 vol% BA in DMF performed at different cathodes (WEs).[a]

Entry	WE	A [b] (cm^2)	t (h)	Q (C)	Conv. (%)	$M_{n,th}$ (10^{-3})	M_n (10^{-3})	k_p^{app} (h^{-1})	$Đ$
1	Pt	5	2	3.0	92	41.4	39.2	1.22	1.14
2	GC	4	2.5	3.3	90	40.4	34.8	0.78	1.13
3	Au	5	2	3.0	90	40.2	32.9	1.10	1.14
4	Fe	4	2	3.0	92	41.4	36.4	1.33	1.15
5	SS304	5	3	3.7	81	36.6	31.2	0.62	1.14
7	NiCr	5	2.5	3.3	89	40.1	37.6	0.92	1.15

[a] Polymerization conditions: $C_{BA}/C_{MBiB}/C_{Cu^{II}(OTf)_2}/C_{Me_6TREN}/C_{Et_4NBr}$ = 349/1/0.1/0.1/0.1 with $C_{Cu^{II}}$ = 10^{-3} M; $C_{Et_4NBF_4}$ = 0.1 M; V_{tot} = 15 mL; T = 45 °C. Applied current/time: I (mA)/t (s): 1.5/100, 1.2/120, 0.9/700, 0.6/1000, 0.4/2000, 0.2/≥3280. [b] Estimated geometric surface area of WE (reprinted with permission from Ref. [10]. Copyright 2016, Royal Chemical Society).

Effect of catalyst loading. Further reduction in production cost can be achieved by lowering catalyst loading, which is also beneficial from an environmental point of view, and dramatically decreases the need of polymer purifications. Potentiostatic *e*ATRPs were carried out with 293, 146 and 73 ppm (defined as $n_{Cu}/n_{monomer}$) of Cu/Me_6TREN, using Pt, Fe and SS304 WEs (**Table 4.4**). Control was preserved for all catalyst loadings, observing a linear increase of MWs with conversion and narrow MW distributions (**Figure 4.9**). Polymerization rate showed a dependence on catalyst concentration, roughly increasing with $(C_{Cu^{II}})^{1/2}$, as previously derived from kinetic analysis of *e*ATRP.[15]

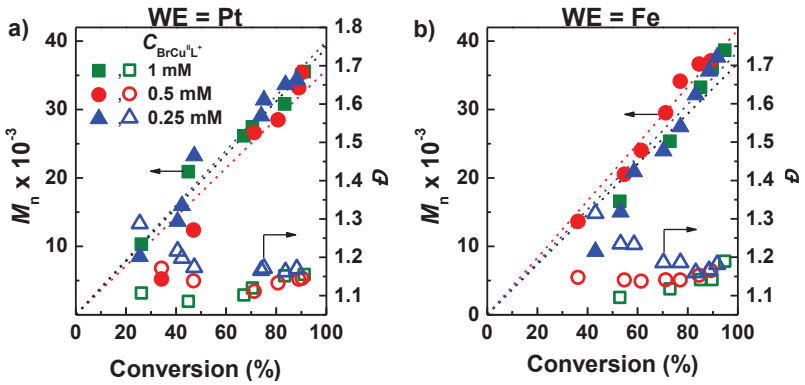

Figure 4.9. Evolution of MWs and $Đ$ *vs.* conversion, in potentiostatic *e*ATRP of 50 vol% BA in DMF + 0.1 M Et_4NBF_4, at different catalyst loadings, performed on WE = a) Pt, and b) Fe. C_{BA}/C_{MBiB} = 349/1, C_{MBiB} = 10^{-2} M, V_{tot} = 15 mL, E_{app} = $E_{1/2}$ – 0.06 V, T = 45 °C (adapted with permission from Ref. [10]. Copyright 2016, Royal Chemical Society).

Table 4.4. Potentiostatic *e*ATRP of 50 vol% BA in DMF with different WEs and catalyst loadings.[a]

Entry	WE	$C_{Cu^{II}}$ (mM)	E_{app}-$E_{1/2}$ (V)	t (h)	Q (C)	Conv. (%)	$M_{n,th}$ (10^{-3})	M_n (10^{-3})	k_p^{app} (h^{-1})	$Đ$
1	Pt	1.0	-0.06	1.5	2.4	91	40.9	35.5	1.83	1.16
2		0.5	-0.06	2	1.6	90	40.5	35.4	1.37	1.15
3		0.25	-0.06	4	2.3	88	39.6	34.4	0.57	1.17
4	Fe	1.0	-0.21	2	2.8	90	40.3	36.1	1.08	1.14
5		0.5	-0.21	2.5	1.9	89	40.1	37.1	0.94	1.16
6		0.25	-0.21	3	1.2	89	39.7	35.6	0.75	1.17
7	SS304	1.0	-0.16	2	1.9	86	38.4	34.7	1.09	1.14
8		0.5	-0.16	2.5	0.95	87	38.9	31.7	0.79	1.15
9		0.25	-0.16	3	1.8	76	32.5	35.3	0.37	1.16

[a] Polymerization conditions: C_{BA}/C_{MBiB} = 349/1, $C_{Cu^{II}(OTf)_2}/C_{Me_6TREN}/C_{Et_4NBr}$ = 1/1/1, with $C_{MBiB} = 10^{-2}$ M; $C_{Et_4NBF_4} = 0.1$ M; $V_{tot} = 15$ mL; $T = 45$ °C (reprinted with permission from Ref. [10]. Copyright 2016, Royal Chemical Society).

Cathodes recyclability. *e*ATRPs with different cathodes, both under potentiostatic and galvanostatic mode, gave high conversions and low dispersity PBA, but prior to all described polymerizations the electrode surface was carefully cleaned and activated. Although fouling of the electrode surface was never observed during these *e*ATRP experiments, practically it is important to check whether the WE could be reused several times without particular surface cleaning. To this end, NiCr was selected because it is the least stable of analyzed electrodes, being a non-noble metal alloy, naturally covered by an oxide layer when exposed to the air. The electrode was used in four sequential polymerizations of BA under galvanostatic conditions (**Table 4.5**). After each experiment, the electrode was simply rinsed with acetone, dilute aqueous HCl, and acetone again. The rate of polymerization was roughly constant throughout the four experiments, with M_n always matching the theoretical values, and consistently maintaining a high degree of control over polymerization, with $Đ \approx 1.1$ in all reactions. This result points out that NiCr electrode was not modified by the *e*ATRP process. Therefore, similar preservation of activity is expected for more stable electrodes such as GC, Au, and stainless steel.

Table 4.5. Consecutive galvanostatic *e*ATRPs of 50 vol% BA in DMF on a NiCr electrode.[a]

Entry	t (h)	Conversion [b] (%)	$M_{n,th}$ (10^{-3})	M_n (10^{-3})	k_p^{app} (h^{-1})	$Đ$
1	2	90	40.6	39.4	1.21	1.13
2	2	89	39.9	36.7	1.23	1.14
3	2	86	38.9	46.0	1.08	1.12
4	2	85	38.2	44.6	1.04	1.11

[a] Polymerization conditions: $C_{BA}/C_{MBiB}/C_{Cu^{II}(OTf)_2}/C_{Me_6TREN}/C_{Et_4NBr}$ = 349/1/0.5/0.5/0.5 with $C_{Cu^{II}} = 5\times10^{-4}$ M; $C_{Et_4NBF_4}$ = 0.1 M; V_{tot} = 15 mL; T = 45 °C. Applied current/time: I (mA)/t (s): 1.3/150, 1.1/150, 0.8/300, 0.55/600, 0.35/1800, 0.18/4200. [b] After 2.3 C of consumed charge.

4.2.2. Pt-free *e*ATRP setup

As mentioned at the beginning of this chapter, a great step toward a more sustainable *e*ATRP was obtained by replacing the Pt CE in a separated compartment with a sacrificial Al wire, directly immersed into the solution.[2] In this way, the experimental setup was simplified and the ohmic drop associated with the presence of separators in divided cells was avoided.

The simplified *e*ATRP (*se*ATRP) approach was combined with the analyzed cathodic materials. The Al wire was activated according to the procedure reported in **Appendix C1** and immersed in the reaction medium. In an undivided cell with an Al anode, the anodic reaction becomes the oxidation of the electrode itself, which releases Al^{3+} ions in solution. Therefore, we checked whether Al^{3+} could interfere with the catalytic system, in particular, if it could compete with Cu ions for the amine ligand.

CVs of $[Cu^{II}Me_6TREN]^{2+}$ recorded in the absence and presence of Al^{3+}, showed a drastic change in the voltammetric response of the catalyst (**Figure 4.10**). Electrolytic oxidation of the Al wire was performed to produce Al^{3+} ions. An anodic current of 2.5 mA was applied for 30 minutes (Q = 4.5 C) at the Al working electrode to produce roughly 1 mM Al^{3+} in solution, which already contained 1 mM $[Cu^{II}Me_6TREN]^{2+}$. When 1 mM Al^{3+} ions were generated, the signal corresponding to Cu^{II} reduction became irreversible and slightly shifted to less negative potentials. When more ligand (1 mM Me_6TREN) was added

to this solution, almost full recovery of the original voltammetric pattern of $[Cu^{II}Me_6TREN]^{2+}$ was observed.

These changes are indicative of the presence of competitive equilibria involving copper ions, Al^{3+} and amine ligand: it seems that Me_6TREN formed complexes with Cu^{2+}, Cu^{+}, and Al^{3+}. Indeed, when Al^{3+} was introduced by electrolysis into a solution of $[Cu^{II}Me_6TREN]^{2+}$ so that $C_{Me_6TREN}/C_{Cu^{2+}}/C_{Al^{3+}}$ = 1/1/1, only a fraction of the copper complex survived, because the ligand was distributed between Cu^{2+} and Al^{3+}. $[Cu^{II}Me_6TREN]^{2+}$ was replenished by further addition of ligand, so that $C_{Me_6TREN}/C_{Cu^{2+}}/C_{Al^{3+}}$ = 2/1/1. Therefore, a sacrificial Al anode can be used in *e*ATRP provided that there is enough ligand in solution for the complexation of both Cu^{2+} and Al^{3+} ions released by the anode.

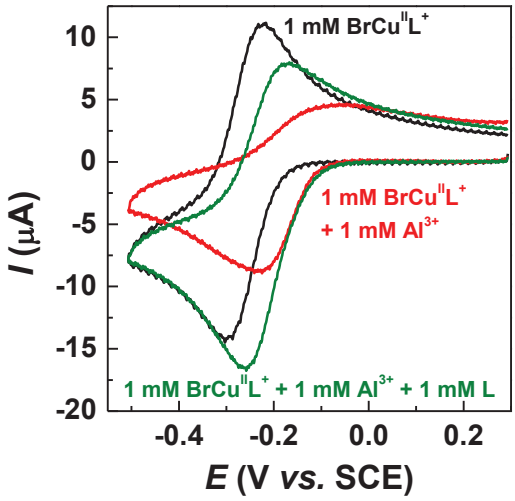

Figure 4.10. CV of 10^{-3} M $[Cu^{II}Me_6TREN]^{2+}$ in DMF + 0.1 M Et_4NBF_4, before (black) and after (red) generating *ca.* 10^{-3} M of Al^{3+} by electrolysis of an Al wire electrode. 10^{-3} M Me_6TREN was added (green) to restore the Cu catalyst. WE = GC, υ = 0.2 V s^{-1}, V_{tot} = 15 mL, T = 25 °C (adapted with permission from Ref. [10]. Copyright 2016, Royal Chemical Society).

In fact, when an *e*ATRP experiment was performed in an undivided cell with an Al anode and without excess ligand with respect to $C_{Cu^{2+}}$, the polymerization was slow and stopped after *ca.* 50% conversion; at the end of the experiment, a deposit of Cu^0 was observed on the WE surface, while cyclic voltammetry on a GC disk showed that $[Cu^{II}Me_6TREN]^{2+}$ was almost absent in solution. When the experiment was repeated with excess ligand ($C_{Me_6TREN}/C_{Cu^{2+}}$ = 2/1), displacement of Cu^{2+} by Al^{3+} from the metal complex was avoided, and the polymerization yielded similar results to that performed in

a divided cell. Previously reported *e*ATRPs with Al sacrificial anode were carried out with $C_L/C_{Cu^{2+}}$ = 2/1,[2] obtaining good results without a deep comprehension of the system. Moreover, the extent of ligand complexation by Al^{3+} can vary with ligand and solvent/monomer nature.

*e*ATRP experiments in an undivided cell with a sacrificial Al anode were then carried out using Fe and SS304 as working electrodes. The catalyst system was composed by 1 mM $Cu^{II}(OTf)_2$ and a two-fold excess (2 mM) of Me_6TREN. In addition, the charge consumption was kept under control to avoid excessive production of Al^{3+} (the charge required to produce 1 mM Al^{3+} was 4.5 C, according to Eq. 4.1). Polymerizations were well-controlled and reached high to very high conversions (**Table 4.6**). *se*ATRP was performed in both potentiostatic and galvanostatic mode, with negligible differences in the produced polymers. These results suggest that non-noble cathodes are completely compatible with a sacrificial anode in both potentiostatic and galvanostatic *e*ATRP, proving the versatility of the method and further simplifying the procedure.

Table 4.6. *e*ATRP of 50 vol% BA in DMF in an undivided cell with an Al anode and an Fe or SS304 cathode.[a]

Entry	WE	E_{app}-$E_{1/2}$ (V)	t (h)	Q (C)	Conv.[b] (%)	$M_{n,th}$ (10^{-3})	M_n (10^{-3})	k_p^{app} (h^{-1})	$Đ$
1	Fe	-0.21	2.5	5.1	90	40.4	37.9	1.01	1.13
2[b]	Fe	-	2.5	4.5	79	35.3	34.4	0.73	1.12
3	SS304	-0.16	4	5.7	77	34.6	31.0	0.44	1.11
4[b]	SS304	-	3	4.9	86	38.6	37.0	0.87	1.10

[a] Polymerization conditions: $C_{BA}/C_{MBiB}/C_{Cu^{II}(OTf)_2}/C_{Me_6TREN}/C_{Et_4NBr}$ = 349/1/0.1/0.1/0.1 with $C_{Cu^{II}}$ = 10^{-3} M; $C_{Et_4NBF_4}$ = 0.1 M; V_{tot} = 15 mL; T = 45 °C. [b] Galvanostatic experiment with 6 current steps. Applied current/time: I (mA)/t (s): 1.5/250, 1.2/300, 0.9/450, 0.6/3000, 0.35/4000, 0.2/≥200 (reprinted with permission from Ref. [10]. Copyright 2016, Royal Chemical Society).

4.3. *e*ATRP of OEOMA in water with non-Pt cathodes

Water is extremely attractive as an environmentally friendly, low-cost solvent for polymerizations. However, triggering controlled polymerizations in water is challenging. As mentioned in **Chapter 2**, only a careful analysis of all equilibria involving system components allowed to obtain nice results in aqueous ATRP.[16, 20]

Briefly, 3 main issues undermine a well-controlled ATRP process in water:

i) Low Cu^{II} halidophilicity:[20] an excess of halide ions should be added to prevent the dissociation of $[X–Cu^{II}L]^+$ to $X^–$ and $[Cu^{II}L]^{2+}$, thereby ensuring the presence of a sufficient amount of deactivator species.

ii) Very high activity of Cu^I species (generally $k_{act} > 10^7$ M^{-1} s^{-1})[21] and high K_{ATRP} (up to 10^{-1}), leading to the generation of a high amount of radicals. Therefore, normally *e*ATRPs are performed at $E_{app} > E^{\ominus}$ of the catalyst to keep the concentration of electrogenerated Cu^I (and hence of radicals) in solution as low as possible.[16, 20]

iii) Fast Cu^I disproportionation, generating Cu^{II} and metallic Cu. For this reason TPMA is normally employed as a ligand, thanks to its ability to strongly bind both Cu^I and Cu^{II}, forming complexes that are stable over a wide range of pH.[20]

Taking these points into account, well-controlled *e*ATRPs of some hydrophilic monomers were reported, by using the traditional electrochemical equipment.[22-24] Nonetheless, a simplified, inexpensive setup is even more desirable in aqueous *e*ATRP to propose a fully sustainable process.

As in organic solvents, a model system was selected to test the new cathodic materials. OEOMA 10 vol% in water was polymerized using $[Br–Cu^{II}TPMA]^+$ as catalyst and HEBiB as initiator, in the presence of 0.1 M Et_4NBr that enhanced the stability of Cu^{II} deactivator and simultaneously served as supporting electrolyte. 10^{-3} M of catalyst was used, with a catalyst/initiator ratio of $C_{[Br-Cu^{II}TPMA]^+}/C_{HEBiB}$ = 1/2, and $E_{app} = E_{1/2} + 0.06$ V = -0.2 V *vs.* SCE.[16, 20]

Not all materials can be used as cathodes in aqueous media, because for example non-noble metals readily undergo oxidation/corrosion. Thus, the oxidation behavior of some materials was studied by means of linear sweep voltammetry, in 10 vol% OEOMA in water. A suitable cathodic material must not be oxidized at the potential applied during polymerization (E_{app} = -0.2 V *vs.* SCE). **Figure 4.11** compares the voltammetric responses of selected materials with the voltammetric pattern of the $[Br–Cu^{II}TPMA]^+$ in the same environment. The anodic onset potential of each material should be compared with the reversible peak couple of the catalyst and, in particular, to the value of applied potential (E_{app} = -0.2 V *vs.* SCE) chosen to run *e*ATRP experiments.

All analyzed materials were stable at E_{app} = -0.2 V *vs.* SCE, except Fe, which is very easily oxidized in aqueous media, and copper, which shows an onset oxidation potential close to E_{app}. The observed anodic currents are due to the oxidation of the electrodes, except in the case of Pt, Au and GC, which do not easily undergo oxidation; indeed, the anodic waves on these electrodes correspond to the electrolyte oxidation. Anyway, the anodic wave defines the working potential window offered by each electrodic material. Therefore, Fe and Cu were discarded as cathodic materials because of their limited electrochemical stability.

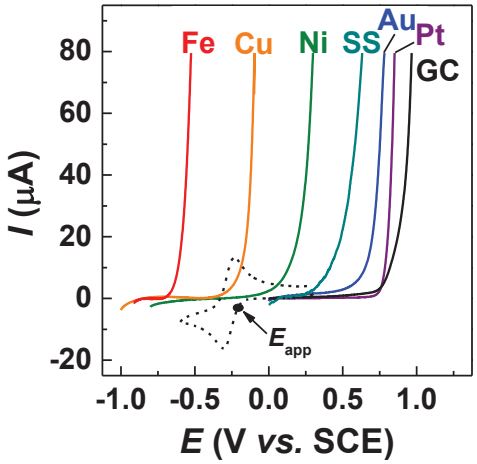

Figure 4.11. Linear sweep voltammetry at v = 0.2 V s^{-1} with tested WEs, labeled on the curves, in 10 vol% OEOMA in water + 0.1 M Et_4NBr. Dashed curve: CV of 10^{-3} M $[Cu^{II}TPMA]^{2+}$ in the same medium, recorded on WE = GC (a 0.3 cm diameter disk), v = 0.2 V s^{-1}, T = 25 °C.

The electrodic materials were then subjected to a blank test to verify their inertness toward the polymerization process. All metals except Fe were tested. As expected, apart from Cu, none of the materials was able to start the polymerization, despite the presence of $[Cu^{II}L]^{2+}$ and RX. Conversely, significant monomer conversion was observed in the presence of a Cu wire. Indeed, metallic Cu generated $[Cu^{I}L]^{+}$ through comproportionation with $[Cu^{II}L]^{2+}$, and Cu^{I} species activated the initiator. The comproportionation between Cu^0 and Cu^{II} species is actually used as a means of Cu^{I} catalyst re-generation in the so-called SARA-ATRP (**Chapter 1**, **Section 1.2**).[26] Normally, an excess of ligand is needed in SARA-ATRP to favor the formation of Cu^{I} in the comproportionation equilibrium, however all ligand present in our system was bound to Cu^{II}, thus the reaction in Eq. 4.2 was suppressed. Nevertheless, Br^- can act as ligand and promote the comproportionation reaction in Eq. 4.3.

$$Cu^0 + [Cu^{II}L]^{2+} + L \rightleftharpoons 2[Cu^{I}L]^{+} \quad (4.2)$$

$$Cu^0 + [Cu^{II}L]^{2+} + 2Br^{-} \rightleftharpoons [Cu^{I}L]^{+} + [Cu^{I}Br_2]^{-} \quad (4.3)$$

The polymerization was fast and well controlled, reaching 96% conversion in 4 h and $Đ$ = 1.18. The ability of metallic Cu to act as supplemental activator and reducing agent in the ATRP equilibrium makes it unsuitable as cathodic material for aqueous *e*ATRP, because the contribution of the comproportionation reaction to the polymerization cannot be suppressed.

4.3.1. Aqueous *e*ATRP with non-Pt cathodes under potentiostatic and galvanostatic control

Potentiostatic *e*ATRP. Pt, Au, glassy carbon (GC), Ti, Ni, 18% NiCr alloy, and 304 stainless steel (SS304) were examined as cathodes (**Figure 4.12**). Before running polymerization experiments, redox properties of the catalyst were investigated on each WE by cyclic voltammetry. CVs of $[Cu^{II}TPMA]^{2+}$ in the polymerization environment, on both small and large GC electrodes showed a quasi-reversible peak couple with $\Delta E_p = E_{pc} - E_{pa}$ = 0.072 V and 0.109 V, respectively (**Figure 4.13**). After the addition of HEBiB a huge increase in the cathodic peak was observed, together with a strong decrease in the anodic peak, as expected considering the high catalytic activity of the Cu complex.[20, 21] Similar voltammetric patterns were observed on Pt and Au. Therefore, during potentiostatic syntheses, the same E_{app} of -0.2 V *vs.* SCE was used for Pt, GC, and Au.

Figure 4.12. Pictures of non-Pt materials used as cathodes for aqueous *e*ATRP (reprinted with permission from Ref. [25]. Copyright 2016, Wiley-VCH).

On non-noble metal electrodes, the voltammetric response was electrochemically much less reversible ($\Delta E_p > 0.25$ V). Highly resistive oxide layers present on the electrode surface increased the overpotential of the electron transfer process, resulting in a cathodic shift of E_{pc} and anodic shift of E_{pa}, hence a higher ΔE_p. Despite the slower electron transfer, the catalytic effect observed on Pt, Au and GC in the presence of HEBiB was evident also on non-noble metal electrodes (*e.g.* on Ni, see **Figure 4.13b**). However, owing to the slower electron transfer on these electrodes, the catalytic reduction wave was shifted to more negative potentials. Therefore, when non-noble metals were used as cathodes for *e*ATRP under potentiostatic mode, E_{app} was shifted to more negative values (**Table 4.7**) to obtain roughly the same cathodic current observed on GC (**Figure 4.13b**), similarly to the procedure adopted in organic solvents (**Section 4.2.1**).

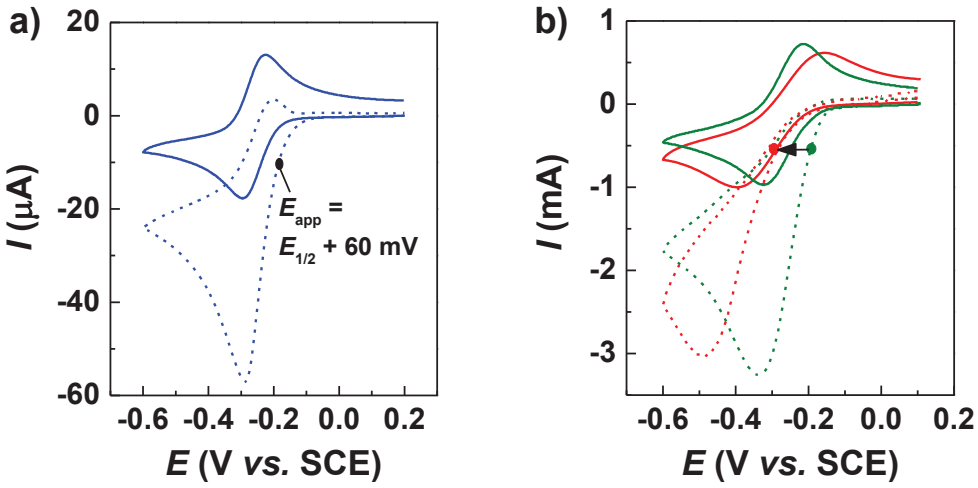

Figure 4.13. Cyclic voltammetry of 10^{-3} M $[Cu^{II}TPMA]^{2+}$ in 10 vol% OEOMA in H_2O + 0.1 M Et_4NBr, on a) a GC disk (d = 3 mm) or b) GC foil (green) or Ni wire (red), recorded at 0.2 V s^{-1} in the absence (solid lines) and presence (dashed lines) of 2×10^{-3} M HEBiB.

Under constant applied potential, Pt provided fast and well-controlled *e*ATRP with 95% conversion in 4 h, $Đ = 1.17$ and high initiator efficiency (I_{eff}), *i.e.* the ratio between experimental and theoretical M_n (**Table 4.7, entry 1**). Similar results were obtained with GC and Au under the same potentiostatic conditions (**Table 4.7, entries 2 and 3**). The apparent propagation rate constant, k_p^{app}, slightly increased with increasing electrode area (A), reflecting the dependence of Cu^{II} reduction rate on A. These results show that it is possible to efficiently trigger and control *e*ATRP of OEOMA at fixed E_{app} on GC and noble metal cathodes (**Figure 4.14**).

Table 4.7. Potentiostatic *e*ATRP of 10 vol% OEOMA in H_2O.[a]

Entry	WE	A (cm^2)	E_{app} (V *vs.* SCE)	t (h)	Q (C)	Conv. (%)	$M_{n,th}$ (10^{-3})	M_n (10^{-3})	k_p^{app} (h^{-1})	$Đ$	I_{eff} (%)
1	Pt	6	-0.2	4	3.2	95	51.5	62.0	0.77	1.17	83
2	Au	5	-0.2	4	3.8	89	48.2	62.0	0.54	1.25	78
3	GC	4	-0.2	5.5	2.0	92	50.1	63.6	0.45	1.15	79
4	Ti	5	-0.2	6	0.2	56	30.5	53.8	0.09	1.17	57
5	Ni	9	-0.32[c]	1.5	3.4	87	46.2	58.2	0.01	1.56	79
6	NiCr	5	-0.32[c]	5.5	0.6	64	35.3	63.9	0.13	1.08	55
7	SS304	5	-0.32[c]	6	3.2	90	48.6	137.1	0.41	1.76	35

[a] Polymerization conditions: $C_{OEOMA}/C_{HEBiB}/C_{Cu^{II}(OTf)_2}/C_{TPMA}/C_{Et_4NBr}$ = 216/2/1/1/100. $C_{Cu^{II}}$ = 10^{-3} M, V_{tot} = 15 mL, T = 25 °C. [b] Estimated geometrical surface area. [c] E_{app} was changed to account for the slower electron transfer (**Figure 4.13b**) (reprinted with permission from Ref. [25]. Copyright 2016, Wiley-VCH).

Conversely, non-noble metal cathodes and alloys did not provide good results in potentiostatic *e*ATRP. Long induction periods, during which no appreciable polymerization occurred, were observed together with and low I_{eff} (*e.g.* 2 h of induction period with NiCr, **Figure 4.14**).

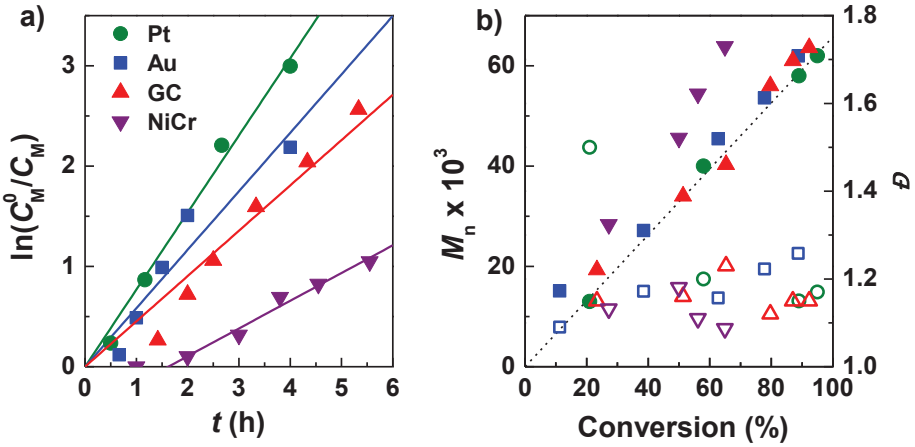

Figure 4.14. Potentiostatic *e*ATRP of OEOMA 10 vol% in H_2O, with different WEs. a) Kinetic plot, b) $Đ$ and MWs evolution *vs.* conversion. Polymerization conditions: $C_{OEOMA}/C_{HEBiB}/\boldsymbol{C_{Cu^{II}(OTf)_2}}/C_{TPMA}/\boldsymbol{C_{Et_4NBr}}$ = 216/2/1/1/100, $\boldsymbol{C_{Cu^{II}}}$ = 10^{-3} M, $E_{app} = E_{1/2} + 0.06$ V, V_{tot} = 15 mL, T = 25 °C (adapted with permission from Ref. [25]. Copyright 2016, Wiley-VCH).

One possible reason for induction periods could be the presence on the electrode surface of a passivating oxide layer, which must be removed before triggering the

polymerization. Actually, during electrolysis at a fixed E_{app} value, the current should decrease because of gradual consumption of Cu^{II} species. Unexpectedly, chronoamperometry recorded during *e*ATRP on Ni (**Figure 4.15a**) and SS304 showed an increase in *I* value during the first 20 minutes of electrolysis, followed by a smooth decay. This unusual behavior is likely due to modifications of surface properties of the metal (*i.e.* removal of oxide layers from the surface) occurring in the initial stages of electrolysis. It follows that the electrode becomes more activated as the electrolysis proceeds, resulting in a decrease of the required overpotential and enhancement of current. This unpredictable increase of current led to fast but poorly controlled polymerization.

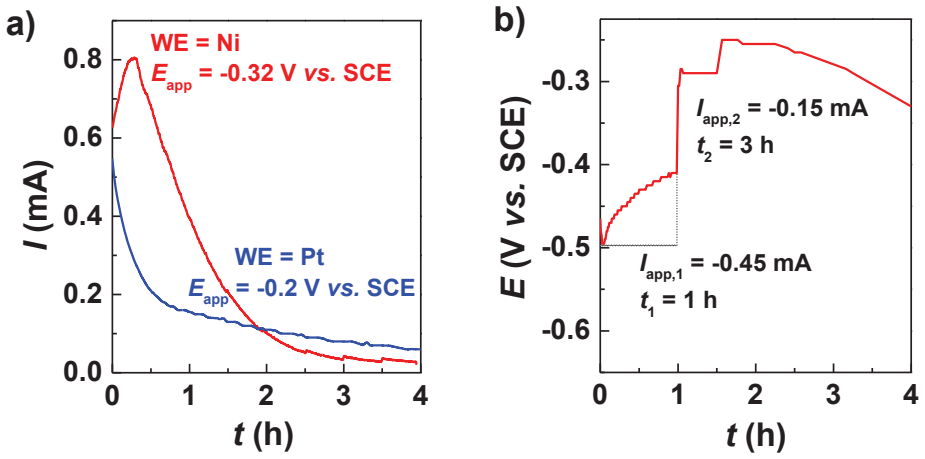

Figure 4.15. a) Chronoamperometry recorded during *e*ATRP of 10 vol% OEOMA in H_2O on Pt at E_{app} = -0.2 V *vs.* SCE (blue line) or Ni at E_{app} = -0.32 V *vs.* SCE (red line). b) Chronopotentiometry recorded during a galvanostatic *e*ATRP of 10 vol% OEOMA in H_2O on Ni. Reaction conditions: $C_{OEOMA}/C_{HEBiB}/C_{Cu^{II}(OTf)_2}/C_{TPMA}/C_{Et_4NBr}$ = 216/2/1/1/100, $C_{Cu^{II}}$ = 10^{-3} M, V_{tot} = 15 mL, T = 25 °C.

Galvanostatic *e*ATRP. The first attempt to avoid induction periods on non-noble metal electrodes consisted in switching from a potentiostatic mode of electrolysis to a galvanostatic approach. Actually, under galvanostatic conditions, the rate of Cu^{II} reduction is less influenced by the nature of electrode material and its surface area. Fixed current steps to be applied were selected by splitting the chronoamperometry curve registered during the potentiostatic *e*ATRP on Pt (**Figure 4.16**). In the first part, a high current was applied to quickly reduce Cu^{II} to Cu^{I}, while in the second part a much lower current was needed to slowly re-generate Cu^{I} by reduction of the deactivator species.[2, 3] This strategy provided a significant improvement of the performances of non-noble metal cathodes, reaching conversions > 80% in 4 h (**Table 4.8**). Nevertheless, induction periods were still observed.

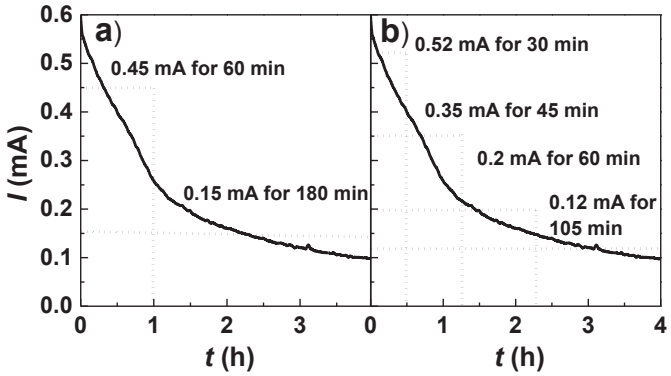

Figure 4.16. Splitting of the chronoamperometry registered on Pt (solid lines) during potentiostatic *e*ATRP (**Table 4.7, entry 1**) in two a) or four b) current steps (reprinted with permission from Ref. [25]. Copyright 2016, Wiley-VCH).

In order to shed some light on issues concerning these materials, the potential of the WE was monitored with respect to a saturated calomel reference electrode during galvanostatic electrolysis. It is expected that *E* will shift to more negative values since, as Cu^{II} is consumed, a higher overpotential is required to maintain the applied constant current.[3] **Figure 4.15b** shows a typical *E vs. t* plot recorded during galvanostatic synthesis with Ni and 304SS cathodes. Initially, the working potential became less negative instead of shifting to more negative values. This unusual behavior is in agreement with the postulated electrode activation during the initial stages of electrolysis, thus requiring a smaller overpotential to maintain the fixed applied current. After *ca.* 2 h, the working potential started to shift cathodically, because of the overpotential produced by the decrease of $[Cu^{II}TPMA]^{2+}$ concentration due to its continuous reduction to $[Cu^{I}TPMA]^{+}$.

Table 4.8. Galvanostatic *e*ATRP of 10 vol% OEOMA in H_2O on non-noble metal cathodes.[a]

Entry	WE	*t* (h)	*Q* (C)	Conv. (%)	$M_{n,th}$ (10^{-3})	M_n (10^{-3})	k_p^{app} (h^{-1})	*Đ*	I_{eff} (%)
1	Ti	3	2.7	81	44.1	91	0.40	2.09	48
2	Ni	4	3.2	83	45.2	91.8	0.50	1.29	48
3	NiCr	5	3.8	93	50.7	86.8	0.61	1.16	58
4	SS304	4	3.2	79	42.7	130	0.30	1.18	33

[a] Polymerization conditions: $C_{OEOMA}/C_{HEBiB}/C_{Cu^{II}(OTf)_2}/C_{TPMA}/C_{Et_4NBr}$ = 216/2/1/1/100, $C_{Cu^{II}}$ = 10^{-3} M, *T* = 25 °C. Current steps: 0.45 mA for 1 h, followed by 0.15 mA for 3 h.

Pre-electrolysis of Cu^{II} species. Low I_{eff} values were observed with non-noble cathodes even by working in a galvanostatic mode. Therefore, another strategy was adopted. The huge discrepancy between experimental M_n and $M_{n,th}$ suggested that a significant portion of RX was consumed in surface-assisted side reactions before reacting with the monomer. To overcome this problem, a pre-electrolysis of Cu^{II} species was performed, meaning that the Cu^{II} complex was partially converted (*ca.* 50%) into the active Cu^{I} species, before adding the initiator (**Scheme 4.1**). In this way, when HEBiB was injected in solution, it immediately reacted with the Cu^{I} species previously generated, thus eliminating any induction period. In fact, galvanostatic *e*ATRP with pre-electrolysis of Cu^{II} showed I_{eff} > 75% (**Table 4.9, entries 1-3**) and no induction period on WE = Ti, NiCr, and SS304 (**Figure 4.17a**). Polymerizations proceeded to > 90% conversion in 3-4 h, with linear first order kinetics. Such results underline that non-noble metals could be efficiently used, adopting a simple galvanostatic mode with delayed introduction of initiator into the reaction medium.

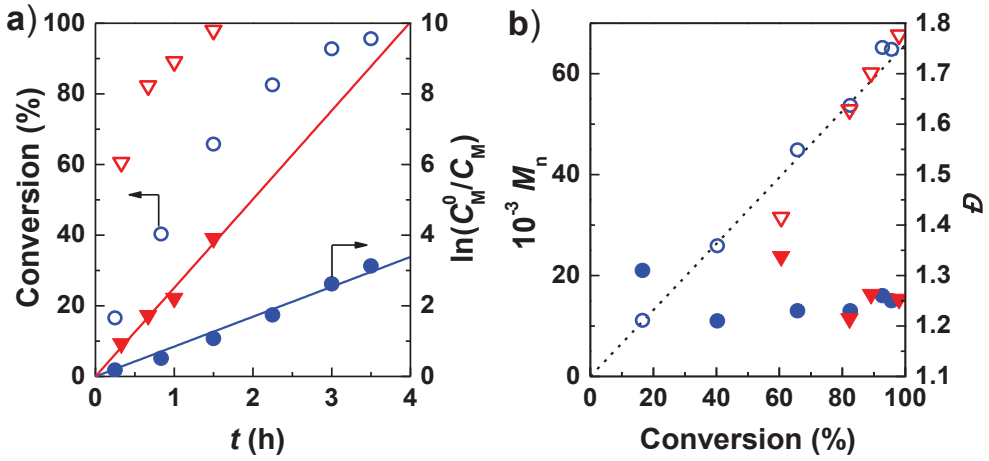

Figure 4.17. Galvanostatic *e*ATRP of OEOMA 10 vol% in H_2O + 0.1 M Et_4NBF_4, on WE = SS304, with (blue) 25 min pre-electrolysis, I = 0.45 mA, and 2 current steps (I_{app} = -0.45, 0.15 mA for t = 35, 180 min), and (red) 22 min pre-electrolysis, I = 0.52 mA, and 4 current steps (I_{app} = 0.52, 0.35, 0.2, 0.12 mA for 8, 45, 60, 130 min). a) Kinetic plot, and b) $Đ$ and MWs evolution *vs.* conversion. Other conditions: $C_{OEOMA}/C_{HEBiB}/C_{Cu^{II}(OTf)_2}/C_{TPMA}/C_{Et_4NBr}$ = 216/2/1/1/100, $C_{Cu^{II}}$ = 10^{-3} M, V_{tot} = 15 mL, T = 25 °C (adapted with permission from Ref. [25]. Copyright 2016, Wiley-VCH).

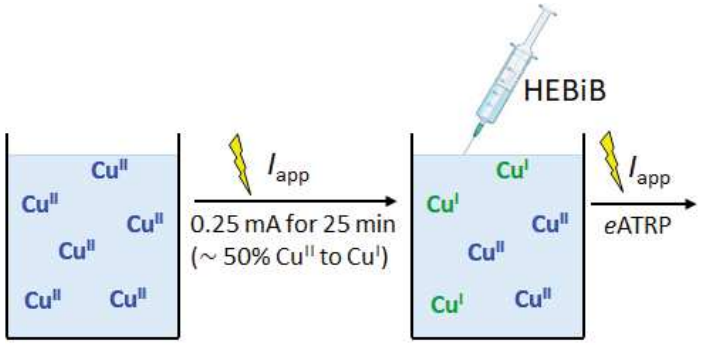

Scheme 4.1. Schematic representation of galvanostatic *e*ATRP with pre-electrolysis of Cu^{II}.

Table 4.9. Galvanostatic *e*ATRP with pre-electrolysis of 10 vol% OEOMA in H_2O.[a]

Entry	WE	Current steps[b]	t (h)	Q (C)	Conv. (%)	$M_{n,th}$ (10^{-3})	M_n (10^{-3})	k_p^{app} (h^{-1})	$Đ$	I_{eff} (%)
1	Ti	2[c]	4	2.97	92	50.1	68.0	0.76	1.32	76
2	NiCr	2	3	2.0	98	53.1	71.7	1.28	1.31	74
3	SS304	2	3.5	2.3	96	51.8	64.8	0.85	1.26	80
4	NiCr	4	2	2.0	92	49.8	58.5	1.33	1.18	85
5	SS304	4	1.5	1.6	98	53.1	67.7	2.51	1.25	78
6[d]	NiCr	4	1.5	1.6	92	49.8	76.1	1.67	1.21	65
7[d]	SS304	4	2	2.0	89	48.3	92.5	0.91	1.39	52

[a] Polymerization conditions: $C_{OEOMA}/C_{HEBiB}/C_{Cu^{II}(OTf)_2}/C_{TPMA}/C_{Et_4NBr}$ = 216/2/1/1/100. Initial $C_{Cu^{II}} = 10^{-3}$ M, T = 25 °C. [b] 2 current steps: 0.45, 0.15 mA for 1 and 3 h, respectively, with pre-electrolysis at I = 0.45 mA for 25 min. 4 current steps: 0.52, 0.35, 0.20, 0.12 mA for 8, 45, 60, 130 min, respectively, with pre-electrolysis at I = 0.52 mA for 22 min. [c] Pre-electrolysis at I = 0.45 mA for 10 min. [d] Undivided cell with Al anode; $C_{Cu^{II}(OTf)_2}/C_{TPMA}$ = 1/2 (reprinted with permission from Ref. [25]. Copyright 2016, Wiley-VCH).

The control over polymer growth was further improved by increasing the number of current steps during galvanostatic *e*ATRPs, preceded by pre-electrolysis of Cu^{II}.[2, 10] By switching from 2 to 4 current steps, $Đ$ decreased and M_n was much closer to $M_{n,th}$ when NiCr was used as cathode, while no significant differences were observed in the case of SS304 (**Table 4.9, entries 4 and 5**).

4.3.2. Pt-free setup for aqueous *e*ATRP

Aqueous *e*ATRP with non-noble metal cathodes was investigated in an undivided cell with a sacrificial Al anode,[2] essentially in a Pt-free setup. To minimize the effect of the

competition between Cu and Al ions in binding the ligand, already observed in organic solvents (**Section 4.2**),[10] these *se*ATRPs were carried out with a $C_{Cu^{II}(OTf)_2}/C_{TPMA}$ ratio 1/2. The reaction was fast, reaching *ca.* 90% in ≤ 2 h, but the dispersity was slightly higher and initiator efficiency lower if compared to experiments run in a divided cell under otherwise identical conditions (**Table 4.9,** compare **entries 4-5** with **6-7**). It is worth noting, however, that this setup is highly simplified and much less expensive than traditional *e*ATRP in divided cells.

ICP-MS analysis of final solutions revealed that a very low amount of metal ions was released from the cathodic materials (**Table 4.10**). Therefore, additional purification procedures were not required after *e*ATRP with any of the tested cathodes. In contrast, when an Al wire was used as a sacrificial anode, some Al ions were found in solution at the end of the polymerization, justifying the use of excess TPMA in *se*ATRPs.

Table 4.10. ICP-MS determination of metal traces in the reaction medium at the end of polymerization.[a]

Cathode	Total concentration of metal ions (M)			
	Fe	Ni	Cr	Al
-[b]	3.6×10^{-6}	$<10^{-6}$	$<10^{-6}$	-
Ni	1.6×10^{-5}	1.4×10^{-5}	$<10^{-6}$	-
304SS	1.6×10^{-4}	1.0×10^{-6}	$<10^{-6}$	-
304SS[c]	8.6×10^{-4}	2.4×10^{-6}	4.0×10^{-6}	2×10^{-3}

[a] Polymerization conditions: $C_{OEOMA}/C_{HEBiB}/C_{Cu^{II}(OTf)_2}/C_{TPMA}/C_{Et_4NBr}$ = 216/2/1/1/100 with initial $C_{Cu^{II}}$ = 10^{-3} M, T = 25 °C. [b] Blank experiment, same setup as *e*ATRP, but without any electrode immersed in solution. [c] Al wire was used as a sacrificial anode in an undivided cell.

Scanning electron microscopy images of Ti and NiCr electrodes, before and after *e*ATRP were recorded to observe possible modifications in electrodic surface morphologies, occurring in the course of the syntheses. **Figure 4.18** shows that surface morphologies were not modified and metal corrosion did not occur, suggesting that the same cathodic material can be reused several times. These images, together with the results of blank experiments and ICP-MS analyses, proved once again that the cathodes were not chemically involved in direct C–X activation, merely acting as a source of electrons for Cu^{II} reduction.

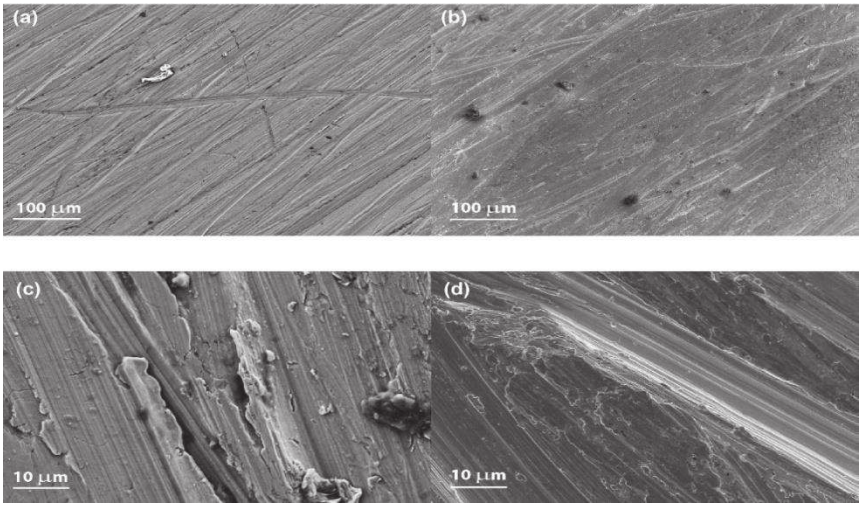

Figure 4.18. Scanning electron microspy images of SS304 a, b) and Ti c, d) electrode surfaces. Images were taken before a, c) and after b, d) *e*ATRP of 10 vol% OEOMA in H_2O.

4.4. Coupled copper cathode/anode for *e*ATRP of BA in DMF

Copper is largely used as electrodic material for electrochemical analysis and applications. However, cathodic materials for *e*ATRP need to be inert toward the polymerization process, thus copper was initially discarded in this work. As previously mentioned, Cu^0 can act as both a reducing agent, by a comproportionation reaction with Cu^{II}, and a supplemental activator, able to reduce RX initiators. For this reason, when Cu^0 is present, the process is called supplemental activator and reducing agent (SARA) ATRP.[8, 9]

In principle, metallic copper can act as an *e*ATRP cathode in the absence of any excess of ligand and halogen ions, because these elements are required to promote the compropotionation reactions, according to Eqs. 4.2 and 4.3. Thus, copper cannot be used as a WE in aqueous media, where an excess of X^- is necessary (**Section 4.3**), but it can be tested in organic solvents, where well-controlled *e*ATRPs were achieved with a ratio $C_{Cu^{II}}/C_L/C_{X^-}$ 1/1/1 (**Section 4.2**). Indeed, a blank test was performed, using the same setup described in **Section 4.2** (1 mM $C_{Cu^{II}}/C_{Me_6TREN}/C_{Br^-}$) and an activated copper wire as WE. No potential was applied, and as expected no conversion was observed even after 4 hours, because neither L nor X^- was available to start the comproportionation reaction; both ligands were engaged in the formation of a highly stable $[X–Cu^{II}Me_6TREN]^+$. *e*ATRP of

BA (50 vol%) in DMF with WE = Cu gave 78% conversion in 2 h, $Đ$ = 1.18 (**Table 4.11, entry 1**), in line with the results obtained with other tested cathodic materials (**Table 4.1**).

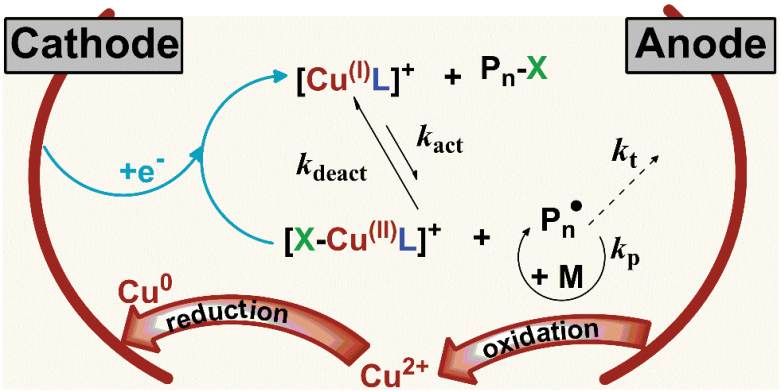

Scheme 4.2. Schematic representation of *e*ATRP mechanism with coupled Cu cathode/anode setup.

Much more interesting will be the use of copper as both cathode and anode for *e*ATRP. Indeed, while employing metallic Cu as a sacrificial anode, Cu^{2+} ions will be released in solution following the anodic oxidation reaction (**Scheme 4.2**). These ions will be reduced again on the cathode and therefore will not affect the polymerization process. However, if an excess of L is present, Cu^{2+} ions can combine with these molecules to give a Cu^{II} complex, $[Cu^{II}L]^{2+}$, that can be reduced to $[Cu^{I}L]^{+}$ at the cathode, thereby catalyzing the polymerization. In this case, the contribution of SARA-ATRP to *e*ATRP cannot be neglected. Indeed, in the presence of excess ligand, $[Cu^{I}L]^{+}$ will be formed also by comproportionation. Therefore, the aim of this work was: *i*) to define the conditions that allow a Cu cathode/anode setup for *e*ATRP, and *ii*) to depict the contribution of both *e*ATRP and SARA-ATRP, while working with a ligand excess.

At first, the activated Cu wire was used only as a sacrificial anode, while a Pt mesh served as the WE. Potentiostatic *e*ATRP was performed with $E_{app} = E_{1/2} - 0.06$ V. The polymerization stopped after 64% conversion in 2 h (**Table 4.11, entry 2**). Cu^0 started depositing on the WE surface few minutes after potential application. Unexpectedly, the recorded current *vs.* time plot (*i.e.* chronoamperometry) showed a rapid enhancement in I, which then remained almost constant at *ca.* 3 mA for the entire duration of the process (**Figure 4.19**). Clearly the charge passed was extremely high, more than 10-times the theoretical value Q_{th} = 1.5 C.

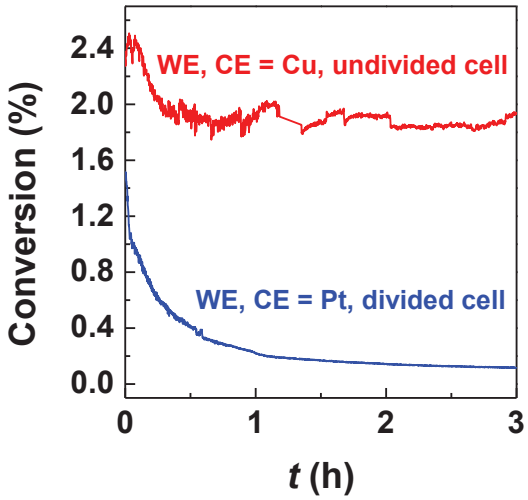

Figure 4.19. Current behavior in *e*ATRP of 50 vol% BA in DMF with a traditional (blue) and new (red) setup (conditions in **Table 4., entry 1** and **Table 4.11, entry 3**).

By replacing the Pt WE with a Cu WE, 83% conversion was achieved in 3 h, with $Đ$ = 1.17 and a linear increase of M_n values with conversion (**Table 4.11, entry 3**). Hence, the coupled copper cathode/anode setup provided a well-controlled process. However, the current behaviour was once again unusual: I remained more or less constant throughout the process, at approximately 2 mA, thus the consumed charge was Q = 20.9 C. By using Eq. 1.27 (**Chapter 1**, **Section 1.4**), which allows to evaluate the extent of radical termination from the amount of electric charge passed, one can estimate the quantity of Cu^0 deposited on the WE surface. This was done by considering that the *e*ATRP was controlled, thus radical termination cannot be higher than 10%, meaning that $n_R \leq 10\% n_{RX}$ (with n_R and n_{RX} standing for the number of moles of terminated chains and initiator, respectively). It follows that the total charge was the sum of Q_{th} = 1.5 C, Q_R = 1.45 C (needed to regenerated Cu^I from Cu^{II} species, if radical termination accounted for 10% of total chains) and the contribution of the bielectronic reduction of Cu^{II} formed at the anode and deposited as Cu^0 at the cathodic surface (Q_{Cu}). This gave Q_{Cu} = 19.4 C, which corresponds to 0.10 mmol of Cu^0 or 1.6 μg of deposited Cu. This estimation does not consider any possible reduction of impurities in solution, or other side-reactions; moreover, the amount of terminated chains might be overestimated. Essentially, a significant amount of metallic copper is deposited on the WE surface and the solution is not very clean. Nevertheless, removal of the WE at the end of electrolysis and column filtration of the final solution can remove Cu^0.

Table 4.11. *e*ATRP of 50 vol% BA in DMF in an undivided cell with a Cu cathode and anode.[a]

Entry	WE	CE	$E_{app} - E_{1/2}$ (V)	I_{app} (mA)	Q^b (C)	t (h)	Conv. (%)	M_n (10^{-3})	$M_{n,th}$ (10^{-3})	k_p^{app} (h^{-1})	$Đ$
1[c]	Cu	Pt	- 0.06	-	1.83	2	78	39.3	35.0	0.85	1.18
2	Pt	Cu	- 0.06	-	20.2	2	64	34.0	28.8	0.51	1.22
3	Cu	Cu	-0.06	-	20.9	3	83	46.1	37.4	0.66	1.17
4	Cu	Cu	-	2	14.4	2	81	41.9	36.4	1.01	1.18
5	Cu	Cu	-	3	21.6	2	82	46.5	36.8	1.01	1.18

[a] Polymerization conditions: $C_{BA}/C_{MBiB}/C_{Cu^{II}(OTf)_2}/C_{Me_6TREN}/C_{Et_4NBr}$ = 349/1/0.1/0.1/0.1, with C_{BA} = 3.49 M; $C_{Et_4NBF_4}$ = 0.1 M; V_{tot} = 15 mL; T = 45 °C. [b] Q (C) = I_{app} (A)*t (s).[c] in divided cell.

The observed constant I value suggested that a galvanostatic *e*ATRP can be performed by applying only one current step. Actually, when I_{app} = 2 mA was applied, the polymerization was well controlled and faster than the potentiostatic synthesis (**Table 4.11, entry 3**). An attempt to increase the polymerization rate by using higher I_{app} did not affect the results, possibly because the process was already diffusion-controlled with I_{app} = 2 mA. Clearly, higher I_{app} means higher charge consumption and hence greater Cu^0 deposit on the WE surface.

Note that it is highly desirable to run a galvanostatic *e*ATRP by appliying only one current value, while preserving the control over the process. In fact, it is extremely simple and inexpensive to connect two Cu wires to a current generator, impose a certain I_{app} and let the system work.

The catalyst loading was drastically reduced from 10^{-3} to 10^{-4} M. Dispersity slightly increased, but the process remained controlled, with M_n matching theoretical values and linearly increasing with conversion (**Table 4.11, entry 2**). The polymerization was slower than in the case of $C_{Cu^{II}} = 10^{-3}$ M, but the process required a very small amount of reagents, as well as a simple, inexpensive setup and facile conditions.

Since the anodic process released Cu^{2+} ions in solution, it would be interesting to use part of these ions as catalyst, *i.e.* avoiding the use of a Cu salt, thus starting with only ligand and Br^- in solution. Therefore, 10^{-4} M Me_6TREN and Br^- were used, and I_{app} = 2 mA. In this case, the contribution of SARA-ATRP must be considered.

Table 4.12. Polymerization of 50 vol% BA in DMF with various techniques. [a]

Entry	Technique	I_{app} (mA)	t (h)	Conv. (%)	M_n (10^{-3})	$M_{n,th}$ (10^{-3})	k_p^{app} (h^{-1})	$Đ$
1	SARA-ATRP[a]	-	3	24	5.53	11.2	0.12	2.49
2	*e*ATRP[b]	2	3.5	73	33.2	32.9	0.39	1.39
3	(SARA+*e*)ATRP[a]	2	3	84	35.4	37.6	0.70	1.30

[a] Initial $C_{Cu^{II}} = 0$ M, $C_{Me_6TREN} = C_{Et_4NBr} = 10^{-4}$ M. [b] $C_{Cu^{II}} = C_{Me_6TREN} = C_{Et_4NBr} = 10^{-4}$ M. General conditions: $C_{BA}/C_{MBiB} = 349/1$ with $C_{BA} = 3.49$ M; $C_{Et_4NBF_4} = 0.1$ M; $V_{tot} = 15$ mL; $T = 45$ °C.

At first, no potential was applied and the system reached 24% conversion in 3 h, but then the process stopped and dispersity was high (**Table 4.12, entry 1**). Such low amounts of L and Br^- seemed not sufficient to ensure a successful SARA-ATRP. Thus, a 2 mA current was applied to the same system in a combination of *e*ATRP and SARA-ATRP, hereafter called (SARA+*e*)ATRP (**Table 4.12, entry 3**). The process was faster and better controlled ($Đ = 1.30$) than the corresponding *e*ATRP, *i.e.* in the presence of Cu salt (**Table 4.12, entry 2**). Interestingly, by overlapping the kinetic plots of SARA-ATRP, *e*ATRP and (SARA+*e*)ATRP, the last appeared as the perfect sum of the other two processes (**Figure 4.20**). The kinetic plot of (SARA+*e*)ATRP was not linear; instead, the conversion sharply increased in the first 30 minutes, then the monomer was much slowly consumed. It seems that the SARA-ATRP mechanism dominated the first part of the reaction, whereas the continuous regeneration of the active catalyst was then ensured by the application of a constant current.

The synergic effect between SARA and *e*ATRP combines a simple setup with the *in situ* generation of both the catalytic species and the reducing agent. Further analysis are required to: *i*) verify the versatility of this approach; *ii*) determine the amount of Cu that remains in produced polymers after removal of the electrodes and simple column filtration.

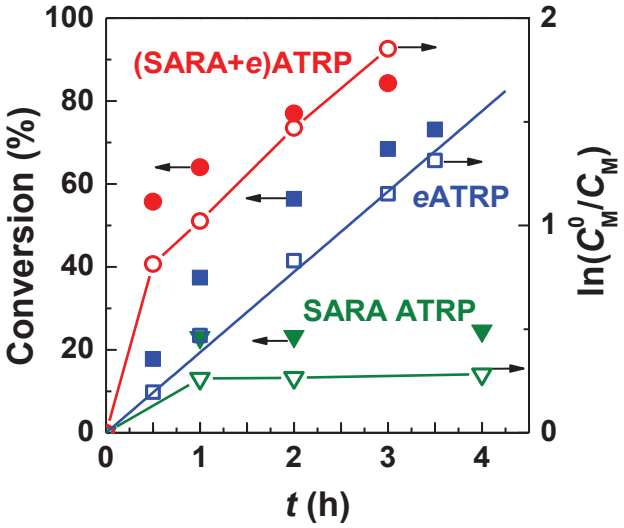

Figure 4.20. Conversion evolution *vs.* time and kinetic plot for the syntheses of 50 vol% BA in DMF. $C_{Cu^{II}} = C_L = C_{Br} = 10^{-4}$ M (blue); $C_{Cu^{II}} = 0$, $C_{Me_6TREN} = C_{Br} = 10^{-4}$ M (green and red).

4.5. Conclusions and perspectives

Non-Platinum electrodes were proved to be effective cathodes for *e*ATRP in both organic and aqueous media. Thus, Pt can be replaced with more affordable and easily functionalizable materials.

Glassy carbon, gold, iron, nickel-chromium, and 304 stainless steel were successfully used as cathodes for *e*ATRP in DMF, operating under both potentiostatic and galvanostatic conditions, and with low catalyst loadings. Non-noble metal electrodes could be used for several consecutive polymerizations, after simple washing in acetone and dilute acid.

Aqueous *e*ATRP performed on glassy carbon, gold, titanium, nickel-chromium, and 304 stainless steel electrodes proceeded with fast kinetics, and the produced POEOMA exhibited low dispersity and good agreement between theoretical and experimental molecular weights. Whereas noble metals and GC worked well under potentiostatic mode, non-noble metals required galvanostatic conditions with pre-electrolysis of Cu^{II} before the addition of RX.

Importantly, ICP-MS analysis confirmed that negligible amounts of metal ions were released during *e*ATRP in both media; therefore, additional polymer purification is not required. Moreover, a Pt-free setup was successfully used, by coupling these cathodes with a sacrificial Al anode, in an undivided cell. When employing a sacrificial Al anode, it is

necessary to use an excess of ligand to prevent the competition between Al^{3+} ions, released by CE oxidation, and Cu^{2+} in binding the ligand.

Finally, some preliminary results were collected on a coupled Cu cathode/anode system, tested in DMF. A "true" galvanostatic approach was possible, with a unique current value applied throughout the process. Furthermore, the copper needed as catalyst can be generated *in situ* from the anodic material oxidation, in a combination of SARA and *e*ATRP.

The proposed setup for *e*ATRP could boost the use of this technique, and pave the way to the scale-up of the process, and the preparation of new functional electrodes and sensors based on inexpensive materials.

References

1. Magenau, A. J.; Strandwitz, N. C.; Gennaro, A.; Matyjaszewski, K. *Science* **2011,** 332, 81-84.
2. Park, S.; Chmielarz, P.; Gennaro, A.; Matyjaszewski, K. *Angewandte Chemie* **2015,** 127, 2418-2422.
3. Magenau, A. J.; Bortolamei, N.; Frick, E.; Park, S.; Gennaro, A.; Matyjaszewski, K. *Macromolecules* **2013,** 46, 4346-4353.
4. Matyjaszewski, K.; Jakubowski, W.; Min, K.; Tang, W.; Huang, J.; Braunecker, W. A.; Tsarevsky, N. V. *Proceedings of the National Academy of Sciences* **2006,** 103, 15309-15314.
5. Li, B.; Yu, B.; Huck, W. T.; Zhou, F.; Liu, W. *Angewandte Chemie* **2012,** 124, 5182-5185.
6. Hosseiny, S. S.; Van Rijn, P. *Polymers* **2013,** 5, 1229-1240.
7. Sun, Y.; Zhang, J.; Li, J.; Zhao, M.; Liu, Y. *RSC Advances* **2017,** 7, 28461-28468.
8. Konkolewicz, D.; Wang, Y.; Zhong, M.; Krys, P.; Isse, A. A.; Gennaro, A.; Matyjaszewski, K. *Macromolecules* **2013,** 46, 8749-8772.
9. Konkolewicz, D.; Wang, Y.; Krys, P.; Zhong, M.; Isse, A. A.; Gennaro, A.; Matyjaszewski, K. *Polymer Chemistry* **2014,** 5, 4396-4417.
10. Lorandi, F.; Fantin, M.; Isse, A. A.; Gennaro, A. *Polymer Chemistry* **2016,** 7, 5357-5365.
11. Bortolamei, N.; Isse, A. A.; Di Marco, V. B.; Gennaro, A.; Matyjaszewski, K. *Macromolecules* **2010,** 43, 9257-9267.
12. De Paoli, P.; Isse, A. A.; Bortolamei, N.; Gennaro, A. *Chemical Communications* **2011,** 47, 3580-3582.
13. Matyjaszewski, K.; Sumerlin, B. S.; Tsarevsky, N. V., *Progress in controlled radical polymerization: mechanisms and techniques*. ACS Publications: 2012.
14. Ribelli, T. G.; Augustine, K. F.; Fantin, M.; Krys, P.; Poli, R.; Matyjaszewski, K. *Macromolecules* **2017**, 50, 7920-7929.
15. Guo, J. K.; Zhou, Y. N.; Luo, Z. H. *AIChE Journal* **2015,** 61, 4347-4357.

16. Bortolamei, N.; Isse, A. A.; Magenau, A. J.; Gennaro, A.; Matyjaszewski, K. *Angewandte Chemie* **2011,** 123, 11593-11596.

17. Konkolewicz, D.; Magenau, A. J.; Averick, S. E.; Simakova, A.; He, H.; Matyjaszewski, K. *Macromolecules* **2012,** 45, 4461-4468.

18. Simakova, A.; Averick, S. E.; Konkolewicz, D.; Matyjaszewski, K. *Macromolecules* **2012,** 45, 6371-6379.

19. Pan, X.; Malhotra, N.; Simakova, A.; Wang, Z.; Konkolewicz, D.; Matyjaszewski, K. *Journal of the American Chemical Society* **2015,** 137, 15430-15433.

20. Fantin, M.; Isse, A. A.; Gennaro, A.; Matyjaszewski, K. *Macromolecules* **2015,** 48, 6862-6875.

21. Fantin, M.; Isse, A. A.; Matyjaszewski, K.; Gennaro, A. *Macromolecules* **2017,** 50, 2696-2705.

22. Chmielarz, P.; Krys, P.; Park, S.; Matyjaszewski, K. *Polymer* **2015,** 71, 143-147.

23. Chmielarz, P.; Park, S.; Simakova, A.; Matyjaszewski, K. *Polymer* **2015,** 60, 302-307.

24. Fantin, M.; Isse, A. A.; Venzo, A.; Gennaro, A.; Matyjaszewski, K. *J. Am. Chem. Soc* **2016,** 138, 7216-7219.

25. Fantin, M.; Lorandi, F.; Isse, A. A.; Gennaro, A. *Macromolecular rapid communications* **2016,** 37, 1318-1322.

26. Konkolewicz, D.; Krys, P.; Góis, J. R.; Mendonça, P. V.; Zhong, M.; Wang, Y.; Gennaro, A.; Isse, A. A.; Fantin, M.; Matyjaszewski, K. *Macromolecules* **2014,** 47, 560-570.

Chapter 5.

Aqueous *e*ATRP of acrylic acid

Table of contentes

5.1. Introduction and aim of the work

ATRP is a versatile and powerful process, however it is extremely challenging to achieve the desired control over polymerizations of some monomers.[1] Particularly, two classes of monomers are requiring great efforts: less active monomers (*i.e.* monomers that do not own a radical stabilizing group in their structure, such as vinyl acetate and alkenes) and acidic monomers.

Focusing on the latter, many reasons were proposed for the failure in controlling polymerizations of methacrylic and acrylic acid (MAA and AA, respectively, **Figure 5.1**), especially in water. The most accredited hypothesis proposed a harmful interaction between monomer molecules or growing chains and the copper catalyst, forming metal carboxylates that are inactive in the ATRP equilibrium.[2, 3] Another reason is the protonation of conventional ATRP catalysts in acidic environments.[4]

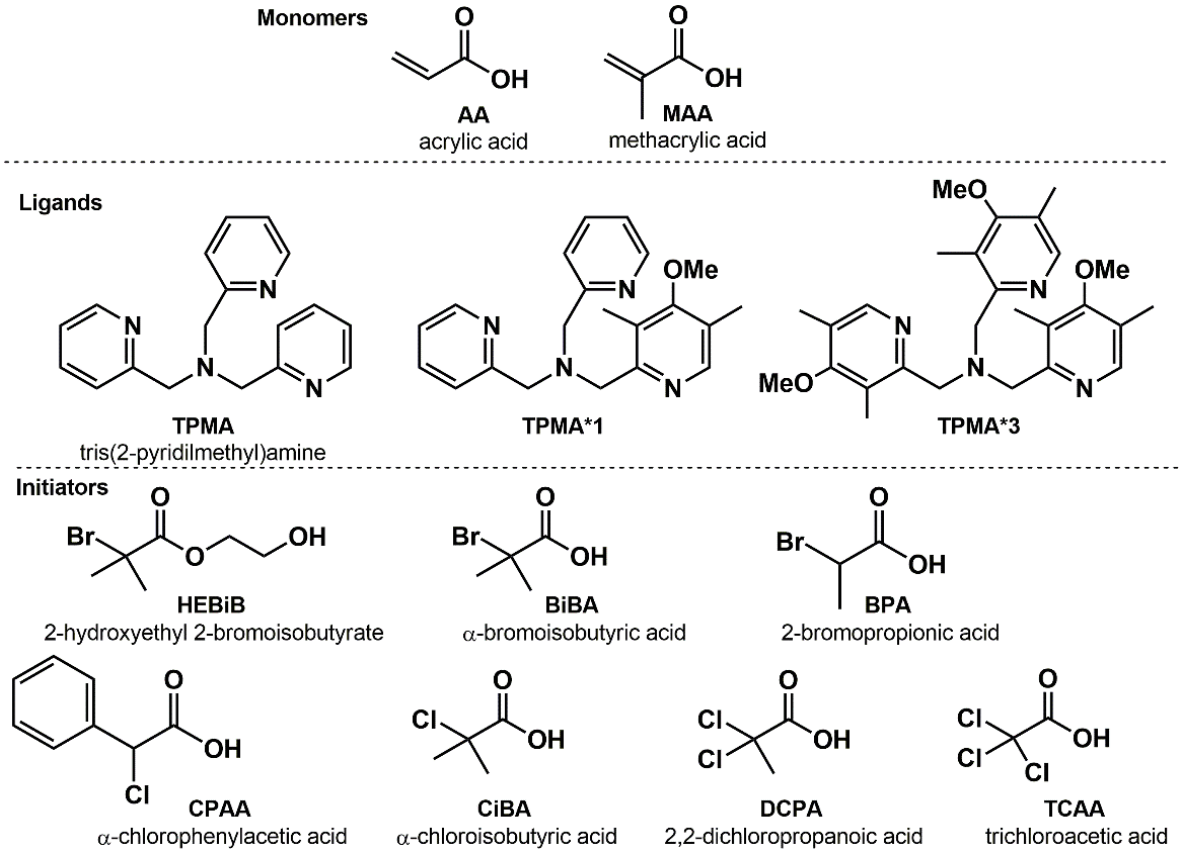

Figure 5.1. Structures of compounds relevant to the present chapter.

Recently, Fantin et al. proved that the real problem affecting ATRP of MAA was cyclization of growing chains (**Figure 5.2a**).[5] This important side reaction led to the formation of lactones, thereby losing the active C–X chain-end, and stopping the propagation process. This lactonization process is thermodynamically triggered by the generation of a stable five-membered cyclic structure. Electrochemical investigations and NMR spectroscopy were crucial in the understanding and detection of this side-reaction.

In order to minimize the extent of cyclization, three different tricks were adopted: *i*) switch from Br to Cl chain end, because Cl^- is a poor living group; *ii*) lower the pH to decrease the amount of nucleophiles; *iii*) increase the polymerization rate to reduce the contribution of side reactions. The selected catalyst was Cu/TPMA, which showed good

stability even under strongly acidic conditions. Successful *e*ATRPs and SARA ATRPs were performed with high excess of Cl^- and pH as low as 0.9. The use of a 4-fold excess of TPMA compared to $C_{Cu^{II}}$ slightly improved polymerization results. First-order kinetics, good accordance between theoretical and experimental MWs and $Đ < 1.5$ were obtained, also targeting DP up to 2000.

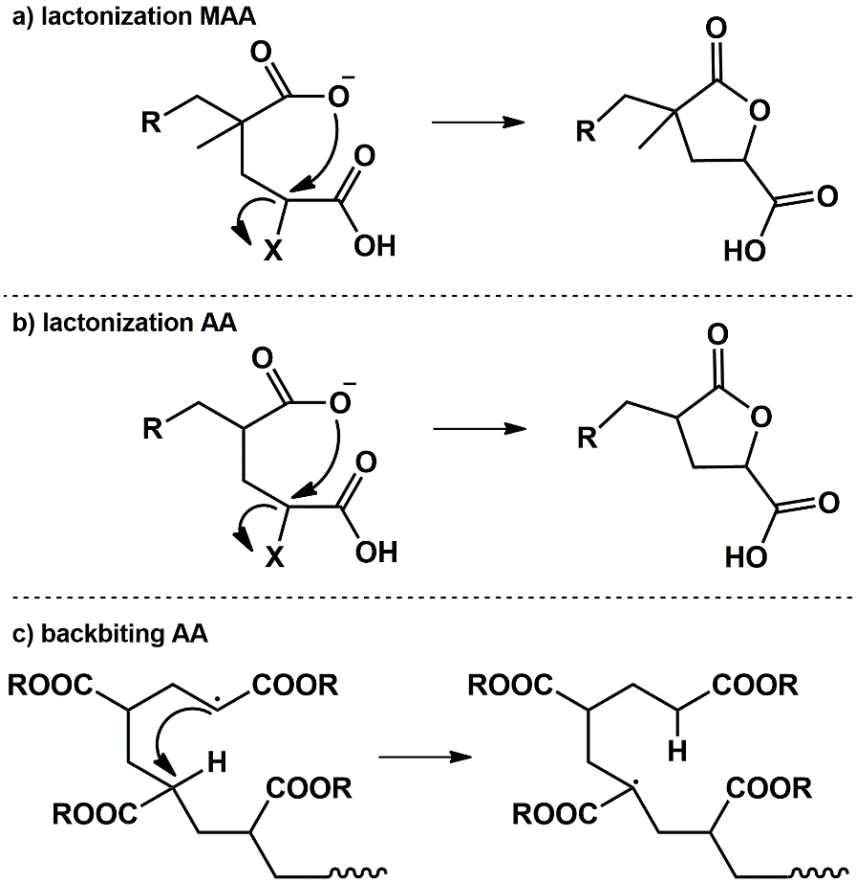

Figure 5.2. Important side reactions in ATRP of acidic monomers: lactonization of growing chains of a) MAA, and b) AA; c) intermolecular chain transfer of PAA chains.

Besides methacrylic acid, also acrylic acid is an important monomer because PAA is largely used as a scale inhibitor and dispersant.[6] These monomers cannot be polymerized by ionic methods, thus radical polymerization techniques are the only way to achieve controlled structures. The pKa of AA in water at room temperature is 4.75. PAA formed by conventional free-radical polymerization is characterized by branching and low MWs.[7] The main cause is the enhanced process of chain transfer to a monomer or polymer chain. The intermolecular chain transfer, also called backbiting, transforms a secondary propagating radical into a tertiary mid-chain radical (**Figure 5.2c**), which is a poorly propagating and terminating species. Thus backbiting strongly affects the degree of branching but also the polymerization kinetics.

Because of steric effects, the backbiting process is much less important for methacrylates than acrylates.[8] It follows that, whereas structural similarities between AA and MAA may suggest that the two monomers will present similar issues during polymerizations, AA may raise additional problems that require different approaches. Controlled polymerizations of AA were reported via NMP[9] in dioxane at 120 °C and RAFT[6] in ethanol at 90 °C. Clearly, milder conditions and the use of water as solvent are desirable for biocompatibility purposes. The following sections report the results obtained in aqueous *e*ATRP of AA, starting from successful conditions for MAA and then adjusting the system to improve the control and better understand reaction mechanisms.

5.2. Effect of halogen ions and initiator structure

By looking at MAA and AA structures it seems reasonable to expect that also acrylic acid will suffer from the lactonization reaction (**Figure 5.2b**).[5] In fact, the cyclization of growing chains will generate once again stable 5-membered cyclic structures that are inactive in the ATRP equilibrium. *e*ATRP of AA (10 vol% in water) was firstly performed in the presence of 0.1 M Br^-, using HEBiB as initiator and $[Cu^{II}TPMA]^{2+}$ as catalyst with $E_{app} > E_{1/2}$, but the process stopped after 3 h with only 5% conversion (**Figure 5.3a**). A very similar result was reported for MAA under identical conditions, supporting the hypothesis that also AA is affected by the cyclization side reaction.

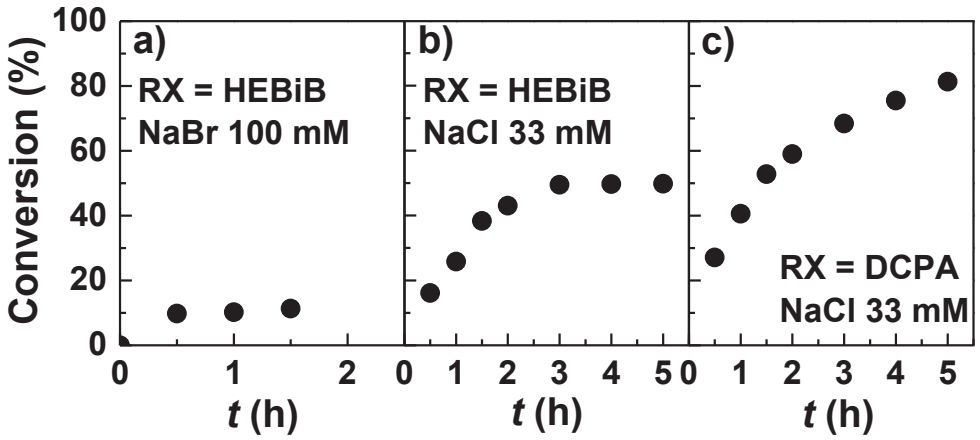

Figure 5.3. Conversion vs. time plots for aqueous *e*ATRP of AA 10 vol% in water performed at 25 °C on a Pt electrode at a) E_{app} = - 0.2 V *vs.* SCE, b,c) E_{app} = - 0.3 V *vs.* SCE. Polymerization conditions: $C_{AA}/C_{RX}/C_{Cu^{II}(OTf)_2}/C_{TPMA}$ = 175/1/0.1/0.4. C_{AA} = 1.46 M. pH = 2.2.

Thus, Br^- ions were replaced with Cl^-, while the pH was not changed at this stage (pH = 2.2 self-imposed by the system). Much more critical is the enhancement of the polymerization rate. Actually, in general, acrylates display at least one-order of magnitude higher propagation rate constants (k_p) compared to methacrylates.[10, 11] However, under standard ATRP conditions their polymerization is much slower. The main cause is the much lower activation rates of acrylate-like dormant species, compared to methacrylate chain ends. The electrochemical mediation of ATRP offered the possibility to affect the overall rate by tuning two different parameters. The most effective one is the applied potential: as previously explained, negative E_{app} values relative to the standard potential of the catalyst determine a huge amount of Cu^I, *i.e.* propagating radicals, in solution. Another possibility is the use of a WE with a large surface area; in fact, a proportionality between the WE area and the polymerization rate was for example observed in **Chapter 1** (**Section 4.3.1**).[12]

Thus, two linked Pt meshes were used as WE (geometrical total area *ca.* 30 cm^2), whereas E_{app} = - 0.3 V *vs.* SCE, which is about 0.06 V more negative than E^e of $[Br–Cu^{II}TPMA]^+$ in the working solution. Moreover, 0.03 M Cl^- was used instead of 0.3 M as in *e*ATRP of MAA. Indeed, excess halide ions increased the stability of $[X–Cu^{II}L]^+$, but they also strongly decreased the polymerization rate.[13, 14] The selected amount of Cl^- ions was aimed to realize a good compromise, ensuring both a sufficiently fast polymerization and enough deactivator species in solution. These conditions gave 50% conversion in 3 h (**Figure 5.3b**), but $Đ$ was still very high and I_{eff} was below 50% (**Table 5.**, **entry 1**).

Table 5.1. Effect of RX nature on *e*ATRP of 10 vol% AA in water at T = 25 °C.[a]

Entry	RX	Q (C)	Conv. (%)[b]	k_p^{app} (h^{-1})	$M_{n,th}$ (10^{-3})	M_n (10^{-3})	I_{eff} (%)	$Đ$
1	HEBiB	13.6	50	0.26	6.4	13.8	46	1.83
2	BIBA	13.9	52	0.19	6.7	15.5	43	1.74
3	BPA	12.9	49	0.15	6.3	12.7	50	1.82
4	DCPA	14.6	81	0.37	10.3	15.7	65	1.43
5	TCAA	21.8	87	0.44	11.0	17.9	61	1.36
6	CIBA	8.8	56	0.17	7.1	12.8	56	1.76
7	CPAA	12.4	56	0.19	7.1	17.5	41	1.72

[a] pH = 2.2. $C_{AA}/C_{RX}/C_{Cu^{II}(OTf)_2}/C_{TPMA}/C_{Cl^-}$ = 175/1/0.1/0.4/4. C_{AA} = 1.46 M. Estimated electrode area 30 cm^2. [b] conversion registered after 5 h.

HEBiB was replaced with RBr initiators bearing a hydroxyl group to better mimic the acidic monomer (**Table 5.1**, **entries 2 and 3**). However, no improvements were observed. The successive step was the use of a chlorinated initiator to have only C-Cl functionalities in the course of the process. Tested RCl initiators are reported in **Figure 5.1**. Surprisingly, high conversions and low dispersity PAA were obtained only with initiators that owned two or three C–Cl bonds in their structures (**Table 5.1**, **entries 4 and 5**). All other RCl initiators were not efficient, although displaying huge reactivity in some cases, with high catalytic reducing currents recorded by CV. 81% conversion was reached in 5 h, with $Đ$ = 1.43 (**Figure 5.3c**), when RX = DCPA, which has two C–Cl bonds, was used. TCAA, which owns 3 C–Cl bonds, gave 87% conversion in 5 h, and PAA with lower dispersity, $Đ$ = 1.36.

For MAA, conversions > 90% were reached in *ca.* 4 h, even by using less reactive initiators. This observation is in line with the lower K_{ATRP} of acrylic monomers, compared to methacrylates.[1] The molecular dispersity values achieved in this work are among the lowest reported so far for PAA,[6, 9] despite seeming quite high if compared to what is observed in ATRP of conventional monomers (an example of GPC traces of PAA obtained herein is reported in **Figure 5.4**). The main reason can be the huge extent of backbiting that occurs during AA polymerizations, which can also be responsible for the strong decrease in ATRP rate at high conversions.[7] Moreover, backbiting leads to a relatively high degree of branching, which explains the discrepancy between theoretical and experimental molecular weights.[8] Actually, the hydrodynamic volume of PAA varies according to the extent of branching.

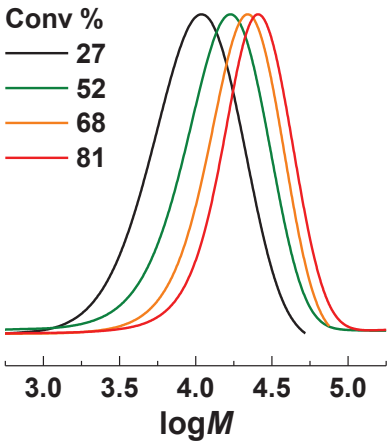

Figure 5.4. GPC traces of PAA obtained by aqueous *e*ATRP, using DCPA as initiator.

The amount of chloride ions was then changed in order to find the best compromise between good control and fastness (**Figure 5.5**). *e*ATRP of AA with RX = DCPA was repeated with C_{Cl^-} = 0.1 M and 0.01 M (**Table 5.2, entries 1 and 3** respectively). With C_{Cl^-} = 0.1 M, the process was slower and the dispersity increased because of the relatively enhanced contribution of the cyclization side-reaction. When C_{Cl^-} was reduced to 0.01 M, conversion reached 92% in 5 h, but dispersity slightly increased, I_{eff} was much smaller and a deviation from linearity was observable in the kinetic plot. Therefore, the amount of Cl^- was fixed to 0.03 M for the following syntheses.

Table 5.2. Effect of concentration of chloride ions on *e*ATRP of 10 vol% AA in water at T = 25 °C.[a]

Entry	C_{DCPA}/C_{Cl^-}	Q (C)	Conv. (%)[b]	k_p^{app} (h^{-1})	$M_{n,th}$ (10^{-3})	M_n (10^{-3})	I_{eff} (%)	$Đ$
1	1/13	16.2	58	0.17	7.4	13.0	57	1.50
2	1/4	14.6	81	0.37	10.3	15.7	65	1.43
3	1/1.3[c]	10.2	92	0.60	11.5	20.3	57	1.45

[a] pH = 2.2. $C_{AA}/C_{DCPA}/C_{Cu^{II}(OTf)_2}/C_{TPMA}$ = 175/1/0.1/0.4. C_{AA} = 1.46 M. WE area *ca.* 30 cm^2. [b]Conversion registered after 5 h. [c] 0.09 M Et_4NBF_4 was added to increase the conductivity of the solution.

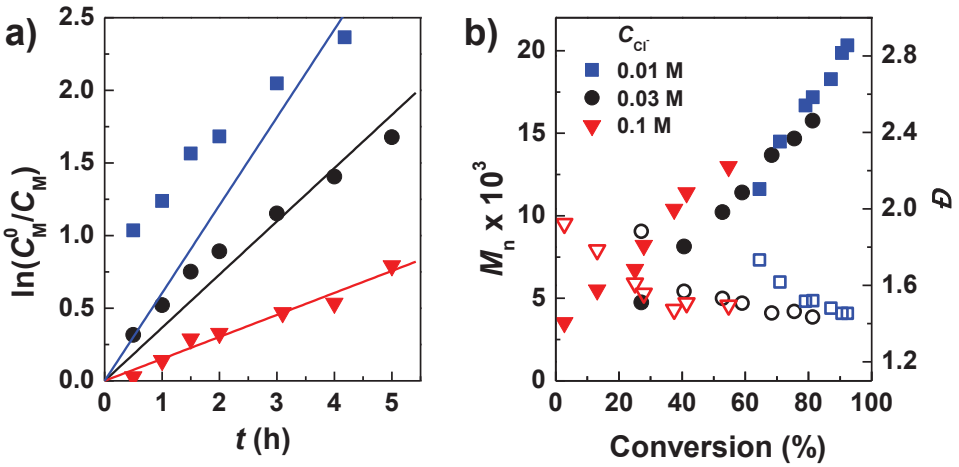

Figure 5.5. *e*ATRP of AA 10 vol% in water with various C_{NaCl}, kinetic plot a) and MWs and $Đ$ evolution *vs.* conversion b). Polymerization conditions: $C_{AA}/C_{DCPA}/C_{Cu^{II}(OTf)_2}/C_{TPMA}$ = 175/1/0.1/0.4. C_{AA} = 1.46 M. C_{NaCl} = 0.01 M (blue squares, + 0.09 M Et_4NBF_4), 0.033 M (black dots), and 0.1 M (red triangles). WE area *ca.* 30 cm^2. V_{tot} = 15 mL, T = 25 °C.

5.3. Effect of pH, temperature, catalyst nature and loading and DP

Since lowering the pH should decrease the extent of cyclization,[5] *e*ATRP of AA was performed at pH 1.4 and 0.9. CIBA was used as initiator, trying to obtain a good control also with a mono-halogenated initiator. However, the polymerization rate decreased by increasing the acidity of the media, whereas the final dispersity increased (**Figure 5.6**). For this reason, pH was not changed in any other synthesis (pH = 2.2), and DCPA and TCAA were then only used as initiators.

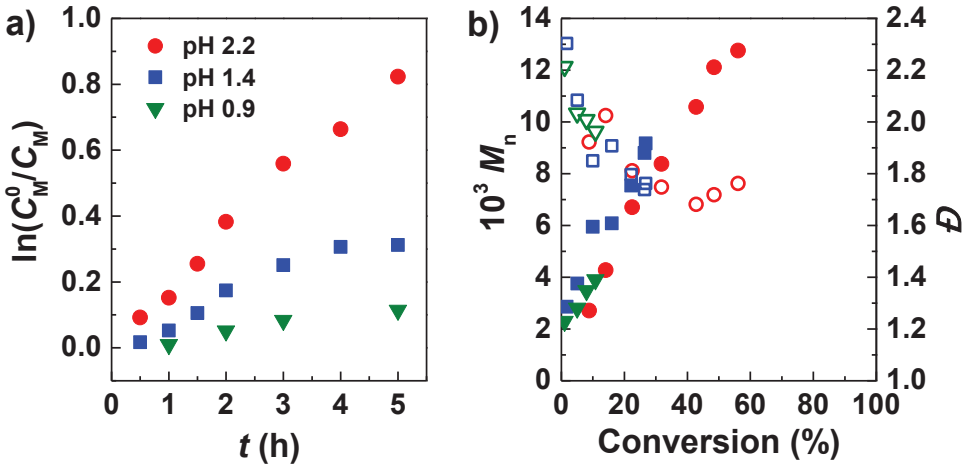

Figure 5.6. *e*ATRP of AA 10 vol% in water at different pH, kinetic plot a) and MWs and dispersity evolution *vs.* conversion b). Polymerization conditions: $C_{AA}/C_{CIBA}/C_{Cu^{II}(OTf)_2}/C_{TPMA}/C_{NaCl}$ = 175/1/0.1/0.4/4. C_{AA} = 1.46 M. WE area *ca.* 30 cm^2. V_{tot} = 15 mL, T = 25 °C.

The effect of catalyst loading was investigated (**Figure 5.7**) not only to use a smaller amount of metal, but also to gain some information about the interplay between propagation and cyclization. DCPA was used as RX. In *e*ATRP and other low-ppm techniques, generally the polymerization rate increases with the square root of catalyst loading (see **Chapter 4**, **Section 4.2.1**).[15, 16] Surprisingly, when the amount of Cu was doubled, the process became slightly slower and, more importantly, the polymerization essentially stopped at 74% conversion (**Table 5.3**, **entry 1**). In contrast, when Cu loading was reduced to *ca.* 0.4 mM, the process was faster, reaching 89% conversion in 5 h, whereas the polymer dispersity remained identical (**Table 5.3**, **entry 2**). These results suggest that the catalyst is involved in the cyclization process, which becomes more important when the catalyst loading is relatively high.

Nevertheless, a further decrease in catalyst loading was not beneficial: $Đ$ increased to 1.58 while the polymerization rate was unaffected (**Table 5.3, entry 3**). It follows that such a low amount of Cu is not effective in tuning the ATRP process of AA, similarly to what is observed for minimeulsion ATRP, where it is possible to reach very low catalyst loadings with methacrylates but not with acrylates (**Chapter 8**, **Section 8.4**).

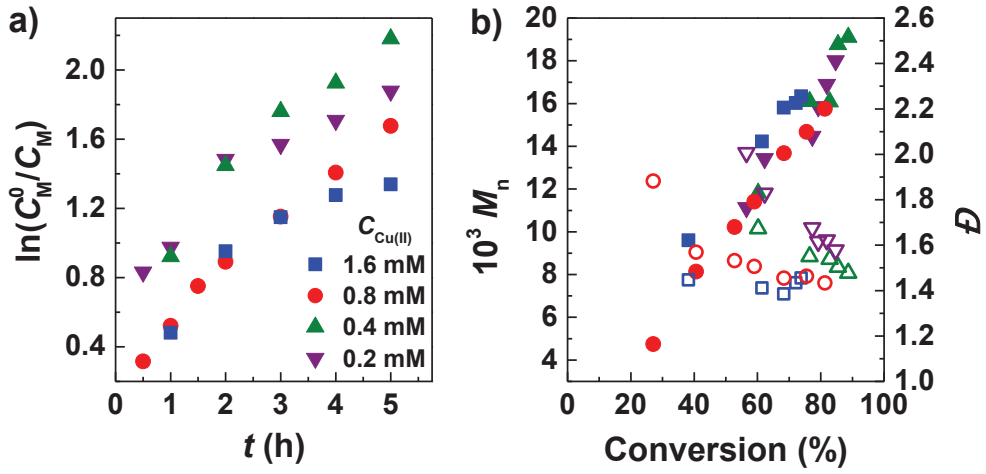

Figure 5.7. *e*ATRP of AA 10 vol% in water with different catalyst loadings, kinetic plot a) and MWs and dispersity evolution *vs.* conversion b). Polymerization conditions: C_{AA}/C_{DCPA} = 175/1. C_{AA} = 1.46 M, $C_{Cu^{II}(OTf)_2}/C_{TPMA}/C_{NaCl}$ = 1/4/40. WE area *ca.* 30 cm^2. V_{tot} = 15 mL, T = 25 °C.

Table 5.3. Effect of catalyst concentration and ligand nature on *e*ATRP of vol% AA in water at 25 °C.[a]

Entry	$C_{DCPA}/C_{Cu^{II}}$	L	Q (C)	Conv. (%)	k_p^{app} (h^{-1})	$M_{n,th}$ (10^{-3})	M_n (10^{-3})	I_{eff} (%)	$Đ$
1	1/0.2	TPMA	31.9	74	0.32	9.4	16.3	57	1.46
2	1/0.05	TPMA	14.4	89	0.50	11.2	19.1	59	1.47
3	1/0.025	TPMA	8.15	85	0.46	10.7	18.0	59	1.58
4	1/0.1	TPMA*1	18	83	0.41	10.5	17.1	61	1.40
5	1/0.1	TPMA*3	8.8	82	0.47	10.4	19.5	54	1.59

[a] pH = 2.2. C_{AA}/C_{DCPA} = 175/1. $C_{Cu^{II}(OTf)_2}/C_{TPMA}/C_{Cl^-}$ = 1/4/40. C_{AA} = 1.46 M. WE area *ca.* 30 cm^2.

Furthermore, to increase the polymerization rate, TPMA was replaced with two different ligands that provide more active copper complexes. As will be better described in **Chapter 6**, the TPMA skeleton was recently modified with methyl and methoxy groups, obtaining new ligands that increased the reducing power of Cu^I.[17] TPMA*1 and TPMA*3 were used herein (**Figure 5.1**), and their activity in ATRP should increase in the order

TPMA < TPMA*1 << TPMA*3. In both cases, $E_{app} = E_{1/2} - 0.06$ V was maintained, using the $E_{1/2}$ value measured for each catalyst. Some improvements were observed with $[Cl{-}Cu^{II}TPMA*1]^+$ in terms of both polymerization rate and degree of control (**Table 5.3**, **entry 4**). Instead, $Đ > 1.5$ was obtained with $[Cl{-}Cu^{II}TPMA*3]^+$ without observing any significant increase in the polymerization rate (**Table 5.3**, **entry 5**). The high dispersity can be explained by the high activity of this catalyst: fast activation of the initiator generated a relatively high quantity of radicals, which immediately terminated, thus accounting for the broad MWs distribution and the low I_{eff}.

The effect of reaction temperature on *e*ATRP of AA was analyzed, using TCAA as initiator. Interestingly, when T was raised to 40 °C the polymerization stopped after reaching 73% conversion in 4 h, accompanied by quite low I_{eff} (**Table 5.4**, **entry 3**). Conversely, when T was decreased to 10 °C the process was obviously slower, but the system reached 92% conversion, even if in 12 h, and $Đ = 1.38$ (**Table 5.4**, **entry 1**). This is reasonable considering that side reactions generally become much more relevant when the operating T is increased, while their effect is minimized at low temperatures.

Table 5.4. Temperature effect on *e*ATRP of 10 vol% AA in water.[a]

Entry	T (°C)	t (h)	Q (C)	Conv. (%)	k_p^{app} (h^{-1})	$M_{n,th}$ (10^{-3})	M_n (10^{-3})	I_{eff} (%)	$Đ$
1	10	12	18.4	92	0.23	11.6	20.0	58	1.38
2	25	5	21.8	87	0.44	11.0	17.9	61	1.36
3	40	3	23	73	0.55	9.3	16.5	56	1.39

[a] pH = 2.2. $C_{AA}/C_{TCAA}/C_{Cu^{II}(OTf)_2}/C_{TPMA}/C_{Cl^-}$ = 175/1/0.1/0.4/4. C_{AA} = 1.46 M. WE area *ca.* 30 cm^2.

Finally, higher monomer percentages were used, leaving unchanged the amount of initiator, TCAA, thus targeting higher degrees of polymerization (**Figure 5.8**). *e*ATRPs of 5, 10, and 20 vol% AA (DP = 88, 175, 350, respectively) gave very similar results, with conversion around 80% in 5 h and $Đ$ = 1.36-1.38 (**Table 5.5, entries 1-3**). However, a monomer percentage as high as 50 % (DP = 875) dramatically slowed down the polymerization, which stopped at 38% conversion, with lower I_{eff}, but acceptable final $Đ$ (1.41, **Table 5.5, entry 4**). Generally, lower $Đ$ values are registered by targeting higher DP, because of the increased number of activation-deactivation cycles.[1] The opposite trend observed herein, and the very low rate could be attributed to the importance of backbiting, which is more effective when higher amounts of monomer are present.[7]

Table 5.5. *e*ATRP of AA in water at $T = 25$ °C.[a]

Entry	AA vol%	DP (X)	t (h)	Q (C)	Conv. (%)	k_p^{app} (h^{-1})	$M_{n,th}$ (10^{-3})	M_n (10^{-3})	I_{eff} (%)	$Đ$
1	5	88	5	30	78	0.35	5.1	8.5	59	1.37
2	10	175	5	21.8	87	0.44	11.0	17.9	61	1.36
3	20	350	5	17.7	81	0.39	20.5	30.2	68	1.38
4	50	875	5	7.8	38	0.12	24	49.8	48	1.41

[a] pH 2.2 was measured. $C_{AA}/C_{TCAA}/C_{Cu^{II}(OTf)_2}/C_{TPMA}/C_{Cl^-}$ = X/1/0.1/0.4/4. C_{AA} = 1.46 M. WE area *ca.* 30 cm^2.

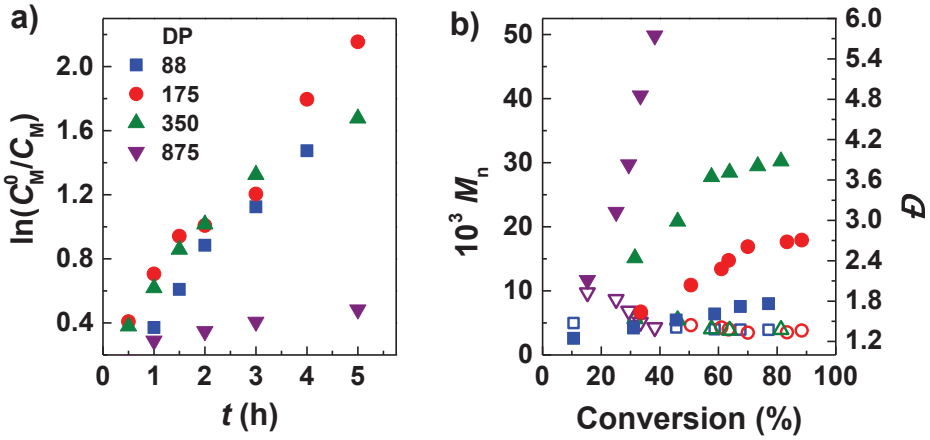

Figure 5.8. *e*ATRP of AA in water by varying monomer loading (5, 10, 20, 50 vol%), kinetic plot a) and MWs and dispersity evolution *vs.* conversion b). Polymerization conditions: $C_{TCAA}/C_{Cu^{II}(OTf)_2}/C_{TPMA}/C_{Cl^-}$ = 1/0.1/0.4/4, $C_{Cu^{II}(OTf)_2} = 0.8 \times 10^{-3}$ M. WE area *ca.* 30 cm^2. V_{tot} = 15 mL, T = 25 °C.

5.4. Conclusions and perspectives

Well-controlled aqueous *e*ATRP of acrylic acid was successfully performed, also analyzing the effect of the amount of halide ions and catalyst, nature of RX and ligands, DP and temperature. Conversions > 80% can be reached in about 5 h, at room temperature, and PAA had final dispersity about 1.4.

As previously proved for controlled polymerization of methacrylic acid, an intramolecular cyclization reaction is the predominant way of termination for growing chains. To prevent this process, bromide ions must be replaced with chloride, and polymerization rate must be maximized.

Interestingly, some improvements in the overall control were observed by diminishing the catalyst loading. The mechanism of the cyclization side reaction is unknown. However, it seems reasonable that the Cu complex is somehow involved in the process. Further study is needed to clarify this point.

Nevertheless, preparation of polymers based on acidic monomers is no more impossible for ATRP. New architectures and hybrid materials based on acrylic and methacrylic acid should be realized, which can be particularly relevant for biological applications.

References

1. Matyjaszewski, K. *Macromolecules* **2012,** 45, 4015-4039.
2. Visnevskij, C.; Ciuta, G.; Ketleriute, S.; Savickaite, M.; Makuska, R. *European Polymer Journal* **2014,** 55, 66-75.
3. Patten, T. E.; Matyjaszewski, K. *Advanced Materials* **1998,** 10, 901-915.
4. Mori, H.; Müller, A. H. *Progress in Polymer Science* **2003,** 28, 1403-1439.
5. Fantin, M.; Isse, A. A.; Venzo, A.; Gennaro, A.; Matyjaszewski, K. *J. Am. Chem. Soc* **2016,** 138, 7216-7219.
6. Ladavière, C.; Dörr, N.; Claverie, J. P. *Macromolecules* **2001,** 34, 5370-5372.
7. Buback, M.; Hesse, P.; Lacík, I. *Macromolecular Rapid Communications* **2007,** 28, 2049-2054.
8. Lacík, I.; Stach, M.; Kasák, P.; Semak, V.; Uhelská, L.; Chovancová, A.; Reinhold, G.; Kilz, P.; Delaittre, G.; Charleux, B. *Macromolecular Chemistry and Physics* **2015,** 216, 23-37.
9. Couvreur, L.; Lefay, C.; Belleney, J.; Charleux, B.; Guerret, O.; Magnet, S. *Macromolecules* **2003,** 36, 8260-8267.
10. Plessis, C.; Arzamendi, G.; Leiza, J. R.; Schoonbrood, H. A. S.; Charmot, D.; Asua, J. M. *Macromolecules* **2000,** 33, 4-7.
11. Lacík, I.; Beuermann, S.; Buback, M. *Macromolecules* **2003,** 36, 9355-9363.
12. Fantin, M.; Lorandi, F.; Isse, A. A.; Gennaro, A. *Macromolecular rapid communications* **2016,** 37, 1318-1322.
13. Bortolamei, N.; Isse, A. A.; Di Marco, V. B.; Gennaro, A.; Matyjaszewski, K. *Macromolecules* **2010,** 43, 9257-9267.
14. Fantin, M.; Isse, A. A.; Gennaro, A.; Matyjaszewski, K. *Macromolecules* **2015,** 48, 6862-6875.
15. Lorandi, F.; Fantin, M.; Isse, A. A.; Gennaro, A. *Polymer Chemistry* **2016,** 7, 5357-5365.
16. Guo, J. K.; Zhou, Y. N.; Luo, Z. H. *AIChE Journal* **2015,** 61, 4347-4357.
17. Kaur, A.; Ribelli, T. G.; Schröder, K.; Matyjaszewski, K.; Pintauer, T. *Inorganic chemistry* **2015,** 54, 1474-1486.

Chapter 6.

New ligands for ATRP

Table of contents

6.1. Introduction and aim of the work

The activity of ATRP catalysts can be tuned by designing new ligands that affect stability and redox properties of the copper centre.[1, 2] The quest to strongly decrease the catalyst loading led to the synthesis of novel ligands that enhance the reducing power of Cu complexes. In fact, traditional ATRP mainly used 2,2'-bipyridine and its derivatives as ligands. Later, new Cu complexes with tris(2-methylpyridyl)amine (TPMA)[3] and tris[2-(dimethylamino)ethyl]amine (Me_6TREN)[4, 5] as ligands exhibited much better performances (**Figure 6.1**). These ligands are commercially available and among the most used nowadays.

Cu/TPMA is the best performing catalyst in aqueous media, mainly because of its stability over a broad range of pH and the low tendency of $[Cu^{I}TPMA]^{+}$ to disproportionate.[6] Particularly, TPMA exhibited unexpected stability under strongly acidic conditions[7] and it is fundamental for ATRP in miniemulsion, if combined with anionic surfactants, as will be explained in details in **Chapter 8**.

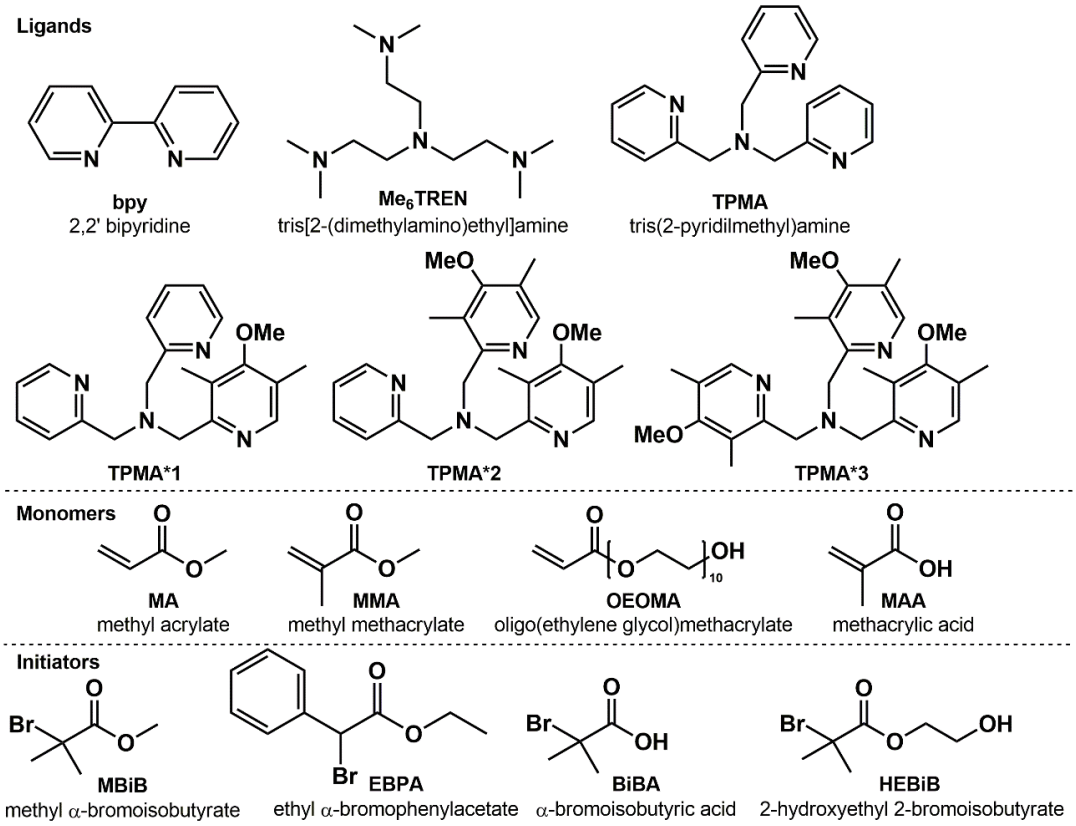

Figure 6.1. Structures of compounds relevant to the present chapter.

Unfortunately, TPMA failed in ATRP of less active monomers, like vinyl acetate, and so did Me_6TREN.[2] For this reason, new structures are continuously designed and tested.[8, 9] Recently, TPMA skeleton was modified by adding methoxy and methyl groups on one or more pyridinic rings (**Figure 6.1**).[9] Cu complexes with the obtained TPMA*1, TPMA*2, and TPMA*3 have increasingly more negative standard reduction potentials, E^{e}, thanks to the ability of the substituent groups on pyridinic rings to donate electrons to the metal centre. In particular, a negative shift in E^{e} is consistent with a ligand able to stronger stabilize the coordination sphere of Cu^{II} compared to Cu^{I}.[10] The reactivity of ATRP catalysts can be directly related to the standard reduction potential of the Cu^{II}/Cu^{I} couple (**Chapter 1**, **Section 1.3.1**). Both the activation rate constant and the equilibrium constant of ATRP increase by enhancing the reducing power of the catalyst, that is, decreasing E^{e} (**Chapter 3**, **Section3.7**).[11, 12]

However, highly active catalysts are not necessary and can be even detrimental in particular environments, like in the presence of water, which dramatically increases the activity of traditional Cu complexes.[6, 13] More important in aqueous media is the stability of the catalyst over a broad range of pH, a requirement that is not fulfilled by many aliphatic ligands, thus TPMA and its analogues are preferred.

In this context, eight novel TPMA copper complexes of the general structure reported in **Figure 6.2** were synthesized by the group of Prof. Zonta, in our Department. Basically, the TPMA skeleton was modified by adding *m*-functionalised phenyl substituents. Their copper complexes were characterized in terms of structural and electrochemical properties, comparing the data with traditional Cu/TPMA under identical conditions. Finally, one of this complex was tested as a catalyst for *e*ATRP in organic solvents and, more interestingly, in aqueous media, where the desired control over the process can benefit from the slightly lower reactivity of the complex. All *e*ATRP experiments were performed with the traditional setup (*i.e.* Pt WE and CE in a divided cell) under potentiostatic control, setting E_{app} to tune the reactivity of the catalyst according to the particular system.

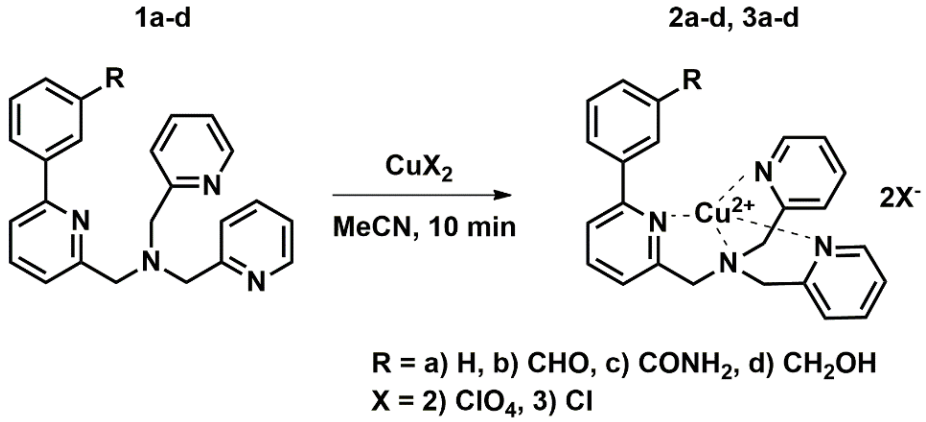

Figure 6.2. Chemical structures of 4 new TPMA-modified ligands and their Cu complexes (adapted with permission from Ref. [14]. Copyright 2017, Elsevier).

6.2. Brief description of ligand syntheses and structural characterization

Briefly, ligands **1a-d** in **Figure 6.2** were prepared by synthesizing a bromo derivative via reductive amination of commercially available 6-bromo-2-pyridinecarboxaldehyde and di(2-picolyl)amine, followed by a Suzuki coupling with appropriate boronic acid. The corresponding copper complexes **2a-d** and **3a-d** were obtained by mixing an equimolar amount of copper(II) perchlorate or chloride with the selected ligand in acetonitrile. The

solution was stirred at room temperature for 10 min and the desired compounds were obtained as crystalline powders or by recrystallization from diethyl ether.[15-17]

ESI-MS, FT-IR spectroscopy and/or elemental analysis confirmed the purity of each compound. Among the different structures, it was possible to obtain crystals suitable for X-ray diffraction of complexes **2a,d** and **3a,c** (**Figure 6.3**). All the monocationic structures exhibited a distinctive Jahn-Teller effect with a strong distorted octahedral coordination for the Cu^{II} centre. The four short bonds of **2a,d** and **3a,c**, were arranged in a square planar manner. These bonds came from *i*) the amino group N(1), *ii*) the two unsubstituted pyridine moieties N(3), N(4), and *iii*) from acetonitrile N(5), for **2a,d**, and from Cl anions in **3a,c**. The elongated bonds at complexes **2a** and **2d** were comparable to well described Cu^{II} complexes of pentadentate bispidine ligands with two amino groups and three pyridine moieties, and a coordinated acetonitrile.[18] Notably, the molecules of **3a,c** form a dimer, whereas the chloride anions generate additional elongated bonds to the other Cu^{II} centre. The dimerization, which was not commonly observed in TPMA modified structures, could be favoured by additive π-π interactions between the pyridine rings. It should be noted that while the reported complexes displayed octahedral geometries in the solid state, and in two cases were dinuclear, previous studies of related complexes performed in solution suggested instead a monomeric character and a C_3 trigonal-bypiramidal symmetry.[9]

2a R = H X = ClO_4 **3a** R = H X = Cl **2d** R = CH_2OH X = ClO_4 **3c** R = $CONH_2$ X = Cl

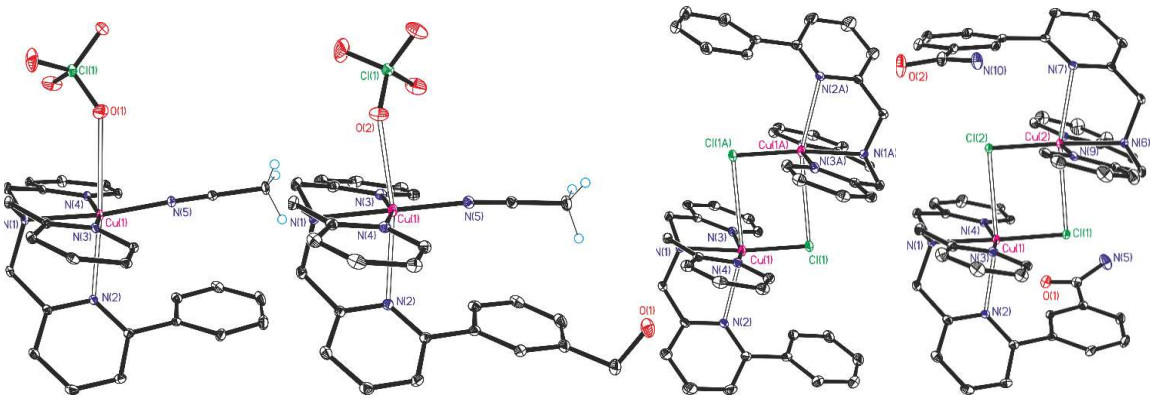

Figure 6.3. X-ray crystal structures of complexes **2a,d** and **3a,c** (reprinted with permission from Ref. [14]. Copyright 2017, Elsevier).

6.3. Electrochemical characterization of new Cu complexes by cyclic voltammetry

The redox properties of the overall complexes were investigated by cyclic voltammetry in acetonitrile. A reversible peak couple, corresponding to one electron transfer was observed for each binary and ternary complex, $[Cu^{II}L]^{2+}/[Cu^{I}L]^{+}$ and $[XCu^{II}L]^{+}/[XCu^{I}L]$, respectively (**Figure 6.4**).

The peak-to-peak separation, ΔE_p, was greater than the typical value for a fast or Nernstian electron transfer (ΔE_p = 60 mV) and increased with the scan rate. These results are indicative of an electron transfer process with a significant reorganization in the geometry of the complex. This is in agreement with previous reports on the electrochemical behaviour of copper-amine complexes employed as catalysts for ATRP.[19]

The standard potential, $E^{\ominus}$, of each Cu^{II}/Cu^{I} couple was as usually determined from the half-wave potential as $E^{\ominus} \approx E_{1/2} = (E_{pc} + E_{pa})/2$. The average of $E_{1/2}$ values measured with scan rates ranging from 0.02 V/s to 0.2 V/s is reported in **Table 6.1** as an estimate of $E^{\ominus}$ for each complex.

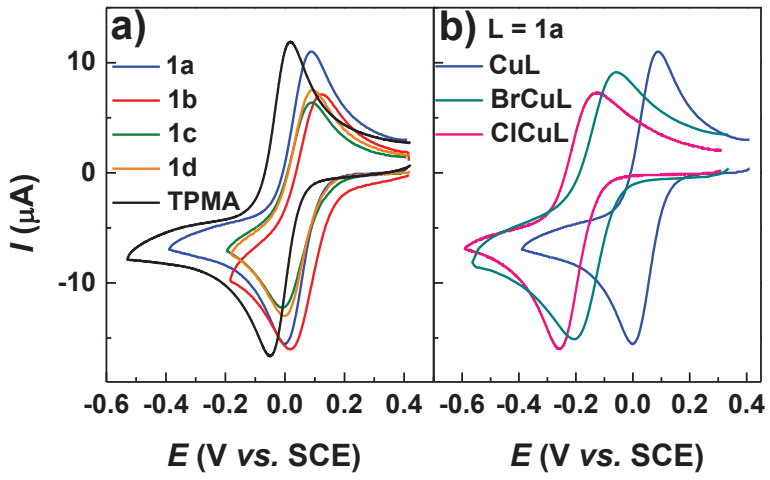

Figure 6.4. Cyclic voltammetry of 1 mM Cu^{II} complexes in CH_3CN + 0.1 M Et_4NBF_4, recorded on a GC electrode at a scan rate of υ = 0.1 V s^{-1} (adaped with permission from Ref. [14]. Copyright 2017, Elsevier).

Compounds formed by Cu^{II} and ligands **1a-d** displayed very small differences in $E^{\ominus}$ values, meaning that their reducing power was weakly affected by the substituent on the phenyl ring probably because of the large distance separating it from the metallic centre. Crystal structures (**Figure 6.3**) supported this hypothesis, evidencing that the biarylic system can rotate, increasing the distance between the substituent and the metal.

Table 6.1. Thermodynamic data for Cu^{II} and Cu^{I} complexes in CH_3CN + 0.1 M Et_4NBF_4 at T = 25 °C.

			$[Cu^{II}L]^{2+}$ [a]		$[ClCu^{II}L]^{+}$ [b]		$[BrCu^{II}L]^{+}$ [c]	
Entry	L	R	$E^{\ominus}$ (V *vs.* SCE)	β^{II}/β^{I} [d]	$E^{\ominus}$ (V *vs.* SCE)	K^{II}_{Cl}/K^{I}_{Cl} [e]	$E^{\ominus}$ (V *vs.* SCE)	K^{II}_{Br}/K^{I}_{Br} [e]
1	- [f]	-	1.056					
2	TPMA	-	-0.019	1.49×10^{18}	-0.363	6.53×10^{5}	-0.282	2.79×10^{4}
3	**1a**	H	0.043	1.33×10^{17}	-0.197	1.14×10^{4}	-0.130	8.40×10^{2}
4	**1b**	CHO	0.071	4.48×10^{16}	-0.203	4.28×10^{4}	-0.157	7.15×10^{3}
5	**1c**	$CONH_2$	0.039	1.56×10^{17}	-0.218	2.21×10^{4}	-0.136	9.08×10^{2}
6	**1d**	CH_2OH	0.045	1.23×10^{17}	-0.200	1.39×10^{4}	-0.131	9.44×10^{2}

[a] Obtained by dissolving the crystalline complexes in acetonitrile. [b] Obtained by dissolving crystalline complexes **2a-d** in acetonitrile, followed by the addition of 2 equivalents of Et_4NCl. [c]Obtained by dissolving crystalline complexes **2a-d** in acetonitrile, followed by the addition of 2 equivalents of Et_4NBr. [d]β^{II} and β^{I} are the stability constants of $[Cu^{II}L]^{2+}$ and $[Cu^{I}L]^{+}$, respectively. [e]K^{II}_{X} and K^{I}_{X} are the association constants of X^{-} with $[Cu^{II}L]^{2+}$ and $[Cu^{I}L]^{+}$, respectively. [f]No added ligand, $E^{\ominus}$ of $Cu^{II}(OTf)_2$ taken from Ref. [10] (reprinted with permission from Ref. [14]. Copyright 2017, Elsevier).

Importantly, $E^{\ominus}$ of these compounds was 58-90 mV more positive than the redox potential of traditional $[Cu^{II}TPMA]^{2+}$ in the same solvent. This difference was caused by the phenyl ring added to the TPMA skeleton, which significantly decreased the charge density on the metal centre, making it more easily reducible. As a consequence, the reactivity of Cu^{I} complexes with these ligands was expected to be smaller than the reactivity of $[Cu^{I}TPMA]^{+}$,[1] which in effect has been confirmed as shown in **Section 6.4**.

The relative stability of Cu^{II} and Cu^{I} species was calculated from the standard potentials of $[Cu^{II}L]^{2+}/[Cu^{I}L]^{+}$ and solvated Cu^{2+}/Cu^{+}, according to Eq. 1.6 in **Chapter 1** (**Section 1.3.1**). Looking at the β^{II}/β^{I} ratio reported in **Table 6.1**, $[Cu^{II}L]^{2+}$ was much more stable than $[Cu^{I}L]^{+}$, as previously found for similar copper-amine complexes.[10, 20] However, the calculated ratio β^{II}/β^{I} was about one order of magnitude lower when **1a-d** were used as ligand, compared to TPMA, because of enhanced Cu^{I} stabilization with the new ligands. Thus, a reduced reactivity of $[Cu^{I}L]^{+}$ (L = **1a-d**) towards RX activation is expected, if compared to $[Cu^{I}TPMA]^{+}$.[21, 22]

Ternary complexes $[XCu^{II}L]^{+}$ were readily formed by adding halide ions to a solution of $[Cu^{II}L]^{2+}$. Cyclic voltammetry of these compounds (**Figure 6.4b**) showed a negative shift of the Cu^{II}/Cu^{I} peak couple, similarly to conventional ATRP catalysts. Standard

reduction potentials of ternary complexes were determined from half-wave potentials (**Table 6.1**), and showed a similar trend to that observed for binary complexes. Indeed, all $[ClCu^{II}L]^+$ complexes exhibited E^e values that were 145-163 mV more positive than E^e of $[ClCu^{II}TPMA]^+$. Analogously, E^e values of $[BrCu^{II}L]^+$ were 125-152 mV more positive than E^e of $[BrCu^{II}TPMA]^+$. Nonetheless, E^e values of $[XCu^{II}L]^+$ were more negative (by 0.18-0.34 V) than those of the corresponding binary complexes $[Cu^{II}L]^{2+}$. From the negative shift of E^e, the relative affinity of $[Cu^{II}L]^{2+}$ and $[Cu^{I}L]^+$ for halide ions (*i.e.* halidophilicity) was determined (according to Eq. 1.16 in **Chapter 1**, **Section 1.3.1**) and reported in **Table 6.1**. The calculated values of K_X^{II}/K_X^{I} varied in the range 10^3-4×10^4, indicating that the affinity for halide ions was much greater for Cu^{II} than Cu^{I} species, with all ligands **1a-d**. This behavior fulfills the fundamental prerequisite for a good ATRP catalyst: Cu^{II} must be predominantly present in the deactivator form, $[X–Cu^{II}L]^+$, while Cu^{I} is desired to give a less stable $[X–Cu^{I}L]$ complex that readily dissociates to regenerate the activator $[Cu^{I}L]^+$.[21, 23]

Overall, the newly synthesized complexes showed more positive reduction potentials than traditional $[X–Cu^{II}TPMA]^+$. Since it was proved that the catalyst activity in ATRP increased with decreasing E^e of $[X–Cu^{II}L]^+$,[11, 23] it can be predicted that the new complexes will have comparable reactivity and will be less active than the copper complex with unmodified TPMA. For this reason, all polymerizations were performed with L = **1a**, chosen as a model catalyst for the new series of copper complexes.

6.4. *e*ATRP in organic solvents catalyzed by Cu/1a and Cu/TPMA

Methyl acrylate (MA) was selected as a monomer for *e*ATRP in CH_3CN, following a previously reported polymerization setup that easily worked with $[Br–Cu^{II}Me_6TREN]^+$ as a catalytyst precursor.[24] However, by using $[Br–Cu^{II}\mathbf{1a}]^+$ no polymer formation was observed after 6 h, despite $E_{app} = E^e - 0.06$ V, thereby establishing a ratio $C_{Cu^I}/C_{Cu^{II}} = 10$, according to Nernst's equation (Eq. 1.26 in **Chapter 1**, **Section 1.4**).

Since a huge amount of generated active species did not enhance the polymerization rate, DMF was used as solvent under otherwise identical conditions. Actually, it was proved that CH_3CN strongly stabilizes $[Cu^{I}L]^+$, thus reducing its activity, if compared to other less coordinating solvents.[11, 25] Nevertheless, no appreciable monomer conversion was observed after few hours. Conversely, when TPMA was tested as ligand in *e*ATRP of MA

in DMF, very high conversion was achieved in 6 h; the polymerization was well-controlled with linear first-order kinetics and very low dispersity (**Figure 6.5**).

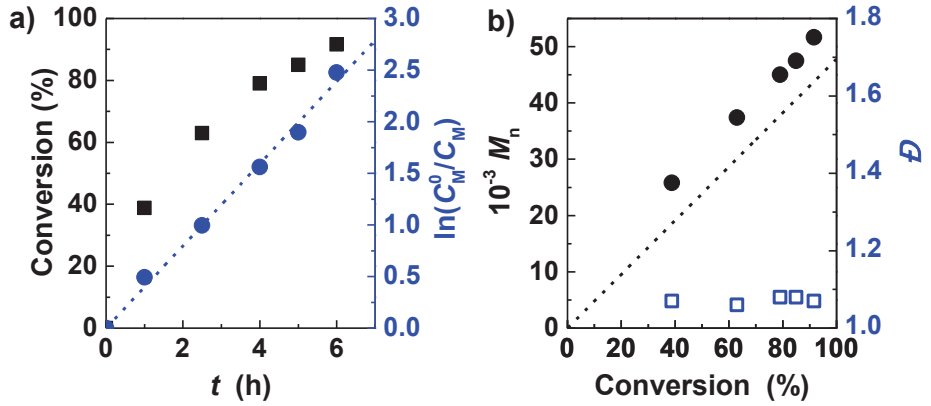

Figure 6.5. *e*ATRP of MA 50 vol% in DMF + 0.1 M Et_4NBF_4. $C_{MA}/C_{MBriB}/C_{[Cu^{II}TPMA]^{2+}}/C_{Br^-}$ = 555/1/0.1/0.2, $E_{app} = E_{1/2} - 0.06$ V, $C_{Cu^{2+}} = 10^{-3}$ M, T = 25°C, V_{tot} = 15 mL. a) Monomer consumption, and first-order kinetic plot, and b) MWs and dispersity evolution *vs.* conversion (adapted with permission from Ref. [14]. Copyright 2017, Elsevier).

A possible explanation for the failure of polymerization with the catalytic system Cu/**1a**/Br^- is the inefficient activation of the secondary alkyl bromide dormant species (R′CH(Br)C(O)OCH_3) by the activator complex $[Cu^IL]^+$ (L = **1a**).[26] In order to validate this hypothesis, the activation rate constants (k_{act}) for the initiator methyl 2-bromoisobutyrate (MBiB) by $[Cu^IL]^+$ in CH_3CN/MA (50% v/v) were measured by using the rotating disk electrode technique (see **Chapter 3** and **Appendix B1** for details on experimental procedures). The activation rate of MBiB by $[Cu^ITPMA]^+$ was expected to be high, thus second order conditions were used (*i.e.* $C_{Cu^I} = C_{MBiB}$). Instead, pseudo-first order conditions were adopted for $[Cu^I\mathbf{1a}]^+$, with $C_{MBiB} = 20C_{Cu^I}$. $k_{act} = 1.1\times10^3$ $mol^{-1}dm^3s^{-1}$ was measured for L = TPMA, whereas the value obtained for L = **1a** was five orders of magnitude lower, $k_{act} = 1.3\times10^{-2}$ $mol^{-1}dm^3s^{-1}$ (**Figure 6.6**). Moreover, k_{act} depends on the structure of RX, increasing in the order primary < secondary < tertiary.[27] The dormant species formed during ATRP of MA is structurally similar to MBiB except being a secondary alkyl halide. Therefore, k_{act} of the dormant species is expected to be at least one order of magnitude lower than k_{act} of MBiB. It follows then, when **1a** was used as ligand, the reactivity of $[Cu^I\mathbf{1a}]^+$ toward the initiator was low and it became even lower when propagating chains were converted to dormant species, P_n–X.

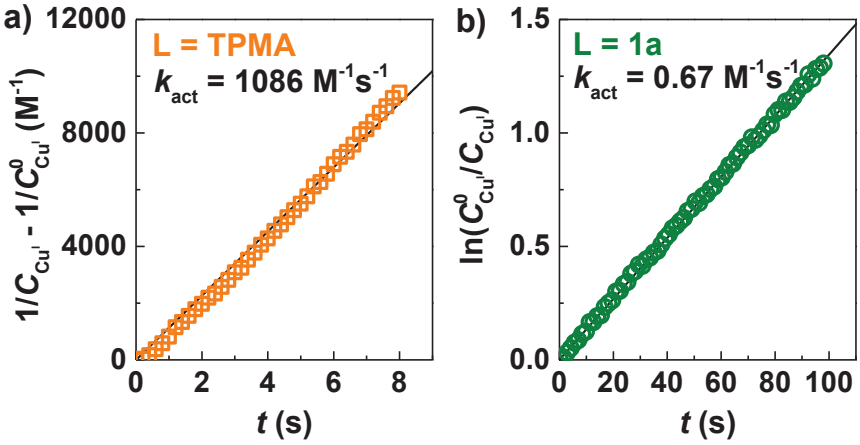

Figure 6.6. Determination of activation rate constants, k_{act}, by RDE, in CH_3CN/MA 1/1 v/v + 0.1 M Et_4NBF_4. a) L = TPMA, second order conditions: $C_{MBriB}/C_{Cu^I}/C_{TPMA}/C_{TEMPO}$ = 1/1/1.1/20. b) L = **1a**, pseudo-first order conditions: $C_{MBriB}/C_{Cu^I}/C_{\mathbf{1a}}/C_{TEMPO}$ = 20/1/1.1/200.

Table 6.2. Potentiostatic *e*ATRP of different monomers catalyzed by $[XCu^{II}L]^+$.[a]

Entry	Solvent	Monomer (vol%)	L	X^-	$E^{\ominus}$ (V)[b]	RX	E_{app} (V)[b]	t (h)	Conv. (%)	Q (C)	k_p^{app} (h^{-1})	M_n (10^{-3})	$M_{n,th}$ (10^{-3})	$Đ$
1	CH_3CN[c]	MA (50%)	**1a**	Br^-	-0.030	MBiB	-0.09	6	0	-	-	-	-	-
2	DMF[c]	MA (50%)	**1a**	Br^-	-0.091	MBiB	-0.15	6	0	-	-	-	-	-
3	DMF[c]	MA (50%)	**TPMA**	Br^-	-0.196	MBiB	-0.26	6	92	4.43	0.40	51.7	43.8	1.07
4	DMF[c]	MMA (50%)	**1a**	Br^-	-0.134	EBPA	-0.19	14	83	8.71	0.12	44.6	38.7	1.21
5	DMF[c]	MMA (50%)	**TPMA**	Br^-	-0.214	EBPA	-0.15	12	77	8.93	0.11	45.9	36.0	1.12
6	H_2O	OEOMA (20%)	**1a**	Br^-	-0.133	HEBiB	-0.07	3	88	0.77	0.84	90.9	96.6	1.16
7[d]	H_2O	OEOMA (10%)	**TPMA**	Br^-	-0.260	HEBiB	-0.20	4	95	3.10		63.0	51.0	1.17
8	H_2O	MAA (10%)[e]	**1a**	Cl^-	-0.120[f]	BiBA	-0.18	5	81	3.56	0.35	21.4	13.9	1.49
9[g]	H_2O	MAA (10%)[e]	**TPMA**	Cl^-	-0.120[f]	BiBA	-0.18	4	96	3.20	0.84	18.0	16.8	1.42

[a] General conditions: $C_{Cu^{II}}$ = 10^{-3} M, T = 25 °C, V_{tot} = 15 mL, $C_M/C_{RX}/C_{Cu^{II}}/C_L/C_{X^-}$: 555/1/0.1/0.1/0.2 (entries 1-3); 467/1/0.1/0.1/0.2 (entries 4-5); 225/1/0.5/0.5/50 (entry 6); 200/1/0.1/0.4/50 (entry 8). [b] vs. SCE. [c] 0.1 M Et_4NBF_4 as supporting electrolyte. [d] Taken from ref. [6]. [e] pH = 0.9 by addition of HCl. [f] Cathodic peak potential, $E_{p,c}$ (irreversible voltammetric response). [g] Taken from ref. [7] (reprinted with permission from Ref. [14]. Copyright 2017, Elsevier).

Aiming to find a suitable system for this catalyst, MA was replaced with MMA. Indeed, k_{act} as well as K_{ATRP} are generally at least one order of magnitude higher for methacrylates than for acrylates, mainly because of the higher stability of tertiary radicals arising from methacrylates than secondary radicals from acrylates.[2] Considering that the polymerization rate of ATRP, R_p, depends linearly on K_{ATRP} (Eq. 1.1 in **Chapter 1**, **Section 1.2**), a faster process is expected with MMA as monomer, compared to MA. Note that homopolymerization of MMA by *e*ATRP catalysed by Cu complexes has never been reported. So far, only the Fe^{II}/Fe^{III} redox couple was used as catalyst. [28, 29]

*e*ATRPs of MMA in DMF were carried out with ethyl α-bromophenylacetate (EBPA) as initiator. The selection of the appropriate initiator for methacrylate polymerization is crucial. In ATRP, methacrylates suffer from the penultimate effect, which leads to low initiator efficiencies and broad $Đ$ values, unless a suitable RX is used.[26] Basically, propagating chains formed at the beginning of the process, when few monomer molecules add to initiator radicals, are highly reactive. Thus, a more reactive RX should be used to ensure a good initiator efficiency. EBPA is the most reactive alkyl halide used in ATRP and it showed good performances for MMA polymerization.[30]

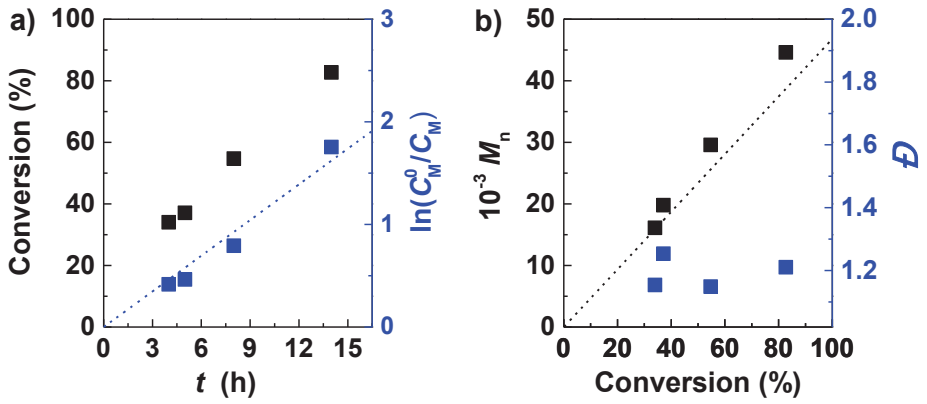

Figure 6.7. *e*ATRP of MMA 50 vol% in DMF + 0.1 M Et_4NBF_4. $C_{MMA}/C_{EBPA}/C_{[Cu^{II}\mathbf{1a}]^{2+}}/C_{Br^-}$ = 467/1/0.1/0.2, $E_{app} = E_{1/2} - 0.06$ V, $C_{Cu^{2+}} = 10^{-3}$ M, T = 25°C, V_{tot} = 15 mL. a) Monomer consumption and first-order kinetic plot, and b) MWs and $Đ$ evolution *vs.* conversion (adapted with permission from Ref. [14]. Copyright 2017, Elsevier).

*e*ATRP of MMA in DMF with $[Br–Cu^{II}\mathbf{1a}]^+$ and $E_{app} = E^{\circ} - 0.06$ V was well-controlled, exhibiting a linear kinetic plot and low dispersity, while reaching 83% conversion in 14 h (**Table 6.2, entry 4** and **Figure 6.7**). Good results were also obtained by using TPMA as ligand, but the huge activity of $[Cu^{I}TPMA]^+$ required a careful tuning

of the applied potential to achieve a controlled polymerization under analogous conditions (**Table 6.3** and **Figure 6.8**). When $E^{\ominus}$ – 0.06 V was applied, dispersity grew with time, reaching $Đ > 2$ after only 40% conversion. Poor control was still observed with $E_{app} = E^{\ominus}$, which implies $C_{Cu^{I}} \approx C_{Cu^{II}}$, while $Đ = 1.12$ and linear first-order kinetics were obtained when Cu^{I}/Cu^{II} ratio was reduced to *ca.* 0.1 by applying $E_{app} = E^{\ominus} + 0.06$ V (**Table 6.2, entry 5**). However, low dispersity was achieved at the expense of the polymerization rate; indeed, the process was slightly slower than with L = **1a**. Moreover, measured MWs exceeded the theoretical values at high conversions, probably because of termination via radical coupling, as proved by a small shoulder at high MWs in the GPC traces (**Figure 6.9**). A better accordance between experimental and theoretical MWs was observed with L =**1a**, despite the slightly higher dispersity, $Đ = 1.2$.

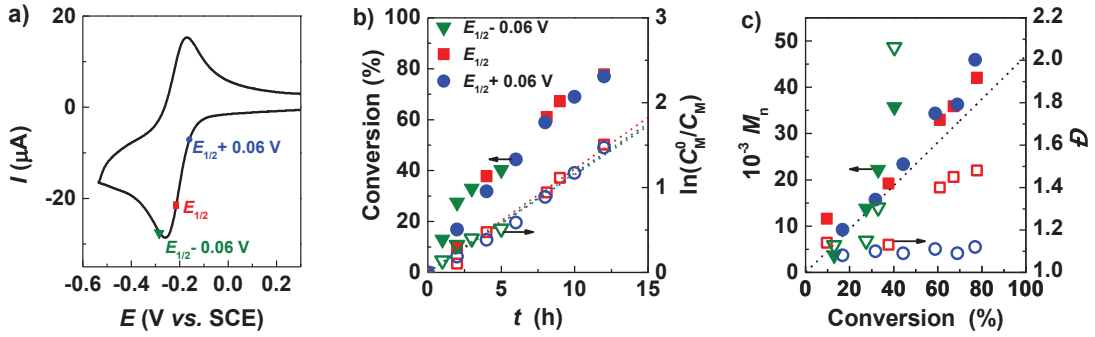

Figure 6.8. a) CV of 10^{-3} M $[BrCu^{II}TPMA]^{+}$ in MMA 50 vol% in DMF + 0.1 M Et_4NBF_4, $\upsilon = 0.2$ Vs^{-1}, $T = 25°C$, $V_{tot} = 20$ mL. b,c) Effect of E_{app} on *e*ATRP of MMA 50 vol% in DMF + 0.1 M Et_4NBF_4. $C_{MMA}/C_{EBPA}/C_{[Cu^{II}TPMA]^{2+}}/C_{Br^-} = 467/1/0.1/0.2$, $C_{Cu^{2+}} = 10^{-3}$ M, $T = 25°C$, $V_{tot} = 20$ mL. b) Monomer consumption and first-order kinetic plot, and c) MWs and $Đ$ evolution *vs.* conversion.

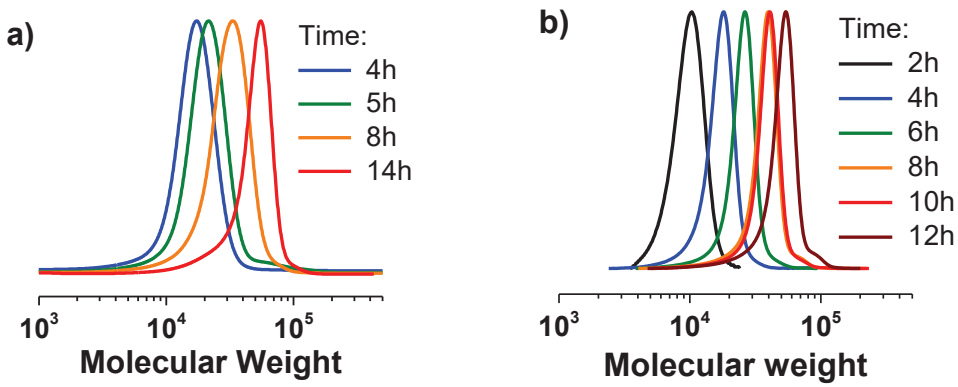

Figure 6.9. GPC traces of PMMA obtained *via* *e*ATRP catalyzed by a) $[Br–Cu^{II}$**1a**$]^{+}$ and b) $[Br–Cu^{II}TPMA]^{+}$. Polymerization conditions in **Table 6.2, entries 4,5**.

Useful information about the effect of E_{app} on *e*ATRP of MMA can be derived from the amount of charge passed during each synthesis (**Table 6.3**), according to the procedure explained in **Chapter 1**, **Section 1.4**. The amount of Cu^{II} converted to Cu^{I} depended on the applied potential, thus the required theoretical charge was different for each synthesis. For $C_{Cu^I} \approx 10 C_{Cu^{II}}$, the theoretical charge can be calculated from Faraday's equation as $Q_{th} = n_{Cu^{2+}} F$ = 1.30 C. Each terminated radical, according to the ATRP equilibrium, accumulates one Cu^{II} species, thus consumed charge exceeding Q_{th} is used to re-generate Cu^{I}. From the excess charge (14.3 – 1.3 = 13 C), the number of terminated chains resulted in n_t = 1.35 × 10^{-4} mol, which equals 90% of the growing chains (the total amount of growing chains was n_{RX} = 1.5 × 10^{-4} mol). Similarly, for $C_{Cu^I} \approx C_{Cu^{II}}$, $Q_{th} = 0.96$ C and n_t = 1.62 × 10^{-4} mol, corresponding to 81% of the growing chains (n_{RX} = 2 × 10^{-4} mol in that case because V_{tot} = 20 mL, see details in **Table 6.3**). Finally, for $C_{Cu^I} \approx 0.1\, C_{Cu^{II}}$, $Q_{th} = 0.19$ C and n_t = 9.1 × 10^{-5} mol, that is, 45% of the growing chains. Using the same procedure to calculate the percentage of terminated chains with **1a** as ligand showed that 57% of the chains were dead, which is consistent with the slightly higher *Đ* value observed comparing entries 4 and 5 of **Table 6.2**. However, these percentages are quite high for controlled processes, probably because these calculations are made considering that none of the charge passed is due to side reactions or impurities. Hence, these values are overestimated, but they give an idea of how the applied potential affects the overall control.

Table 6.3. *e*ATRP of MMA catalyzed by Cu/TPMA, with different applied potentials.[a]

Entry	E_{app} (V *vs.* SCE)	Q (C)	t (h)	Conv. (%)	k_p^{app} (h^{-1})	$M_{n,th}$ (10^{-3})	M_n (10^{-3})	*Đ*
1[b]	-0.27	14.3	5	40	0.11	18.8	35.7	2.06
2	-0.21	16.6	12	78	0.12	36.4	42.1	1.49
3	-0.15	8.94	12	77	0.11	36.0	45.9	1.12

[a] General conditions in **Figure 6.8**. $E_{1/2}$ = -0.214 V *vs.* SCE. [b] V_{tot} = 15 mL.

6.5. *e*ATRP in aqueous media catalyzed by Cu/1a and Cu/TPMA

*e*ATRP of oligo(ethylene glycol) methyl ether methacrylate (OEOMA) was performed with $[Cu^{II}\mathbf{1a}]^{2+}$ according to the guidelines defined for aqueous *e*ATRP: large Br^- excess, low monomer percentage, and $E_{app} > E^{\circ}$.[6, 13] The process was well-controlled showing linear first-order kinetics and good agreement between experimental and theoretical

molecular weights (**Figure 6.10**). The reaction reached 88% conversion in 3 h with very low dispersity. The result well matches the literature data with $[Cu^{II}TPMA]^{2+}$ as catalyst for the same system: 95% conversion in 4 h with $Đ = 1.17$.[6] Moreover, only 10 vol% of monomer was used in the previous work, while 20 vol% of OEOMA was processed herein, proving that a slight increase in monomer loading is not harmful, thus higher amount of produced polymer can be targeted with this system.

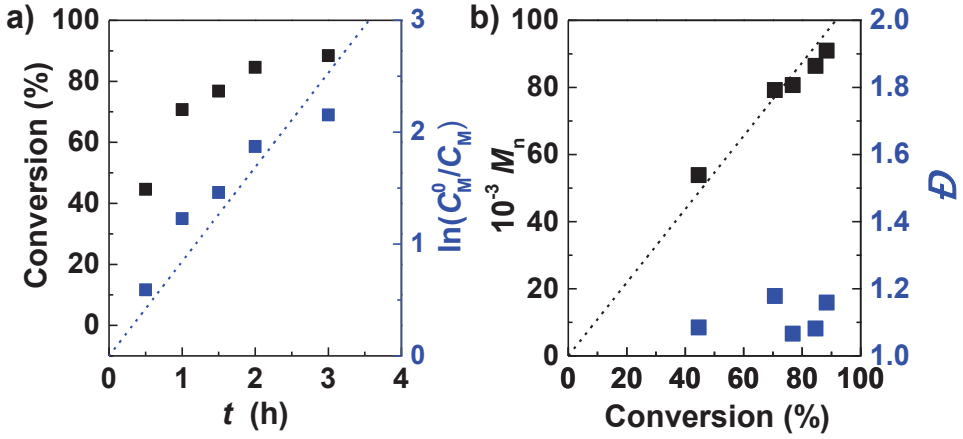

Figure 6.10. *e*ATRP of OEOMA 20 vol% in H_2O. $C_{OEOMA}/C_{HEBiB}/C_{[Cu^{II}\mathbf{1a}]^{2+}}/C_{Br^-}$ = 225/1/0.5/50, $C_{Cu^{2+}} = 10^{-3}$ M, $T = 25°C$, $V_{tot} = 15$ mL. a) Monomer consumption and first-order kinetic plot and b) MWs and dispersity evolution *vs.* conversion (adapted with permission from Ref. [14]. Copyright 2017, Elsevier).

Finally, aqueous *e*ATRP of methacrylic acid was tested with the new catalyst, considering the excellent results obtained recently with TPMA.[7] Indeed, the phenyl group on the TPMA skeleton seemed to not strongly affect the properties of the ligand, thus it is reasonable to expect a good stability for **1a** at very low pH, similarly to TPMA. As described in **Chapter 5**, 3 solutions were adopted to defeat the intramolecular cyclization process hampering well-controlled ATRP of MAA through the formation of a lactone: *i*) low pH, *ii*) excess of Cl^- instead of Br^-, and *iii*) $E_{app} < E^{\circ}$. *e*ATRP of MAA using TPMA as a ligand reached 96% conversion in 4 h, and the final polymer had $Đ = 1.49$, by working at pH = 0.9, $C_{NaCl} = 0.3$ M and $E_{app} = E^{\circ} - 0.12$ V (**Table 6.2, entry 9**). An excess of TPMA was proved to be beneficial, endorsing a better control and a slightly faster polymerization. By replacing TPMA with **1a**, a comparable result was obtained with 83% conversion in 5 h and $Đ = 1.49$ (**Table 6.2, entry 8** and **Figure 6.11**).

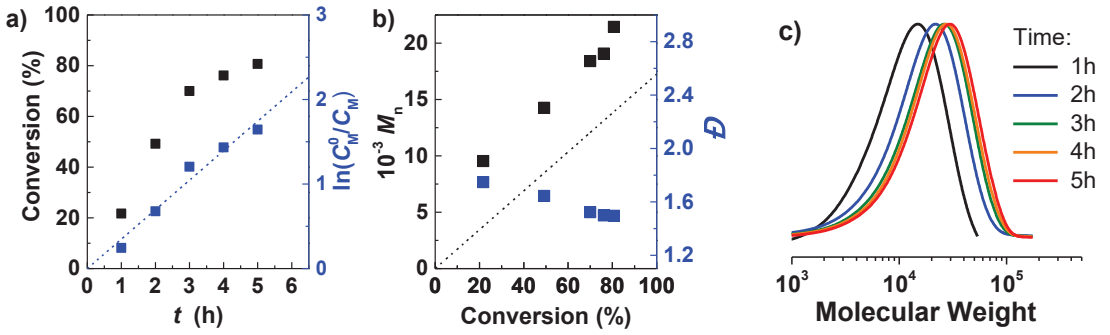

Figure 6.11. *e*ATRP of MAA 10 vol% in H_2O. $C_{MAA}/C_{BiBA}/C_{Cu^{II}}/C_{\mathbf{1a}}/C_{Cl^-}$ = 200/1/0.1/0.4/50, $C_{Cu^{2+}} = 10^{-3}$ M, T = 25°C, V_{tot} = 15 mL. a) Monomer consumption and first-order kinetic plot, and b) MWs and dispersity evolution *vs.* conversion, and c) GPC traces (adapted with permission from Ref. [14]. Copyright 2017, Elsevier).

Overall, the copper complex with **1a** is a suitable catalyst for aqueous *e*ATRP, even in acidic conditions, providing a catalytic efficiency comparable to the one observed with copper/TPMA under identical conditions.

6.6. Conclusions and perspectives

Eight novel copper catalysts have been synthesized and characterized in terms of structural and electrochemical properties. CV studies showed a small influence of the substituents in the phenyl ring on the redox properties of the catalyst and hence on its reactivity, the dominant effect being the electron-withdrawing nature of the phenyl substituent itself. The small influence of the substituents can be explained considering that the possible rotation of the biarylic system moves the substituents away from the metal centre.

Surprisingly, the presence of one phenyl ring on the TPMA backbone reduced significantly the activity of $[Cu^{I}L]^{+}$, while substituents on that ring had virtually no effect on catalyst activity. Nevertheless, Cu/**1a** complex resulted a robust and suitable catalyst for *e*ATRP in organic solvents with reactive monomers such as methyl methacrylate or in aqueous media, even operating at very low pH. Electrochemical studies suggested that all these new complexes have similar catalytic activities in *e*ATRP. Although the new catalyts are less reactive than the parent TPMA complex, their lower catalytic activity may be exploited to gain easy control of extremely reactive systems, where the activation rate is not an issue.

References

1. Tang, W.; Matyjaszewski, K. *Macromolecules* **2006,** 39, 4953-4959.
2. Matyjaszewski, K. *Macromolecules* **2012,** 45, 4015-4039.
3. Schröder, K.; Mathers, R. T.; Buback, J.; Konkolewicz, D.; Magenau, A. J.; Matyjaszewski, K. *ACS Macro Letters* **2012,** 1, 1037-1040.
4. Xia, J.; Gaynor, S. G.; Matyjaszewski, K. *Macromolecules* **1998,** 31, 5958-5959.
5. Kwak, Y.; Magenau, A. J.; Matyjaszewski, K. *Macromolecules* **2011,** 44, 811-819.
6. Fantin, M.; Isse, A. A.; Gennaro, A.; Matyjaszewski, K. *Macromolecules* **2015,** 48, 6862-6875.
7. Fantin, M.; Isse, A. A.; Venzo, A.; Gennaro, A.; Matyjaszewski, K. *J. Am. Chem. Soc* **2016,** 138, 7216-7219.
8. Elsen, A. M.; Burdyńska, J.; Park, S.; Matyjaszewski, K. *Macromolecules* **2012,** 45, 7356-7363.
9. Kaur, A.; Ribelli, T. G.; Schröder, K.; Matyjaszewski, K.; Pintauer, T. *Inorganic chemistry* **2015,** 54, 1474-1486.
10. Bortolamei, N.; Isse, A. A.; Di Marco, V. B.; Gennaro, A.; Matyjaszewski, K. *Macromolecules* **2010,** 43, 9257-9267.
11. Braunecker, W. A.; Tsarevsky, N. V.; Gennaro, A.; Matyjaszewski, K. *Macromolecules* **2009,** 42, 6348-6360.
12. Fantin, M.; Isse, A. A.; Bortolamei, N.; Matyjaszewski, K.; Gennaro, A. *Electrochimica Acta* **2016,** 222, 393-401.
13. Bortolamei, N.; Isse, A. A.; Magenau, A. J.; Gennaro, A.; Matyjaszewski, K. *Angewandte Chemie* **2011,** 123, 11593-11596.
14. Carmo dos Santos, N. A.; Lorandi, F.; Badetti, E.; Wurst, K.; Isse, A. A.; Gennaro, A.; Licini, G.; Zonta, C. *Polymer* **2017,** 128, 169-176.
15. Badetti, E.; Wurst, K.; Licini, G.; Zonta, C. *Chemistry-A European Journal* **2016,** 22, 6515-6518.
16. Berardozzi, R.; Badetti, E.; dos Santos, N. A. C.; Wurst, K.; Licini, G.; Pescitelli, G.; Zonta, C.; Di Bari, L. *Chemical Communications* **2016,** 54, 8428-8431.
17. Natali, M.; Badetti, E.; Deponti, E.; Gamberoni, M.; Scaramuzzo, F. A.; Sartorel, A.; Zonta, C. *Dalton Transactions* **2016,** 45, 14764-14773.
18. Comba, P.; Hauser, A.; Kerscher, M.; Pritzkow, H. *Angewandte Chemie International Edition* **2003,** 42, 4536-4540.
19. Qiu, J.; Matyjaszewski, K.; Thouin, L.; Amatore, C. *Macromolecular Chemistry and Physics* **2000,** 201, 1625-1631.
20. Lorandi, F.; Fantin, M.; Isse, A. A.; Gennaro, A. *Polymer* **2015,** 72, 238-245.
21. De Paoli, P.; Isse, A. A.; Bortolamei, N.; Gennaro, A. *Chemical Communications* **2011,** 47, 3580-3582.
22. Isse, A. A.; Bortolamei, N.; De Paoli, P.; Gennaro, A. *Electrochimica Acta* **2013,** 110, 655-662.
23. Fantin, M.; Lorandi, F.; Gennaro, A.; Isse, A. A.; Matyjaszewski, K. *Synthesis* **2017,** 49, 3311-3322.
24. Magenau, A. J.; Strandwitz, N. C.; Gennaro, A.; Matyjaszewski, K. *Science* **2011,** 332, 81-84.
25. Horn, M.; Matyjaszewski, K. *Macromolecules* **2013,** 46, 3350-3357.
26. Nanda, A. K.; Matyjaszewski, K. *Macromolecules* **2003,** 36, 8222-8224.

27. Tang, W.; Matyjaszewski, K. *Macromolecules* **2007,** 40, 1858-1863.
28. Guo, J. K.; Yin-Ning, Z.; Zheng-Hong, L. *AIChE Journal* **2017**, DOI: 10.1002/aic.15978.
29. Guo, J.-K.; Zhou, Y.-N.; Luo, Z.-H. *Macromolecules* **2016,** 49, 4038-4046.
30. Jakubowski, W.; Matyjaszewski, K. *Angewandte Chemie* **2006,** 118, 4594-4598.

Chapter 7.

Characterization of common ATRP catalysts and initiators in an Ionic Liquid

Table of contents

7.1. Introduction and aim of the work

In the last two decades, Ionic Liquids (ILs) gained a leading role in many fields of chemistry, mainly because of their low-toxicity, low-volatility and recyclability. Concerning polymerization processes, ILs have been largely employed as green solvents or even monomers.[1]

By definition, ILs are composed by anions and cations and melt below 373 K; in particular, the melting point of room temperature ionic liquids (RTILs) is around or below 298 K. Alkylammonium, alkylphosphonium, N,N'-dialkylimidazolium, N-alkylpyridinium cations are the most used cations in combination with tetrafluoroborate (BF_4^-), hexafluorophosphate (PF_6^-), trifluoromethansulfonate (OTf^-) and bis(trifluoromethylsulfonyl)imide (NTf_2^-) anions.

The physical properties of RTILs strongly depend on the particular cation/anion couple. Generally, they are highly viscous liquids, and greater viscosity is found for small symmetrical and non-planar anions and/or branched cations, or cationic structures bearing long alkyl chains.

Regarding their electrochemical properties, the conductivity of ILs is generally low, due to the high viscosity, the correlated motion of cations and anions, their size and the ability in delocalizing the anionic charge.[2] Nevertheless, their conductivity is sufficiently high to perform electrochemical measurements in the absence of any added supporting electrolyte. A related advantage is the exceptionally wide electrochemical stability window of ILs, which is narrower in ordinary solvents, mainly because of redox reactions involving the supporting electrolyte.[3, 4]

The electrochemical stability can however be weakened by oxygen, which exhibits high solubility in ILs, or by water and halide anions impurities descending from the production process.[5, 6] As reported recently, residual halide ions can be easily removed through electrochemical deposition on a silver electrode.[7] Electrochemical analysis in ILs suffers from low mass transport due to the high viscosity of the medium.[8] Moreover, some compounds showed a large difference between diffusion coefficients, *D*, of reduced and oxidized species.[9]

ILs showed some attractive features when used as ATRP solvents. Carmichael et al. reported the first traditional ATRP of methyl methacrylate (MMA) in RTILs, precisely in [BMIm][PF_6], triggered by CuBr/N-propyl-2pyridilmethyl amine (NPrPMI), and ethyl-α-bromo isobutyrate (EBiB) as initiator.[10] The polymerization rate was comparable to common organic solvents, the system presented always one phase and the IL with solubilized catalyst was successfully separated during polymer extraction with toluene, taking advantage of the insolubility of Cu complexes in this solvent. This promising synthesis led to several ATRPs in a series of ILs with different cations, all able to solubilize

monomers such as MMA and AN.[11, 12] Instead, the partial or complete insolubility of various monomers in some ILs became an advantage because the growing chains resided in the organic phase, while the catalyst was confined in the IL together with few radicals, thus preventing termination reactions. Various copolymers were synthesized by ATRP in [BMIm][PF_6], displaying very low dispersities.[13, 14] Moreover some ILs were simultaneously used as ligand and solvent for copper and iron mediated ATRP of MMA and AN, avoiding the need of externally added organic ligands.[15] In ARGET-ATRP of MMA and AN in various ILs, a strong effect of the cation on k_p was observed, with propagation rates that increased by increasing the alkyl chain length.[12] ICAR[16] and photo-ATRP[17] in ILs were also reported. Finally some attempts were made to induce tacticity in generated polymers by using chiral ILs that can interact with the propagating macroradicals.[18]

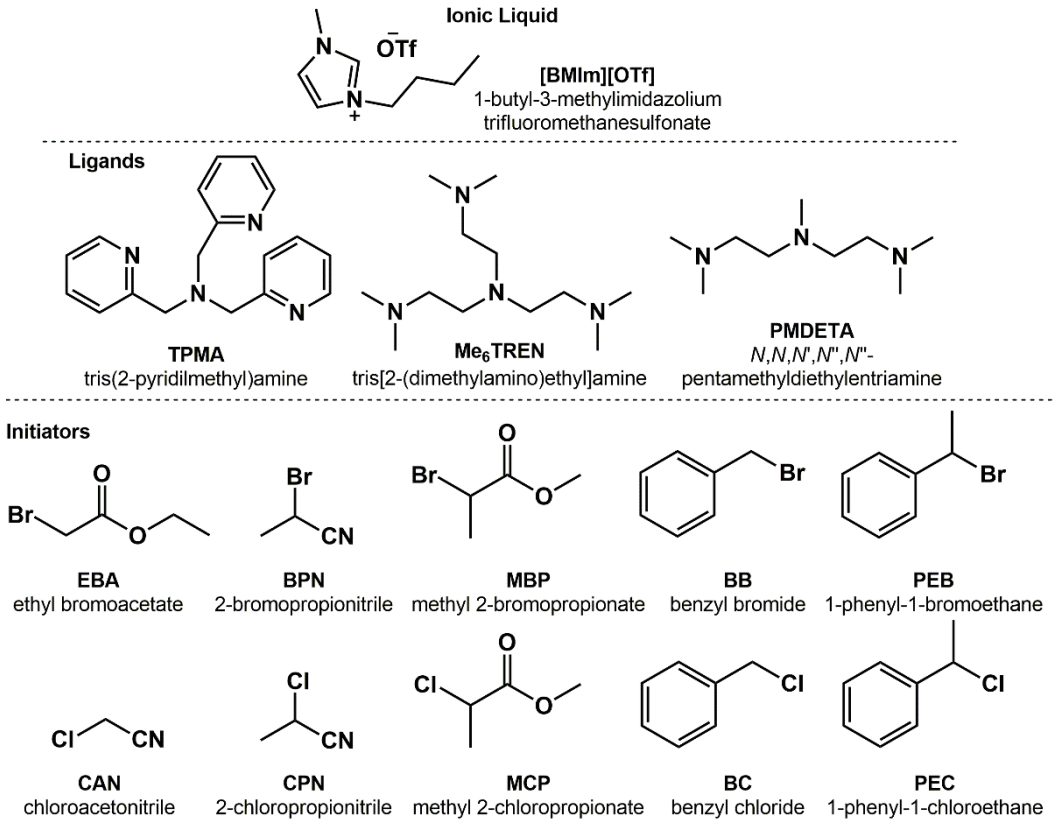

Figure 7.1. Structures of compounds relevant to the present Chapter.

Despite such a widespread application of ILs in ATRP, chemical and electrochemical properties of common catalysts and initiators were never analyzed in these media. For this reason, a basic electrochemical study was conducted on some commonly used ATRP catalysts and initiators (**Figure 7.1**) in [BMIm][OTf]. This IL was selected because of its relatively low viscosity and the good solubility displayed by conventional monomers (*e.g.*

methyl acrylate, methyl methacrylate, styrene) in this medium. The operating temperature was fixed at 50 °C to further reduce the viscosity and enhance the diffusion coefficient of redox probes and therefore the recorded current. The activation kinetics of analyzed initiators were also investigated by means of a rotating disk electrode.

7.2. Redox properties of common ATRP catalysts in [BMIm][OTf]

Cyclic voltammetry was performed in [BMIm][OTf] without adding any supporting electrolyte. All copper complexes were prepared *in situ* by stepwise addition of equimolar amounts of $Cu^{II}(OTf)_2$, a ligand (TPMA, Me_6TREN, or PMDETA), and Et_4NBr or Et_4NCl as halogen ions source for the ternary complexes.

CVs of binary complexes $[Cu^{II}L]^{2+}$ showed a quasi-reversible peak couple for the reduction of Cu^{II} to Cu^{I} (**Figure 7.2a**) and the standard reduction potential of each complex was estimated from the half-wave potential $E_{1/2} = (E_{pa} + E_{pc})/2$ (**Table 7.**). E^{e} of $[Cu^{II}L]^{2+}/[Cu^{I}L]^{+}$ showed a strong dependence on ligand type, decreasing in the order PMDETA ≅ Me_6TREN > TPMA, which is slightly different from the trend (PMDETA > TPMA > Me_6TREN) observed in traditional solvents.[19, 20]

Addition of X^{-} yielded ternary complexes $[X–Cu^{II}L]^{+}$, which exhibited similar CV pattern as $[Cu^{II}L]^{2+}$, albeit at more negative potentials (**Figure 7.2b and c**). An exception to this behavior, which is normally observed for ATRP catalysts in organic solvents, is represented by $[Br–Cu^{II}TPMA]^{+}$ and $[Br–Cu^{II}PMDETA]^{+}$, whose E^{e} is practically identical to E^{e} of $[Cu^{II}TPMA]^{+}$ and $[Cu^{II}PMDETA]^{+}$, respectively (**Table 7.**). The shift in the redox potential depends on the relative stability of Cu^{I} and Cu^{II} complexes: more negative potentials for ternary complexes compared to binary ones, observed in organic solvents, arise from the enhanced stabilization of Cu^{II}.[22] Conversely, in water this negative shift can be observed only with TPMA,[23] similarly to what is reported herein for [BMIm][OTf]. All $[Cl\text{-}Cu^{II}L]^{+}$ complexes showed E^{e} values more negative than those of their respective $[Br\text{-}Cu^{II}L]^{+}$ complexes, accounting for the stronger affinity of Cu^{II} complexes (*i.e.* halidophilicity) for Cl^{-} than Br^{-}, in agreement with trend already observed in acetonitrile.[24] The reduction potentials of ternary complexes followed the expected trend (PMDETA > TPMA > Me_6TREN) for both $[Cl–Cu^{II}L]^{+}$ and $[Br–Cu^{II}L]^{+}$.[20]

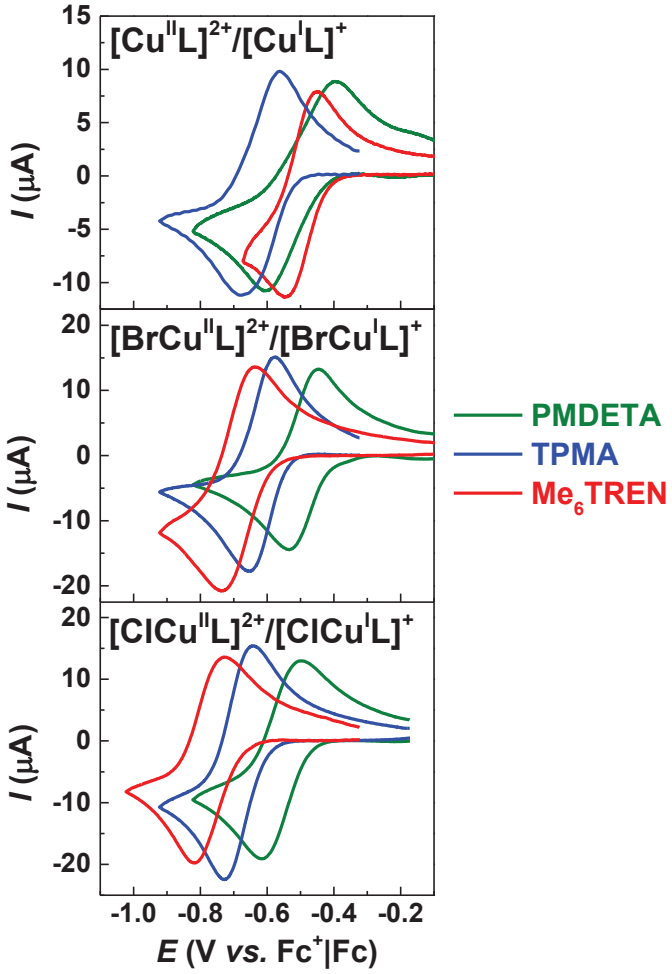

Figure 7.2. CVs of 10^{-2} M a) $[Cu^{II}L]^{2+}$, b) $[BrCu^{II}L]^{+}$ and c) $[ClCu^{II}L]^{+}$ in [BMIm][OTf] at $\upsilon = 0.1$ V s^{-1} and $T = 50$ °C; L = TPMA, PMDETA or Me_6TREN (adapted with permission from Ref. [21]. Copyright 2017, Elsevier).

Table 7.1. Standard reduction potentials of Cu^{II}/L/X^- complexes in [BMIm][OTf], $T = 50$ °C.

	$E^{\ominus}$ (V *vs.* Fc^+|Fc) [a]		
Redox couple	L = Me_6TREN	L = TPMA	L = PMDETA
$[Cu^{II}L]^{2+}/[Cu^{I}L]^{+}$	-0.51	-0.62	-0.50
$[BrCu^{II}L]^{+}/[BrCu^{I}L]$	-0.69	-0.61	-0.49
$[ClCu^{II}L]^{+}/[ClCu^{I}L]$	-0.78	-0.69	-0.56

[a] $E^{\ominus}$ values were calculated as the average of half-wave potentials, $E_{1/2} = (E_{pc} + E_{pa})/2$, measured over scan rates ranging from 0.02 to 1 V s^{-1}.

7.3. Redox properties of some ATRP initiators in [BMIm][OTf]

As described in **Chapter 1** (**Section 1.3.2**), alkyl halides used as initiators in ATRP undergo a dissociative electron transfer promoted by $[Cu^{I}L]^{+}$.[21] DET reactions in organic halides have been extensively studied. In general, DET can follow two different pathways: *i*) a stepwise pathway involving the formation of a radical anion intermediate ($RX^{\bullet -}$), which quickly dissociates generating $R^{\bullet}$ and X^{-}, *ii*) a concerted mechanism with the electron transfer occurring simultaneously with bond rupture to form $R^{\bullet}$ and X^{-} (**Scheme 7.1**).[25] Theoretical and experimental studies showed that the stepwise mechanism is traditionally preferred by aromatic RX, able to accommodate the electron in a low energy π* orbital, generating a detectable radical anion. Then, the electron shifts into the σ* molecular orbital of the C–X bond, which finally breaks (intramolecular DET).[26] Conversely, aliphatic halides need to place the electron in a high energy σ* orbital, thus the simultaneous formation of two fragments is thermodinamically favored, but the ET becomes very slow.[27]

$R^{\bullet}$ formed during the DET is generally unstable and subjected to a second electron transfer to form a carbanion. In fact, if the potential of the second ET (E_2) is more positive than the potential of the DET (E_1), when the applied potential equals E_1 the radical is immediately reduced to a carbanion. This is commonly observed on non-catalytic electrodes, like glassy carbon.[28] Instead, on catalytic electrodes such as Ag, it is possible that $E_2 < E_1$. In such cases the radical is not further reduced at E_1.[29] Besides the nature of the electrode material, the difference between E_1 and E_2 depends on the nature of substituents in α position to C–X.

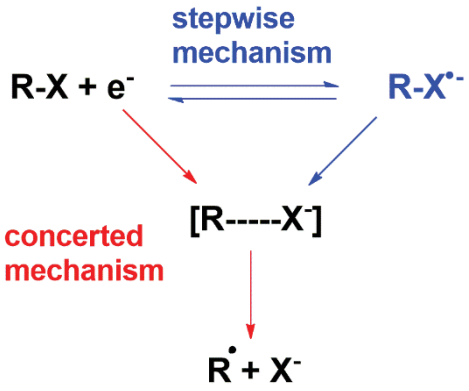

Scheme 7.1. Dissociative electron transfer mechanisms for alkyl halides used as ATRP initiators, and successive reduction to carbanions.

Previous works on the reduction of RX in organic solvents showed that in the case of compounds bearing a C–H group with a strong electron withdrawing substituent (*e.g.* Z = CN, COOMe) in α position, R^- can be protonated by the parent RX (Eq. 7.1).[30] To avoid possible self-protonation reactions, all CV investigations were performed in the presence of acetic acid (HAc) in slight excess over RX (Eq. 7.2).

$$(\mathrm{RCHZ})^- + \mathrm{RCH(Z)X} \rightleftharpoons \mathrm{RCH_2Z} + (\mathrm{RC(Z)X})^- \quad (7.1)$$

$$\mathrm{R}^- + \mathrm{HAc} \rightleftharpoons \mathrm{RH} + \mathrm{Ac}^- \quad (7.2)$$

CV of the analyzed alkyl halides exhibited an irreversible cathodic peak attributable to a $2e^-$ reduction of RX to R^- and X^-, as already observed in $[BMIm][BF_4]$[31] and acetonitrile.[32] The peak remained irreversible, shifted to more negative potentials and became more stretched upon increasing the scan rate, thus confirming the total irreversibility of the redox reaction. This observation is consistent with a dissociative electron transfer leading to the formation of two fragments, R• and X^-. Regardless of DET mechanism, a second TE, occurring at a more positive potential, caused the immediate reduction of R• to a carbanion.

Considering the aliphatic nature of selected alkyl halides, a concerted dissociative electron transfer mechanism was expected. The transfer coefficient α can be calculated from the dependence of peak potential, E_p, on scan rate,[31, 32] according to Eq. 7.3.

$$\frac{\partial E_p}{\partial \log v} = -1.15\frac{RT}{\alpha F} \quad (7.3)$$

All RX exhibited a transfer coefficient α much lower than 0.5, as expected for a concerted DET (**Table 7.2**).

E_p depends on molecular structure of RX: in general, E_p(RCl) < E_p(RBr), whereas within a series of chlorides or bromides E_p depends on the electron withdrawing power of the α-substituent, decreasing in the order CN > CO_2Me >> Ph.[33] More important, E_p of RX is more than 1.0 V more negative than E^e of the copper complexes, excluding the risk of undesired RX reduction in *e*ATRP.

Table 7.2. Electrochemical parameters of initiators and k_{act} for the activation reaction by Cu^{I}/TPMA/Br^{-} in [BMIm][OTf], T = 50 °C.

Entry	RX	E_p [a] (V)	α [b]	k_{act} ($M^{-1}s^{-1}$) [c]
1	EBA	-1.88	0.37	5.6
2	BB	-1.94	0.31	1.6×10^2
3	MBP	-1.82	0.39	2.1×10^2
4	PEB	-1.83	0.26	1.6×10^3 [d]
5	BPN	-1.71	0.34	-
6	BC	-2.41	0.27	3.9
7	MCP	-2.18	0.27	9.7
8	PEC	-2.39	0.32	3.3×10^1
9	CAN	-2.14	0.34	2.3×10^2
10	CPN	-2.17	0.30	9.0×10^2

[a] *vs.* Fc^{+}|Fc measured at υ = 0.1 V s^{-1}. [b] Determined from the slopes ($\partial E_p/\partial \log \upsilon = -1.15RT/\alpha F$) of E_p versus $\log\upsilon$ plots. [c] Reaction between RX and $[Cu^{I}TPMA]^{+}$ in the presence of TEMPO and X^{-} ($C_{Cu^{I}}/C_{TEMPO}/C_{X^{-}}$: 1/10/2). Unless otherwise stated, k_{act} accuracy was ± 5-10%. [d] k_{act} accuracy ± 20%.

7.4. Activation kinetics of selected RX by $[Cu^{I}TPMA]^{+}$ in [BMIm][OTf]

The kinetics of ATRP activation in ILs was investigated by monitoring the decrease of $[Cu^{I}L]^{+}$ concentration at a rotating disk electrode. TEMPO was used as a radical scavenger to kinetically isolate the activation step, by irreversibly trapping all generated radicals.[30] All kinetic analyses were performed in the presence of a 10-fold excess of TEMPO over $[Cu^{I}L]^{+}$. Halide ions were also added ($C_{Cu^{I}}/C_{X^{-}}$: 1/2) since typically ATRP is performed starting with $Cu^{II}X_2$ and therefore X^{-} is always present in the reaction medium. Rigorously, the activation rate constant measured under described conditions is an apparent constant, whose value depends on $C_{X^{-}}$,[34] as explained for K_{ATRP} measurement in **Chapter 3**.

From an experimental point of view, a solution of $C_{TPMA}/C_{X^{-}}/C_{TEMPO}$ = 1/2/10 in [BMIm][OTf] was prepared and carefully degassed. Cu^{I} was withdrawn from a stock solution, under inert atmosphere, and injected into the cell. A fixed potential (E_{app} = -0.3 V *vs.* Fc^{+}|Fc) was applied to provide diffusion-controlled oxidation of Cu^{I} (**Figure 7.3a**) and the corresponding limiting current (I_L) was recorded (see Levich equation, Eq. 3.1 in **Chapter 3**, **Section 3.2**). Immediately after, RX was injected and I_L decay was monitored.

All investigated initiators were sufficiently reactive to adopt a second-order kinetic regime with $C_{RX} = C_{Cu^I}$ = 2-10 × 10^{-3} M. It must be mentioned that Cu^I species are typically involved in disproportionation equilibria, which however were proven to be much slower than RX activation.[34] Considering that under the adopted experimental conditions Cu^I concentration is proportional to I_L, the kinetic rate law is

$$\frac{1}{C_{[Cu^I L]^+}} - \frac{1}{C^0_{[Cu^I L]^+}} = \frac{I^0_L}{I_L C^0_{[Cu^I L]^+}} - \frac{1}{C^0_{[Cu^I L]^+}} = k_{act} t \quad (7.4)$$

where the superscript "0" indicates the values of I_L and $[Cu^ITPMA]^+$ concentration at t = 0. All systems gave the expected linear behavior from which k_{act} was extracted. k_{act} for BPN could not be measured (Cu^I lifetime < 1 s).

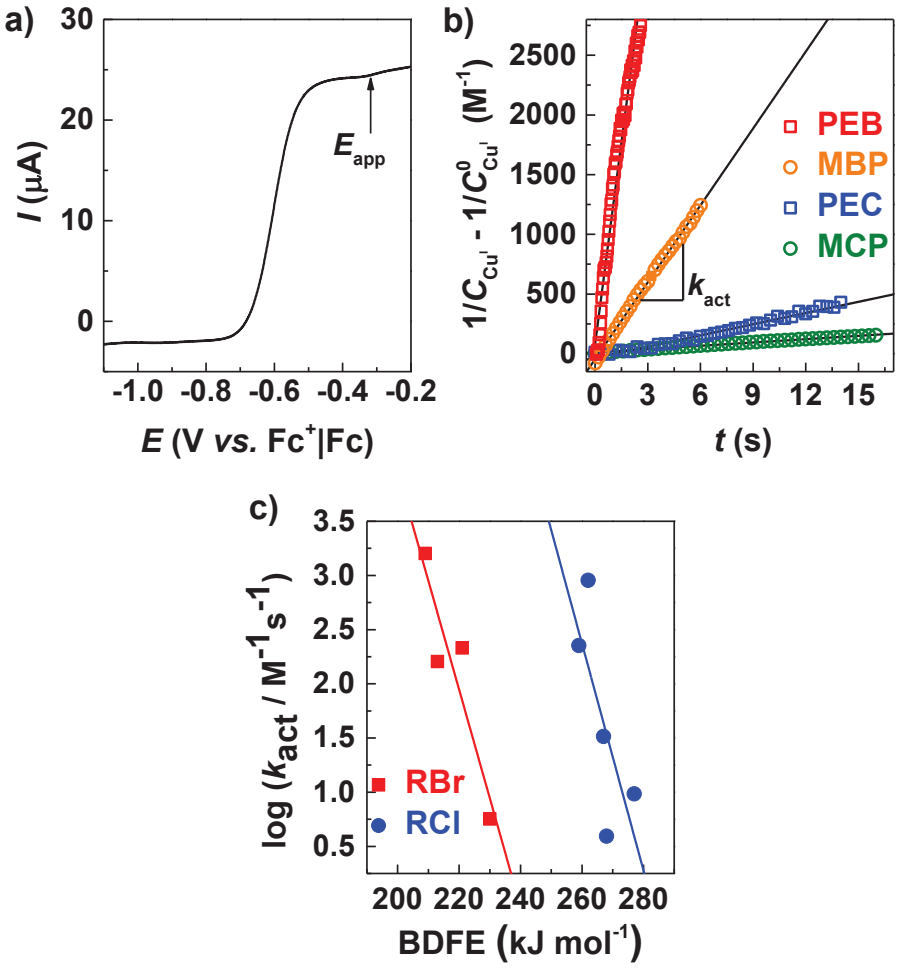

Figure 7.3. a) Linear sweep voltammetry of 5 mM $[BrCu^ITPMA]$ in [BMIm][OTf] at RDE, υ = 0.005 V s^{-1}, ω_{RDE} = 4000 rpm (the arrow indicates E_{app} during RX activation experiments). b) Kinetic analysis of RX activation by $[Cu^ITPMA]^+$. c) Correlation between k_{act} and bond dissociation free energy (BDFE) of R−X (adapted with permission from Ref. [21]. Copyright 2017, Elsevier).

As expected, RBr was more reactive than RCl of the same structure ($k_{act(RBr)} > 10\ k_{act(RCl)}$), accounting for the weaker C–X bond in the initiator when X = Br than X = Cl (**Table 7.2**).[35] The overall structure of RX also strongly affected k_{act}. Secondary RX were more reactive than primary alkyl halides of the same type, as previously reported. This is most likely due to the higher stability of secondary alkyl radicals than primary R•.[36] Considering the effect of the substituent on α position of C–X, the following order of increasing k_{act} was observed: $CO_2Me < Ph < CN$. Activation rate constants in [BMIm][OTf] were of the same order of magnitude of k_{act} values reported in acetonitrile or DMSO.[20, 34] However it should be highlighted that k_{act} values measured in ILs are slightly underestimated, due to the presence of halide ions that decreased the amount of catalytic $[Cu^{I}L]^{+}$ (as explained in **Chapter 3**, **Section 3.7**).[37]

Seeking a useful structure-reactivity relationship, the overall activation reaction can be split, from the thermodynamic point of view, into 4 steps (Eq. 7.5-7.9). A thermochemical cycle can be written to evaluate the Gibbs free energy of the overall activation reaction, $\Delta_r G^{\ominus}_{ATRP}$, which is equal to the sum of the Gibbs free energies of the separate steps.[20]

i) $\mathrm{R-X} \rightleftharpoons \mathrm{R^{\bullet} + X^{\bullet}}$ $\Delta_r G_i^{\ominus} = \mathrm{BDFE}$ (7.5)

ii) $\mathrm{X^{\bullet} + e^{-} \rightleftharpoons X^{-}}$ $\Delta_r G_{ii}^{\ominus} = -FE^{\ominus}_{X/X^-}$ (7.6)

iii) $[\mathrm{XCu^{I}L}] \rightleftharpoons [\mathrm{XCu^{II}L}]^{+} + e^{-}$ $\Delta_r G_{iii}^{\ominus} = E^{\ominus}_{[XCu^{II}L]^+/[XCu^{I}L]}$ (7.7)

iv) $[\mathrm{Cu^{I}L}]^{+} + \mathrm{X^{-}} \rightleftharpoons [\mathrm{XCu^{I}L}]$ $\Delta_r G_{iv}^{\ominus} = -RT \ln K_X^I$ (7.8)

$\mathrm{R-X} + [\mathrm{Cu^{I}L}]^{+} \rightleftharpoons [\mathrm{XCu^{II}L}]^{+} + \mathrm{R^{\bullet}}$ $\Delta_r G^{\ominus}_{ATRP} = -RT \ln K_{ATRP}$ (7.9)

For a selected catalyst and a series of RCl or RBr, three out of four reactions remain fixed: only R–X dissociation to R• and X• changes (Eq. 7.5). Therefore, $\Delta_r G^{\ominus}_{ATRP}$ depends exclusively on the bond dissociation free energy (BDFE) of RX. It follows that k_{act} can be correlated with the BDFE of the initiator (**Figure 7.3c**). A roughly linear plot was obtained for each series, suggesting that k_{act} of different RX should be predictable, if the relative BDFEs are known. Actually, BDFEs were not available in ILs and their solvation effects might significantly differ from those of traditional solvents, thus BDFE values calculated in vacuum were used.[35]

7.5. Conclusions and perspectives

The redox properties of common ATRP catalysts and initiators were analyzed in [BMIm][OTf], one of the imidazolium-based Ionic Liquids mostly used as a solvent in radical polymerizations. This study confirms that Cu complexes and RX behavior is similar in ILs and in organic solvents. In general, E^e of $[XCu^{II}L]^+$ is more negative than that of $[Cu^{II}L]^{2+}$, indicating that X^- stabilizes more Cu^{II} than Cu^{I}, which is a crucial requisite of a good ATRP catalyst. Reductive cleavage of R–X follows a concerted mechanism that requires potentials much more negative than the typical cathodic potentials used in *e*ATRP.

Activation rate constants of selected RX by $[Cu^{I}TPMA]^+$ were measured by means of a rotating disk electrode. Measured values were comparable to activation rate constants reported in common solvents. Also structure-reactivity correlations similar to those observed in molecular solvents were found.

In conclusion, [BMIm][OTf] is a suitable solvent for ATRP catalyzed by copper complexes. Very recently in fact, the first *e*ATRP in IL was successfully performed.[38] Collected data provide a useful database for the selection of the appropriate catalytic systems in ILs.

References

1. Kubisa, P. *Progress in Polymer Science* **2004,** 29, 3-12.
2. Every, H. A.; Bishop, A. G.; MacFarlane, D. R.; Orädd, G.; Forsyth, M. *Physical chemistry chemical physics* **2004,** 6, 1758-1765.
3. Bonhote, P.; Dias, A.-P.; Papageorgiou, N.; Kalyanasundaram, K.; Grätzel, M. *Inorganic chemistry* **1996,** 35, 1168-1178.
4. MacFarlane, D.; Meakin, P.; Sun, J.; Amini, N.; Forsyth, M. *The Journal of Physical Chemistry B* **1999,** 103, 4164-4170.
5. Seddon, K. R.; Stark, A.; Torres, M.-J. *Pure and Applied Chemistry* **2000,** 72, 2275-2287.
6. Widegren, J. A.; Laesecke, A.; Magee, J. W. *Chemical Communications* **2005**, 1610-1612.
7. Arnaboldi, S.; Magni, M.; Mussini, P. R.; Gennaro, A.; Isse, A. A. *Electrochemistry Communications* **2015,** 51, 46-49.
8. Zistler, M.; Wachter, P.; Wasserscheid, P.; Gerhard, D.; Hinsch, A.; Sastrawan, R.; Gores, H. *Electrochimica acta* **2006,** 52, 161-169.
9. Evans, R. G.; Klymenko, O. V.; Hardacre, C.; Seddon, K. R.; Compton, R. G. *Journal of Electroanalytical Chemistry* **2003,** 556, 179-188.

10. Carmichael, A. J.; Haddleton, D. M.; Bon, S. A.; Seddon, K. R. *Chemical Communications* **2000**, 1237-1238.

11. Biedroń, T.; Kubisa, P. *Macromolecular Rapid Communications* **2001,** 22, 1237-1242.

12. Chen, H.; Liu, D.; Song, Y.; Qu, R.; Wang, C. *Polymers for Advanced Technologies* **2011,** 22, 1513-1517.

13. Wang, G.-X.; Lu, M.; Hou, Z.-H.; Wu, H. *Journal of Polymer Research* **2013,** 20, 80.

14. Shim, J.-J. *Colloid and Polymer Science* **2015,** 293, 617-623.

15. Chen, H.; Wang, C.; Liu, D.; Wang, M.; Ji, C. *Journal of Applied Polymer Science* **2011,** 122, 3298-3302.

16. Wang, G.; Lu, M.; Zhong, M.; Wu, H. *Journal of Polymer Research* **2012,** 19, 9782.

17. Wang, G.-X.; Lu, M.; Hou, Z.-H.; Yang, C.-A.; Liang, E.-X.; Liu, L.-c.; Wu, H.; Li, X.-L.; Xu, Y.-X. *Journal of Polymer Research* **2015,** 22, 60.

18. Biedroń, T.; Kubisa, P. *Journal of Polymer Science Part A: Polymer Chemistry* **2005,** 43, 3454-3459.

19. Braunecker, W. A.; Tsarevsky, N. V.; Gennaro, A.; Matyjaszewski, K. *Macromolecules* **2009,** 42, 6348-6360.

20. Fantin, M.; Isse, A. A.; Bortolamei, N.; Matyjaszewski, K.; Gennaro, A. *Electrochimica Acta* **2016,** 222, 393-401.

21. Lorandi, F.; De Bon, F.; Fantin, M.; Isse, A. A.; Gennaro, A. *Electrochemistry Communications* **2017,** 77, 116-119.

22. Bortolamei, N.; Isse, A. A.; Magenau, A. J.; Gennaro, A.; Matyjaszewski, K. *Angewandte Chemie* **2011,** 123, 11593-11596.

23. Fantin, M.; Isse, A. A.; Gennaro, A.; Matyjaszewski, K. *Macromolecules* **2015,** 48, 6862-6875.

24. Bortolamei, N.; Isse, A. A.; Di Marco, V. B.; Gennaro, A.; Matyjaszewski, K. *Macromolecules* **2010,** 43, 9257-9267.

25. Costentin, C.; Robert, M.; Savéant, J.-M. *Chemical physics* **2006,** 324, 40-56.

26. Andrieux, C. P.; Savéant, J.-M.; Tallec, A.; Tardivel, R.; Tardy, C. *Journal of the American Chemical Society* **1997,** 119, 2420-2429.

27. Cardinale, A.; Isse, A. A.; Gennaro, A.; Robert, M.; Savéant, J.-M. *Journal of the American Chemical Society* **2002,** 124, 13533-13539.

28. Savéant, J.-M., Single Electron Transfer and Nucleophilic Substitution. In *Advances in Physical Organic Chemistry*, Bethell, D., Ed. Academic Press: 1991; Vol. Volume 26, pp 1-130.

29. Isse, A. A.; De Giusti, A.; Gennaro, A. *Tetrahedron letters* **2006,** 47, 7735-7739.

30. Isse, A. A.; Bortolamei, N.; De Paoli, P.; Gennaro, A. *Electrochimica Acta* **2013,** 110, 655-662.

31. Isse, A. A.; Scarpa, L.; Durante, C.; Gennaro, A. *Physical Chemistry Chemical Physics* **2015,** 17, 31228-31236.

32. Isse, A. A.; Berzi, G.; Falciola, L.; Rossi, M.; Mussini, P. R.; Gennaro, A. *Journal of Applied Electrochemistry* **2009,** 39, 2217.

33. Isse, A. A.; Lin, C. Y.; Coote, M. L.; Gennaro, A. *The Journal of Physical Chemistry B* **2010,** 115, 678-684.

34. Lorandi, F.; Fantin, M.; Isse, A. A.; Gennaro, A. *Polymer* **2015,** 72, 238-245.

35. Lin, C. Y.; Coote, M. L.; Gennaro, A.; Matyjaszewski, K. *Journal of the American Chemical Society* **2008,** 130, 12762-12774.

36. Tang, W.; Matyjaszewski, K. *Macromolecules* **2007,** 40, 1858-1863.

37. De Paoli, P.; Isse, A. A.; Bortolamei, N.; Gennaro, A. *Chemical Communications* **2011,** 47, 3580-3582.

38. De Bon, F.; Fantin, M.; Isse, A. A.; Gennaro, A. *Polymer Chemistry*, *submitted*.

Chapter 8.

Hydrophilic catalyst and anionic surfactant: a powerful interacting system for (mini)emulsion ATRP

Table of contents

8.1. Introduction and aim of the work

Dispersed media are eco-friendly systems, less toxic and less expensive than most organic solvents. Polymerizations in dispersed media, such as microemulsion, miniemulsion, emulsion, and dispersion, are extremely attractive for the excellent heat transfer properties and low environmental impact.[1-3] In particular, oil-in-water miniemulsions allow the preparation of nanoparticles with different morphology that can find applications in biomedicine, pharmaceutics and nanotechnology.[4]

In polymerizations in miniemulsion, monomer droplets act as "nanoreactors", where the polymerization process occurs.[4] Therefore, in ATRP, both the catalyst and the initiator should be sufficiently hydrophobic to reside in the droplets (**Scheme 8.1**). Many efforts were indeed devoted to the synthesis of extremely hydrophobic ligands able to form active Cu complexes confined inside the polymerization *loci*. BPMODA and BPMODA* (**Figure 8.1**), which own a pyridinic structure and a long alkylic chain, gave optimum results in miniemulsion ATRP with low-ppm catalyst loading.[5, 6]

Other fundamental components of a miniemulsion system are the surfactant and the co-surfactant. In ATRP, generally non-ionic surfactants are employed to avoid any interaction with the Cu complex.[1] The co-surfactant is a hydrophobic molecule, which prevents the Ostwald-ripening of droplets during the polymerization. Hexadecane (HD) is typically used. Miniemulsions are generated by mixing all components and applying high shearing forces, like ultrasound or microwave, until a stable "milky" solution is obtained.

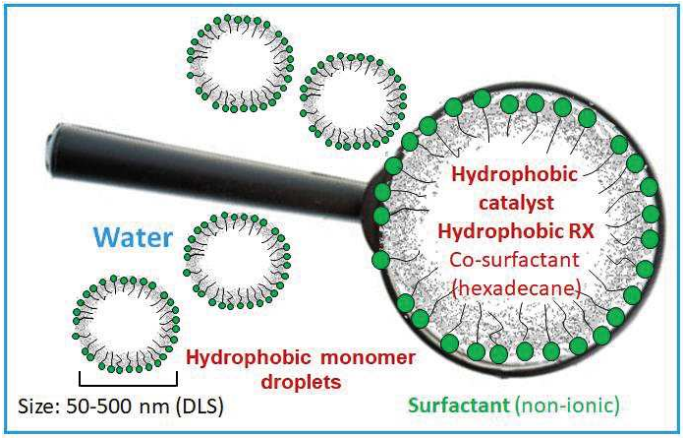

Scheme 8.1. Schematic representation of the traditional composition of a miniemulsion ATRP system.

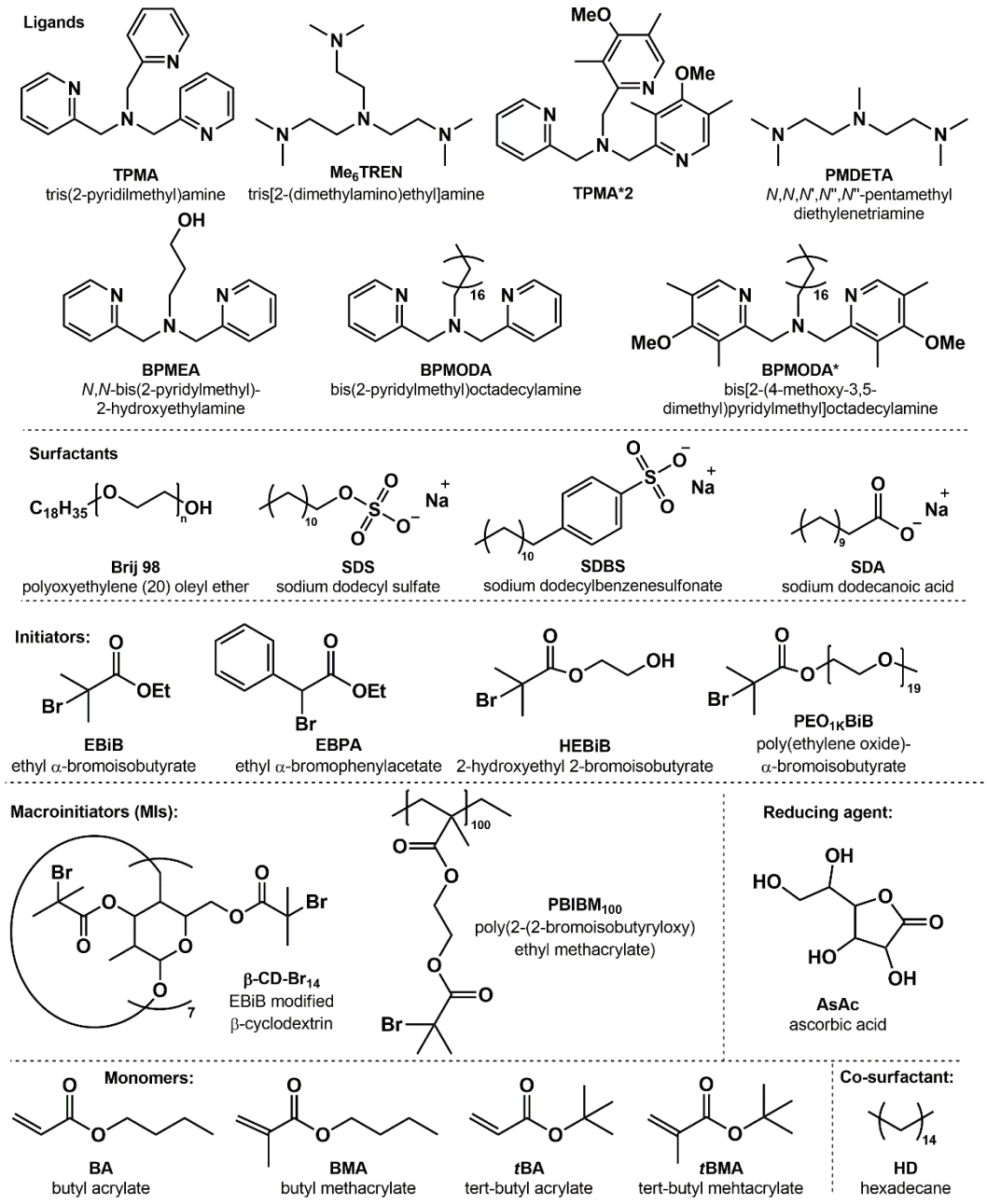

Figure 8.1. Chemical structures of compounds relevant to the present chapter.

A great advantage of miniemulsion (and emulsion) systems is the compartmentalization of catalyst molecules and radicals. This phenomenon, whose entity strongly depends on droplet (particles) size, as well as on the amount of catalyst and radicals, has two main effects. *i*) The segregation effect: radicals located in different particles cannot react with each other, thus reducing the odds of terminations; *ii*) the confined space effects: the reaction rate between two molecules located in the same small space is enhanced with decreasing the particles size. Essentially, polymerizations should become faster by decreasing particles size, whereas dispersity of the generated polymer should decrease.[7-9]

Combining eco-friendly (mini)emulsions with electrosynthetic methods offers an additional advantage, since the use of electrons as reagents does not involve the formation of any of the by-products observed when using reducing or oxidizing agents.[10]

*e*ATRP under heterogeneous conditions is challenging, because in (mini)emulsion, electrode and reactants are separated: the electrode is in contact with the continuous aqueous phase, while polymerization reactants (monomer, initiator, and radicals) are dispersed in the organic phase.[11] Therefore, to trigger the polymerization the electrochemical stimulus must reach the aqueous phase (crossing a first electrode|liquid interface) and then shuttle to the dispersed phase (crossing a second liquid|liquid interface). Moreover, radicals must be continuously activated/deactivated once the electrochemical stimulus has reached the organic phase.

These observations led to the development of a dual catalytic system for *e*ATRP in miniemulsion, composed of one hydrophobic and one hydrophilic copper catalyst.[11] The water-soluble catalyst was needed to close the electrochemical circuit between the WE and the hydrophobic catalyst. Thus, the WE was in contact with the aqueous phase, from which the water-soluble catalyst shuttled the electrochemical stimulus to the hydrophobic catalyst confined in monomer droplets. A series of Cu complexes and polymerization conditions (E_{app}, catalyst loading, DP) was tested for miniemulsion *e*ATRP of BA. The best dual-catalyst system was the one composed of hydrophilic Cu/BPMEA and hydrophobic Cu/BPMODA*. Interestingly, the partition of the two complexes was much more relevant to polymerization outcomes than the activity of the catalysts.

Nonetheless, a much simpler approach can be used to effectively run *e*ATRP in miniemulsion. Indeed, we showed that some hydrophilic Cu complexes can interact with anionic surfactants, generating neutral ion pairs that can enter the hydrophobic droplets and catalyze the polymerization process.[12] Besides simplifying the previously proposed setup, this approach suggested a paradigm shift in miniemulsion ATRP. Actually, super hydrophobic ligands (*e.g.* BPMODA, BPMODA*), specifically designed to confine the catalyst in droplets, and non-ionic surfactants are now replaced by commercial catalysts and inexpensive anionic surfactants. Moreover, to be removed from the final polymer, hydrophobic catalysts required complex purification procedures. Instead, simple crushing of the miniemulsion by dilution and centrifugation showed complete migration of the hydrophilic complex to the aqueous phase, leaving only few ppm of metal in the precipitated polymer. Cu/TPMA and sodium dodecyl sulfate (SDS) turned out as the best

combination of catalyst and surfactant, providing well-controlled homopolymers, block copolymers and more complex architectures, such as stars and brushes, *via e*ATRP and ARGET-ATRP.

A detailed electrochemical analysis was performed to study the interaction between selected catalysts and surfactants, whereas partition experiments confirmed the presence of some hydrophilic copper complex inside the hydrophobic monomer. These investigations are reported in the following sections, together with some outstanding results obtained with the new catalytic system in miniemulsion *e*ATRP and ARGET ATRP.[13]

The last part of this chapter shows some preliminary results concerning the successful application of this catalytic system to *ab initio* emulsion ARGET ATRP, despite the substantial differences between the two types of dispersed media. Indeed, polymerizations in emulsion require a hydrophilic initiator to start the process inside the monomer-swollen micelles. The largest part of the monomer forms some reservoirs from which monomer molecules diffuse toward the polymerization *loci*. Also, the catalyst needs to be water-soluble, thus Cu/TPMA-SDS system seemed a promising candidate for this environment.

8.2. Characterization of $[Br–Cu^{II}L]^+$/SDS interaction

8.2.1. Electrochemical study of $[Br–Cu^{II}L]^+$/SDS interaction

Cyclic voltammetry was used to analyze the behavior of three $[Br–Cu^{II}L]^+$ complexes at different SDS concentrations (**Figure 8.2**). The electrochemical response of all catalysts drastically changed when the surfactant was added.

In "pure" aqueous media (water + 0.1 M NaBr), the standard reduction potential of the redox couple $[Br–Cu^{II}TPMA]^+/[Br–Cu^{I}TPMA]$ was determined as $E_{1/2}$ = -0.307 V *vs.* SCE, in good agreement with previously reported values,[14] while ΔE_p = 80 mV (υ = 0.1 V s^{-1}, T = 65 °C). In the presence of SDS, both the cathodic and anodic peaks decreased in intensity (**Figure 8.2a**). By increasing the surfactant amount, the peak couple shifted toward more negative potentials, and a stable value of $E_{1/2}$ = -0.331 V *vs.* SCE was registered for C_{SDS} > 9 mM, while ΔE_p remained approximately constant at 95 mV.

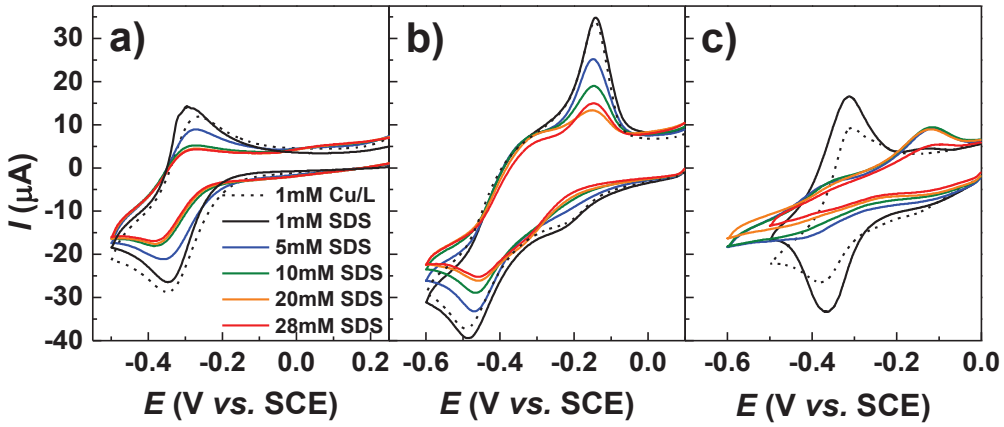

Figure 8.2. CVs of 10^{-3} M a) [Br–Cu^{II}TPMA]$^+$, b) [Br–Cu^{II}Me$_6$TREN]$^+$ and c) [Br–Cu^{II}(TPMA*2)]$^+$, in water + 0.1 NaBr with increasing amounts of SDS. WE = Pt, $\upsilon = 0.1$ Vs^{-1}, $T = 65$ °C.

A similar behavior was previously reported for various cobalt and copper complexes.[15-18] The decrease in i is a direct consequence of the lower diffusion coefficients of the micelle-bound complexes. Bonding of the complexes to the micelles is also responsible of the increased irreversibility of the electron transfer, *i.e.* larger ΔE_p values. Essentially, the catalyst moves through the solution with the smaller diffusion coefficient of the much bigger micelles. This electrochemical behavior indicated that the cationic Cu species progressively bound to the anionic micelles. The shift in the $E_{1/2}$ ($\approx E^{\ominus}$) value (*ca.* 30 mV) suggested that [Br–Cu^{II}L]$^+$ interacted more strongly than [Br–Cu^{I}L].[19] Defining K^{II}_{SDS} and K^{I}_{SDS} as the affinity constants of the Cu^{II} and Cu^{I} oxidation states for the micellar SDS, Eq. 8.1 can be derived:

$$E^{\ominus}_{[\mathrm{Br-Cu^{II}L}]^+_{SDS}/[\mathrm{Br-Cu^{I}L}]_{SDS}} = E^{\ominus}_{[\mathrm{Br-Cu^{II}L}]^+/[\mathrm{Br-Cu^{I}L}]} + \frac{RT}{F}\ln\frac{K^{I}_{SDS}}{K^{II}_{SDS}} \quad (8.1)$$

from which $K^{II}_{SDS}/K^{I}_{SDS} = 3$ was calculated. This is desirable during polymerization because more Cu^{II} deactivator is attracted to the micelles (or droplets), improving the chance of deactivation and polymerization control. In conclusion, both [Br–Cu^{II}TPMA]$^+$ and [Br–Cu^{I}TPMA] resided in the micellar environment. Further addition of SDS after $C_{SDS} \approx 9$ mM did not significantly alter the voltammetric response.

Table 8.1 lists the voltammetric data with different scan rates for 1 mM [Br–Cu^{II}TPMA]$^+$, in the presence of a relatively high amount of SDS, $C_{SDS} = 28$ mM. The redox process involving the Cu^{II}/Cu^{I} couple was diffusion controlled (i_{pc} *vs.* $\upsilon^{1/2}$ plot was linear and passed through the origin, **Figure 8.3**). The ratio between the cathodic and anodic peak

currents was *ca.* 1. Therefore, in the presence of SDS, Cu^{II}/Cu^{I} is a quasi-reversible redox couple like traditional ATRP catalysts.

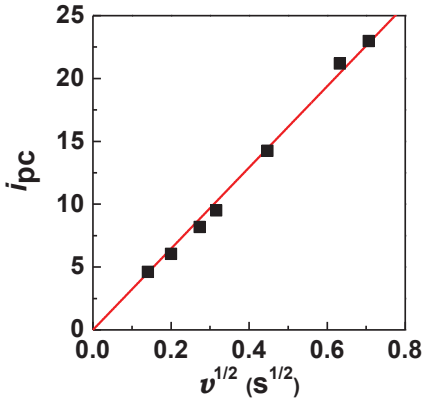

Figure 8.3. Linear fit of cathodic peak current values at different scan rates for 10^{-3} M [Br–Cu^{II}TPMA]$^+$, in water + 0.1 M NaBr + 0.028 M SDS, T = 65 °C.

Table 8.1. Voltammetric data for 10^{-3} M [Br–Cu^{II}TPMA]$^+$ in water + 0.1 M NaBr + 0.028 M SDS, T = 65 °C.

v (Vs^{-1})	E_{pc} (V *vs.* SCE)	$-i_{pc}$ (μA)	$E_{1/2}$ (V *vs.* SCE)	ΔE_p (mV)
0.02	-0.369	4.61	-0.337	65
0.04	-0.369	6.04	-0.333	72
0.08	-0.371	8.18	-0.330	82
0.1	-0.374	9.51	-0.331	87
0.2	-0.379	14.25	-0.328	103
0.4	-0.393	21.18	-0.326	134
0.5	-0.402	22.97	-0.326	152

Moving to another catalyst, [Br–$Cu^{II}Me_6$TREN]$^+$ exhibited almost the same variations in the intensity of the signal observed for [Br–Cu^{II}TPMA]$^+$ after increasing C_{SDS} (**Figure 8.2b**). However, the voltammetric pattern was quite complex: the cathodic scan showed two ill-separated reduction peaks, while a sharp symmetric oxidation peak at ~ -0.2 V *vs.* SCE appeared in the reverse scan. This peak is characteristic of the oxidation of Cu^0 deposited on the electrode. Therefore, the two cathodic peaks can be attributed to the stepwise reduction of Cu^{II} to Cu^{I} and then to Cu^0.[14] Successive additions of SDS progressively decreased the intensity of all peaks, while the first cathodic peak shifted to more negative potentials. Despite the unclear pattern, [Br–$Cu^{II}Me_6$TREN]$^+$ seemed to be, at least partially, bound to micelles. However, the weaker interaction of Cu^{II} with the

micelles can explain the poor control in *e*ATRP with this catalyst, as will be shown later in the chapter.

$[Br–Cu^{II}(TPMA*2)]^+$ displayed a huge reduction in the intensity of the signal even with low C_{SDS} (**Figure 8.2c**). The standard reduction potential shifted toward more negative values, similarly to $[Br–Cu^{II}TPMA]^+$. Thus, Cu^{II} is more stabilized than Cu^{I} by the interaction with SDS, which can favor deactivator build-up in the micelles and therefore controlled polymerization. Unfortunately, the electro-reduction of this catalyst is complicated by strong adsorption of both Cu^{II} and Cu^{I} at the electrode surface. The symmetrical reversible peak couple observed after the first addition of SDS is typical of strongly adsorbed species. Such strong adsorption might lead to passivation of the electrode with negative impact on the overall rate of polymerization.

Aiming to calculate the partition of $[Br–Cu^{II}TPMA]^+$ between water and micelles, the diffusion coefficient (D) of the electrochemical probe ($[Br–Cu^{II}TPMA]^+$) was computed at different C_{SDS}.[15] D values were measured from the slope of i_{pc} *vs.* $\upsilon^{1/2}$ plot by applying the Randles-Ševčík equation (Eq. 8.2) to CVs recorded at different scan rates.

$$i_{\mathrm{pc}} = 0.4463\mathrm{n}FA\left(\frac{\mathrm{n}F}{RT}\right)^{1/2} D^{1/2}\upsilon^{1/2}C_{\mathrm{p}} \qquad (8.2)$$

where i_{pc} is the cathodic peak current, υ is the scan rate, C_p is the bulk concentration of the electroactive species, and n is the number of exchanged electrons (n = 1 in this case).

A fundamental parameter required to assess the system is the critical micelle concentration (cmc) of the surfactant in the operating solution.[15, 16] An electrochemical determination of cmc is possible by analyzing the variation of redox parameters (cathodic peak current, i_{pc}, and halfwave potential, $E_{1/2}$) of the electrochemical probe, while increasing C_{SDS}. i_{pc} and $E_{1/2}$ exhibited two different regimes if plotted versus C_{SDS}: they sharply varied below ~8-9 mM SDS, then remained approximately constant for higher C_{SDS} (**Figure 8.4**). Linear regressions were performed for the i_{pc} *vs.* C_{SDS} and $E_{1/2}$ *vs.* C_{SDS} plots before and after the regime changed. From the intersection between the two straight lines, cmc = 8.9 mM was determined as average of the values derived from the i_{pc} *vs.* C_{SDS} and $E_{1/2}$ *vs.* C_{SDS} plots.

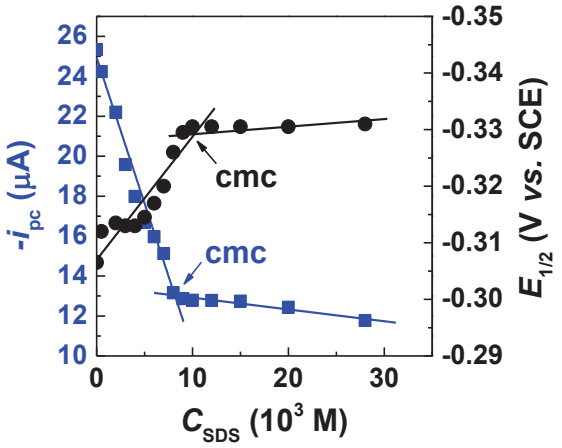

Figure 8.4. Determination of SDS cmc in water + 0.1 M NaBr, T = 65 °C. Elaboration of electrochemical parameters derived from CVs in **Figure 8.2** ($C_{[BrCu^{II}TPMA]^+}$ = 10^{-3} M, C_{SDS} = 0.5, 2, 3, 4, 5, 6, 7, 8, 9, 10, 12, 15, 20, 28 × 10^{-3} M).

Below the cmc, a sharp decrease in current was observed because of the formation of SDS aggregates that can bound to the Cu complex.[17] The aggregates become fully-formed micelles above the cmc. The small variation of the peak currents above the cmc is due to increasing amount of Cu^{II} bound to micelles and also to increased viscosity, which alters diffusion rate of the micelle-bound species. Moreover, excess surfactant can adsorb on the electrode surface, slowing or even preventing ET at very high C_{SDS}.

In the literature, cmc of SDS was accurately determined in water and in water + 0.1 M NaCl,[20, 21] but few studies were conducted in water + 0.1 M NaBr.[22] A value of cmc = 4.3 mM can be derived from reference[22] in water + 0.1 M NaBr at T = 40 °C. Cmc quickly increases with increasing temperature (for T > 25 °C both in water and in water + 0.1 M NaCl),[21] thus the obtained value, cmc = 8.9 mM in 0.1 M NaBr at 65 °C, is in line with other literature values.

Above the cmc, the interaction between the micelles and the probe significantly affected the diffusion coefficients of $[Br–Cu^{II}TPMA]^+$, allowing to analyze the distribution of the Cu complex between water and micelles. The experimentally determined diffusion coefficient of the electroactive species can be expressed by Eq. 8.3:

$$D_{exp}^{1/2} = \frac{D_m^{1/2} K(C_{SDS} - cmc) + D_w^{1/2}}{1 + K(C_{SDS} - cmc)} \quad (8.3)$$

where D_m is the micelles diffusion coefficient, K is the partition coefficient of the probe, and D_w is the diffusion coefficient of the probe in the absence of SDS.[15, 16] The diffusion coefficients at different C_{SDS} were calculated from Eq. 8.2. Then, Eq. 8.3 was fitted on the

experimental D_{exp} values to obtain D_m and K as fitting parameters (**Figure 8.5**). The fitting procedure returned the values reported in **Table 8.2**.

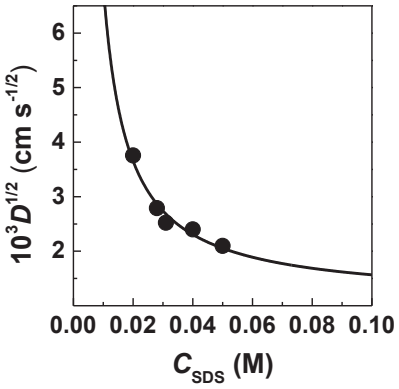

Figure 8.5. D_{exp} of $[Br–Cu^{II}TPMA]^+$ at different C_{SDS} and the best fitting curve according to Eq. 8.3.

Table 8.2. Diffusion coefficient of $[Br–Cu^{II}TPMA]^+$ in the absence of surfactant, self-diffusion coefficient of the micelles and partition coefficient of the complex, in water + 0.1 M NaBr, T = 65 °C.

$10^6 D_w$ (cm^2 s^{-1})[a]	$10^6 D_m$ (cm^2 s^{-1})[b]	K (M^{-1})[b]
60.3 ± 9.9	1.10 ± 0.48	146 ± 23

[a] determined from Eq. 8.2. [b] Computed through a non-linear regression of $D^{1/2}$ *vs.* C_{SDS}, according to Eq. 8.3.

Determined $D_m = 1.10 \times 10^{-6}$ cm^2 s^{-1} for 0.028 M SDS in 0.1 M NaBr is well comparable to literature data obtained under similar conditions. $D_m = 8.0 \times 10^{-7}$ cm^2 s^{-1} was measured for 0.1 M SDS in pure water at T = 25°C (D_m was proved to decrease when reducing the amount of the surfactant, and to increase with raising T).[23] $D_m = 1.9 \times 10^{-6}$ cm^2 s^{-1} was obtained for 0.069 M SDS in water + 0.6 M NaCl at T = 65°C. This value decreased with reducing C_{NaCl}.[24]

K values ranging between 10^1 and 5×10^3 were determined using this method for cobalt and iron complexes interacting with SDS micelles under similar conditions.[15, 16] The value obtained for the present case, K = 146, was consistent with this range, and indicates a mildly strong interaction. Several studies were devoted to accurately refine the determination of K; in particular, Rusling et al. underlined the dependence of this parameter on the concentration of the electrochemical probe,[25] while Mandal et al. verified the decrease of K when increasing $C_{surfactant}$.[16] However, such detailed analysis is beyond the scope of this work.

Conveniently, the fraction of catalyst bound to micelles can be directly computed from Eq. 8.4, and the results are reported in **Table 8.3** for [Br–Cu^{II}TPMA]$^+$ in the presence of SDS.

$$D_{\mathrm{exp}}^{1/2} = f_{\mathrm{bound}} D_{\mathrm{m}}^{1/2} + (1 - f_{\mathrm{bound}}) D_{\mathrm{w}}^{1/2} \quad (8.4)$$

Eq. 8.4 was never applied to a miniemulsion system to evaluate the partition of the probe between water and monomer droplets. In miniemulsion, the droplets are essentially monomer-swollen micelles, with bigger size but similar surface structure. The electrochemical behavior of [Br–Cu^{II}TPMA]$^+$ was essentially the same in the presence of SDS micelles (**Figure 8.2a**) or in the presence of SDS-stabilized droplets (**Figure 8.6a**). Indeed, a drastic drop of current was observed in miniemulsion because the probe is bound to the surface of monomer droplets swollen by SDS. The effect was greater for [Br–Cu^{II}TPMA]$^+$ than for the other catalysts (**Figure 8.6**), due to the higher affinity of [Br–Cu^{II}TPMA]$^+$ for the surfactant. The recorded small current was due to the partition the complex inside the droplets, from where the catalyst could not be reduced at the WE.

Due to the similar behavior of the copper complexes in the presence of micelles or monomer droplets, Eq. 8.4 was redefined to take into account the formation of SDS-stabilized monomer droplets:

$$D_{\mathrm{exp}}^{1/2} = f_{\mathrm{bound}} D_{\mathrm{d}}^{1/2} + (1 - f_{\mathrm{bound}}) D_{\mathrm{w}}^{1/2} \quad (8.5)$$

where D_{d} is the diffusion coefficient of the droplets, which was estimated by means of the Stokes-Einstein equation (Eq. 8.6):

$$D_{\mathrm{d}} = \frac{k_{\mathrm{B}} T}{6\pi\eta r_{\mathrm{d}}} \quad (8.6)$$

where k_{B} is the Boltzmann constant, η is the viscosity of the solution, and r_{d} is the droplet radius, which was obtained from DLS measurements. Viscosity was considered the same as for pure water at T = 65 °C (η = 0.4339 mPa s^{-1}).[26] Particle radius r_{d} was determined by DLS measurements before the polymerization ($d_{\mathrm{Z\text{-}ave}}$ = 126±1 nm; similar values were obtained in all experiments performed with the same amount of BA and SDS). D_{d} = 8.8 × 10^{-8} cm^2 s^{-1} was obtained. Eq. 8.5 requires also the diffusion coefficient of the probe in the miniemulsion environment, D_{exp}, and in water, D_{w}, which were determined by CV at different scan rates (Eq. 8.2). CVs in miniemulsion were poorly reproducible because of adsorption of surfactant or monomer molecules on the electrode surface; to minimize this issue, the electrode surface was cleaned before each CV run.

Table 8.3. Computed physico-chemical parameters for 10^{-3} M [Br–Cu^{II}L]$^+$ in pure water, SDS micelles and in miniemulsion, T = 65 °C.

Entry	L	Environment	10^6 D_{exp} (cm^2 s^{-1})[a]	10^6 D_w (cm^2 s^{-1})[a]	f_{bound}
1	TPMA	Micelles[b]	3.44	60.3	0.79
2	TPMA	Miniemulsion[c]	0.44	60.3	0.95
3	Me_6TREN	Miniemulsion[c]	17.1	36.4	<0.50
4	BPMEA	Miniemulsion[c]	3.33	20.5	0.64

[a] D_w values were measured with $C_L/C_{Cu^{II}}$ = 1, while a ratio $C_L/C_{Cu^{II}}$ = 2 was used for D_{exp}. [b] water + 0.1 M NaBr + 10^{-3} M [Br–Cu^{II}TPMA]$^+$ + 0.028 M SDS. [c] $C_{BA}/C_{NaBr}/C_{[Cu^{II}Br_2]}/C_L$= 280/20/0.2/0.4, BA 19 vol% in H_2O, C_{SDS} = 6.2 wt % rel. to BA, C_{HD} = 10.8 wt % rel. to BA, V_{tot} = 20 mL (reprinted with permission from Ref. [12]. Copyright American Chemical Society, 2017).

The f_{bound} values in **Table 8.3** show that [Br–Cu^{II}TPMA]$^+$ was binding very strongly to both micelles and droplets, confirming the similar behavior of this catalyst in both environments. Instead, [Br–Cu^{II}BPMEA]$^+$ and [Br–$Cu^{II}Me_6$TREN]$^+$ interacted much less with the droplets surface. Taking into account the poor reversibility of the CV signal of [Br–$Cu^{II}Me_6$TREN]$^+$ and the uncertainty over the response in miniemulsion, a more approximate value of f_{bound} was computed for this species.

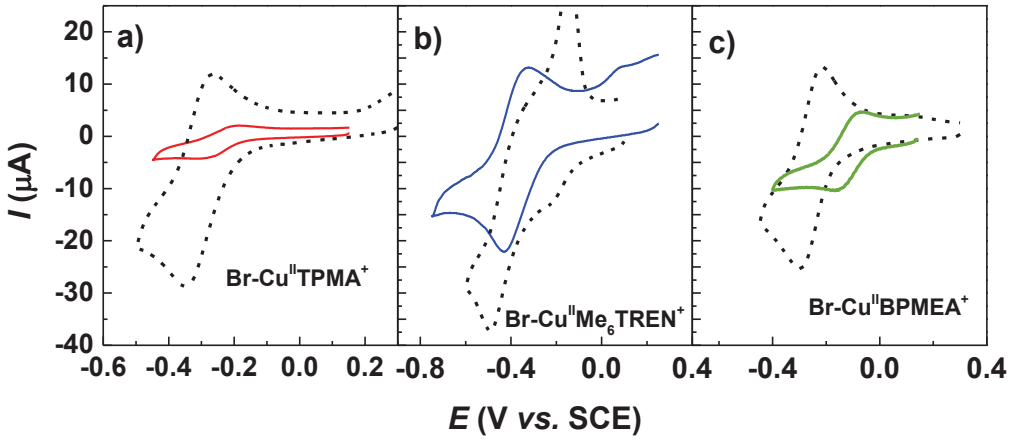

Figure 8.6. CVs of 10^{-3} M a) [Br–Cu^{II}TPMA]$^+$, b) [Br–$Cu^{II}Me_6$TREN]$^+$, and c) [Br–Cu^{II}BPMEA]$^+$ in miniemulsion (solid lines) and in water + 0.1 M NaBr (dashed lines). WE = Pt, υ = 0.1 Vs^{-1}, T = 65 °C. Other conditions for miniemulsion: $C_{BA}/C_{NaBr}/C_{Cu^{II}Br_2}/C_L$= 280/20/0.2/0.4, BA 19 vol% in H_2O, C_{SDS} = 6.2 wt% relative to BA, C_{HD} = 10.8 wt% rel. to BA, V_{tot} = 20 mL (reprinted with permission from Ref. [12]. Copyright American Chemical Society, 2017).

The slight discrepancy between f_{bound} for [Br–Cu^{II}TPMA]$^+$ in the presence of micelles (0.79) and in the presence of droplets (0.95) might arise from the following reasons: *i*) the

slightly higher C_{SDS} used in miniemulsion (38 mM *vs.* 28 mM); *ii*) in miniemulsion a significant part of the catalyst molecules on the droplet surface might not undergo reduction, which would cause an underestimate of D_{exp} and thus an overestimation of f_{bound}; *iii*) the presence of BA, which is slightly soluble in water, can change the relative affinity of the complex for water or the SDS-rich interface.

In conclusion, a large fraction of $[Br–Cu^{II}TPMA]^+$ was present at the droplets' surface, from where it could activate and deactivate the growing chains by an interfacial catalysis procedure. However, such heterogeneous catalysts are typically inefficient deactivators which would lead to broad $Đ$.[27, 28] Therefore, we investigated if, in the presence of SDS, some of the catalyst molecules could be transported inside monomer droplets, acting as a traditional homogenous catalyst and supplementing the interfacial catalysis.

8.2.2. Partition evaluation *via* UV-visible spectroscopy

In the absence of surfactant, no Cu^{II} complexes were detected in the Visible-NIR spectrum of the organic phase, indicating that $[Br–Cu^{II}TPMA]^+$ was completely distributed in the aqueous phase. The same was observed in the presence of Brij-98. Conversely, partition experiment in the presence of SDS (**Figure 8.7**) showed that 0.4% of the catalyst was present in the organic phase (*i.e. ca.* 3 ppm of Cu, out of a total 700 ppm Cu). This indicated that $[Br–Cu^{II}TPMA]^+$ and DS^- formed hydrophobic ion pairs that transported some deactivator molecules into the organic phase, enhancing deactivation.

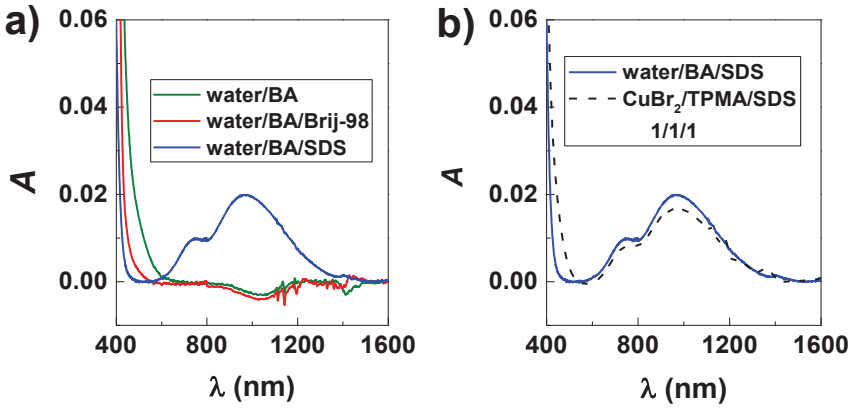

Figure 8.7. a) Visible-NIR spectra of BA phase (BA 20 vol% in water + 0.1 M NaBr) in the absence and presence of different surfactants. b) Comparison of Vis-NIR spectra of Cu^{II} complexes in the organic phase after partition experiment and after addition of $\boldsymbol{C_{Cu^{II}Br_2}}/C_{TPMA}/C_{SDS}$ 1/1/1 (reprinted with permission from Ref. [12]. Copyright American Chemical Society, 2017).

The partition coefficients (water/BA) of $[Br–Cu^{II}TPMA]^+$ in the presence of different surfactants were measured by recording catalyst absorbance through a UV-Vis spectrophotometer at a fixed wavelength (λ_{max}, 970 nm). Solutions of $Cu^{II}Br_2$/TPMA were prepared in water/BA at different but relatively high concentrations as to be able to accurately detect the small amount of catalyst partitioned in the hydrophobic phase. Therefore, the aqueous and organic phases were put carefully in the same vial to form a macroscopic two-phase system. Then, the mixture was let to equilibrate for 3 days under gentle rocking on a platform rocker (more drastic mixing procedures led to the formation of a dispersion). After 3 days, the mixture was still macroscopically well separated; it was centrifuged at 5000 rpm for 15 min to obtain a cleaner separation between the two phases. Finally, the organic top layer was withdrawn and analyzed by Vis-NIR spectroscopy. The linear calibration was obtained by recording the absorbance of a series of solutions with varying C_{Cu}, but fixed ratio of $C_{Cu^{II}Br_2}/C_{TPMA}/C_{SDS}$ 1/1/1, in BA + a few drops of H_2O.

Figure 8.7a shows the Visible-NIR spectra of the BA phase. No Cu^{II} complexes were detected in the presence of Brij-98 or in the absence of surfactant. Conversely, a Cu^{II} complex was detected in the presence of SDS, thus this surfactant was effectively able to transport some of the hydrophilic deactivator catalyst inside the organic phase. **Figure 8.7b** shows that the Visible-NIR spectra recorded after the partition experiment was similar to that of the complex obtained by mixing $C_{Cu^{II}Br_2}/C_{TPMA}/C_{SDS}$ 1/1/1 in BA. The resulting Cu complexes have very similar absorption spectra. From the calibration curve, it was determined that only 0.11 mM $Br\text{-}Cu^{II}\text{-}TPMA^+$, corresponding to 0.4% of the catalyst, migrated to the organic phase. Under polymerization conditions, lower $Cu^{II}Br_2$/TPMA concentrations were used (1 or even 0.5 mM, corresponding to 700 and 300 ppm, respectively). In those cases, catalyst loading in the monomer droplets should be only 3 and 1.5 ppm, considering that a similar amount of catalyst (0.4%) was distributed into the organic phase.

This indicated that $[Br–Cu^{II}TPMA]^+$ and $DS^–$ formed hydrophobic ion pairs that transported some deactivator molecules into the organic phase, enhancing deactivation.

8.3. Ion-pair and interfacial catalysis in minimeulsion *e*ATRP

A typical list of reagents used in miniemulsion *e*ATRP in the presence of hydrophilic catalyst and anionic surfactant is shown in **Table 8.4**. NaBr (0.1 M) was added to increase the stability of the $[Br–Cu^{II}L]^+$ deactivator, which could otherwise dissociate to $[Cu^{II}L]^{2+}$ + $Br^–$ in aqueous media.[14]

Table 8.4. Composition of organic and aqueous phases in a typical miniemulsion polymerization.[a]

Component	Weight (g)	Comments
Organic phase		
BA	7.12	20 vol% (18 wt%) to total
EBiB	0.039[b]	C_{BA}/C_{EBiB} = 280/1
HD	0.77	10.8 wt% to BA
Aqueous phase		
Water	32	Distilled water
SDS	0.44	6.2 wt% to BA
NaBr	0.41	C_{NaBr} = 0.1 M
$Cu^{II}Br_2$	8.9×10^{-3}	1 mM with respect to V_{tot}
TPMA	0.023	$C_{Cu^{II}Br_2}/C_L$ = 1/2

[a]Polymerization conditions: T = 65 °C, V_{tot} = 40 mL; [b]Initiator concentration, C_{EBiB}, was varied to target different DPs (reprinted with permission from Ref. [12]. Copyright American Chemical Society, 2017)..

In order to verify that hydrophilic catalysts have to be combined with an anionic surfactant to effectively tune *e*ATRPs in miniemulsion, one synthesis was conducted in the presence of the non-ionic surfactant Brij-98. The polymerization was uncontrolled and very broad MW distribution was observed (**Table 8.5, entry 1**), suggesting the presence of an insufficient amount of deactivator in polymerizing monomer droplets. Conversely, using an anionic surfactant, SDS, $Đ$ = 1.18 (**Table 8.5, entry 2**), confirming the presence of a specific interaction between $[Br–Cu^{II}L]^+$ and SDS that enabled a controlled process.

Table 8.5. *e*ATRP of BA in miniemulsion with different surfactants and catalysts, T = 65 °C.[a]

Entry	L	Surfactant	$E_{pc} - E_{app}$ (V)	t (h)	Q (C)	Conv. (%)	k_p^{app} (h^{-1})	M_n (10^{-3})	$M_{n,th}$ (10^{-3})	$Đ$
1	TPMA	Brij 98	0.03	7.5	16.2	90	0.60	27.8	3.2	4.77
2	TPMA	SDS	0.03	7.5	3.9	75	0.18	28.4	27.3	1.18
3	TPMA*[2]	SDS	0.03	7.5	3.3	38	0.07	15.9	14.1	1.32
4	Me_6TREN	SDS	0.03	1.5	7.3	93	0.40	59.8	33.8	1.94
5	Me_6TREN	SDS	– 0.12	5	4.6	77	0.55	38.7	27.9	1.56
6[b]	BPMEA	SDS	0	24	2.0	66	0.06	29.1	24.3	4.62

[a]Conditions as in **Table 8.4**, unless otherwise stated. [b]From Ref. [11] (reprinted with permission from Ref. [12]. Copyright American Chemical Society, 2017).

8.3.1. Proposed mechanism of miniemulsion *e*ATRP catalyzed by [Br–Cu^{II}TPMA]$^+$/DS^-

Scheme 8.2 presents the proposed mechanism of miniemulsion *e*ATRP with [Br–Cu^{II}TPMA]$^+$/SDS catalytic system. Atom transfer was carried out both by catalyst molecules bound to the droplets' surface, "interfacial catalysis", and by ion pairs distributed in monomer droplets, "ion-pair catalysis". Electrochemical regeneration of the catalyst involved both a small amount of [Br–Cu^{II}L]$^+$ dissolved in the aqueous phase and [Br–Cu^{II}L]$^+$ bound to the droplets' interface. The same catalyst could be used for activator regeneration at the WE and polymerization control in the monomer droplets, without the need of a dual (hydrophilic + hydrophobic) catalytic system.

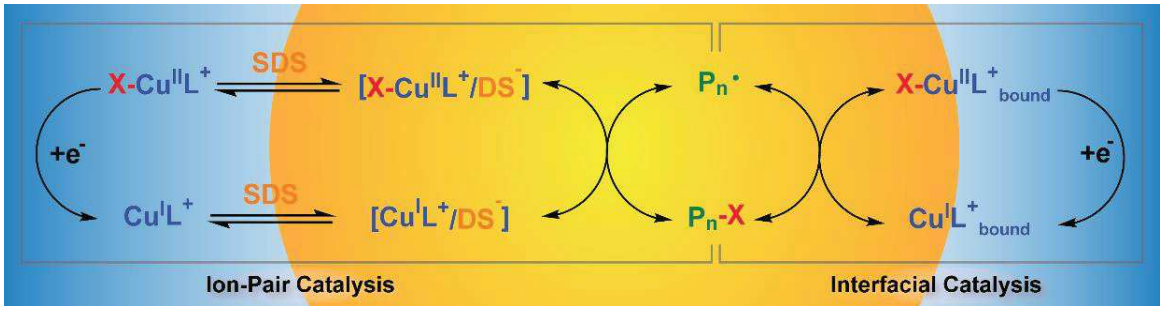

Scheme 8.2. Proposed mechanism of ion-pair and interfacial catalysis combination, in miniemulsion *e*ATRP (reprinted with permission from Ref. [12]. Copyright American Chemical Society, 2017).

Table 8.9 presents a molecular description of the ATRP catalytic system in a single miniemulsion droplet, which can be considered an individual *mini-bulk* polymerization reactor.[4] For a reaction volume of 40 mL, the number of droplets was determined as 7.6×10^{15}, considering each droplet as a sphere with diameter 126 nm (measured by DLS). The average amount of each reagent in a single droplet was computed by determining the number of particles (N) of each species and dividing it by the number of droplets. The amount of catalyst inside each droplet was derived from the average 14 ppm of residual copper as determined by ICP-MS. Finally, the catalyst at the interface was calculated as 95% of the total catalyst concentration (**Table 8.3**).

With 700 ppm of total copper present in the miniemulsion, each ion-pair catalyst was responsible for the activation/deactivation of 260 chain ends. Conversely, each catalyst bound to the interface activated and deactivated an average of 5 chains. On the surface, one catalyst molecule ($[Br–Cu^{II}TPMA]^+_{bound}$) was present every ~30 surfactant molecules. Interestingly, during polymerization only 1 in 1200 droplets was active (*i.e.* contained an active radical) at any given moment, which suggests that radical-radical termination events could be limited, thanks to the compartmentalization phenomenon.[7-9]

Table 8.6. Molecular description of the $[Br–Cu^{II}TPMA]^+$/SDS system in a single miniemulsion droplet[a]

Species	Concentration (M)[b]	N[c]	Ratio[d]
SDS[e]	-	9.2×10^4	1.5×10^3
Hexadecane	-	2.7×10^5	4.4×10^3
$[Br–Cu^{II}TPMA]^+_{bound}$	-	3.0×10^3	48
$[Br–Cu^{II}TPMA]^+/DS^–$	9.9×10^{-5}	62	1
BA	7.0	4.4×10^6	7.1×10^5
EBiB	2.5×10^{-2}	1.6×10^4	2.6×10^2
$P_n^{\bullet}$[f]	$0/11.7 \times 10^{-6}$	0/1	$0/2.9 \times 10^{-2}$
	(1.3×10^{-9})	(8.2×10^{-4})	(2.3×10^{-5})

[a]Conditions as in **Table 8.4**. [b]Concentration of the species in the organic phase (V = 8 mL). [c]Average number of particles of each species in a single droplet. [d]$N/N_{catalyst}$. [e]The surfactant available to stabilize the droplets was considered as C_{SDS} – cmc. [f]Two different values are reported, considering that during polymerization the number of radicals in most droplets is either 0 or 1. In parentheses the average of the whole organic phase (reprinted with permission from Ref. [12]. Copyright American Chemical Society, 2017).

Regarding the activator complex, the ion pair $[Cu^{I}L]^{+}/DS^{-}$ or the "traditional" $[Cu^{I}L]^{+}$, a $C_{Cu^{I}}/C_{Cu^{II}}$ ratio of *ca.* 0.1 in the monomer droplets was estimated by considering Eq. 8.7:

$$K_{ATRP} = \frac{C_{[Br\text{-}Cu^{II}L]} + C_{P_n^{\bullet}}}{C_{[Cu^{I}L]} + C_{[P_n\text{-}X]}} \quad (8.7)$$

$C_{[P_n-X]}$ = 25 mM, whereas $C_{P_n^{\bullet}}$ = 1.3 × 10^{-9} M was calculated from measured $k_p^{app} = k_p C_{P_n^{\bullet}}$ = 0.18 h^{-1} (**Table 8.5**, **entry 2)**, together with k_p = 3.8×10^4 M^{-1} s^{-1} from Ref. [36] Last, K_{ATRP} = 1.8 × 10^{-6} was determined for the Cu^{I}/TPMA catalyst in butyl acrylate/acetonitrile 50/50 (v/v) at 25 °C (**Chapter 3**, **Table 3.3**). K_{ATRP} increases with increasing *T*, thus a slightly higher value should be used in Eq. 8.7.

Unexpectedly, the super-active catalyst,[29] $[Br–Cu^{II}(TPMA*^{2})]^{+}$, provided slower polymerization rate and poorer control (**Table 8.5, entry 3**), indicating that catalyst distribution and interfacial dynamics may play a more important role than the thermodynamics of RX activation.

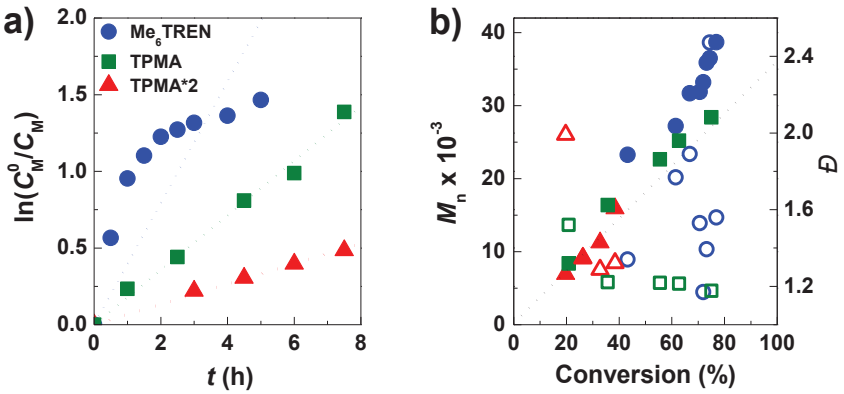

Figure 8.8. Miniemulsion *e*ATRP of BA 20 vol%, with different Cu complexes (L = TPMA, TPMA*^{2}, and Me_6TREN). a) Kinetic plot and b) MWs and *Đ* evolution *vs.* monomer conversion. Reaction conditions as in **Table 8.4** (adapted with permission from Ref. [12]. Copyright American Chemical Society, 2017).

Overall, catalyst hydrophilicity or nature of the surfactant affected *e*ATRP much more than the rate and amount of Cu^{I} generation (**Figure 8.8**). For example, control only partially improved by decreasing the rate of regeneration of $[Cu^{I}Me_6TREN]^{+}$ (**Table 8.5, entry 4 *vs.* 5**). The rate of Cu^{II} reduction was diminished by positively shifting E_{app} by 0.15 V, which led to ~300 times lower Cu^{I}/Cu^{II} ratio on the surface of the WE. Despite this drastic decrease in Cu^{II} reduction rate, the polymerization was not well-controlled, lowering *Đ* from 1.94 to 1.56.

Cu^{I} generation rate was also varied in the case of $[Br–Cu^{II}TPMA]^{+}$, with even smaller effects on polymerization control, which was always good (**Figure 8.9** and **Table 8.7**). These results confirmed that the specific catalyst/surfactant interaction was the most important parameter affecting control.

Table 8.7. *e*ATRP of BA in miniemulsion with $[Br–Cu^{II}TPMA]^{+}$/SDS at different applied potentials.[a]

Entry	$E_{pc} - E_{app}$ (V)	t (h)	Q (C)	Conv. (%)	k_p^{app} (h^{-1})	M_n	$M_{n,th}$	$Đ$	$d_{v,final}$ (nm)
1	0.015 V	7.5	0.9	68	0.14	28.6	24.5	1.24	174±1
2	0.03 V	7.5	3.9	75	0.18	28.4	27.3	1.18	126±2
3	0.09 V	7.5	7.9	79	0.21	32.3	28.7	1.24	156±2

[a] Conditions as in **Table 8.4** unless otherwise stated.

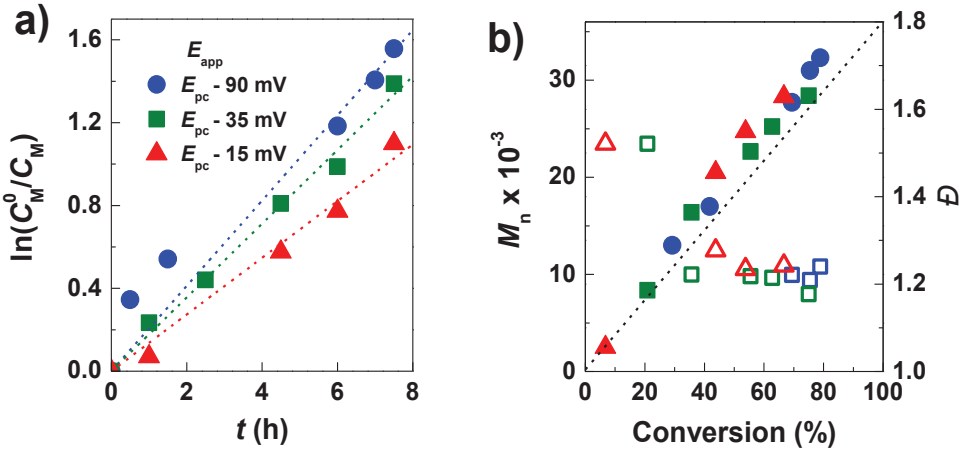

Figure 8.9. Miniemulsion *e*ATRP of BA as a function of E_{app}. a) Kinetic plot and b) MWs and $Đ$ evolution *vs.* monomer conversion for different E_{app} values. Reaction conditions as in **Table 8.4**.

The best performing system, $[Br\text{-}Cu^{II}TPMA]^{+}$/SDS, was also used to produce very well defined PBA ($Đ$ = 1.1) in a simplified *e*ATRP system (*se*ATRP), thus using a two-electrode setup with a sacrificial Al anode under fixed current conditions (**Figure 8.10**).[30]

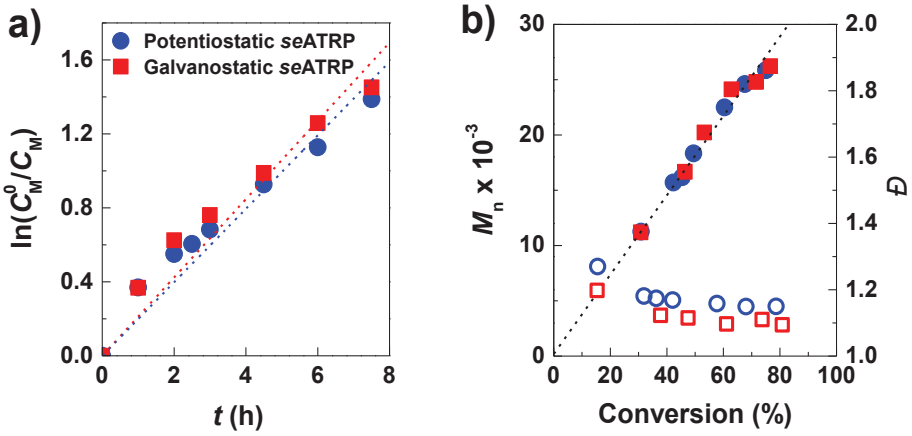

Figure 8.10. Miniemulsion *se*ATRP of BA 20 vol%, under potentiostatic and galvanostatic conditions. a) Kinetic plot and b) MW and *Đ* evolution *vs.* monomer conversion. Other conditions as in **Table 8.4**.

The efficiency of the [Br-Cu^{II}TPMA]$^+$/SDS catalytic system was tested over the range of 1200-300 ppm of Cu (**Table 8.8, entries 1-3**). Controlled *e*ATRP was obtained in each case, with linear increase of MW with conversion. However, polymerization rate tended to decrease at high conversions with lower catalyst ampunt.[31, 32] Higher catalyst loadings provided higher rates of polymerization and higher conversions with narrower *Đ*.

*e*ATRPs of BA were also performed at three different C_{BA}/C_{EBiB} ratios, targeting DP = 100, 280, and 500 (**Table 8.8, entries 4-6**). Polymerizations were well controlled with linear first-order kinetics, M_n matching the theoretical values, and low *Đ* (**Figure 8.11**). As expected, dispersity and polymerization rate decreased with increasing C_{BA}/C_{EBiB}.[33]

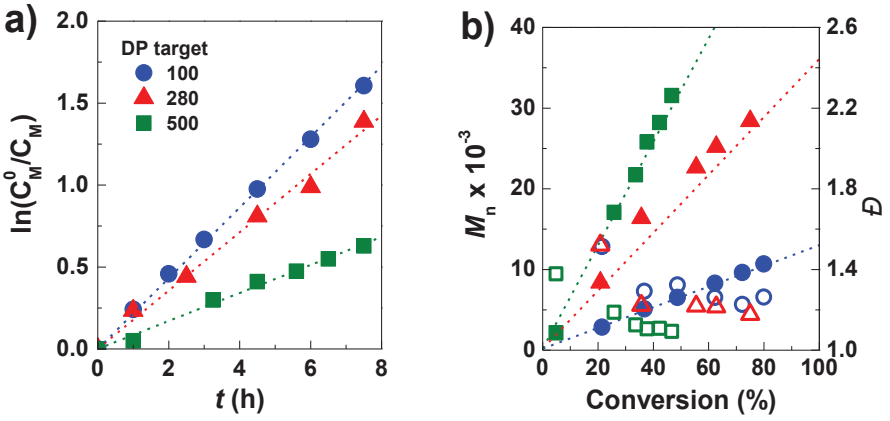

Figure 8.11. Miniemulsion *e*ATRP of BA with different target DPs. a) Kinetic plot and b) MW and *Đ* evolution *vs.* monomer conversion. Other conditions as in **Table 8.4** (adapted with permission from Ref. [12]. Copyright American Chemical Society, 2017).

Table 8.8. *e*ATRP of BA in miniemulsion at different copper concentrations and degree of polymerization.[a]

Entry	$C_{BA}/C_{EBiB}/C_{[Cu^{II}Br_2]}$	Q (C)	Conv. (%)	k_p^{app} (h^{-1})	M_n (10^{-3})	$M_{n,th}$ (10^{-3})	$Đ$	$d_{v,final}$[b] (nm)
1	280/1/0.09	2.6	60	0.14	24.6	21.8	1.19	105±1
2	280/1/0.20	3.9	75	0.18	28.4	27.3	1.18	126±2
3	280/1/0.34	4.8	87	0.27	33.7	31.9	1.16	174±1
4	100/1/0.07	4.9	80	0.22	10.7	10.6	1.26	117±1
5	500/1/0.36	1.8	47	0.09	31.6	30.2	1.09	100±1

[a]Conditions as in **Table 8.4** unless otherwise stated; $E_{app} = E_{pc} - 0.03$ V, selected from CV response; reaction time = 7.5 h. [b]Final average particle diameter, calculated from volume, determined by dynamic light scattering (reprinted with permission from Ref. [12]. Copyright American Chemical Society, 2017).

8.3.2. Chain-end fidelity and quantification of radical terminations

Chain-end functionality was completely retained, within the GPC detection limit (**Figure 8.12**), which was proved by chain extension of a PBA_{78}-Br macroinitiator prepared by miniemulsion s*e*ATRP (*i.e.* Al wire sacrificial anode in an undivided cell with [Br-Cu^{II}TPMA]$^+$/SDS, DP = 78.

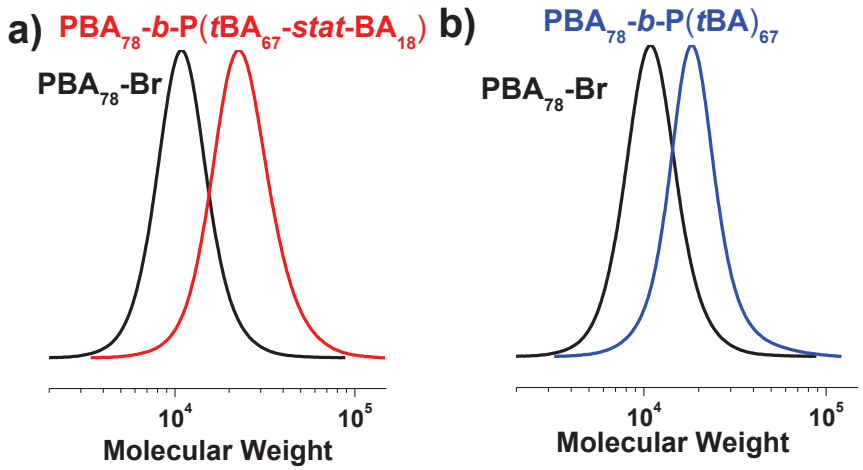

Figure 8.12. GPC traces of copolymers formed by chain extension of PBA_{78}-Br by *se*ATRP in miniemulsion. a) *in situ* chain extension, b) chain extension after purification of the PBA-Br macroinitiator. Reaction conditions as in **Table 8.4**, with $C_{tBA}/C_{PBA_{78}-Br}/C_{Cu^{II}}$ = 80/1/0.06, 20 vol% *t*BA (adapted with permission from Ref. [12]. Copyright American Chemical Society, 2017).

PBA$_{78}$-Br was seamlessly extended with *t*BA *in situ*, generating PBA$_{78}$-*b*-P(*t*BA$_{67}$-*stat*-BA$_{18}$), where *stat* indicates the formation of a statistical copolymer with composition ratio *t*BA/BA 67/18. PBA$_{78}$-Br was also chain extended after purification of the macroinitiator and re-emulsification, generating PBA$_{78}$-*b*-P(*t*BA)$_{67}$. In each case, linear first-order kinetics, predetermined MWs, and low dispersities were obtained.

Table 8.9. Preparation of PBA-Br macroinitiator and chain extension with *t*BA by *se*ATRP in miniemulsion.[a]

Entry	RX	M	$C_M/C_{RX}/C_{Cu^{II}}$	Q (C)	Conv. (%)	k_p^{app} (h^{-1})	M_n (10^{-3})	$M_{n,th}$ (10^{-3})	$Đ$	$d_{v,final}$ (nm)
1[b]	EBiB	BA	100/1/0.07	12.1	78	0.21	10.2	10.3	1.16	120±1
2	PBA-Br	*t*BA[c]	80/1/0.06	2.1	83	0.24	21.5	21.1	1.19	130±1
3	PBA-Br	*t*BA	80/1/0.06	4.8	80	0.21	17.5	18.4	1.16	115±1

[a] General conditions as in **Table 8.4**, reaction time = 7.5 h.. [b] Preparation of the PBA-Br macroinitiator. [c] Unreacted BA (0.27 M, 22% of starting concentration) was still present in the reaction mixture (reprinted with permission from Ref. [12]. Copyright American Chemical Society, 2017).

By recording the total consumed charge (Q) during *e*ATRP (**Table 8.9**), it was determined, according to the procedure reported in **Chapter 1** (**Section 1.4**), that ≤1% of chains terminated by radical−radical reactions. Considering that at the beginning of the experiment, copper is present as Cu^{II}, the total measured charge Q is the sum of two contributions (Eq. 1.27 in **Chapter 1**, **Section 1.4**): *i*) $Q_0 = n_0F$ for the initial reduction of Cu^{II} species to Cu^{I}; *ii*) Q_R for the reduction of Cu^{II} species accumulated due to the radical-radical terminations. n_0 was estimated by using the Nernst equation (Eq. 1.26 in **Chapter 1**, **Section 1.4**) . In most experiments, $E_{app} = E_{pc} - 0.03$ V was used, which corresponds to roughly $E_{app} = E^o - 0.08$ V ≈ $E_{1/2} - 0.08$ V. At this E_{app}, the $C_{Cu^I}/C_{Cu^{II}}$ ratio at the electrode is ~0.05, therefore *ca.* 95% of the Cu^{II} species are converted to Cu^{I}. In the experiments with 700 ppm of initial Cu^{II}, $n_0 = 3.7\times10^{-5}$ mol and $Q_0 = 3.5$ C were calculated. Subtracting this value from the average $Q = 3.7$ C leaves $Q_R = 0.2$ C; it follows that the amount of terminated radicals is $n_R = 2\times10^{-6}$ mol. The number of growing chains is equal to the number of moles of initiator, $n_{RX} = 2.0\times10^{-4}$ mol. Therefore, the fraction of radical-radical terminated chains, n_R/n_{RX}, was only ~1% of the total number of chains. Actually, the fraction of radical-radical terminated chains is ≤ 1%, because the measured charge Q might contain minor

contributions from reduction of oxygen or other impurities. Therefore, most of the chain-end functionality was preserved.

Finally, ICP-MS of the obtained polymer, before any purification procedure, showed the presence of a small amount (< 20 ppm) of copper, which can also improve the stability of the latex.[34 35] Polymers obtained with $[Br–Cu^{II}TPMA]^+$/SDS were perfectly clear and transparent; in comparison, samples obtained with similar amounts of hydrophobic complexes contained > 400 ppm of residual Cu and were intensely colored (**Figure 8.13**).

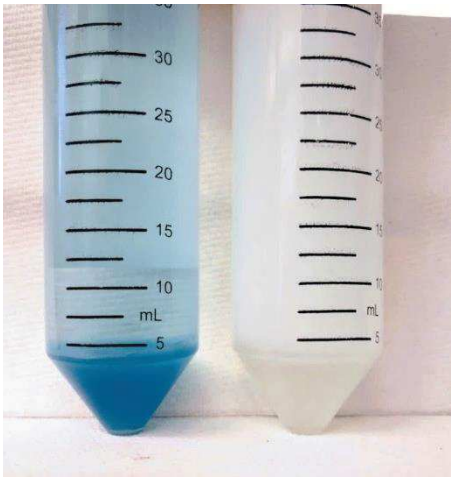

Figure 8.13. Comparison between polymer produced with dual catalytic system (left, *ca.* 1000 ppm of hydrophobic catalyst $[Br–CuBPMODA*]^+$ and $[Br–CuBPMEA]^+$) and single hydrophilic catalytic system (right, *ca.* 700 ppm of $[Br–CuTPMA]^+$) (reprinted with permission from Ref. [12]. Copyright American Chemical Society, 2017).

8.4. Ion-pair and interfacial catalysis in miniemulsion ARGET-ATRP

A typical list of reagents used in miniemulsion ARGET-ATRP in the presence of a hydrophilic catalyst and anionic surfactant is shown in **Table 8.10**. The composition was in fact very similar to the system used in *e*ATRP, but the electrochemical stimulus was replaced by a reducing agent. To this end, ascorbic acid (AsAc) was selected because of its good solubility in water.

Table 8.10. Composition of organic and aqueous phases in a typical miniemulsion ARGET-ATRP.[a]

Component	Weight (g)	Comments
Organic phase		
Monomer	1.79	20 vol% (18 wt%)
RX [b,c]	0.0098 (EBiB)	$C_{Monomer}/C_{RX}$ = 280/1
	0.012 (EBPA)	
HD	0.19	10.8 wt% to monomer
Aqueous phase		
Water	8	Distilled water
SDS[c]	0.082	4.6 wt% to monomer
NaBr	0.103	C_{NaBr} = 0.1 M with respect to V_{tot}
$Cu^{II}Br_2$	2.2×10^{-3}	1 mM with respect to V_{tot}
TPMA	3.2×10^{-3}	1.1 mM with respect to V_{tot}
AsAc	varied	Specified in each table

[a]Polymerization conditions: T = 65 °C, V_{tot} = 10 mL. [b] C_{RX} was varied to target different degrees of polymerization (reprinted with permission from Ref. [13]. Copyright American Chemical Society, 2017).

Cu complexes with pyridinic ligands, $[Br–Cu^{II}TPMA]^+$ and $[Br–Cu^{II}(TPMA*2)]^+$, provided well-controlled polymerizations of BA, with $Đ \approx 1.2$ and M_n close to theoretical values (**Table 8.11, entries 1-3**). Obtained latexes were stable for several months, and particle sizes measured by dynamic light scattering before and after polymerizations varied less than 15%. Comparable results were obtained by using either NaBr or Et_4NBr as source of $Br^–$ for $[Br–Cu^{II}TPMA]^+$ (**Table 8.11, entry 1 *vs.* 2**). Et_4NBr produced larger monomer droplets, indicating that $[Et_4N]^+$ can slightly destabilize latex formation.

The polymerization rate was almost the same with $[Br–Cu^{II}TPMA]^+$ and $[Br–Cu^{II}(TPMA*2)]^+$, despite the much higher redox activity of the latter catalyst.[29] Actually, the interaction between $[Br–Cu^{II}(TPMA*2)]^+$ and SDS seemed to be comparable to the $[Br–Cu^{II}TPMA]^+$/SDS interaction (**Figure 8.2**). Similarly to miniemulsion *e*ATRP with this catalytic system, the catalyst activity is not a critical parameter. Essentially, key factors are catalyst interaction with the surfactant and the consequent partition of the catalyst between organic and aqueous phases.

Table 8.11. ARGET-ATRP of BA in miniemulsion with various ligand-surfactant combinations.[a]

Entry	Ligand	Surfactant	t (h)	Conv. (%)	k_p^{app} (h^{-1})	M_n (10^{-3})	$M_{n,th}$ (10^{-3})	$Đ$	d_Z[b] (nm)
1	TPMA	SDS	6	66	0.25	30.9	24.4	1.17	117±2
2	TPMA[c]	SDS	5	70	0.31	24.1	25.5	1.14	152±1
3	TPMA*2	SDS	3	40	0.21	10.0	14.5	1.24	114±1
4	PMDETA	SDS	2	79	1.42	38.5	28.8	5.02	161±1
5	Me_6TREN	SDS	1.1	89	2.21	32.4	32.2	2.65	152±2
6	TPMA	SDBS	3	84	0.63	29.8	30.4	1.32	153±1
7	TPMA	SDS+SDA[d]	5	74	0.31	27.4	27.0	1.25	273±3

[a]General conditions as in **Table 8.10**. $C_{AsAc}/C_{Cu^{II}} = 0.5$, AsAc injected dropwise at $t = 0$ h. [b] Z-Average particles diameter, measured by DLS. [c] Et_4NBr replaced NaBr. [d] $C_{SDS} = 4.6$ wt% and $C_{SDA} = 0.5$ wt% relative to BA (reprinted with permission from Ref. [13]. Copyright American Chemical Society, 2017).

Me_6TREN and PMDETA were also tested under otherwise identical conditions. 6–9 times faster polymerizations compared to TPMA were obtained, but the control was very poor (**Table 8.11, entries 3-4**). Bad results were observed also in *e*ATRP with Me_6TREN and were attributed to the too weak interaction between $[Br–Cu^{II}Me_6TREN]^+$ and SDS, supported by electrochemical studies (**Figure 8.2** and **Table 8.3**). From CV data it is reasonable to expect that few deactivator molecules were present in polymerization *loci*. In fact, GPC traces revealed a sharp peak followed by a broad signal at high MWs, indicating the presence of droplets with none or very little $[Br–Cu^{II}Me_6TREN]^+/DS^-$ deactivator (**Figure 8.14**).

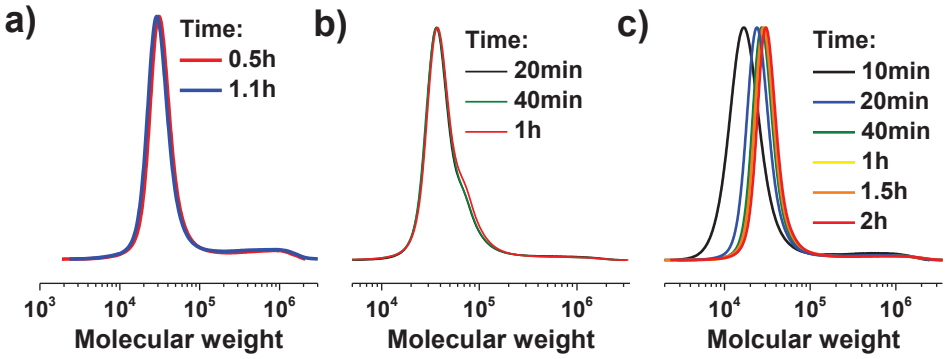

Figure 8.14. GPC traces of PBA in miniemulsion with Cu^{II}/Me_6TREN as catalyst: effect of $C_{AsAc}/C_{Cu^{II}}$ ratio. Conditions in **Table 8.12**, **entry 1** a), **entry 5** b), **entry 6** c).

Considering that under homogeneous conditions, $[Cu^{I}Me_6TREN]^+$ is at least one order of magnitude more active than $[Cu^{I}TPMA]^+$, several attempts were made to improve the control by slowing down the process: *i*) reduce catalyst and/or ascorbic acid loadings, *ii*) use of NaCl instead of NaBr, *iii*) replace the initiator EBiB with MBP, which has a secondary alkyl structure, thus it is less reactive.[37] Nevertheless, relatively fast polymerization and large $Đ$ were always obtained (**Table 8.12**).

$[Cu^{I}PMDETA]^+$ is much less active as homogeneous ATRP catalyst than both $[Cu^{I}Me_6TREN]^+$ and $[Cu^{I}TPMA]^+$.[38] Therefore, the very poor control observed with $[Br–Cu^{II}PMDETA]^+$ suggested that the interaction of this complex with SDS was very weak.

Table 8.12. ARGET ATRP of BA in miniemulsion catalyzed by Cu/Me_6TREN.[a]

Entry	Surfactant	$C_{Cu^{II}}$ (ppm)	$C_{AsAc}/C_{Cu^{II}}$	t (h)	Conv. (%)	k_p^{app} (h^{-1})	$M_{n,th}$ (10^{-3})	M_n (10^{-3})	$Đ$	d_Z (nm)[b]
1	SDS	720	0.5	1.1	89	2.21	32.2	32.4	2.65	152±2
2	SDS+SDA[c]	720	0.5	1	85	2.22	30.9	33.4	2.61	149±2
3	SDS+SDA[c]	360	0.5	1	90	2.63	32.9	31.9	3.56	138±1
4	SDS+SDA[c]	72	0.5	4	0	-	-	-	-	-
5	SDS	720	0.25	1	93	3.29	33.8	38.6	1.82	144±2
6	SDS	720	0.125	2	87	1.30	31.7	32.1	2.36	133±1
7[d]	SDS	720	0.5	1	85	2.20	30.9	27.4	3.24	128±1
8[e]	SDS	720	0.5	1	88	2.62	31.9	32.7	2.43	129±1

[a]General conditions as in **Table 8.10**. [b]Z-Average particle diameter measured by DLS. [c] C_{SDS} = 4.6 wt%, C_{SDA} = 0.5 wt% rel. to BA. [d] NaBr was replaced with NaCl. [e] RX = MBP.

In order to effectively interact with the cationic catalyst the surfactant has to be anionic, therefore, different anionic surfactants were tested: SDS, sodium dodecylbenzene sulfonate (SDBS), and sodium dodecanoate (SDA).

SDBS provided a fast polymerization, reaching 84% conversion in 3 h (**Table 8.11, entry 6**), albeit $Đ$ = 1.32, slightly higher than with SDS under identical conditions. The higher polymerization rate and the slight decrease in control may be caused by a weaker interaction between $[Br–Cu^{II}TPMA]^+$ and SDBS, leading to a lower amount of Cu^{II} species inside the droplets.

SDA alone could not stabilize the BA miniemulsion, therefore a combination of SDS and SDA was tested (4.6 wt% SDS + 0.5 wt% SDA relative to BA, **Table 8.11, entry 7**).

The obtained miniemulsion was stable, but particle size increased to *ca.* 270 nm (almost twice larger than with other surfactants). Polymerization was slightly faster than with SDS alone, with $Đ$ = 1.25. Therefore, SDA can be used to tune the particle size without destabilizing the final latex.

Finally, the SDS amount was varied to change latex properties and polymerization kinetics (**Table 8.13** and **Figure 8.15**). By lowering C_{SDS}, k_p^{app} decreased and first-order kinetics deviated from linearity. However, controlled polymerization was obtained with C_{SDS} as low as 1.15 wt% relative to monomer, which is below the cmc of the surfactant in the polymerization media (cmc = 8.9 mM, **Section 8.2.1**). By reducing C_{SDS}, control decreased because less catalyst was bound to droplets' surface and less ion pairs were formed. Polymerization rate decreased as a consequence of the increased droplets size, which lowered the overall interfacial area, slowing down the kinetics of mass transport. This is in contrast with what is predicted from the catalyst compartmentalization effect in miniemulsion ATRP.[7-9] The reason can be that smaller particles and/or less catalyst molecules are needed to obtain an effective compartmentalization. Nevertheless, the process remained controlled ($Đ$ = 1.1–1.3) and the final latexes were stable, meaning that C_{SDS} can be varied to tune particles dimension.

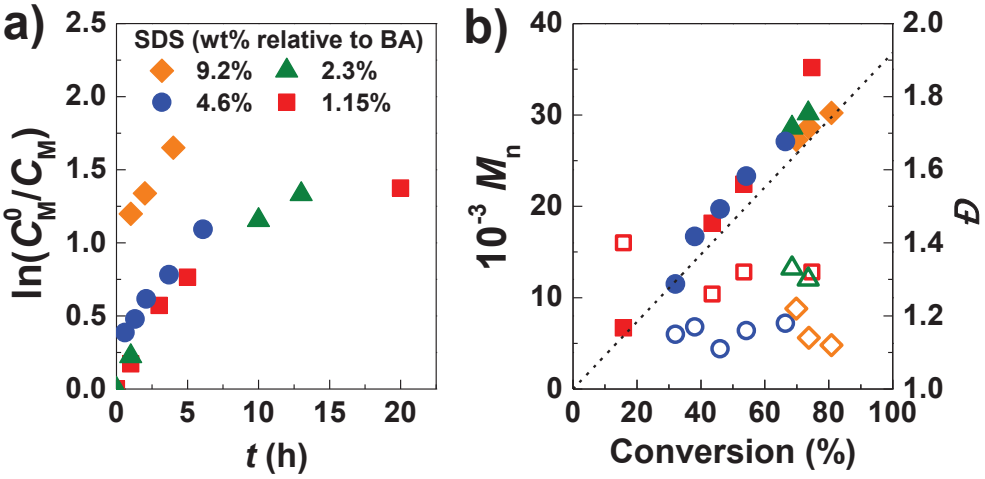

Figure 8.15. ARGET-ATRP of BA in miniemulsion with different SDS amounts (**Table 8.13**). a) Kinetic plot, and b) MW and $Đ$ evolution *vs.* conversion. $C_{AsAc}/\boldsymbol{C}_{\boldsymbol{Cu^{II}}}$ = 0.5 added dropwise at t = 0 h. Other conditions as in **Table 8.10** (reprinted with permission from Ref. [13]. Copyright American Chemical Society, 2017).

Table 8.13. ARGET-ATRP of BA in miniemulsion with different amounts of SDS.[a]

Entry	C_{SDS} (wt% rel. to BA)	t (h)	Conv. (%)	k_p^{app} (h^{-1})	M_n (10^{-3})	$M_{n,th}$ (10^{-3})	$Đ$	d_Z [c] (nm)
1	9.2	4	81	0.50	30.2	29.4	1.12	106±2
2	4.6	6	66	0.25	30.9	24.4	1.17	117±2
3	2.3	13	74	0.12	30.2	26.7	1.30	161±1
4	1.15	20	74	0.16	35.2	27.2	1.32	207±2

[a]General conditions as in **Table 8.10**. $C_{AsAc}/C_{Cu^{II}} = 0.5$, AsAc injected dropwise at $t = 0$ h. [b]Z-Average particle diameter measured by DLS (reprinted with permission from Ref. [13]. Copyright American Chemical Society, 2017).

The effect of catalyst loading was then studied on the system $[Br–Cu^{II}TPMA]^+/DS^-$. The amount of copper complex was reduced from 719, to 360 and 144 ppm (**Table 8.14**). Lowering catalyst loading did not significantly affect polymerization rate. However, the $Đ$ increased with decreasing catalyst loading, in agreement with a general trend often observed in ATRP and predicted by Eq. 1.2 in **Chapter 1** (**Section 1.3**).

Control over BA polymerization was lost when only 144 ppm of catalyst were used ($Đ$ = 1.65). Conversely, 360 ppm of catalyst ensured a well-controlled polymerization, even if, based on data in **Table 8.3**, less than 10 ppm of copper species were present inside the monomer droplets under these conditions.

Higher degrees of polymerization were targeted by lowering initiator concentration. PBA with DP > 700 was obtained with $Đ$ = 1.25 and good agreement between theoretical and experimental MWs. Polymerization rate decreased with reducing C_{EBiB}, as expected from Eq. 1.1 in **Chapter 1** (**Section 1.3**), due to lower amount of generated radicals (**Table 8.14, entry 4**).

Monomer nature was then changed to prove the efficacy of the catalyst also in the polymerization of methacrylates. ARGET-ATRP of BMA was similar to BA polymerization. In fact, $[Br–Cu^{II}TPMA]^+$ is insoluble in both BA and BMA, and therefore entered monomer droplets only when paired with SDS. ARGET-ATRP of BMA required careful selection of the initiator: tertiary alkyl halides, such as EBiB, are less efficient initiators for methacrylates, due to penultimate effect.[39] Instead, EBPA, which is more reactive than EBiB, provided a well-controlled process, reaching 34% conversion within 2 h with $Đ$ = 1.13 (**Table 8.14, entry 5**).[37, 40] However, polymerization stopped after 2 h, suggesting that the initial addition of AsAc ($C_{AsAc}/C_{Cu^{II}} = 0.5$) did not provide continuous

regeneration of the active catalyst. Hence, several strategies of AsAc feeding were implemented. The best result in terms of both rate and control was obtained by simply injecting 0.4 equivalents of AsAc, with respect to initial $C_{Cu^{II}}$, at t = 0 h and then every 30 minutes. 82% conversion was reached after only 1 h, with $Đ$ = 1.26 and good agreement between experimental and theoretical MWs (**Table 8.14, entry 6**).

Table 8.14. ARGET-ATRP of BA and BMA in miniemulsion with different catalyst loadings and degrees of polymerization.[a]

Entry	$C_{[Br-Cu^{II}TPMA]^+}$ (ppm)	DP	t (h)	Conv. (%)	k_p^{app} (h^{-1})	M_n (10^{-3})	$M_{n,th}$ (10^{-3})	$Đ$	d_Z[b] (nm)
monomer = BA, RX = EBiB [c]									
1	719	280	6	66	0.25	24.4	30.9	1.17	117±2
2	360	280	4	70	0.34	25.6	34.1	1.24	126±2
3	144	280	4	71	0.31	26.1	36.7	1.65	121±1
4	719	1000	20	71	0.07	91.6	101.8	1.25	126±1
monomer = BMA, RX = EBPA[d]									
5	800	280	2	34	0.25	14.6	13.8	1.13	144±3
6	800	280	1	82	1.60	36.3	32.9	1.26	135±2
7	200	280	2	90	1.05	36.3	36.1	1.33	132±3
8	50	280	2	77	0.72	31.6	30.9	1.31	139±3
9	800	600	2.5	82	0.52	70.0	70.2	1.20	138±2
10	800	1200	4	76	0.38	118.6	129.3	1.42	131±2
11[e]	800	280	6	92	0.35	34.5	36.9	1.18	193±1

[a]General conditions as in **Table 8.10**. [b]Z-Average particles diameter by DLS before polymerization. [c] $C_{AsAc}/C_{Cu^{II}}$ = 0.5, AsAc injected dropwise at t = 0 h. [d] $C_{AsAc}/C_{Cu^{II}}$ = 0.4 injected dropwise every 30 minutes, except for entry 10, $C_{AsAc}/C_{Cu^{II}}$ = 0.5 injected at t = 0 h. [e][Br–Cu^{II}BPMODA*]$^+$ was used as catalyst (reprinted with permission from Ref. [13]. Copyright American Chemical Society, 2017).

Catalyst loading was then successfully reduced from 800 ppm to 50 ppm (**Table 8.14, entries 6-8**). Polymerization rate (R_p) decreased with decreasing $C_{[Br-Cu^{II}TPMA]^+}$, exhibiting a good proportionality between R_p and the square root of catalyst loading, as observed in **Chapter 4** (**Section 4.2**).

50 ppm of [Br–Cu^{II}TPMA]$^{+}$, corresponding to 6.25 × 10^{-5} M, provided 77% conversion in 2 h with final $Đ$ = 1.31. However, MW distribution was broader during the first hour, due to the slow ATRP deactivation with such a low catalyst loading (**Figure 8.16**).[31] Compared to BA, BMA has a much lower propagation rate constant, k_p,[36, 41] thereby allowing well-controlled process with few ppm of catalyst ($Đ$ and k_p are directly proportional according to Eq. 1.2 in Chapter 1, **Section 1.3**).

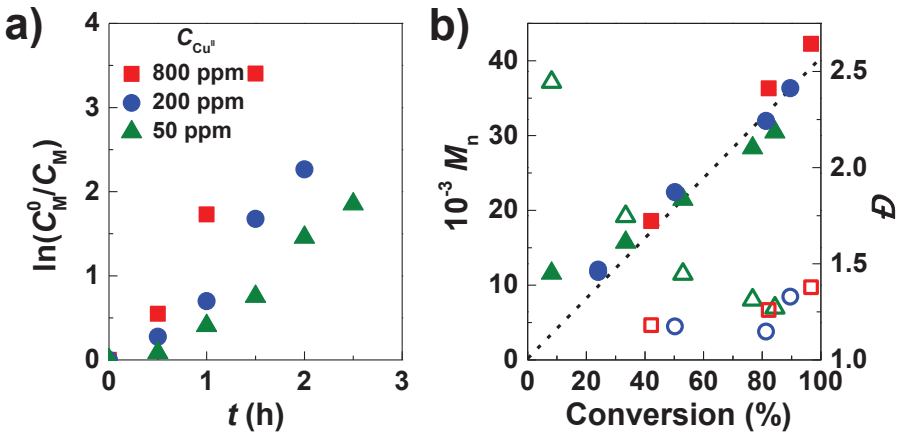

Figure 8.16. Miniemulsion ARGET-ATRP of BMA with various catalyst loadings. a) Kinetic plot and b) MW and $Đ$ evolution *vs.* monomer conversion. C_{AsAc}/ $C_{Cu^{II}}$ = 0.4, injected dropwise every 30 min. Other reaction conditions are listed in **Table 8.10** (adapted with permission from Ref. [13]. Copyright American Chemical Society, 2017).

High MW PBMA was obtained by targeting DP = 600 and 1200 (**Table 8.14, entries 9-10**). Polymerization rates were proportional to C_{EBPA}. By switching from target DP = 280 to 600, $Đ$ diminished from 1.25 to 1.20, in agreement with Eq. 1.2 in **Chapter 1, Section 1.3**. However, $Đ$ increased to 1.42 for DP = 1200. A possible reason can be the high viscosity in the polymerizing droplets. An increase of viscosity, besides slowing down termination events, can hamper the effective deactivation of propagating radicals by the few Cu^{II} species inside the droplets. High viscosity can also support the "auto-acceleration" of the polymerization after 2 h, which was concomitant to the increase in dispersity (**Figure 8.17**).

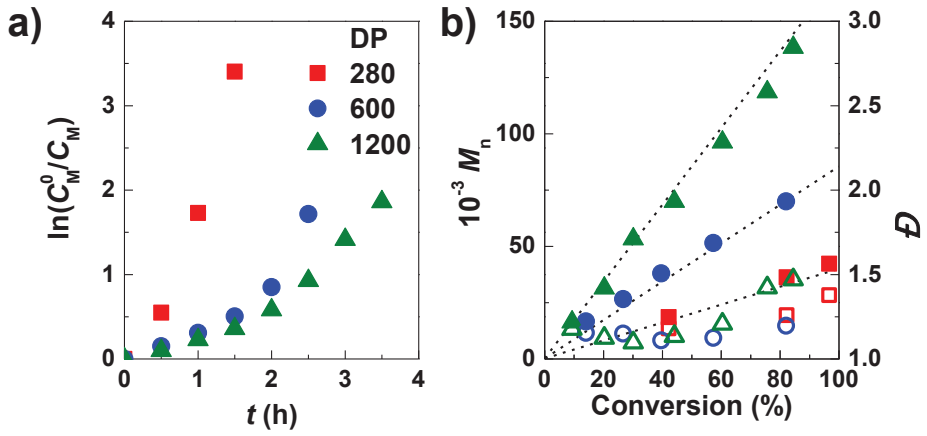

Figure 8.17. Miniemulsion ARGET-ATRP of BMA with different target DPs (280, 600 and 1200). a) Kinetic plot and b) MW and $Đ$ vs. monomer conversion. $C_{AsAc}/C_{Cu^{II}} = 0.5$. Other reaction conditions listed in **Table 8.10** (adapted with permission from Ref. [13]. Copyright American Chemical Society, 2017).

8.4.1. Residual catalyst in precipitated polymers

ICP-MS measurements of the precipitated polymers revealed residual copper contents as low as 4.5, 1.6 and 0.3 ppm (defined as $m_{Cu}/m_{polymer}$), with initial catalyst loadings of 800, 200 and 50 ppm (defined as $n_{Cu}/n_{monomer}$), respectively. Remarkably, less than 1% of the initial copper content remained in the final polymer after precipitation. Metal contamination in the ppb range makes the polymer suitable for some applications without any purification procedure.

For comparison, ARGET-ATRP of BMA in miniemulsion was carried out with a traditionally used super-hydrophobic complex (**Table 8.14, entry 11**), namely BPMODA*. Under the same conditions used for Cu/TPMA, Cu/BPMODA* gave well-controlled polymers, but particles size was 80% larger, suggesting potential destabilization of the droplets' surface. Starting from 800 ppm of $[Br–Cu^{II}BPMODA*]^+$, ICP-MS measurements showed 45 ppm of residual copper in the precipitated polymer, 10 times higher than with $[Br–Cu^{II}TPMA]^+/DS^-$.

8.4.2. Complex macromolecular architectures *via* ARGET-ATRP in miniemulsion

Chain extension experiments. To test chain-end fidelity of the obtained polymers, a PBMA macroinitiator (PBMA-MI) was prepared by miniemulsion ARGET-ATRP with $[Br–Cu^{II}TPMA]^+/DS^-$. After purification, the macroinitiator had M_n = 4000 and $Đ$ = 1.31. Chain extensions were performed with both BA (**Table 8.15, entry 1**) and *t*BMA (**Table 8.15, entry 2**). **Figure 8.18a** and **Figure 8.18b** show a clean shift of MWs in both cases, with monomodal MW distributions, confirming the retention of chain-end functionality in the first block. The second block was also well-controlled, with $Đ_2$ = 1.34 for *t*BMA and $Đ_2$ = 1.15 for BA, calculated as $Đ - 1 = w_1^2(Đ_1 - 1) + w_2^2(Đ_2 - 1)$, where w_1 and w_2 are the weight fractions of the first and second blocks, respectively.[42, 43] Confirmed high chain-end fidelity led to the synthesis of more complex structures by miniemulsion ARGET-ATRP, such as star and brush-like polymers.

Table 8.15. Preparation of polymers with complex structures by ARGET-ATRP in miniemulsion.[a]

Entry	Initiator	Polymer	*t* (h)	Conv. (%)	k_p^{app} (h^{-1})	M_n ($\times10^{-3}$)	$M_{n,th}$ ($\times10^{-3}$)	$Đ$	d_Z[b] (nm)
1[c]	PBMA-Br	PBMA-*block*-PBA	2	30	0.20	13.0	11.7	1.10	118±1
2[d]	PBMA-Br	PBMA-*block*-P*t*BMA	1	30	0.35	16.1	12.6	1.19	119±1
3[d]	β-CD-Br_{14}	β-CD-*star*-PBA	2	73	0.70	47.7	65.7	1.39	118±2
4[d]	β-CD-Br_{14}	β-CD-*star*-PBMA	2	76	0.95	82.2	78.1	1.54	138±2
5[e]	$PBiBM_{100}$	$PBiBM_{100}$-*graft*-PBA	4	94	0.44	357	125	1.29	194±2
6[e]	$PBiBM_{100}$	$PBiBM_{100}$-*graft*-PBA	7	57	0.15	775	347	1.28	155±1

[a]General conditions: monomer 20 vol% in H_2O + 0.1 M NaBr, T = 65 °C; V_{tot} = 10 mL, $C_{Cu^{II}}/C_{TPMA}$ = 1 mM, C_{SDS} = 4.6 wt%, C_{HD} = 10.8 wt% relative to monomer. [b]Z-Average particle diameter by DLS before polymerization. [c]AsAc feeding rate = 3 μmol/h. [d]AsAc feeding rate = 2 μmol/h. [e] V_{tot} = 5 mL, AsAc feeding rate = 50 nmol/h (reprinted with permission from Ref. [13]. Copyright American Chemical Society, 2017).

Synthesis of star polymers. PBA and PBMA stars were prepared by grafting from a β-cyclodextrin core (β-CD-Br_{14}), which was functionalized with 14 ATRP initiators (**Figure 8.1**). With both PBA and PBMA, a clean shift of MW was observed in the GPC traces (**Figure 8.18c** and **Figure 8.18d**). PBA star polymers were well-defined (**Table 8.15,**

entry 3), with $M_{n,} < M_{n,th}$ because the hydrodynamic volume of a star polymer is lower than that of its linear analogue with the same MW. PBMA star polymer was less controlled (**Table 8.15, entry 4**), with M_n higher than $M_{n,th}$. As discussed above, EBiB-type initiators are less efficient for methacrylates, which hamper concurrent growth of all arms from the star core.

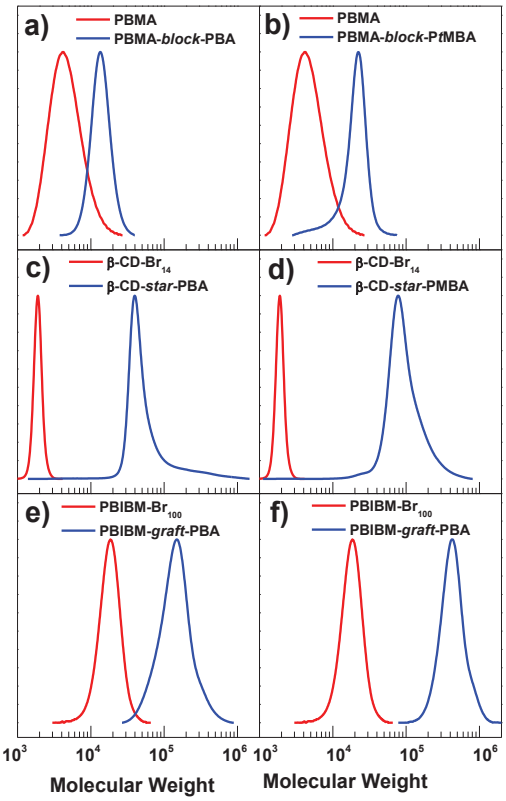

Figure 8.18. GPC traces of different architectures from ARGET-ATRP in miniemulsion. Chain extensions of PBMA-MI with a) *t*BMA and b) BA; multi-arm star polymers from β-CD-Br_{14} macroinitiator and c) BA or d) BMA; PBA molecular brushes with DP target e) 25 and f) 100. Other reaction conditions in **Table 8.10** (reprinted with permission from Ref. [13]. Copyright American Chemical Society, 2017).

Synthesis of molecular brushes. Molecular brushes were successfully prepared in miniemulsion by grafting BA from the $PBiBM_{100}$ macroinitiator. The latter has a methacrylate backbone functionalized with 100 EBiB-like initiating sites (**Figure 8.1**). Successful synthesis of molecular brushes requires minimal termination to avoid coupling between multifunctional macromolecules.[44] Indeed, direct injection of AsAc at the beginning of the reaction produced too many radicals and resulted in coupled chains, *i.e.* gelation. Therefore, the concentration of radicals was lowered by *i*) decreasing C_{SDS} and *ii*) gradually feeding AsAc to slowly reduce Cu^{II} to the active Cu^{I} state (**Table 8.15**, **entries 5 and 6**). Slightly larger particles were obtained according to DLS, as expected from the

lower C_{SDS}; the final miniemulsion was stable and no gelation was observed. Molecular brushes with side chain length of DP = 24 and 57 were prepared. In both cases, radical termination by coupling was minimal, according to the small shoulders in the GPC traces (**Figure 8.18e** and **Figure 8.18f**). Again, $M_{n,app} < M_{n,th}$, due to the very compact nature of molecular brushes.[44]

8.5. Ab *initio* emulsion ARGET-ATRP with [Br–Cu^{II}TPMA]$^+$/SDS

Polymerizations in emulsion systems are even more attractive than miniemulsion, mainly because of the scalability and extremely low cost of the process.[2, 45] Indeed, monomer dispersion in emulsion does not require the application of a high shearing force and latex products should be ready to use. The system is simply composed by water, a monomer with low water-solubility, a water-soluble initiator and a surfactant. Industrial emulsion polymerization asks for small amount of surfactant (typically < 3 wt% relative to monomer).

The main difference between emulsion and miniemulsion concerns the *locus* of polymerization: in emulsion, the process starts in the aqueous phase, whereas in miniemulsion chains grow inside monomer droplets. For this reason, a suitable initiator for emulsion polymerization must be water soluble, whereas its partitioning between the two phases can destabilize the process. The monomer, instead, before starting the polymerization is partitioned in 3 phases. *i*) Large monomer droplets stabilized by the surfactant, *ii*) into the aqueous phase (until saturation), together with the initiator and free surfactant molecules, and *iii*) into the micelles.[46] Clearly, micelles formed only if the amount of surfactant is above its cmc.

A typical *ab initio* emulsion polymerization is composed by 3 intervals (**Scheme 8.3**). Interval I sees the formation of particles through complex mechanisms of nucleation. Interval II starts when particles are mature and their number becomes constant. Particles grow by propagation in the presence of monomer droplets, which supply monomer molecules that reach polymerization *loci* by diffusing through the water phase. This interval may extend from 5-10% conversion until 30-70%, depending on many factors, and it ends when monomer droplets disappear. Finally, during Interval III monomer molecules remained inside particles are polymerized. It should be highlighted that polymerization

does not happen inside monomer droplets, which act as a monomer reservoir. Stabilization of growing particles is ensured by a continuous redistribution of surfactant molecules.

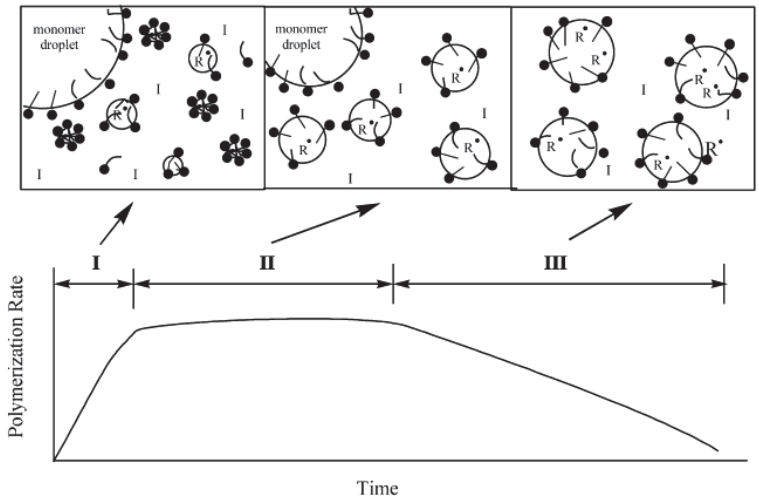

Scheme 8.3. Intervals I-III in a typical *ab initio* emulsion polymerization with their relative kinetics (reprinted with permission from Ref. [46]. Copyright 2001, Elsevier).

Interval I can be avoided in order to precisely know the number of particles inside the system. To this end, pre-formed polymer particles should be present in the emulsified solution, and this approach is called seeded emulsion polymerization.[47, 48] However, seeded method, as well as detailed kinetic descriptions of emulsion polymerizations, will not be treated in this work.

When adapted to ATRP, emulsion setup requires a copper catalyst that should display some solubility in both organic and aqueous phases to efficiently tune the polymerization. In this way it should be able to activate the initiator in water, but also to intermittently activate and deactivate the growing chains, from both inside and outside of the particles. Therefore, $[Br–Cu^{II}TPMA]^+$ seemed an excellent candidate, being extremely water-soluble but also forming ion pairs with SDS that can efficiently catalyze the process.

Ascorbic acid can be conveniently used as a reducing agent also in emulsion, thanks to its good water-solubility. More stringent is the requirement of a water-soluble initiator. Indeed, so far very few "true" *ab initio* emulsion ATRP were reported. In many cases, catalysts that can effectively distribute between the two phases were used (*i.e.* ligands owing less hydrophilic character than TPMA),[49, 50] but the same applies also to the selected RX. Moreover, the few works employing highly water-soluble RX showed very low initiator efficiencies, and poor latex stabilities, despite quite narrow MWs distributions.[49, 51, 52] An original and successful approach was proposed by Min et al., who

realized a two-step *ab initio* emulsion ATRP.[47] In the first step BA was polymerized in microemulsion via AGET ATRP, then a second part of deoxygenated BA was added, thereby forming the emulsion *in situ*.

This section presents preliminary results concerning the use of the [Br–Cu^{II}TPMA]$^+$/SDS catalytic system in ARGET-ATRP of BA, by means of an *ab initio* emulsion approach. EBiB, used as initiator in miniemulsion, was replaced with HEBiB and PEO_{1K}BiB, which should exhibit higher solubility in water. Interestingly, the pre-emulsification procedure is crucial: by stirring the solution for a long time before starting the polymerization, the reaction components are allowed to distribute between the two phases. Thus, different populations of chains were observed because the process started both inside monomer droplets and in monomer-swollen particles. Moreover, the stirring rate drastically affects the control and the stability of the latex.

8.5.1. Effect of pre-emulsification procedure on *ab initio* emulsion ARGET-ATRP of BA

First emulsion ARGET-ATRP of BA was performed with the optimized conditions for this monomer in miniemulsion (**Table 8.11, entry 1**), except replacing the initiator EBiB with HEBiB, which has higher water-solubility, while retaining a similar structure. The two phases were pre-emulsified by vigorous stirring (ca. 750 rpm) for 1 h at r.t. Then AsAc was injected to start the polymerization, while stirring rate and T were raised to 1500 rpm and 65 °C, respectively. 70% conversion was reached in 4 h. However, the process was uncontrolled ($Đ > 1.8$). More important, severe coagulation was observed after 2 h.

In order to improve the stability of the emulsion, C_{SDS} was increased from 4.6 to 9.2 wt% (relative to monomer), and AsAc was slowly fed throughout the synthesis. Nevertheless, serious coagulation was observed. Thus C_{SDS} = 18.4 wt% (relative to BA) was used, finally obtaining a stable emulsion (**Table 8.16, entry 1**). However, the system reached 89% conversion in 5 h, but $Đ > 2$. GPC traces in Figure 8.19 show the curious evolution of MWs distribution. Indeed, after 30 minutes only one peak was present, but shifted to higher M_n compared to theoretical value. After 1 h a second peak appeared at lower M_n. Then, the second peak increased in intensity while shifting to higher M_n values, while the first one slightly shifted to higher M_n, but it became relatively less significant.

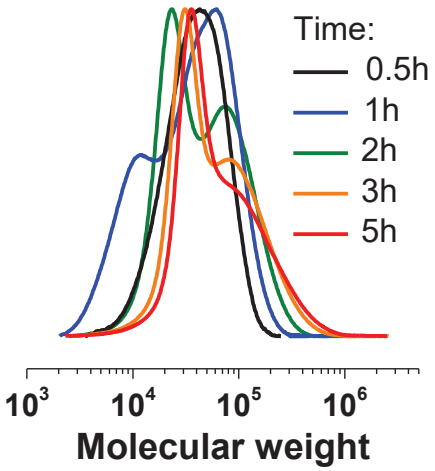

Figure 8.19. GPC traces of *ab initio* emulsion of BA 20 vol% in H_2O, with 18.4 wt% SDS (relative to BA) and 1 h of stirring at 750 rpm as pre-emulsification procedure. Other conditions as in **Table 8.16**, **entry 1**.

One reasonable explanation of the observed MWs evolution is the presence of two populations of growing chains. One population formed in monomer droplets, where polymerization was quick and poorly controlled, as depicted from the relatively large peak at high M_n. The second population originated in the water phase, as expected from a true emulsion system. A possible cause of the double distribution can be partitioning of HEBiB between the two phases. Indeed, HEBiB has a certain solubility in BA and the long-time stirring can favor its partitioning. Moreover, the stirring can create monomer "agglomerations" with different size, thus hindering the homogeneity of the solution.[53]

Table 8.16. Effect of the pre-emulsification procedure on *ab initio* emulsion ARGET-ATRP of BA, T = 65 °C.[a]

Entry	Pre-emulsification procedure	t (h)	Conv. (%)	k_p^{app} (h^{-1})	$M_{n,th}$ (10^{-3})	M_n (10^{-3})	$Đ$	$d_{Z\text{-ave}}$ (nm)[b]
1[c]	1 h mixing	5	89	0.45	32.9	34.4	2.11	161.8±0.4
2	10 min mixing	5	74	0.25	27.3	34.0	1.67	157.8±0.8
3	No mixing	5	82	0.33	30.0	30.4	1.59	182.2±1.3
4	Feeding BA	5	74	0.25	27.3	31.3	4.02	114.2±0.1

[a] $C_{BA}/C_{HEBiB}/C_{Cu^{II}Br_2}/C_{TPMA}$ = 280/1/0.2/0.22, BA 20 vol% in H_2O + 0.1 M NaBr, C_{SDS} = 18.4 wt% rel to BA, V_{tot} = 10 mL. 800 nmol AA injected at t = 0, then AA was fed with a syringe pump, feeding rate = 800 nmol/h. Stirring rate = 500 rpm. [b] Particles size at the end of the polymerization, measured by DLS. [c] stirring rate = 1500 rpm.

After this unsatisfactory result, the pre-emulsification procedure was changed. Firstly, the two phases were mixed for ten minutes, then the stirring was started simultaneously to AsAc injection (**Table 8.16, entries 2 and 3**). Moreover, the stirring rate during polymerization was reduced to 500 rpm. *Đ* decreased to 1.67 and 1.59, respectively, while polymerization rate remained similar. In the case of no-mixing, GPC trace after 30 minutes already exhibited two peaks (**Figure 8.20a**), supporting the enhancement of the population formed in water.

An attempt of feeding the monomer while injecting AsAc provided a very promising MW distribution after 30 minutes (**Figure 8.20a** and **Table 8.16, entry 4**). However, after few hours a small and broad peak at very high MWs was observed, thus monomer feeding was no more used.

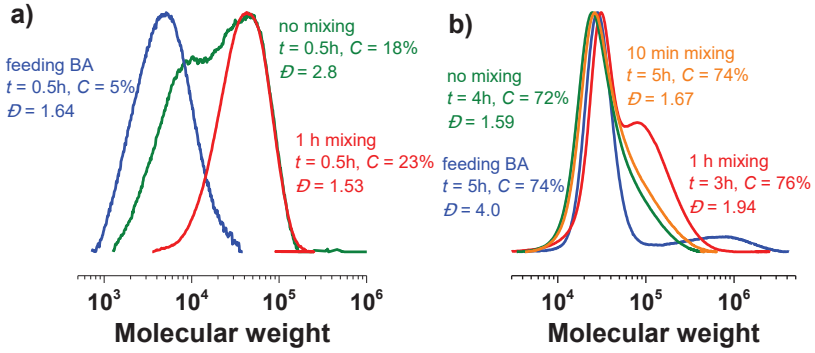

Figure 8.20. GPC traces of PBA *via* emulsion ARGET-ATRP with different procedures of pre-emulsification. Conditions in **Table 8.16**.

In order to reduce the final dispersity, DP = 500 was targeted instead of 280. Indeed, generally higher DPs favor lower *Đ* values,[33] but also the decrease in C_{HEBiB} should modify its solubilization equilibria. Surprisingly, a huge improvement was observed with dispersity dropping to 1.15. The process was slower, reaching 77% conversion in 7h (**Table 8.17, entry 2**). The high MW population was never observed (**Figure 8.21**). Moreover, the particle size growth, followed by DLS, started from a very small value, as expected from the initial absence of nucleated micelles. The particles size greatly enlarged in the first stages of the process and finally remained almost unchanged (**Figure 8.22**). To the best of our knowledge, this is the greatest result so far obtained for a one-step *ab initio* emulsion ATRP.

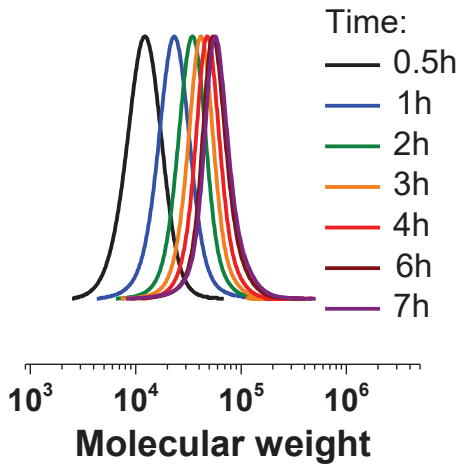

Figure 8.21. GPC traces of *ab initio* emulsion ARGET-ATRP of BA 20 vol% in H_2O, with 18.4 wt% SDS (relative to BA) and DP 500. Other conditions in **Table 8.17**, **entry 2**.

Conversion %	$d_{Z\text{-ave}}$ (nm)
17	69.4±0.4
28	95.9±0.4
42	93.8±0.5
52	105.0±0.2
62	105.8±0.2
77	109.2±0.5

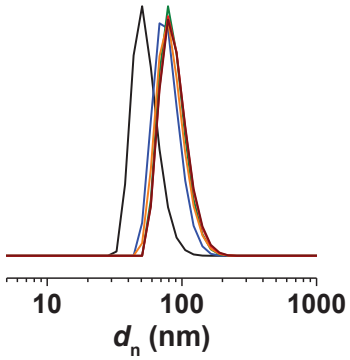

Figure 8.22. DLS measurements of particles size during *ab initio* emulsion ARGET-ATRP of BA (**Table 8.17**, **entry 2**).

However, C_{SDS} was very high if compared to industrial requirements. It should be noted that literature data normally report surfactant amounts ranging from 9 to 20 wt% relative to monomer.[2, 50-52] Hence, C_{SDS} was lowered to 9.2 and 4.6 wt% (relative to BA). As expected, final latex size increased and the polymerization rate slightly decreased (**Table 8.17, entries 3 and 4**). Unfortunately, small but not negligible coagulation was observed in both syntheses.

Table 8.17. *Ab initio* emulsion ARGET-ATRP of BA, with different hydrophilic RX, T = 65 °C.[a]

Entry	RX	C_{SDS} (wt%)[b]	DP	t (h)	Conv. (%)	k_p^{app} (h^{-1})	$M_{n,th}$ (10^{-3})	M_n (10^{-3})	$Đ$	$d_{Z\text{-ave}}$ (nm)[c]	
1	HEBiB	18.4	280	5	82	0.33	30.0	30.4	1.59	182.2±1.3	
2	HEBiB	18.4	500	7	77	0.23	49.9	55.8	1.15	109.2±0.5	
3	HEBiB	9.2	500	8	75	0.17	48.1	62.0	1.13	122.4±0.3	coagulation
4	HEBiB	4.6	500	6	61	0.16	39.2	55.8	1.21	158.4±2.1	coagulation
5 [d]	HEBiB	4.6	500	21	77	0.07	49.7	64.2	1.16	176.6±0.2	
6	PEO_{1K}BiB	18.4	280	4	63	0.22	24.7	20.9	1.28	81±16	
7 [e]	PEO_{1K}BiB	18.4	280	7	67	0.16	26.1	33.0	1.10	159±33	
8	PEO_{1K}BiB	4.6	500	18	78	0.08	52.0	69.9	1.27	102.1±2.5	

[a] $C_{BA}/C_{RX}/C_{NaBr}/C_{[Cu^{II}TPMA]^{2+}}$ = 500/1/20/0.2, BA 20 vol% in H_2O, V_{tot} = 10 mL. 800 nmol AA injected at t = 0, then AA was fed with a syringe pump, feeding rate = 800 nmol/h. Stirring rate = 500 rpm. [b] Relative to monomer. [c] Particles size at the end of the polymerization, measured by DLS. [d] Stirring rate = 250 rpm, with a bigger magnetic stirrer. [e] Feeding rate = 500 nmol/h.

Besides the pre-emulsification procedure, also the stirring rate during the process seemed to affect emulsion stability,[54] thus its effect was evaluated by repeating the experiment with a lower amount of SDS, and changing the stirring rate from 250 to 1000 rpm (**Figure 8.23**). The latter drastically destabilized the emulsion and conversion stopped at 26% after few hours. Instead, by stirring at 250 rpm the process was slower but a small coagulation was still detected. However, by using a bigger magnetic stirrer, which ensured a good mass transportation around the whole Schlenk, and by stirring at 250 rpm, no coagulation was observed even after 21 h of polymerization (**Table 8.17, entry 5**).

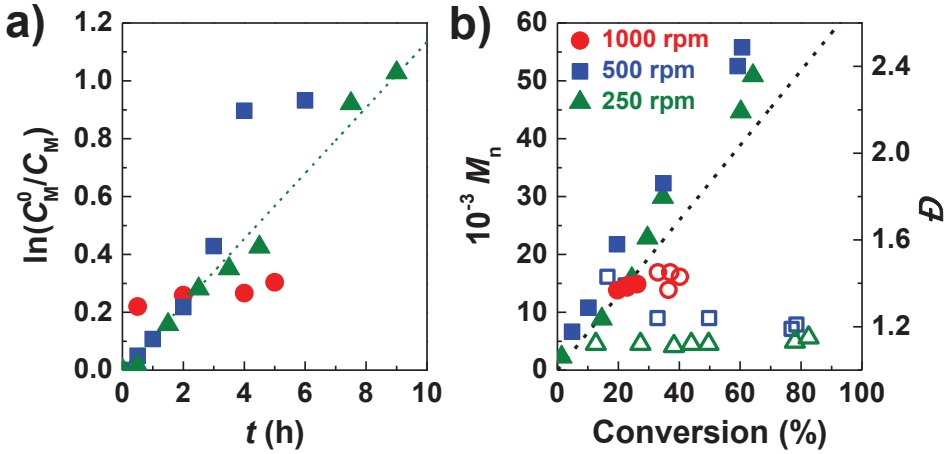

Figure 8.23. Emulsion ARGET ATRP of BA with C_{SDS} = 4.6 wt% rel. to BA and different stirring rate during polymerizations. Kinetic plot a) and MWs and dispersity evolution *vs.* conversion b). Conditions in **Table 8.17**.

Since the solubility in water of the initiator is a critical parameter, $PEO_{1K}BiB$ was tested, considering the great water-solubility of PEO. No pre-emulsification was performed also with this initiator, and the stirring (500 rpm) was started together with AsAc injection. At first, DP = 280 was targeted with C_{SDS} = 18.4 wt% (relative to BA). 63% conversion was reached within 4 h (**Table 8.17, entry 6**), and $Đ$ = 1.28. GPC traces revealed two peaks after 30 minutes, but the one at high M_n was relatively much less important, and a final monomodal narrow distribution was obtained (**Figure 8.24**).

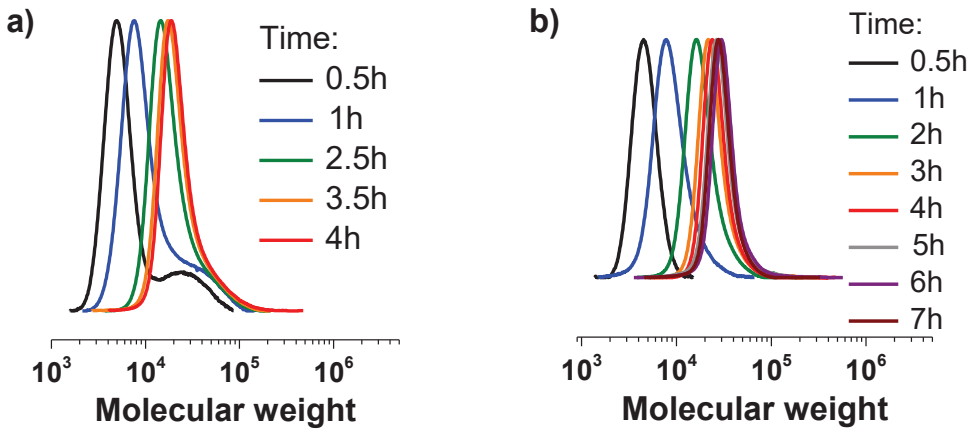

Figure 8.24. GPC traces of *ab initio* emulsion of BA 20 vol% in H_2O, with RX = $PEO_{1K}BiB$ and AsAc feeding rate = 800 nmol/h a), and 500 nmol/h b). Other conditions in **Table 8.17, entry 6, 7**.

Unexpectedly, the final solution, despite not presenting any coagulation, was much less stable than in the of RX = HEBiB, and immediately after the solution was transferred into a vail, the organic phase settled on the bottom (**Figure 8.25**). The aqueous phase appeared quite blue, while the organic phase was white, suggesting that copper complexes were mainly in water. Further characterizations on metal residues and particles stability are needed, however this easy separation may be profitable.

Figure 8.25. A picutre of final solutions obtained from *ab initio* emulsion ARGET-ATRP of BA, by using HEBiB of $PEO_{1K}BiB$ as initiator.

Slowing down the feeding rate of AsAc injection did not cause any improvement (**Table 8.17, entry 7**) in terms of overall stability, but $Đ$ decreased to 1.10. Finally, C_{SDS} was decreased to 4.6 wt% (relative to monomer), while DP = 500 was targeted, as in the case of HEBiB. The process was slower, reaching 78% conversion in 18 h, but no coagulation was observed. Measured M_n matched theoretical values and dispersity was low. The final solution almost immediately split in two phases with markedly different coloration.

In summary, one-step *ab initio* emulsion ARGET-ATRP of BA is possible, by using water-soluble initiators. The best results in terms of control and emulsion stability were obtained by avoiding any pre-mixing of the two phases before starting the polymerization. Thus, the most delicate step of the process concerns particles nucleation in the aqueous phase. The stirring rate during the polymerization also strongly affected the reaction, with very slow stirring providing higher conversions and improved stability. Two highly water-soluble RX were tested. In both cases, C_{SDS} could be lowered below 5 wt% relative to monomer, and low dispersities were attained. However, the slow stirring made the process relatively slow, reaching conversion > 75% in *ca.* 20 h. Interestingly, when HEBiB was used as initiator, the final emulsion was stable for days, even months. Instead, with RX =

$PEO_{1K}BiB$, the final, unstirred solution almost immediately divided into a white organic phase and a blue aqueous phase, which presumably contained the major part of catalyst molecules.

8.6. Conclusions and perspectives

A novel catalytic system was developed for ATRP in miniemulsion, based on the interaction between hydrophilic catalysts and anionic surfactants. The combination of ion-pair and interfacial catalysis was used to control *e*ATRP and ARGET-ATRP in miniemulsion. Expensive ligands, specifically designed for miniemulsion ATRP, were successfully replaced with commercially available ligands (*e.g.* TPMA) and inexpensive anionic surfactants such as SDS.

Catalyst loading can be decreased to few ppm; particularly ARGET-ATRP of BMA in miniemulsion was well-controlled with only 50 ppm of Cu. Residual copper in the final latex was lower than 1 ppm. Indeed, by crashing the miniemulsion by dilution, the hydrophilic complex $[Br–Cu^{II}TPMA]^+$ migrated in the aqueous phase. Thus, with this catalyst system the residual Cu content was at least 10 times lower than when using traditional hydrophobic ligands.

PBA and PBMA homopolymers with various MWs and low dispersity, as well as PBA-*stat*-PBA, PBA-*b*-PtBA, PBMA-*b*-PBA, and PBMA-*b*-PtBMA block copolymers, βCD-*star*-PBA, and βCD-*star*-PBMA polymer stars, and PBIBM-*graft*-PBA polymer brushes, were produced. Designing complex architectures in this system is relatively simple, thus new structures should be addressed, with different monomers and inorganic materials.

The same catalytic system was adopted in *ab initio* emulsion ARGET-ATRP, to fulfill the requirement of a hydrophilic catalyst for this medium. Preliminary experiments were very promising, firstly for the novelty of the one-step *ab initio* emulsion ATRP and secondly because such a low amount of surfactant (< 5 wt% relative to monomer) was never reported in a well-controlled emulsion ATRP. Clearly, further studies are needed. For example, other monomers, as well as higher DP and even lower C_{SDS}, should be tested. Moreover, *in situ* formation of well-defined hydrophobic copolymers is one of the most attractive goals of emulsion polymerizations and should be targeted with this system.

References

1. Min, K.; Matyjaszewski, K. *Central European Journal of Chemistry* **2009,** 7, 657.
2. Charleux, B.; Monteiro, M. J.; Heuts, H. *Chemistry and Technology of Emulsion Polymerisation, Second Edition* **2013**, 105-143.
3. Zetterlund, P. B.; Thickett, S. C.; Perrier, S. b.; Bourgeat-Lami, E.; Lansalot, M. *Chemical reviews* **2015,** 115, 9745-9800.
4. Asua, J. M. *Progress in polymer science* **2002,** 27, 1283-1346.
5. Elsen, A. M.; Burdyńska, J.; Park, S.; Matyjaszewski, K. *Macromolecules* **2012,** 45, 7356-7363.
6. Min, K.; Gao, H.; Matyjaszewski, K. *Journal of the American Chemical Society* **2005,** 127, 3825-3830.
7. Kagawa, Y.; Zetterlund, P. B.; Minami, H.; Okubo, M. *Macromolecular theory and simulations* **2006,** 15, 608-613.
8. Thomson, M. E.; Cunningham, M. F. *Macromolecules* **2010,** 43, 2772-2779.
9. Zetterlund, P. B.; Kagawa, Y.; Okubo, M. *Macromolecules* **2009,** 42, 2488-2496.
10. Magenau, A. J.; Strandwitz, N. C.; Gennaro, A.; Matyjaszewski, K. *Science* **2011,** 332, 81-84.
11. Fantin, M.; Park, S.; Wang, Y.; Matyjaszewski, K. *Macromolecules* **2016,** 49, 8838-8847.
12. Fantin, M.; Chmielarz, P.; Wang, Y.; Lorandi, F.; Isse, A. A.; Gennaro, A.; Matyjaszewski, K. *Macromolecules* **2017,** 50, 3726-3732.
13. Wang, Y.; Lorandi, F.; Fantin, M.; Chmielarz, P.; Isse, A. A.; Gennaro, A.; Matyjaszewski, K. *Macromolecules* **2017**, ASAP.
14. Fantin, M.; Isse, A. A.; Gennaro, A.; Matyjaszewski, K. *Macromolecules* **2015,** 48, 6862-6875.
15. Mandal, A. B.; Nair, B. U.; Ramaswamy, D. *Langmuir* **1988,** 4, 736-739.
16. Mandal, A. B.; Nair, B. U. *The Journal of Physical Chemistry* **1991,** 95, 9008-9013.
17. Anitha, N.; Balamurugan, R.; Palaniandavar, M. *Journal of colloid and interface science* **2011,** 362, 243-252.
18. Sivagnanam, U.; Palaniandavar, M. *Journal of Electroanalytical Chemistry* **1996,** 410, 43-53.
19. Bortolamei, N.; Isse, A. A.; Di Marco, V. B.; Gennaro, A.; Matyjaszewski, K. *Macromolecules* **2010,** 43, 9257-9267.
20. Cifuentes, A.; Bernal, J. L.; Diez-Masa, J. C. *Analytical Chemistry* **1997,** 69, 4271-4274.
21. Paula, S.; Sues, W.; Tuchtenhagen, J.; Blume, A. *The Journal of Physical Chemistry* **1995,** 99, 11742-11751.
22. Bergström, M.; Pedersen, J. S. *Physical Chemistry Chemical Physics* **1999,** 1, 4437-4446.
23. McIntire, G. L.; Chiappardi, D. M.; Casselberry, R. L.; Blount, H. N. *The Journal of Physical Chemistry* **1982,** 86, 2632-2640.
24. Collura, J.; Harrison, D.; Richards, C.; Kole, T.; Fisch, M. *The Journal of Physical Chemistry B* **2001,** 105, 4846-4852.
25. Rusling, J. F.; Shi, C. N.; Kumosinski, T. F. *Analytical chemistry* **1988,** 60, 1260-1267.
26. Kestin, J.; Sokolov, M.; Wakeham, W. A. *Journal of Physical and Chemical Reference Data* **1978,** 7, 941-948.
27. Hong, S. C.; Paik, H.-j.; Matyjaszewski, K. *Macromolecules* **2001,** 34, 5099-5102.

28. Wei, Y.; Jia, Y.; Wang, W.-J.; Li, B.-G.; Zhu, S. *Macromolecules* **2014,** 47, 7701-7706.

29. Kaur, A.; Ribelli, T. G.; Schröder, K.; Matyjaszewski, K.; Pintauer, T. *Inorganic chemistry* **2015,** 54, 1474-1486.

30. Park, S.; Chmielarz, P.; Gennaro, A.; Matyjaszewski, K. *Angewandte Chemie* **2015,** 127, 2418-2422.

31. Guo, J. K.; Zhou, Y. N.; Luo, Z. H. *AIChE Journal* **2015,** 61, 4347-4357.

32. Lorandi, F.; Fantin, M.; Isse, A. A.; Gennaro, A. *Polymer Chemistry* **2016,** 7, 5357-5365.

33. Matyjaszewski, K. *Macromolecules* **2012,** 45, 4015-4039.

34. Wei, Y.; Liu, P.; Wang, W.-J.; Li, B.-G.; Zhu, S. *Polymer Chemistry* **2015,** 6, 2837-2843.

35. Wei, Y.; Zhang, Q.; Wang, W.-J.; Li, B.-G.; Zhu, S. *Polymer* **2016,** 106, 261-266.

36. Asua, J. M.; Beuermann, S.; Buback, M.; Castignolles, P.; Charleux, B.; Gilbert, R. G.; Hutchinson, R. A.; Leiza, J. R.; Nikitin, A. N.; Vairon, J. P. *Macromolecular Chemistry and Physics* **2004,** 205, 2151-2160.

37. Tang, W.; Matyjaszewski, K. *Macromolecules* **2007,** 40, 1858-1863.

38. Tang, W.; Matyjaszewski, K. *Macromolecules* **2006,** 39, 4953-4959.

39. Nanda, A. K.; Matyjaszewski, K. *Macromolecules* **2003,** 36, 8222-8224.

40. Jakubowski, W.; Matyjaszewski, K. *Angewandte Chemie* **2006,** 118, 4594-4598.

41. Beuermann, S.; Buback, M.; Davis, T. P.; Gilbert, R. G.; Hutchinson, R. A.; Kajiwara, A.; Klumperman, B.; Russell, G. T. *Macromolecular Chemistry and Physics* **2000,** 201, 1355-1364.

42. Fukuda, T.; Goto, A. *Macromolecular rapid communications* **1997,** 18, 683-688.

43. Chmielarz, P.; Krys, P.; Park, S.; Matyjaszewski, K. *Polymer* **2015,** 71, 143-147.

44. Min, K.; Yu, S.; Lee, H.-i.; Mueller, L.; Sheiko, S. S.; Matyjaszewski, K. *Macromolecules* **2007,** 40, 6557-6563.

45. Asua, J. M. *Journal of Polymer Science Part A: Polymer Chemistry* **2004,** 42, 1025-1041.

46. Qiu, J.; Charleux, B.; Matyjaszewski, K. *Progress in Polymer Science* **2001,** 26, 2083-2134.

47. Min, K.; Gao, H.; Matyjaszewski, K. *Journal of the American Chemical Society* **2006,** 128, 10521-10526.

48. Okubo, M.; Minami, H.; Zhou, J. *Colloid and Polymer Science* **2004,** 282, 747-752.

49. Jousset, S.; Qiu, J.; Matyjaszewski, K.; Granel, C. *Macromolecules* **2001,** 34, 6641-6648.

50. Rusen, E.; Mocanu, A. *Colloid and Polymer Science* **2013,** 291, 2253-2257.

51. Qiu, J.; Gaynor, S. G.; Matyjaszewski, K. *Macromolecules* **1999,** 32, 2872-2875.

52. Chambard, G.; De Man, P.; Klumperman, B. In *Atom transfer radical polymerisation in emulsion*, Macromolecular Symposia, 2000; Wiley Online Library: 2000; pp 45-51.

53. Durbin, D.; El-Aasser, M.; Poehlein, G.; Vanderhoff, J. *Journal of Applied Polymer Science* **1979,** 24, 703-707.

54. Moribe, H.; Kitayama, Y.; Suzuki, T.; Okubo, M. *Macromolecules* **2010,** 44, 263-268.

Conclusion and perspectives

Electrochemistry provides sustainable, flexible, and robust tools to trigger polymerization processes and analyze reaction mechanisms. Electrochemically mediated atom transfer radical polymerization (*e*ATRP) enables the synthesis of precisely controlled polymers with complex architectures, by using electrons as driving force of the process. *e*ATRP is a clean and simple technique, free of by-products and it can be conveniently performed by means of a common current generator.

Actually, the setup of *e*ATRP has been highly simplified over the last three years. The Platinum counter electrode was at first replaced with a sacrificial Aluminum wire, then, it was proved during this thesis work that several non-noble, inexpensive materials can replace the Pt cathode. Thus, potentiostatic and galvanostatic *e*ATRP can be run in organic and aqueous media with an affordable Pt-free setup. In contrast to Platinum, these electrodic materials are functionalizable; they can be decorated with ATRP initiating sites and further used as a platform to grow polymer chains. Polymer-grafted electrodes find considerable applications in the field of bio-sensors and membranes.

A sustainable polymerization process requires not only a cost-effective setup, but also the use of green, recyclable compounds. For this reason, the use of Ionic Liquids (ILs) as ATRP solvents should be promoted. The reported characterization of common ATRP catalysts and initiators in [BMIm][OTf] provides useful guidelines to selecting the proper system composition for polymerizations. The behavior of the analyzed compounds well-matched the one observed in traditional organic solvents, but with the advantage that ILs, with solubilized catalysts, can be easily recovered and recycled. Finally, ILs are particularly interesting for *e*ATRP because they do not require any supporting electrolyte. Thus, various monomers should be polymerized *via e*ATRP in ILs, also attempting to *in situ* building multiblock-copolymers.

Polymerizations in dispersed media, such as miniemulsion, microemulsion, nanoemulsion, emulsion and dispersion, are another environmentally friendly approach to polymer synthesis. Industrial plants are mainly based on heterogenous processes, although academic research is generally more focused on homogeneous systems. In this context, the proposed effective combination of commercial hydrophilic ligands and inexpensive anionic surfactants can raise the interest toward (mini)emulsion ATRP. Particularly, emulsions

fulfill the criteria of low-cost, simplicity and sustainability mentioned above. Therefore, the reported work on ARGET-ATRP in emulsion should be expanded to various hydrophobic monomers, and more importantly to build (multi)block copolymers. The optimized conditions of pre-emulsification and stirring should be scaled to higher volumes. Finally, the amount of surfactant, which currently ranges from 4.5-18 wt% (relative to monomer), should be further decreased below 3 wt% to satisfy industrial requirements.

The strength of polymerizations in dispersed systems is the use of water as solvent for non water-soluble monomers and polymers. This non-toxic, cheap and biocompatible solvent, however, posed many challenges to well-controlled ATRPs, even in the synthesis of hydrophilic polymers. Actually, aqueous *e*ATRPs of very few monomers were reported so far. Thus, polymerizations of novel hydrophilic monomers should be addressed by *e*ATRP, also because of the increasing interest toward the synthesis and application of double hydrophilic block copolymers. These architectures, indeed, show high responsiveness to pH and temperature.

The aqueous *e*ATRP of acrylic acid reported in this thesis work, together with published *e*ATRP and SARA-ATRP of methacrylic acid represent a major achievement in the field of controlled polymerizations. These monomers were considered a limit to ATRP applicability for many years. Poly(acrylic acid) is biocompatible and a fundamental component of many polymeric architectures used as drug carriers, surfactants and polyelectrolytes.

The successful *e*ATRP of acidic monomers is encouraging us to tackle the controlled polymerization of other “difficult” monomers, like vinyl acetate, and similar less activated monomers, on one side, and strongly activated monomers like cianoacrylates, on the other side.

Great results in *e*ATRP would have been impossible without a continuous attentive analysis of atom and electron transfer mechanisms in ATRP. Electrochemistry, more than any other discipline, provides easy-access to several thermodynamic and kinetic parameters, facilitating the prediction of synthetic results. Common practice to define the suitability of newly synthesized Cu complexes for ATRP involves *i*) determination of standard redox potentials, *ii*) estimation of halogen affinity via cyclic voltammetry and *iii*) electrochemical measurements of activation rate constant. In addition, a fast and reproducible electrochemical procedure to determine K_{ATRP} is now available. Creation of a

big database that contains K_{ATRP}, k_{act} and k_{deact} values for a wide series of ligands, initiators, solvents and monomers is the natural prosecution of the work started during my doctorate.

Electrochemical analysis should now focus on a better definition of side reactions that hamper ATRP catalysts. Creative ligand design can help electrochemistry in this task. Indeed, the synthesis of new structures should target the preparation of much more active Cu complexes to enhance ATRP rate. Also, stability, solubility and steric features can be tuned by modifying the ligand.

In conclusion, this work provides several steps forward *e*ATRP implementation and mechanistic understanding. These achievements are marked in red in **Figure I** and **Figure II,** but they are in fact starting points for new challenges that will confirm ATRP as the leading technique in polymer synthesis.

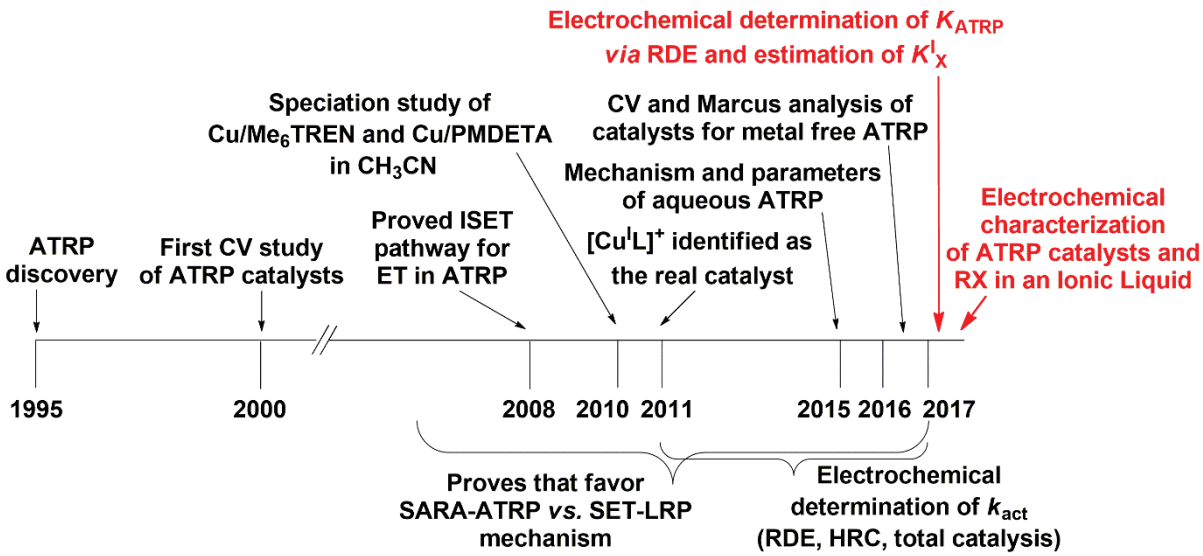

Figure I. Timeline of fundamental contributions of electrochemistry to the study of ATRP mechanism. The work presented in this thesis is reported in red.

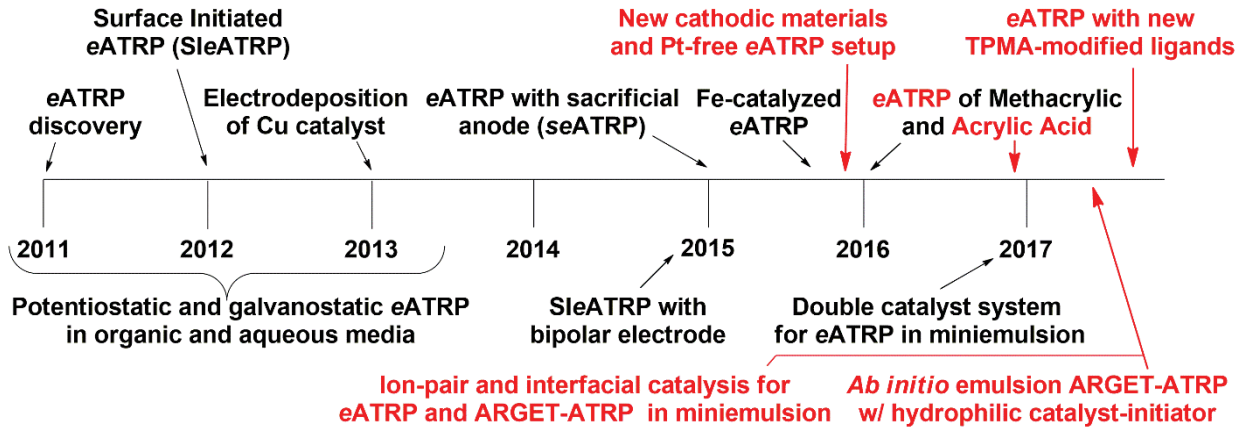

Figure II. Timeline of major landmarks in *e*ATRP history, my contribution is reported in red.

Appendix A.

Materials and instruments

Table of contents

A1. Materials and purification procedures

Solvents : acetonitrile (CH_3CN, Sigma-Aldrich, ≥99.9%), *N*,*N*-dimethylformamide (DMF, VWR, 99.9%), stabilized tetrahydrofuran (THF, Romyl, with BHT as stabilizer), were used as received.

Water was purified by double distillation in the presence of potassium permanganate.

3-butyl-1-methylimidazolium triflate ([BMIm][OTf], Iolitech, ≥ 98%) was purified by mixing 20 mL of Ionic Liquid with 80 mL of double-distilled water and neutralized to pH 7 with 0.07 M KOH. After removing water by a rotary evaporator, the IL was purified by extraction with diethyl ether (2×50 mL, followed by 1×100 mL) after vigorous mixing for at least 3 h. The IL was dried first at a rotary evaporator to remove the residual ether and then under high vacuum (≈ 0.03 mbar) at 110 °C for at least 24 hours.

Deuterated solvents ($CDCl_3$, Sigma Aldrich, 99.8%, and D_2O, Sigma Aldrich, 99.9%) for NMR spectroscopy were used as received.

Monomers: *n*-Butyl acrylate (BA, Sigma-Aldrich, ≥99%), oligo(ethylene glycol) methyl ether methacrylate (OEOMA, Sigma-Aldrich, average molecular weight = 500), methyl methacrylate (MMA, Sigma-Aldrich, 99%), methyl acrylate (MA, Sigma-Aldrich, 99%), *n*-Butyl methacrylate (BMA, 99%, Aldrich), *t*-butyl acrylate (*t*BA, 98%, Aldrich), *t*-butyl methacrylate (*t*BMA, 98%, Aldrich) were purified by passing through a column filled with activated basic alumine (Al_2O_3, VWR, 58 Å) to remove the polymerization inhibitor.

Methacrylic acid (MAA, Sigma-Aldrich, 99%) and acrylic acid (AA, Sigma-Aldrich, 99%) were distilled through a 10 cm Vigreux column to remove polymerization inhibitors.

Ligands: tris[2-(dimethylamino)ethyl]amine (Me_6TREN, VWR, 99+%), tris(2-pyridylmethyl)amine (TPMA, Sigma-Aldrich, 98%), N,N,N′,N″,N″-Pentamethyldiethylenetriamine (PMDETA, Sigma-Aldrich, 99%) were used as received. In some cases, TPMA was prepared according to a published procedure.[1] (4-methoxy-3,5-dimethyl-pyridin-2-ylmethyl)-pyridin-2-ylmethyl-amine (TPMA*1), and parent TPMA*2 and TPMA*3, were prepared according to a previously published procedure.[2] Bis(2-pyridylmethyl)octadecylamine (BPMODA) and bis[2-(4-methoxy-3,5-dimethyl)pyridylmethyl]octadecylamine (BPMODA*) were prepared as previously described.[1, 3]

Initiators: methyl 2-bromopropionate (MBP, Sigma-Aldrich, 98%), ethyl 2-chloropropionate (ECP, Sigma-Aldrich, 97%), methyl α-bromoisobutyrate (MBiB, Sigma-Aldrich, >99%), 2-hydroxyethyl 2-bromo-isobutyrate (HEBiB, Sigma-Aldrich, 95%), α-bromoisobutyric acid (BiBA, Sigma-Aldrich, 98%), 2-bromopropionic acid (BPA, Sigma-Aldrich, ≥99%), α-chlorophenylacetic acid (CPAA, Sigma-Aldrich, 97%), α-chloroisobutyric acid (CiBA, Sigma-Aldrich, 97%), 2,2-dichloropropanoic acid (Delapon, Sigma-Aldrich), trichloroacetic acid (TCAA, Sigma-Aldrich, ≥99%), ethyl α-bromophenylacetate (EBPA, Sigma-Aldrich, 97%), ethyl bromoacetate (EBA, Sigma-Aldrich, 98%), benzyl bromide (BB, Sigma-Aldrich, 98%), 1-phenyl-1-bromoethane (PEB, Sigma-Aldrich, 97%), 2-bromopropionitrile (BPN, Sigma-Aldrich, 97%), benzyl chloride (BC, Sigma-Aldrich, 99%), methyl 2-chloropropionate (MCP, Sigma-Aldrich, 97%), 1-phenyl-1-chloroethane (PEC, Sigma-Aldrich, 99%), chloroacetonitrile (CAN, Sigma-Aldrich, 98%), chloropropionitrile (CPN, Sigma-Aldrich, 95%), ethyl α-bromoisobutyrate (EBiB, Sigma-Aldrich, 98%) were used as received.

EBiB-modified β-cyclodextrin (β-CD-Br_{14}), and poly(2-(2-bromoisobutyryloxy)ethyl methacrylate) ($PBiBM_{100}$) were prepared according to published procedures.[4, 5]

Others: Cu^{II} trifluoromethanesulfonate ($Cu^{II}(OTf)_2$, Alfa Aesar, 99%), copper(II) bromide ($CuBr_2$, Sigma-Aldrich, 99%), 2,2,6,6-tetramethyl-1-piperidinyloxy (TEMPO, Sigma-Aldrich, 98%), tetrabutylammonium hexafluorophosphate ($TBAPF_6$, Sigma-Aldrich, 98%), methylated cellulose (Tylose, MH = 300, Sigma-Aldrich), hexadecane (HD, Sigma-Aldrich, 99%), sodium bromide (NaBr, Acros, 99%), polyoxyethylene (20) oleyl ether (Brij 98, Acros), sodium dodecyl sulfate (SDS, Sigma-Aldrich, 99%), sodium dodecylbenzenesulfonate (SDBS, Sigma-Aldrich, technical grade), ascorbic acid (AsAc, Sigma-Aldrich) were used as received.

Dodecanoic acid (DA, 98%, Sigma-Aldrich) was neutralized with NaOH to prepare sodium dodecanoate (SDA).

Tetraethylammonium tetrafluoroborate (Et_4NBF_4, Alfa Aesar, 99%), used as supporting electrolyte, was recrystallized from ethanol and dried in a vacuum oven at 70 °C for 24 h. Tetraethylammonium bromide (Et_4NBr, Sigma-Aldrich, 98%) and tetraethylammonium chloride (Et_4NCl, Sigma-Aldrich, ≥98%) were recrystallized from ethanol and from a mixture of ethanol/diethyl ether, respectively, and dried in a vacuum oven at 70 °C for 24 h.

A2. Instruments

Potentiostat: all electrochemical characterizations and electrolysis experiments were carried out in a three-electrode cell by using an Autolab PGSTAT 30 potentiostat/galvanostat (EcoChemie, The Netherlands) run by a PC with GPES software, or an Autolab PGSTAT302N potentiostat/galvanostat, run by a PC with NOVA 2.1 software (EcoChemie, The Netherlands), or a PARC 273A potentiostat/galvanostat (EG&G Princeton Applied Research) run by a PC with Echem software, or a Gamry Ref-600 potentiostat/galvanostat.

Electrochemical cell was always equipped with a 3-electrode setup. The reference electrode was an Ag|AgI| 0.1 M Bu_4NI in DMF for organic solvents, IL, and miniemulsion, whereas a saturated calomel electrode (SCE) was used in water. The counter electrode was a small Pt ring for voltammetric characterizations and a Pt foil for *e*ATRPs. The Pt CE was separated from the working solution through a glass frit, filled with a methylcellulose-based gel. For *se*ATRP, the Pt foil was replaced by an activated Aluminum wire directly immersed in solution. Finally the working electrode for electrochemical characterizations

was a small glassy carbon disk (3 mm dia., TOKAI, GC-20), polished with a 0.25-µm diamond paste, and ultrasonically rinsed in ethanol for 5 minutes. During electrolysis, the selected bulk working electrode was used after activation, according to procedures that will be described in next sections.

The ferrocenium/ferrocene (Fc^+/Fc) redox couple was used as internal standard, added at the end of each characterization/kinetic experiment, to convert all potentials to the aqueous saturated calomel electrode (SCE). The known values of $E^e(Fc^+/Fc)$ *vs.* SCE: -0.390 V in CH_3CN, and-0.476 V in DMF were used.[6]

Gel permeation chromatography (GPC): equipped with Agilent PLgel columns (guard, 50, 50) connected in series, and a refractive index detector (RID), provided the number average molecular weight (M_n) and the molecular-weight dispersity ($Đ$) values. For the analysis of PBA and POEOMA the eluent was DMF + 1% v/v triethylenamine + 1% v/v glacial acetic acid, at a flow rate of 1 mL/min. Columns were thermostated at 70 °C, while the RID temperature was set at 50 °C. The columns were calibrated with 12 linear poly(methyl methacrylate) standards (M_n = 634-1944000). For characterizing PMA and PMMA the eluent was stabilized THF at a flow rate of 1 mL/min. Both columns and RID temperature was set at 35 °C. The columns were calibrated with mentioned PMMA standards.

The set of columns was changed for the analysis of PAA and PMA: PL aquagel-OH columns (guard, 30, 50) were used at 30 °C; the RID was set at 35 °C. The mobile phase was aqueous 0.1 M Na_2HPO_4 at a flow rate of 1 mL/min.

Finally, polymers obtained by polymerizations in (mini)emulsion were characterized through a GPC equipped with Polymer Standards Services (PSS) columns (guard, 10^5, 10^3, and 10^2 Å) and a differential refractive index detector (Waters, 2410), with THF as eluent at a flow rate of 1.00 mL/min (T = 35 °C). GPC traces were processed by WinGPC 8.0 software (PSS) using a calibration based on linear polystyrene (PS) standards.

Before injection into the GPC, samples were always filtered over neutral alumina, and 200 nm PTFE filter, to remove the copper catalyst.

^{1}H-NMR: a Varian 300 MHz or a Bruker 200 MHz instrument was used to determine monomer conversion. All spectra were recorded in $CDCl_3$ for *e*ATRPs in organic solvents, and in D_2O for *e*ATRPs in water.

Thermostat: Thermo Scientific, HAAKE SC100, connected to the external jacket of electrochemical cells.

UV-Visible-NIR spectroscopy: UV-Visible-NIR spectra were recorded by Agilent Cary 5000 or Agilent 8453 with a quartz or glass cuvette (length = 1 cm).

Inductively coupled plasma-mass spectrometry (ICP-MS): samples were prepared by digesting the solutions in 10 mL of 2% HNO_3 matrix at 90 °C for 30 min. The concentrations of copper (Cu) in solutions were measured by an Agilent Technologies 7700× ICP-MS system (Agilent Technologies International Japan, Ltd., Tokyo, Japan), whereas in precipitated polymers after miniemulsion polymerizations were determined using Thermo-Finnigan Element XR ICP-MS. Instruments were calibrated with standard solutions. Elemental results were within the calibration range.

Scanning electron microscopy (SEM): SEM images in **Chapter 4** were acquired using a field emission source equipped with a GEMINI column (Zeiss Supra VP35).

X-ray data: crystallographic data of polydentate amine ligands presented in **Chapter 6** were deposited as CCDC-1542046-49 (2a 1542046, 2d 1542047, 3a 1542048 and 3c 1542049). Copies of the data can be obtained, free of charge, at the Cambridge Crystallographic Data Centre.

Ultrasound: miniemulsions were generated by means of a Ultrasonics W-385 sonicator.

Dynamic light scattering (DLS): particle size and size distribution in (mini)emulsion were determined by using a Zetasizer Nano from Malvern Instruments, Ltd.

A3. Materials used as electrodes

Platinum gauze (Alfa Aesar, 99.9 % metals basis), Gold foil (0.25 mm foil; Alfa Aesar, 99.95 % metals basis), Glassy carbon (GC, Tokai GC-20) plate, Titanium foil (0.25 mm foil; Aldrich, 99.7% trace metals basis), Nickel foil (0.25 mm foil; Aldrich, 99.9%), Iron wire (2 mm, Alfa Aesar, 99% metal basis),Nickel Cromium wire (1 mm diameter, Alfa Aesar, Ni:Cr = 80:20 wt%, 99% metal basis) and stainless steel SS304 (0.5 mm foil, Alfa Aesar, Fe:Cr:Ni = 70:19:11 wt%) foil. Aluminum wire (1 mm diameter; Carlo Erba, 99.5%) Copper wire (1 mm diameter, annealed, Alfa Aesar, 99.9% metal basis).

References

1. Xia, J.; Matyjaszewski, K. *Macromolecules* **1999,** 32, 2434-2437.
2. Kaur, A.; Ribelli, T. G.; Schröder, K.; Matyjaszewski, K.; Pintauer, T. *Inorganic chemistry* **2015,** 54, (4), 1474-1486.
3. Elsen, A. M.; Burdyńska, J.; Park, S.; Matyjaszewski, K. *Macromolecules* **2012,** 45, 7356-7363.
4. Chmielarz, P.; Park, S.; Sobkowiak, A.; Matyjaszewski, K. *Polymer* **2016,** 88, 36-42.
5. Beers, K. L.; Gaynor, S. G.; Matyjaszewski, K.; Sheiko, S. S.; Möller, M. *Macromolecules* **1998,** 31, 9413-9415.
6. L. Falciola, A. Gennaro, A. A. Isse, P. R. Mussini and M. Rossi, *Journal of Electroanalytical Chemistry* **2006**, 593, 47-56.

Appendix B.

Experimental and theoretical details for the electrochemical determination of k_{act} and K_{ATRP}

Table of contents

B1. General procedure for k_{act} determination *via* rotating disk electrode

This procedure was applied to all measurements of ATRP activation rate constant k_{act}, *i.e.* kinetics in **Chapter 3**, **Chapter 6** and **Chapter 7**.

A stock solution of Cu^{I} in CH_3CN was prepared by using the comproportionation reaction between $Cu^{II}(OTf)_2$ and a Cu wire, activated by cleaning with CH_3OH/HCl 3/1 and rinsed with water and acetone. The concentration of $Cu^{I}OTf$ was determined by spectrophotometric analysis, using 2,9-dimethyl-1,10-phenanthroline as a specific ligand (ε = 8458 M^{-1} cm^{-1}) in a 3-fold excess with respect to the metal.[1]

The counter and reference electrodes (a Pt ring and an Ag|AgI|0.1 M *n*-Bu_4NI in DMF, respectively) were put into the electrochemical cell. The working electrode was a 3 mm glassy carbon disk for the rotating disk electrode (RDE). The disk was polished with a 0.25 mm diamond paste and utlrasonically rinsed in ethanol, washed with abundant distilled water and acetone and put into the cell.

Recrystallized Et_4NBF_4 supporting electrolyte, 0.3256 g, and 15 mL of pure solvent or solvent/monomer mixture were inserted into the cell. Then, the desired amount of ligand and radical scavenger TEMPO were added into the solution. After degassing the solution for *ca.* 15 min, cyclic voltammetry was run to check for impurities and verify the absence of oxygen. The RDE rotation was set at 4000 rpm and started, while a constant potential was applied.

E_{app} values were selected as to follow the diffusion-controlled oxidation of $[Cu^{I}TPMA]^{+}$ in a potential range were no other processes were occurring: therefore, E_{app} = 0.28, or 0.38 V vs. SCE in CH_3CN/BA (1/1 v/v), and DMF/BA (1/1 v/v), respectively. The required amount of Cu^{I} was withdrawn with a syringe from the stock solution, under inert atmosphere, and injected into the cell. The needed amount of initiator was put into the cell few instants after Cu^{I} injection. In many cases, stock solutions of RX in the desired solvent were previously prepared and degassed as to facilitate the injection of small amounts without opening the cell. At the end of measurements, a final CV was always recorded to check the stability and the potential of the Cu catalyst. The ferrocenium/ferrocene redox couple was added and its standard potential was measured to convert all potentials to the aqueous SCE.

B2. General procedure for K_{ATRP} determination *via* rotating disk electrode

The same procedure described for k_{act} determination was used also for K_{ATRP} measurements, but the radical scavenger TEMPO was not put into the cell. RDE rotation was set at 2500 rpm, while E_{app} = 0.48 or 0.28 V vs. SCE for L = Me_6TREN, and TPMA, respectively, in both CH_3CN, and CH_3CN/BA (1/1 v/v), while E_{app} = 0.58, or 0.38 V vs. SCE for L = Me_6TREN, and TPMA, respectively, in both DMF, and DMF/BA (1/1 v/v).

For relatively slow reactions with low ATRP equilibrium constants, k_{act} and K_{ATRP} were measured concurrently, by adopting the described procedure and adding a degassed concentrated solution of TEMPO in CH_3CN or DMF, *ca.* 1 minute after RX injection. The amount of TEMPO in the operating solution was 10- to 20-fold in excess over $[Cu^{I}L]^{+}$, to assure that all generated radicals were immediately trapped by the nitroxide.

B3. Definition of K_{ATRP}^{app} and its relation with K_{ATRP}

In the presence of halogen ions, two equilibria should be considered when evaluating the thermodynamic of ATRP: *i*) the ATRP equilibrium, Eq. B1, *ii*) the association of X^{-} to $Cu^{I}L^{+}$, Eq. B2.

$$[Cu^{I}L]^{+} + RX \rightleftharpoons [XCu^{II}L]^{+} + R^{\bullet} \qquad K_{ATRP} = \frac{C_{[XCu^{II}L]^{+}} C_{R^{\bullet}}}{C_{[Cu^{I}L]^{+}} C_{RX}} \qquad \text{(B1)}$$

$$[\mathrm{Cu^{I}L}]^{+} + \mathrm{X}^{-} \rightleftharpoons \mathrm{XCu^{I}L} \qquad K_{\mathrm{X}}^{\mathrm{I}} = \frac{C_{\mathrm{XCu^{I}L}}}{C_{[\mathrm{Cu^{I}L}]^{+}} C_{\mathrm{X}^{-}}} \tag{B2}$$

The total amount of Cu^{I} and X^{-} in solution at the equilibrium is calculated by Eqs. B3 and B4, assuming that all Cu^{I} species other than $[Cu^{I}L]^{+}$ and $XCu^{I}L$ are negligible.

$$C_{\mathrm{Cu^{I}}}^{0} = C_{[\mathrm{Cu^{I}L}]^{+}} + C_{\mathrm{XCu^{I}L}} + C_{[\mathrm{XCu^{II}L}]^{+}} \tag{B3}$$

$$C_{\mathrm{X}^{-}}^{0} = C_{\mathrm{X}^{-}} + C_{\mathrm{XCu^{I}L}} \tag{B4}$$

where the superscript "0" indicates the initially added amount of Cu^{I} and X^{-}. Eqs. B3 and B4 can be re-written as:

$$C_{\mathrm{X}^{-}} = C_{\mathrm{X}^{-}}^{0} - C_{\mathrm{XCu^{I}L}} \tag{B5}$$

$$\begin{aligned} C_{[\mathrm{Cu^{I}L}]^{+}} &= C_{\mathrm{Cu^{I}}}^{0} - C_{\mathrm{XCu^{I}L}} - C_{[\mathrm{XCu^{II}L}]^{+}} = C_{\mathrm{Cu^{I}}}^{0} - K_{\mathrm{X}}^{\mathrm{I}} C_{[\mathrm{Cu^{I}L}]^{+}} C_{\mathrm{X}^{-}} - C_{[\mathrm{XCu^{II}L}]^{+}} \\ &= C_{\mathrm{Cu^{I}}}^{0} - K_{\mathrm{X}}^{\mathrm{I}} C_{[\mathrm{Cu^{I}L}]^{+}} \left(C_{\mathrm{X}^{-}}^{0} - C_{\mathrm{XCu^{I}L}}\right) - C_{[\mathrm{XCu^{II}L}]^{+}} \end{aligned}$$

$$C_{[\mathrm{Cu^{I}L}]^{+}} = \frac{C_{\mathrm{Cu^{I}}}^{0} - C_{[\mathrm{XCu^{II}L}]^{+}}}{1 + K_{\mathrm{X}}^{\mathrm{I}} \left(C_{\mathrm{X}^{-}}^{0} - C_{\mathrm{XCu^{I}L}}\right)} \tag{B6}$$

By substituting Eq. B6 in the expression for K_{ATRP}, dictated by Eq. B1:

$$K_{\mathrm{ATRP}} = \frac{C_{\mathrm{XCu^{II}L}} + C_{\mathrm{R}^{\bullet}}}{\left(C_{\mathrm{Cu^{I}}}^{0} - C_{[\mathrm{XCu^{II}L}]^{+}}\right) C_{\mathrm{RX}}} \left[1 + K_{\mathrm{X}}^{\mathrm{I}} \left(C_{\mathrm{X}^{-}}^{0} - C_{\mathrm{XCu^{I}L}}\right)\right] = K_{\mathrm{ATRP}}^{\mathrm{app}} \left[1 + K_{\mathrm{X}}^{\mathrm{I}} \left(C_{\mathrm{X}^{-}}^{0} - C_{\mathrm{XCu^{I}L}}\right)\right] \tag{B7}$$

Eq. B7 highlights that, by increasing $C_{\mathrm{X}^{-}}^{0}$, $K_{\mathrm{ATRP}}^{\mathrm{app}}$ should decrease, to keep constant the value of K_{ATRP}. Thus, the ratio between the equilibrium constant in the presence and absence of halide ions, expressed by Eq. B8, is always < 1, as seen in **Figure 3.9** (**Chapter 3**, **Section 3.7**).

$$\frac{K_{\mathrm{ATRP}}^{\mathrm{app}}}{K_{\mathrm{ATRP}}} = \frac{1}{\left[1 + K_{\mathrm{X}}^{\mathrm{I}} \left(C_{\mathrm{X}^{-}}^{0} - C_{\mathrm{XCu^{I}L}}\right)\right]} \tag{B8}$$

$$K_{\mathrm{ATRP}}^{\mathrm{app}} = \frac{K_{\mathrm{ATRP}}}{\left[1 + K_{\mathrm{X}}^{\mathrm{I}} \left(C_{\mathrm{X}^{-}}^{0} - C_{\mathrm{XCu^{I}L}}\right)\right]} \tag{B9}$$

Finally, if $C_{\mathrm{X}^{-}}^{0} \gg C_{\mathrm{Cu^{I}}}^{0}$, Eq. B9 reduces to Eq. B10:

$$K_{\mathrm{ATRP}}^{\mathrm{app}} = \frac{K_{\mathrm{ATRP}}}{1 + K_{\mathrm{X}}^{\mathrm{I}} C_{\mathrm{X}^{-}}^{0}} \tag{B10}$$

Moreover, from Eq. B7, $K_{\mathrm{ATRP}}^{\mathrm{app}}$ is defined as:

$$K_{\mathrm{ATRP}}^{\mathrm{app}} = \frac{C_{[\mathrm{XCu^{II}L}]^+} C_{\mathrm{R}^\bullet}}{\left(C_{\mathrm{Cu^I}}^0 - C_{[\mathrm{XCu^{II}L}]^+}\right) C_{\mathrm{RX}}} \tag{B11}$$

Considering the Eq. B3 for $C_{\mathrm{Cu^I}}^0$, in the absence of added X^-, Eq. B11 reduces to the expression for K_{ATRP}. Thus the ratio $K_{\mathrm{ATRP}}^{\mathrm{app}}/K_{\mathrm{ATRP}}$ equals the ratio $C_{[\mathrm{Cu^IL}]^+}/C_{\mathrm{Cu^I}}^0$, if the amount of $XCu^{II}L$ is negligible:

$$\frac{K_{\mathrm{ATRP}}^{\mathrm{app}}}{K_{\mathrm{ATRP}}} = \frac{C_{[\mathrm{Cu^IL}]^+}}{C_{\mathrm{Cu^I}}^0 - C_{[\mathrm{XCu^{II}L}]^+}} \approx \frac{C_{[\mathrm{Cu^IL}]^+}}{C_{\mathrm{Cu^I}}^0} \tag{B12}$$

Note that Eq. B12 can also be derived from Eq. B8, considering Eq. B4 and the expression for $K_{\mathrm{X}}^{\mathrm{I}}$.

The equilibrium concentration of $[Cu^IL]^+$, $C_{[\mathrm{Cu^IL}]^+}$, is derived from the equilibrium in Eq. B2, considering that $C_{\mathrm{Cu^I}}^0$ and $C_{\mathrm{X}^-}^0$ are the initial concentrations of Cu^I and X^-, respectively, thus their equilibrium concentrations are $C_{\mathrm{Cu^I}}^0 - C_{[\mathrm{Cu^IL}]^+}$, and $C_{\mathrm{X}^-}^0 - C_{[\mathrm{Cu^IL}]^+}$. By solving the second order equation:

$$C_{[\mathrm{Cu^IL}]^+} = \frac{K_{\mathrm{X}}^{\mathrm{I}} C_{\mathrm{Cu^I}}^0 + K_{\mathrm{X}}^{\mathrm{I}} C_{\mathrm{X}^-}^0 + 1 + \left[\left(K_{\mathrm{X}}^{\mathrm{I}} C_{\mathrm{Cu^I}}^0 + K_{\mathrm{X}}^{\mathrm{I}} C_{\mathrm{X}^-}^0 + 1\right)^2 - 4\left(K_{\mathrm{X}}^{\mathrm{I}}\right)^2 C_{\mathrm{X}^-}^0 C_{\mathrm{Cu^I}}^0\right]^{1/2}}{2K_{\mathrm{X}}^{\mathrm{I}}} \tag{B13}$$

References

1. Gahler, A. R. *Analytical Chemistry* **1954,** 26, 577-579.

Appendix C.

Experimental details for *e*ATRPs in organic and aqueous media

Table of contents

C1. Procedures of electrochemical, chemical or mechanical activation of electrodic materials

To effectively conduct electrons, electrodic materials need to be activated with either electrochemical, chemical or mechanical procedures.

- Platinum mesh electrode was electrochemically activated in 0.5 M H_2SO_4 by first applying a series of anodic/cathodic steps of 6 s each, with a current density of ca 0.4 mA/cm^2, for a total time of 15 min, and then 50 voltammetric cycles at 0.1 V/s in a potential range between -0.7 and 1.0 V vs. Hg/$HgSO_4$ reference electrode.
- GC foil was polished with 1000, 2500, 4000 silicon carbide papers and 3-, 1-, 0.25-µm diamond pastes. Each polishing step was followed by ultrasonic rinsing in ethanol for 5 minutes.
- Gold foil was cleaned with aqua regia (HCl/HNO_3 = 3/1, v/v) and then washed with deionized water. Then, similarly to Pt, it was electrochemically activated in 0.5 M H_2SO_4 with cyclic anodic/cathodic steps of 6 s each, with a current density of ca 0.4 mA/cm^2, for a total time of 15 min, followed by 50 CV cycles at 0.2 V/s in a potential range between -0.7 and 1.2 V vs. Hg/$HgSO_4$ reference electrode.
- Ti and Ni foils, NiCr wire, Fe wire, and 304SS foil were polished with 1000, 2500, 4000 silicon carbide papers and 3-, 1-, 0.25-µm diamond pastes, with ultrasonic rinsing in ethanol for 5 minutes after each polishing step. They were then chemically activated by

soaking in a dilute solution of HCl for 10 minutes. NiCr wire was also immersed in dilute HNO_3 after polishing. Finally the electrodes were rinsed with plenty of distilled water.

- Al wire was chemically activated by immersion in a HCl/H_2O 1/1 (v/v) solution and then rinsed with plenty of distilled water.
- Cu wire was chemically activated by immersion in a CH_3OH/HCl 3/1 (v/v) solution and then rinsed with distilled water and acetone.

C2. General procedure of potentiostatic and galvanostatic *e*ATRP

The following steps were followed for all *e*ATRPs reported in **Chapter 4** (except for aqueous *e*ATRP with pre-electrolysis of Cu^{II}, see **Section C3**), **Chapter 5**, and **Chapter 6**.

A six-neck electrochemical cell was purged with Ar and maintained at the desired temperature with a thermostat. A 3 mm diameter GC disk used for voltammetric analysis, a bulk WE (of different materials) for electrolysis and a counter electrode made of Pt in a separated compartment were inserted. The decided amount of supporting electrolyte, solvent and monomer were put into the cell, together with a magnetic stirrer. Selected volumes of $Cu^{II}(OTf)_2$, polydentate amine ligand, and halogen ions were withdrawn from stock solutions and added into the cell. A CV of the ATRP catalyst was recorded on the GC disk electrode. Then, the initiator was injected into the solution and another CV was recorded, to verify the catalytic effect. The solution was then degassed for 30 minutes, under vigorous magnetic stirring. At this point, the bulk WE, which was previously activated (**Section C1**) and already in the cell, above the solution, was immersed into the solution and a fixed potential (or a current program) was applied to the system. Samples were withdrawn periodically to follow the polymerization kinetic.

In case of a *se*ATRP, the CE was an activated Al wire, directly immersed into the working solution.

C3. Procedure for galvanostatic *e*ATRP with pre-electrolysis of Cu^{II}

This procedure was adopted for aquoues *e*ATRP of OEOMA on non-noble metal cathodes (see **Chapter 4**, **Section 4.3**). The same steps described in **Section C2** were performed, except that the current program was started before RX injection. Cu^{II} was reduced by applying a cathodic current of 0.45 mA for 25 min (in the case of a two steps

galvanostatic *e*ATRP) or a cathodic current of 0.52 mA for 22 min (in the case of a four steps galvanostatic synthesis). A theoretical charge corresponding to ca 50% conversion of Cu^{II} to Cu^{I} was passed, but the effective Cu^{II} reduction was less than 50% as significant portion of the charge was consumed to activate the electrode by removal of surface oxides. After pre-electrolysis, the required amount of RX was added, withdrawn from a degassed stock solution, and the chosen current program was applied to start the *e*ATRP.

Appendix D

Experimental details for *e*ATRP and ARGET-ATRP in (mini)emulsion

Table of contents

D1. Electrochemical characterization of Cu complexes-SDS interaction

A literature procedure was followed to determine the fraction of catalyst bound to micelles (f_{bound}, **Chapter 1**, **Section 8.2.1**).[1] In this experiment, probe and surfactant concentrations (C_p and C_{SDS} respectively) were both varied to maintain a constant ratio $C_p/C_{mic} \approx 1$, where $C_{mic} = (C_{SDS} - cmc)/N$. N is the aggregation number of SDS, which depends on the operating conditions. In literature, N = 82 was measured for *ca.* 0.038 M SDS in water + 0.1 M NaBr, at $T = 40$ °C.[2] Considering that N varies with T in pure water as: $N = 520 - 1.52*T(K)$, we assumed that a similar trend is valid also in the presence of 0.1 M NaBr, that is the slope of the curve N vs. T is the same. From N = 82 for $T = 40$ °C a new intercept was determined as 558, thus N = 44 for $T = 65$ °C.[3] CVs of the catalytic system were recorded at different scan rates, for 5 C_{SDS} values.

D2. Description of partition experiments

Aqueous solutions of $Cu^{II}Br_2$/ligand (1/2 by mole) were prepared at various concentrations. Catalyst absorbance was recorded by UV-Visible spectroscopy (maximum wavelength, λ_{max}, 867 nm)., and a linear calibration was obtained from the correlation

between A values and catalyst concentration. Solutions of copper complex in water were prepared at various concentrations and then mixed with different monomer volumes. Mixtures were vigorously stirred using a Vortex Mixer at either RT or 60 °C. The aqueous phase was collected and absorbance at λ_{max} was recorded by UV-Vis spectrometer. Percentage of copper complex remaining in the aqueous phase was then calculated.

In order to detect the minimum amount of hydrophilic catalyst distributed in the organic phase, the latter was spectroscopically analyzed. A higher amount of $Cu^{II}Br_2$/L was used to detect more accurately the small amount of catalyst in the organic phase. The linear calibration was obtained as before, but using $C_{Cu^{II}Br_2}/C_{TPMA}/C_{SDS}$ 1/1/1 in BA + a few drops of H_2O. This allowed to saturate the BA phase in water, as occurs during a miniemulsion experiment. In the presence of surfactant, the analyzed solution was not vigorously mixed, in order to avoid formation of a dispersion. Therefore, aqueous and organic phase were put carefully in the same vial to form a macroscopic two-phase system. Then, the mixture was let to equilibrate for three days under gentle rocking on a platform rocker. After three days the mixture was still macroscopically well separated, but was centrifuged at 5000 rpm for 15 minutes to obtain a cleaner separation between the two phases. Finally, the organic top layer was withdrawn and analyzed by Visible-NIR spectroscopy.

D3. General procedure of *e*ATRP and *se*ATRP in minemulsion

A stock solution of monomer, RX (the required amount to target the desired degree of polymerization), and co-surfactant was prepared. The selected amount of $Cu^{II}Br_2$, ligand, NaBr and surfactant were dissolved in the desired volume of distilled water. Precise volumes of organic and aqueous solutions were mixed, placed in an ice bath, and dispersed by a probe sonicator, amplitude = 70% for 15 min; (application and rest time of 1 s each). At the end, particle size was measured by diluting in 1.5 mL of water 3 drops of the emulsified solution, and analyze the sample by DLS. Nitrogen was bubbled through the miniemulsion solution for 40 min, prior to recording a CV, which allowed for accurate selection of the applied potential E_{app}. The electrolysis was performed at the selected E_{app}. Samples were withdrawn periodically to follow the monomer conversion by gravimetric analysis, while M_n and $Đ$ were determined by GPC. Gravimetric analysis was performed by putting few drops of polymerizing solution on an Al plate, which was located in an oven

for at least 40 minutes. The weights of the empty plate, and before and after the evaporation in the oven, were recorded and allowed for the determination of monomer conversion.

In case of *se*ATRP, the CE was an activated Al wire directly immersed into the working solution.

For chain extension experiments, the macroinitiator (MI, first block) was prepared *via se*ATRP method described above, by targeting DP = 100. When the polymerization was stopped, the final solution was divided into 2 parts. *i*) the first one was used for *in situ* chain extension with a second monomer: MI and monomer solutions were mixed, placed in an ice bath, and dispersed by a probe sonicator, amplitude = 70% for 15 min; (application and rest time of 1 s each). Nitrogen was bubbled through the miniemulsion solution for 40 min, then the selected E_{app} was applied to start the polymerization. *ii*) the second part was purified: dried at 100 °C for 1 day, dissolved in THF, precipitated in methanol/water mixture three times, passed through *a* neutral alumina column in order to remove catalyst, and dried under vacuum for 2 days. Finally, the purified MI was used as initiator for *se*ATRP of the second monomer, according to the normal procedure.

D4. General procedure for ARGET-ATRP in miniemulsion

Monomer, co-surfactant, and the required amount of RX to target selected DP, were mixed to form the organic phase. $Cu^{II}Br_2$/TPMA stock solution, NaBr, and SDS were dissolved in distilled water. The organic and aqueous solutions were mixed, placed in an ice bath, and dispersed by probe sonicator, amplitude = 70% for 15 min (application and rest time of 1 s each). Nitrogen was bubbled through the miniemulsion solution for 30 minutes. The flask was immersed in a 65 °C oil bath and then an ascorbic acid solution (in water) was slowly injected over 3 minutes to start the reaction. Then, the reducing agent was intermittently added dropwise or continuously by means of a syringe pump, depending on the selected feeding strategy. Samples were withdrawn periodically to follow the monomer conversion by gravimetric analysis, while M_n and $Đ$ were determined by GPC. Particle size was measured by DLS before and after polymerization, by diluting 3 drops of the solution in 1.5 mL of water.

For chain extension experiments, the MI was prepared following the described procedure, but targeting low DP. The product was precipitated into CH_3OH/H_2O (1/1 by v/v), re-dissolved in THF, passed through neutral alumina column and dried in vacuum.

The purified MI was then used as initiator for the ARGET-ATRP of the second block, by following the usual procedure.

After *e*ATRP or ARGET-ATRP, some solutions were analyzed by ICP-MS. For this purpose, 5 mL of polymerization solution were transferred to a 50 mL centrifuge tube. 20 mL of water and 20 mL of MeOH were added and then the tubes were placed in the centrifuge for 20 min at 5000 rpm.

D5. General procedure for ARGET-ATRP in emulsion

The aqueous phase was prepared by dissolving in distilled water the desired amount of $Cu^{II}Br_2$, ligand, NaBr and SDS. Nitrogen was bubbled through the aqueous solution for 30 minutes. Meanwhile, the monomer was also degassed in a separated flask. The flask containing the aqueous phase was immersed in a 65 °C oil bath and the desired amount of degassed monomer was gently injected. Stirring was started at the selected rate. Depending on the pre-emulsification procedure, the ascorbic acid was injected after some time or immediately when stirring was started (no pre-emulsification). The ascorbic acid solution (in water) was continuously injected by means of a syringe pump, at the set feeding rate. Samples were withdrawn periodically to follow the monomer conversion by gravimetric analysis, while M_n and $Đ$ were determined by GPC. Particle size was measured by DLS before and after polymerization (or in one case at fixed intervals), by diluting few drops of solution in 1.5 mL of water.

References

1. Mandal, A. B.; Nair, B. U.; Ramaswamy, D. *Langmuir* **1988,** 4, 736-739.
2. Bergström, M.; Pedersen, J. S. *Physical Chemistry Chemical Physics* **1999,** 1, 4437-4446.
3. Shah, S.; Jamroz, N.; Sharif, Q. *Colloids and Surfaces A: Physicochemical and Engineering Aspects* **2001,** 178, 199-206.